Small signal modelling of power electronic converters, for the study of time-domain waveforms, harmonic domain spectra, and control interactions

Geoffrey Neal Love

A thesis presented for the degree of
Doctor of Philosophy
in
Electrical and Computer Engineering
at the
University of Canterbury,
Christchurch, New Zealand.

January 2007

ABSTRACT

This thesis describes the development of several small signal analysis methods for the modelling of power electronic converters. The methods are written generally and are intended to be able to be applied to all converter classes. In the penultimate chapter these general models are used to model the capacitor commutated converter.

All the contained methods are based around a time domain small signal model. This time domain small model is a linearization of a power electronic system of passive components and ideal switches described as a hybrid system. The key problem in the derivation of the small signal model is the correct determination and description of the linearized effect of switching instant variation.

Three analysis methods based upon the small signal model are advanced in this thesis, these are; time domain sensitivity matrices for use in a Newton determination of the cyclic steady state of a power electronic converter, partial waveform construction of harmonic sensitivity matrices for studying sensitivity of converters to harmonic disturbances, and harmonic state space models also for the construction of harmonic sensitivity matrices and for study of dynamic systems. Each modelling technique is applied to the more common converter topologies of the Buck-Boost converter and the Graetz Bridge before being finally applied to the capacitor commutated converter. Each technique is compared to PSCAD-EMTDC simulations for verification.

ACKNOWLEDGEMENTS

Firstly I would like to thank my supervisor Dr Alan Wood. Thanks Al for your time and patients over these years in listening, discussing, and editing my thoughts. I always found your door open when I sort it. Thanks for taking the risk and giving me a large amount of freedom, and I hope it didn't cause you too much stress!

Secondly I would like to thank my senior colleagues Dr David Hume and Chris Osauskas. Your work and the conversations I have had with you both were invaluable in setting the direction of my PhD. Thank you for being so generous with both your time and your ideas.

Thanks is also due to the rest of the academic and technical staff at the Electrical and Computer Engineering Department, special thanks go to Ken Smart, Dr Chris Arnold, Assoc. Professor Neville Watson, Pieter Kikstra, and Professor Pat Bodger.

I would also like to thank my colleagues over the years, Dr Christoph Sainter, Dr Kent Yu, Dr Bernard Perera, Dr Chris Collins, Dr John Schnberger, Dr Liu Yonghe, Dr Mohamed Zaid, DC++, Dave Rentoul, Suman Poudel, Jiak-San Tan, Nikki Newham, Nick Murray, Lance Frater, Simon Bell, William, and Jordon.

Thanks to Mum and Dad for their Love and for their finanical support during my undergrad years.

To my friends I thank you for distracted me from my PhD over these years, not that distracting me from my PhD was that hard! Thank you; Alex Goldsbrough, Ali Rad, Ahmed Mohamed, Amy Cruickshank, Ben McQueen, Catherine Paquette, Chris Forne, David Lim, Emily Wall, Jason McEwen, Julie Jansen, Leigh Clark, Matthew Jones, Miho Tanaka, Nadine Clayton, Prow Tovaranonte, Savva Kerdemelidis, Sandy Quick, Susan Gill, Stacy Malloch and Tim Hawkins.

Thank-you Miss Susan Lee for your love and support whilst I was writing this thesis, I wish you the best for the future.

CONTENTS

GLOSSARY

AC	Alternating Current
CCC	Capacitor Commutated Converter
CSS	Cyclic Steady State
DC	Direct Current
DE	Differential Equation
EMP	Exponential Modulate Periodic (system)
FSCI	Fourier Series Coefficient Integral
HD	Harmonic Domain
HSM	Harmonic Sensitivity Matrix
HSS	Harmonic State Space
HTF	Harmonic Transfer Function
HVdc	High Voltage Direct Current
I/O	Input Output
LTI	Linear Time Invariant (system)
LTISS	Linear Time Invariant State Space
LTP	Linear Time Periodic (system)
LTPSS	Linear Time Periodic State Space
MPBV	Multi Point Boundary Value (problem)
PD	Partial Derivative
PR	Partial Resonance
PSS	Partial Steady State
PT	Partial Transient
PW	Partial Waveform
PWL	Piece Wise Linear
S-domain	Complex Frequency Domain
SCR	Short Circuit Ratio
SI	Switching Instant
SIV	Switching Instant Variation
STM	State Transition Matrix
TPBV	Two Point Boundary Value (problem)

Chapter 1

INTRODUCTION

The main motivation of this thesis is the the development of analysis techniques that can be applied to a general power electronic circuit. This kind of general technique is lacking in power electronic analysis with the only technique time-domain simulation being truly general.

In a time-domain simulation, the digital computer with its program instructions and memory registers is used to mimic the behavior of a power electronic circuit using the laws of circuit theory. This mimicking of one physically real system with another, even one buried deep with a computer, is the essence of simulation and it is a powerful and general technique that can model complex and detailed topologies. Unfortunately, in some cases it does not provide the insights or the form required for tasks such as controller design, filter design and stability analysis. Additionally the computational effort required to perform a simulation can be great, especially the mass simulations needed for a contingency style analysis.

The alternatives to time-domain simulation developed so far in the study of power electronic devices are very case specific often taking advantages of peculiarities of specific topologies. For example s-domain models have been constructed for both DC:DC style converters [1] and separately for HVdc converters [2], [3], and [4], but how to apply the techniques developed for one converter class (DC:DC or HVdc) to another is not readily apparent. When new topologies such as the capacitor commutated converter come into vogue then alternatives to time domain simulation are unavailable. It is the intention of the work in this thesis to not only build alternative analysis techniques for the study of Capacitor Commutated converters, but to outline their construction in such a way that the techniques can be applied to any converter topography.

The alternative analysis methods advanced in this thesis are all based on the premise that in studying the response of a system to small perturbations the effect can be extrapolated to larger perturbations. This notion is called linearization, or the small signal model, and as the name suggests works best for those systems that are either highly linear[5] or in the study of *small* disturbances. In this thesis small signal techniques are developed for three sorts of models; time domain sensitivity matrices for a Newton's solution to the cyclic

steady state problem, harmonic sensitivity matrices, and s-domain dynamic models using the harmonic state space (HSS).

1.1 PRELIMINARIES :DOMAINS

In this thesis, already several *domains* have been referred to; Time Domain, Frequency Domain, Harmonic Domain and the s-domain. As each of these domains have crucial importance in this thesis, some time is taken here to describe exactly what each domain is.

Time Domain *In the Time Domain all signals are functions of time, $f(t)$, where t is time.*

Discrete Time Domain *In the Discrete Time Domain all signals are functions of discrete (or event) time, $f(k)$, where k is a discrete (or event) time point.*

Complex Frequency or s-Domain *In the s-domain all signals are functions of complex frequency $f(s)$, where s is a complex frequency $\sigma + j\omega$.*

Frequency Domain *In the Frequency Domain all signals are functions of frequency $f(\omega)$, where ω is frequency.*

The frequency domain is a subset of the s-domain. Using the s-plane (the plane of complex numbers) the frequency domain lies on the imaginary axis. If a frequency domain signal is shown in the s-plane it will appear at two points, $(+j\omega, -j\omega)$.

Harmonic Domain *Harmonic domain signals are signals which are functions of the harmonic frequencies of the pumping frequency, $f(\omega_1 k)$, where k is an integer, and ω_1 is the pumping frequency.*

The harmonic domain is a subset of the frequency domain, and consequently a subset of the s-domain. In this thesis harmonic domain signals are represented in the complex exponential form of a Fourier series, others including [6] [7] [5] use a real-imaginary form. The real-imaginary form has some implementation advantages but the complex form is easier to manipulate and arrange so is the form used within this thesis. However any of the results obtained in this thesis can be equivalently written in the real-imaginary form.

The harmonic domain is exclusive to power systems literature and has been used in development of techniques for finding the harmonic steady state and the harmonic coupling of various power systems components, including synchronous machines [8] and power electronic converters [6] [7]. Despite the term being exclusive to power systems literature, this type of domain has a long history under different guises [9].

1.2 CHAPTER SUMMARY

The layout of the thesis is as follows.

Chapter 2: Hybrid Modelling of Power Electronic Circuits In this chapter a general model of the power electronic system is developed. It is based upon the structure and terminology of hybrid system theory [10] [11], adapted to take account of the peculiarities specific to power electronic systems. The main aim of the model is to formalize and generalize the dynamic interactions and behavior in power electronic systems from which to base the analysis techniques that follow.

Chapter 3: Small Signal Modelling In this chapter the small signal model of the hybrid model of Chapter 2 is described. A small signal model can be defined with the use of Taylor's theorem. In Taylor's theorem, any function (where in this thesis the functions are the actions of the power electronic converters) can be described in terms of a set of its derivatives. A small signal model assumes that the function is sufficiently linear that it can be described by its first derivative. This assumption sacrifices model accuracy to produce a model that is amenable to analysis, but is a valid assumption for power electronic converters as they have been demonstrated to be highly linear [5].

The linearization of a converter is mostly trivial where the Differential Equations DEs that describe each mode's continuous evolution in the hybrid model can be recycled for use in the small signal model. The key difficulty occurs at the switching points, where currents and voltages are step changed to take account of the linearized effects of switching instant variations (SIVs).

Chapter 4: Steady State Analysis The small signal model forms the basis for several analysis techniques and other models. The first of these, and the most widely reported is finding the steady state operating point of a power electronic system subject to periodic excitation. In this chapter, this is achieved by a Newton's solution to a two point boundary value problem. The small signal model is used to form the Jacobian for the Newton's technique.

Chapter 5: Harmonic Sensitivity Matrices Harmonic Sensitivity Matrices map input distortion described in the harmonic domain to the output. This style of model has been constructed for converters numerically [12] [13], and analytically [6], [7], [14], [15] and [5] for studying converter harmonics in power quality studies, filter design and in [6], [7], they are used for the Newton's solution of the harmonic operating point of a HVdc link.

In this chapter the harmonic sensitivity matrices are constructed from the small signal model using a partial waveform shaping technique. This technique is similar to the technique outlined in [15] and [5], but is extended to the general case.

Chapter 6: Harmonic State Space Model Power Electronic Converters have been previously modeled using the HSS framework [16] but currently no generalized technique has been developed. In particular, autonomous switches with states in their commutation circuits have been largely ignored. In this chapter a general technique has been developed based on the time domain small signal model.

Once produced the HSS is by itself a powerful model but in addition it can be used in the construction of the harmonic sensitivity matrices and also for s-domain models for dynamic analysis. The development of these models is the major contribution of the work presented in this thesis.

Chapter 7: Capacitor Commutated Converter In this chapter, the techniques developed in the previous chapters are used to model the Capacitor Commutated Converter (CCC). The addition of the capacitor in each phase increases the complexity of the commutation circuit and increases the difficulty of the modelling problem - however with the application of the above formalized techniques the steady state, the harmonic sensitivity, and the dynamic s-domain description are constructed systematically and with ease.

Chapter 2

HYBRID MODEL OF A POWER ELECTRONIC SYSTEM WITH IDEAL SWITCHES

2.1 INTRODUCTION

Hybrid systems theory is an emerging field of research within Circuits, Systems and Control literature [11]. The aim of the research is to create methods of analysis and control for systems that fall between the tradition boundaries of continuous systems and discrete systems – the so called hybrid systems.

Briefly, *a hybrid system is a collection of dynamic systems with a set of rules for jumping between them* [10]. In power electronics, the *dynamic systems* are the electrical systems associated with each switching configuration i.e the stages. The *rules* are the inequalities for each switch that determines when they can or must change position.

The aim of this chapter is to build a formal model of an ideal power electronic system using the terms and formalization found in hybrid systems theory.

2.2 POWER ELECTRONIC SYSTEM

In this thesis, a power electronics system has the following definition.

Definition 2.1 (Power Electronic System) *A power electronic system is system containing at least one power electronic switch, any number of passive electrical components (transformers, resistors,capacitors, and inductors) and any number of ideal current and voltage sources.*

Definition 2.1 defines the power electronic system to be separate from its controller. This split enables the characteristics of the power electronic system to be generalized without considering the unrestricted complexity of the controller. As a block diagram, the model of a power electronic system is that of Figure 2.1.

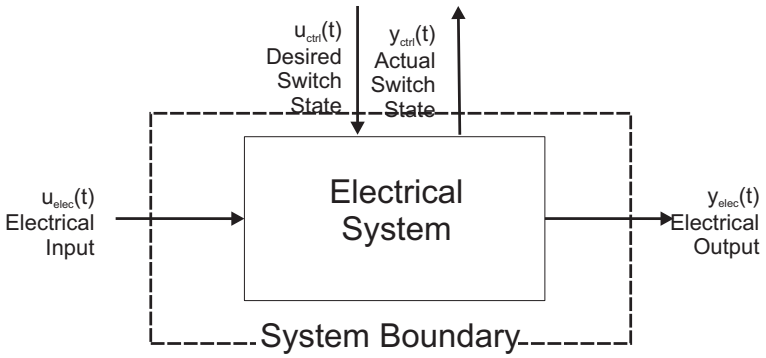

Figure 2.1 Power Electronic system, and its signals. y_{elec} and u_{elec} together form the electrical ports of the system, y_{ctrl} are discrete control observers, and u_{ctrl} are the discrete control commands

As should be apparent from the names of the signals there are two categories of input/output (I/O) signals that interact with the system, electrical signals and control signals. Electrical signals have the subscript suffix $_{elec}$, and control signals have the subscript $_{ctrl}$.

Control system commands are sent to the power electronic system via the discrete vector $u_{ctrl}(t)$, this signal contains the desired switch positions. Feedback from the power electronic system to the controller is carried out by discrete vector $y_{ctrl}(t)$ which contains the switching position of both controlled and autonomous switches. The vectors $u_{ctrl}(t)$, and $y_{ctrl}(t)$ may disagree as the ordered and actual switch positions could be inconsistent.

The external electrical systems interact with the power electronic system via the electrical ports. Here, these vectors are displayed as the I/O pairs, $y_{elec}(t)$ and $u_{elec}(t)$. The vector y_{elec} can be modified to include observers of electrical signals that are internal quantities.

Determining the boundaries of the power electronic system and deciding which devices are part of the system is subjective. However, some passive elements belong with the switches if their dependency is directly affected by the switch position.

2.2.1 Power Electronic Devices

Power electronic switches have a great range of structural, capacity, and control differences. For example a typical modern IGBT can switch at 50kHz, but can only handle 500A, compared to a GTO which has a much slower switching frequency of 1 kHz, but can handle a much larger current of 2000A [17]. They are driven differently as well; a GTO is turned on and off with a pulse, whilst a IGBT needs a constant gate current to remain on. However, their operation from a control point of view is essentially the same; they are both controllable unidirectional devices, are both able to turn on when positively biased, can turn-off when carrying current, and are forced to turn-off if subjected to negative directional current. From this ideal point of view both switches are the same, their speed and current carrying differences are dictated by their real world application. Using this ideal perspective there are three classes of switches.

- **Type I:** Type 1 devices are uni-directional devices whose on and off states are autonomously determined. Diodes are the sole member of this group.
- **Type II:** Type II devices are uni-directional devices whose on state can be controlled and whose off state is autonomously determined when forward biased. Thyristors (or SCRs) are the sole member of this group.
- **Type III:** Type III devices are uni-directional devices whose on and off state can be controlled when forward biased. This group is made up from many members, (BJTs, Mosfets, IGBTs GTOs, MCTs), all of which have different power handling characteristics.

Most varieties of switches are Type III, with diodes and thyristor being the sole members of the Type I and Type II classes respectively. Although the types are all uni-directional, bi-directional devices types can be constructed from two uni-directional devices paralleled back to back. For example a triac consists of two type II devices paralleled back to back.

Definitions of the behavior of these three types are as follows. Included in these definitions are the switch inequalities which govern when a switch can (or must) change position. Figure 2.2 defines the variables used in these formal definitions.

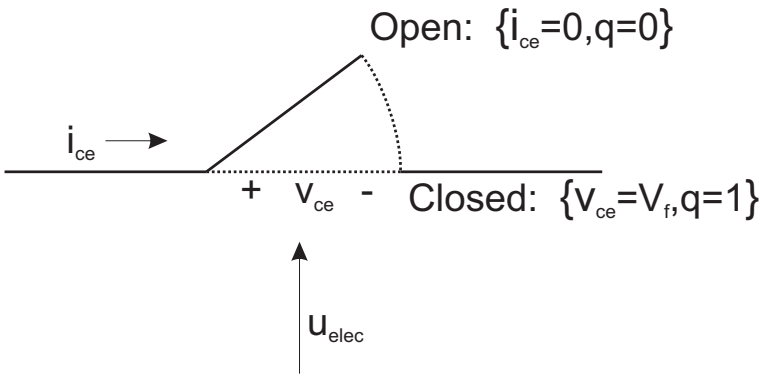

Figure 2.2 Power Electronic Switch and its variables. v_{ce} is the voltage across the switch, i_{ce} is the current through the switch, and V_f is the turn on voltage across the switch when it is closed. The variable q is the discrete state of the switch, $q = 1$ when the switch is closed, and $q = 0$ when the switch is open. Depending on the switch type the discrete control signal u_{ctrl} can also be present. The terminal labels C and E stands for *collector* and *emitter* respectively and originate from labels used in BJT, here they are just labels and nothing more is implied by their use.

Definition 2.2 (Type I) *Type I devices turn on when the voltage, v_{ce}, across the switch is greater than the voltage V_f and turn off when the current through the switch is less than or equal to 0.*

Switch Inequalities

Device turns on, $q = 1$, when the following inequality is met.

$$v_{ce} > V_f \tag{2.1}$$

Device turns off, $Q = 0$, when the following inequality is met.

$$i_{ce} \leq 0 \tag{2.2}$$

Definition 2.3 (Type II) *Type II devices turn on when the forward voltage, v_{ce}, across the switch is greater than V_f and the switch is given an "on" signal. An "on" signal is represented by $u_{ctrl} = 1$. Turn off occurs when the current through the switch is less than or equal to 0.*

Switch Inequalities

Device turns on, $q = 1$, when the following conditions are met.

$$v_{ce} > V_f \tag{2.3}$$
$$and \ u_{ctrl} = 1 \tag{2.4}$$

Device turns off $q = 0$, when the following inequality is met.

$$i_{ce} \leq 0 \tag{2.5}$$

Definition 2.4 (Type III) *Type III devices turns on when the forward voltage, v_{ce}, across the switch is greater than v_f and the switch is given an "on" signal. An on signal is represented by $u_{ctrl} = 1$. Turn off occurs when the current through the switch is less than or equal to 0, or when the switch is given an off signal. An off signal is represented by $u_{_{ctrl}} = 0$.*

Switch Inequalities

Device turns on, $q = 1$, when the both the inequality 2.6, and boolean equation 2.7 are met.

$$v_{ce} > V_f \tag{2.6}$$
$$and \ u_{ctrl} = 1 \tag{2.7}$$

Device turns off $Q = 0$, when either the inequality 2.8, and boolean equation 2.9 are met.

$$i_{ce} \leq 0 \tag{2.8}$$
$$or \ u_{ctrl} = 0 \tag{2.9}$$

Typically V_f is equal to zero, however a value of 0.6V that is found across real switches [17] could be used. In this thesis V_f is assumed to be zero.

In the definitions given the "on" inequalities are exclusive of the boundary, ($>$), whilst the "off" inequalities are inclusive ($\leq$). If both were exclusive or inclusive then the position of the switch would be ambiguous at the boundary.

2.3 HYBRID SYSTEMS

Restating Branicky's hybrid system definition [10] used in the introduction of this chapter: *a hybrid system is a collection of dynamic systems with a set of rules for jumping between them.* The dynamic systems can be of any sort (difference equation, Petri nets, etc) but here they are assumed to be continuous state space systems described using a 1st order set of DE's. These 1st order systems are collectively called the *continuous dynamics*, and they determine the evolutions of the *continuous state*.

In power electronic circuits the DE's are formed from passive circuit elements. It is assumed here that these state space models are easily obtainable, and in general the circuits used in this thesis are simple enough that they can be derived by simple circuit analysis. For more complex systems bond-graph theory [18] or some other automated technique could be used.

Every 1st order set of DEs is associated with a discrete state of the hybrid system. In a power electronic system these are the switch positions. Together each 1st order set of DEs and its associated discrete state are collectively known as a stage of system. In a system with n switches there are 2^n possible discrete states, however in most systems only a subset of these are typically used.

Two sets of rules are used to determine discrete state of a hybrid system. Collectively the rules are the *discrete dynamics* of the system. The first group, called jump sets, determine when a system should jump and are defined as areas within the spaces of a stage. The second group, called jump destination maps are used once a jump-set has been satisfied and determine the new discrete state of the system, and where within the continuous state of the new stage the evolution begins.

In summary a hybrid system containing both discrete dynamics and continuous dynamics is made from the following constituent parts.

- Discrete States
- Set of continuous dynamic systems
- Jump Sets
- Jump destination maps

A visual representation of these parts is depicted in Figure 2.3. These parts and their place in a power electronics model are expanded upon in the remained of this section.

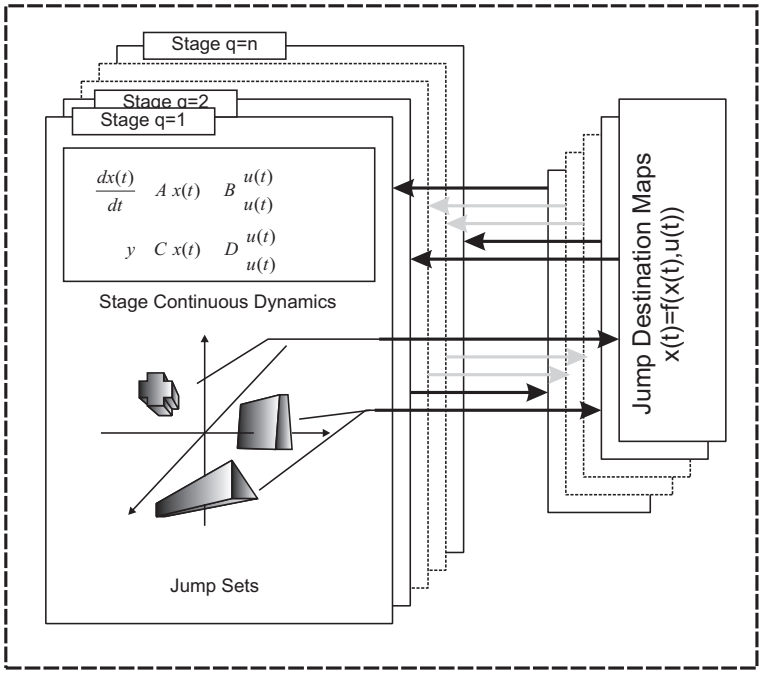

Figure 2.3 Visual representation of a hybrid system. The stages, and their associated jump sets are stacked on the left, the Jump destination maps are stacked on the right.

2.3.1 Stages: Discrete States and Continuous Systems

In a power electronic system the discrete state represents the positions of the system's switches - and as discussed for a system with i switches there are $n = 2^i$ switch configurations. Each configuration is associated with a continuous dynamic system that in power electronic systems are describe as state space equations, as in equation 2.10.

$$\begin{aligned} \frac{dx_n(t)}{dt} &= A_n x_n(t) + B_n \begin{bmatrix} u_{elec}(\tau) \\ \dot{u}_{elec}(\tau) \end{bmatrix} \\ y_{elec}(t) &= C_n x_n(t) + D_n \begin{bmatrix} u_{elec}(\tau) \\ \dot{u}_{elec}(\tau) \end{bmatrix} \end{aligned} \tag{2.10}$$

The integral form is that of equation 2.11.

$$x_n(t) = e^{A_n(t-t_0)} x_n(t_0) + \int_{t_0}^{t} e^{A_n(t-\tau)} B_n(\tau) \begin{bmatrix} u_{elec}(\tau) \\ \dot{u}_{elec}(\tau) \end{bmatrix} d\tau \tag{2.11}$$

The state vector of the stage $x_n(t)$, is a function of the dynamically independent energy [19] [1] in the system and unless stated it is assumed that the states are formed from capacitor voltages and inductor currents[2]. The gradient of the input is required if the output is a function of a source dependent component. The rigorous formation of the state space description can be achieved using bond-graph theory [18].

2.3.2 Jump Sets

Each stage contains a set of jump sets that determine when a system stops evolving in that stage and begins evolving in the next. These jump sets are realized as areas within the spaces of each stage, in power electronic systems the jump sets fall into two classes; controlled and autonomous. If a stage has an autonomous jump set the system jumps the moment it finds itself within the set. In a controlled jump set the system will only jump when ordered by an external control to do so. Formally the definitions of these autonomous and controlled jump sets are as follows.

Definition 2.5 (Autonomous Jump Set) *Within every n^{th} stage there possibly exists K autonomous jump sets. The boundaries of the k^{th} autonomous jump set are defined by the function $v_k(x_n, u_{elec})$. If the system enters the jump set, or lies on its boundaries then an autonomous jump occurs.*

Definition 2.6 (Controlled Jump Set) *Within every n^{th} stage there possibly exists R controlled jump sets. The boundaries of the k^{th} controlled jump set are defined by the function $f_k(x_n, u_{elec})$. If the system enters the jump set, or lies on its boundaries then the system can make an controlled jump set.*

The definition of autonomous used here differs from that used in Branicky's work [10]. In Branicky's work autonomous jump sets are only functions of the state space of each stage; here they are function of the electrical input as well. This altered definition reflects the more usual condition of controlled and autonomous switches found in power electronics literature.

For the power electronic system the boundaries of the jump set are defined by the switch inequalities. Type I switches have only autonomous jump sets, whilst type II and type III have a mix of both autonomous and controlled jump sets. The autonomous and controlled jump sets in a power electronic system are as follows (where $V_f(t)$ is set to zero).

Autonomous Jump Sets in a power electronic system

[1] Independent energy is stored in those components whose energy is determined by the dynamic evolution of the system. Dynamically dependent energy is attributed to components with energy that is directly dependent on a source, or a switch position. An example of a dependent component is an inductor in series with a current source.

[2] Although any orthogonal basis could be used for simplification it is usually assumed in this thesis that each state is a capacitor voltage or an inductor current.

- For every type I switch that is off during a particular stage, there exists an autonomous jump set described by $v_{ce} > 0$
- For every type I,II, and III switch that is on during a particular stage, there exists an autonomous jump set described by $i_{ce} \leq 0$

Controlled Jump sets in a power electronic system

- For every type II,III switch that is off during a particular stage, there exists a controlled jump set described by $v_{ce} > 0$
- For every type III switch that is on during a particular stage, there exists a controlled jump set described by $v_{ce} > 0$

v_{ce}, and i_{ce} are normally functions of the variables of each stage, i.e $[x_n(t), u_{elec}(t)]$.

2.3.3 Jump Destination Maps

When a jump set or group of jump sets is satisfied the system changes its discrete state and jumps to a new stage, this transition is performed by one of the system's jump destination maps. In a system with continuous modes each map has two parts, a discrete map and a continuous map. The discrete map declares what two stages the system evolves between, in most hybrid systems this map is obvious. Figure 2.4 shows a three stage system and the discrete portion of the six unique jump destination maps between them.

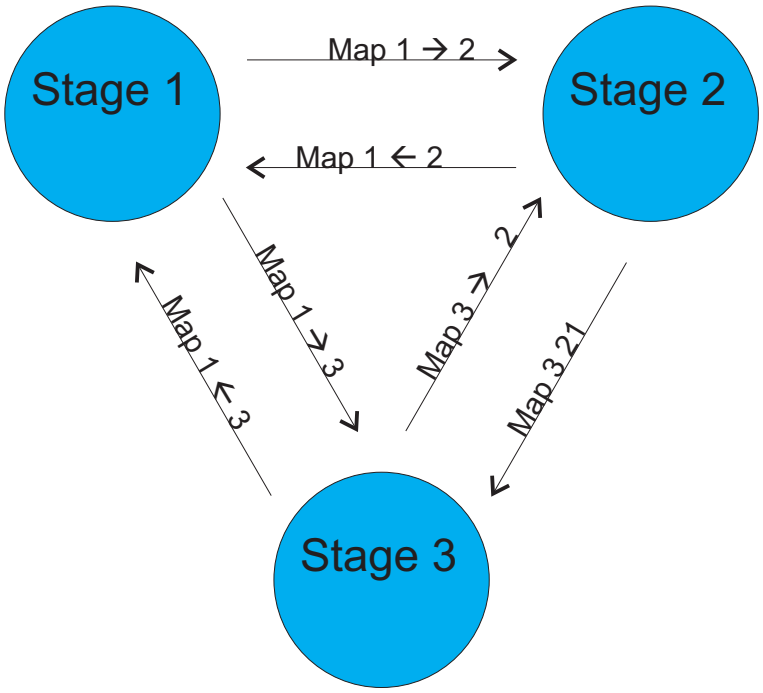

Figure 2.4 Three stage and the jump transition maps between them

The form of the continuous map shown in equation 2.12.

$$x_{n+1}(t_{\theta_n}^+) = P[n+1,n]x_n(t_{\theta_n}^-) + Q[n+1,n]u_{elec}(t_{\theta_n}) \tag{2.12}$$

The matrix $P[n+1,n]$ is called the projection matrix, and it transforms the independent energy in the old stage n to the new stage $n+1$. The matrix, $Q[n+1,n]$ is called the injection matrix and it injects (or extracts) energy from the continuous input to the continuous states of the new stage. In power electronic systems the projection and injection matrixes are found by using the laws of flux and charge conservation [20] and [21].

Determining which map to invoke is a function of the satisfied jump sets. Every jump set and every overlap of jump sets is potentially associated with a different map. For example in Figure 2.5 two overlapping jump sets, one autonomous and one controlled are depicted. Together these sets are associated with three maps; one associated with the autonomous region, one associated with the controlled region, and one associated with the overlapping region. The map associated with the overlap is used only when both the autonomous and controlled jump sets are satisfied; otherwise unless the control jump set is *primed* when the system enters the overlap then the map associated with the autonomous region is invoked.

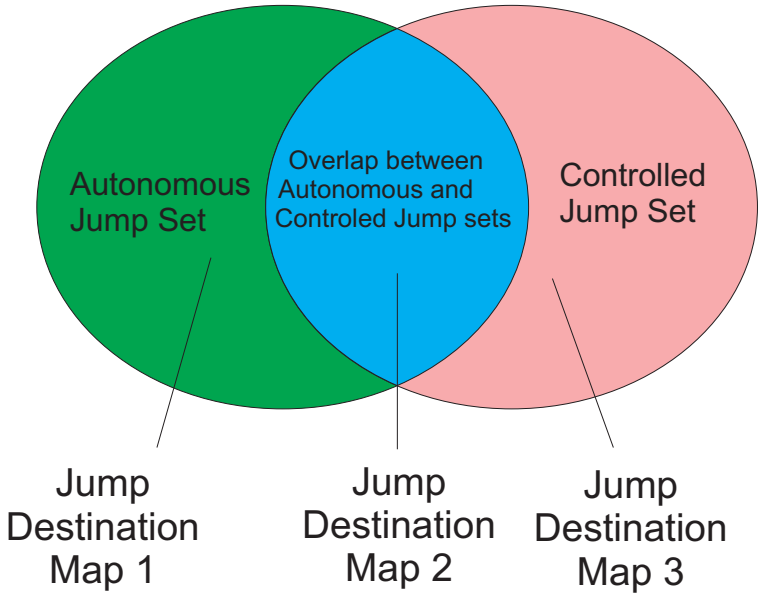

Figure 2.5 Overlapping jump sets and the associated jump destination maps

2.3.4 Evolution of a hybrid System

Together the discrete states, the continuous systems, the jump sets and the jump destination maps form a hybrid system. In Figure 2.6 the stylized evolution of a system with four stages is shown. In each stage there is a mix of both controlled and autonomous jump sets.

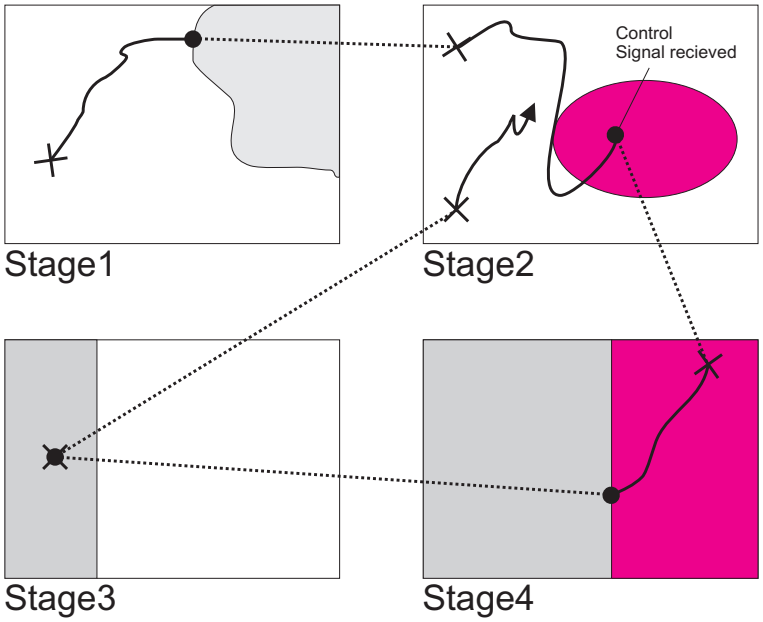

Figure 2.6 Evolution of *Branicky* hybrid system. Autonomous jump sets are light grey areas, controlled jump sets are dark grey, and areas which are white are not members of any jump set

2.3.5 Formal Definition

Formally, a hybrid control system, for a power electronic system using a definition based on [10], is a system of the form of Definition 2.7.

Definition 2.7 (Hybrid system description of a power electronic system) *A hybrid system of a power electronic system, $H = [Q, \Sigma, V, F, G]$ is defined by the following parts.*

- *Q is a set of labels that form the discrete states of the system. Each discrete state isassociated with a dynamic system. Together the discrete state and its associated dynamic system form a stage of the system.*
- *$\{\Sigma_n\}_{n \in Q}$ is the collection of dynamic systems, one for every discrete state. Each dynamic system is made from the following constituent parts $[x_n, A_n, B_n, C_n, D_n]$. x_n is the continuous state and A_n, B_n, C_n, D_n determine the continuous dynamics of the stage using the following differential equation.*

$$\begin{aligned} \frac{dx_n(t)}{dt} &= A_n x_n(t) + B_n \begin{bmatrix} u_{elec}(\tau) \\ \dot{u}_{elec}(\tau) \end{bmatrix} \\ y(t) &= C_n x_n(t) + D_n \begin{bmatrix} u_{elec}(\tau) \\ \dot{u}_{elec}(\tau) \end{bmatrix} \end{aligned}$$

- *$\{V_k\}_{\forall\, n \in Q}$ are the sets of K autonomous jump sets associated with the N stages. The*

region of the k^{th} jump set is defined by an inequality of the form $V_k \leq g_1 x_n + g_2 u$ or the form $V_k < g_1 x_n + g_2 u$ [3].

- *$\{F_k\}_{\forall\, n \in Q}$ are the sets of R controlled jump sets associated with the N stages. The region of the k^{th} jump set is defined by an inequality of the form $F_k \leq g_3 x_n + g_4 u$ or the form $F_k < g_3 x_n + g_4 u$ [3].*

- *$\{G\}$ is the set of of jump destination maps. The jump destination map $G[i,k]$ is the jump destination map from stage j to stage i, its continuous part is described by the difference equation $x_i = P[i,j]x_n + Q[i,j]u$. Each jump destination map is associated with a jump set or a union of jump sets.*

2.4 EXAMPLE OF HYBRID MODEL

In this section a hybrid model is built that will describe the evolution of a discontinuously operated buck-boost converter.

I/O of Buck-Boost Converter The electrical port of a buck-boost converter is nominally connected to a DC voltage source. There is a single controllable switch and the control input vector u_{elec} contains only a single variable, there are no input dependent storage components so the input's gradient is not needed. If desired additional measurement outputs for both electrical and control quantities can be included, however these additions are not pursued here.

$$u_{elec}(t) = \begin{bmatrix} v_{dc}(t) \end{bmatrix} \quad y_{elec}(t) = \begin{bmatrix} i_{dc}(t) \end{bmatrix} \tag{2.13}$$

Stages The buck-boost converter has four possible stages, the schematics of each stage are depicted in Figure 2.7, whilst the differential equations of the three stages visited by a discontinuous operated buck boost converter are described below.

- **Stage 1**

$$\begin{aligned} \begin{bmatrix} \dot{v}_c(t) \end{bmatrix} &= \begin{bmatrix} -\frac{1}{CR} \end{bmatrix} \begin{bmatrix} v_c(t) \end{bmatrix} + \begin{bmatrix} 0 \end{bmatrix} \begin{bmatrix} v_{dc}(t) \end{bmatrix} \\ \begin{bmatrix} \dot{i}_{dc}(t) \end{bmatrix} &= \begin{bmatrix} 0 \end{bmatrix} \begin{bmatrix} v_c(t) \end{bmatrix} + \begin{bmatrix} 0 \end{bmatrix} \begin{bmatrix} v_{dc}(t) \end{bmatrix} \end{aligned}$$

[3] *The less than ($<$) form is needed for turn "on" jump sets and the ($\leq$) is needed for turn "off" jump sets as discussed in section 2.2.1. The general form requires that switch "on" inequalities need to be re-written in the less than form. This requirement is needed by the small signal model developed in the following chapter.*

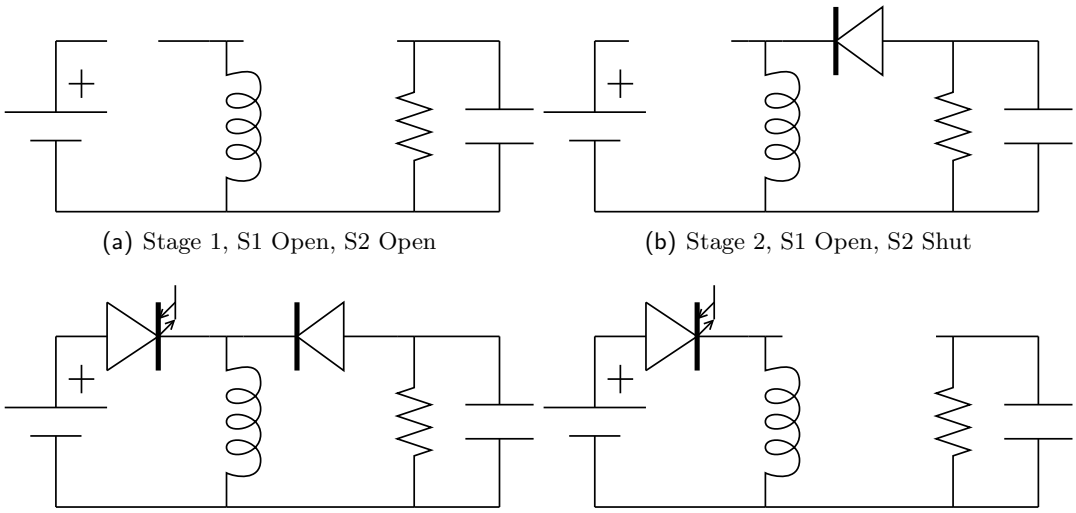

(a) Stage 1, S1 Open, S2 Open

(b) Stage 2, S1 Open, S2 Shut

(c) Stage 3, S1 shut, S2 Shut

(d) Stage 4, S1 Shut, S2 Open

Figure 2.7 Schematics of the four stages of the buck-boost converter

- **Stage 2**

$$\begin{bmatrix} \dot{i}_l(t) \\ \dot{v}_c(t) \end{bmatrix} = \begin{bmatrix} 0 & \frac{1}{L} \\ -\frac{1}{C} & -\frac{1}{CR} \end{bmatrix} \begin{bmatrix} i_l(t) \\ v_c(t) \end{bmatrix} + \begin{bmatrix} 0 \\ 0 \end{bmatrix} \begin{bmatrix} v_{dc}(t) \end{bmatrix}$$

$$\begin{bmatrix} i_{dc}(t) \end{bmatrix} = \begin{bmatrix} 0 & 0 \end{bmatrix} \begin{bmatrix} i_l(t) \\ v_c(t) \end{bmatrix} + \begin{bmatrix} 0 \end{bmatrix} \begin{bmatrix} v_{dc}(t) \end{bmatrix}$$

- **Stage 4**

$$\begin{bmatrix} \dot{i}_l(t) \\ \dot{v}_c(t) \end{bmatrix} = \begin{bmatrix} 0 & 0 \\ 0 & -\frac{1}{CR} \end{bmatrix} \begin{bmatrix} i_l(t) \\ v_c(t) \end{bmatrix} + \begin{bmatrix} \frac{1}{L} \\ 0 \end{bmatrix} \begin{bmatrix} v_{dc}(t) \end{bmatrix}$$

$$\begin{bmatrix} i_{dc}(t) \end{bmatrix} = \begin{bmatrix} 1 \\ 0 \end{bmatrix} \begin{bmatrix} i_l(t) \\ v_c(t) \end{bmatrix} + \begin{bmatrix} 0 \end{bmatrix} \begin{bmatrix} v_{dc}(t) \end{bmatrix}$$

Jump Sets and Jump destination maps In the complete hybrid model of a buck-boost converter each stage has at least two and possibly three jump sets. Defining all these jump sets and their destination maps is laborious for anything other than a simple case. During discontinuous operation of the buck-boost converter, the converter jumps from stage 4 to stage 2, from stage 2 to stage 1, and then from stage 1 back to stage 4. In Table 2.1 the three jump sets triggered and the three corresponding jump destination maps are detailed. Each jump is labelled per the scheme {Stage, Switch, Controllability}. For example S1S1A, is a jump in stage 1, caused by switch 1, and is autonomous.

Jump Label	Current Stage	Switch (and position)	Jump inequality	Type	Destination Stage	P	Q
S1S1C	1	S1 type III Open	$v_{dc}(t) - v_l(t) > 0$	C	4	$\begin{bmatrix} 0 \\ 1 \end{bmatrix}$	$\begin{bmatrix} 0 \\ 0 \end{bmatrix}$
S2S2A	2	S2 type I Closed	$i_l(t) \geq 0$	A	1	$\begin{bmatrix} 0 & 1 \end{bmatrix}$	$\begin{bmatrix} 0 \end{bmatrix}$
S4S1A	4	S1 type I Closed	$v_{dc}(t) - v_l(t) > 0$	C	2	$\begin{bmatrix} 0 & 0 \\ 0 & 1 \end{bmatrix}$	$\begin{bmatrix} 0 \\ 0 \end{bmatrix}$

Table 2.1 Jump Sets of the buck-boost converter

2.4.1 Example of Time Domain Evolution

In Figure 2.8 the hybrid model is used to form the time domain waveforms of the buck-boost converter. The details of the converter operation are outlined below.

- Starting in stage 4. Current builds in the inductor that is switched to the DC voltage source. The capacitor is discharging into the load.
- At $t = t_{\theta_2}$ an *off* control signal is sent to the type III controllable switch as the system is traversing controlled jump set S4S1C. The switch turns *off*. By jump destination map $G[4, 2]$ the system jumps to stage 2, in which the type I, diode also begins conducting.
- In stage 2 the capacitor is connected in parallel with the load resistor to the inductor. Current decreases in the inductor, whilst the voltage in the capacitor rises initially before falling. At $t = t_{\theta_3}$ the current in the inductor drops to zero and the system enters autonomous jump set S2S2A.
- By jump destination map $G[2, 1]$ the system enters stage 1 in which the type I diode is turned *off* and the capacitor is left to discharge through the load resistor.
- The system is inside the controlled jump set S1S1C and at $t = t_{\theta_4}$ an *on* control signal is sent to the type III controllable switch. The switch begins conducting and by jump destination map $G[4, 1]$ the system returns to stage 4.

2.5 DISCUSSION

Switching Cascade When the system of Figure 2.6 jumped from stage 4 to stage 2 it actually landed within an autonomous jump set of stage 1 before instantaneously jumping to stage 2. This kind of jump is an example of a cascade, where several jumps occur at the same continuous point in time. These kinds of intermediate stages are a mechanism that can be used to model complex switching cascades, such as those found in the discontinuous buck-boost converter. In the hybrid model built here no attempt was made to model this behavior as it is not necessary for the small signal models built in the following chapters.

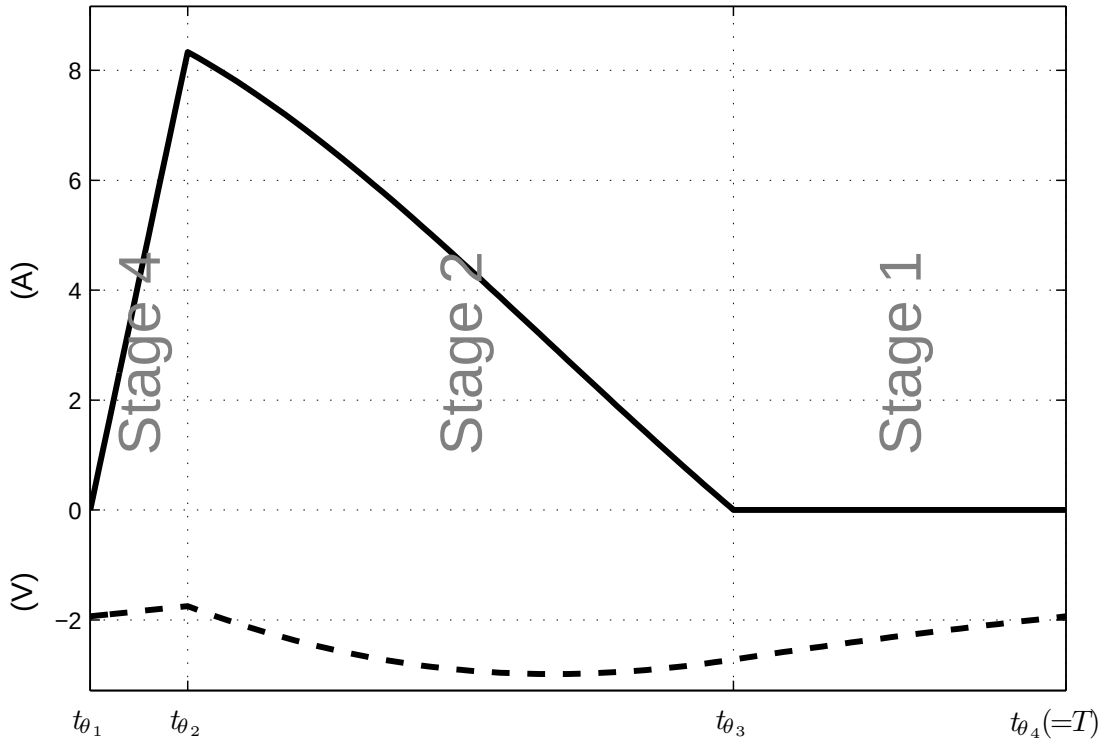

Figure 2.8 Evolution of the hybrid model of a buck boost converter. **Solid** inductor current **Dashed** capacitor voltage.

A small signal model only requires a jump destination map of the final from the initial stage, the cascade is hidden due to the small signal assumption.

Despite this lack of attention to cascades in this thesis the hybrid model presented here can be extended to include them using techniques similar to those of [22], [23] and [24]. In the reported methods state gradients are allowed to include an impulse following a jump. These impulses are then used to satisfy the jump sets of the following stages to let a cascade occur.

2.6 CONCLUSION

In this chapter a model of a power electronic system with ideal autonomous and controlled switches has been presented. The model is built upon the terminology and structure used in Hybrid System's theory and is able to model any non-contradictory arrangement of switches, sources and passive components. A hybrid model of a buck-boost converter was built and the model was used to describe the time domain evolution of the converter.

Chapter 3

SMALL SIGNAL MODEL OF A SWITCHING SYSTEM

3.1 INTRODUCTION

The general hybrid power electronic model described in the previous chapter mimics the behavior of a system of power electronic switches, passive devices, and ideal sources. However, by itself it is not easily solvable either analytically or numerically due to the non-linear problem of guaranteeing the correct location of the switching instants. Fortunately a more readily solvable model can be obtained by reducing the hybrid model to its small signal equivalent. The construction of this small signal equivalent is the topic of this chapter.

Small signal analysis is the study of deviations from an operating point for a system subjected to small disturbances. The assumption made by this method is that the disturbances are so small that the deviation of the system can be described linearly. Whilst the small signal model is strictly only accurate for infinitesimal disturbances, it can be used to predict the behavior of systems subjected to larger non-infinitesimal disturbances. Of course the larger the disturbance and the more non-linear the system the more inaccurate the result. However, the small signal model is easier to manipulate and for many applications this tradeoff between model accuracy and model form is worthwhile.

Small signal analysis has commonly appeared in power electronics and power systems [25] literature in various forms. In particular for power electronics, linearized state space averaging, linearized dynamic phasors, Newton time domain shooting methods and Newton haromonic domain methods are all based around small signal models.

The key difficulty in developing the small signal model of a power electronic system is defining the small signal evolution of the system across a switching instant. Here, the switching instant evolution is described as a difference equation and an impulse implemented as a dirac delta function. The difference equation is used to relate the states across a switching instant, and the impulse is injected into the output at the switching instant. Describing and proving the relationship between the post and pre switching instant, the magnitude of the output impulse, and the magnitude of the switching instant variation (SIV) itself are the contributions of this chapter.

3.2 SMALL SIGNAL ANALYSIS

Small signal analysis[1] examines the response of a device to small signal deviations from a known operating point. Formally, the concept of a small signal representation is derived with the help of Taylor's Theorem. Taylor's theorem states that a function's evolution can be exactly described with the use of a power series expansion of its derivatives. The formal definition of single variable Taylor's Theorem is defined below in definition 3.1.

Theorem 3.1 (Single-variable Taylor's Theorem) *Suppose we have a single variable function of the form of equation 3.1*

$$y(x) = f(x) \tag{3.1}$$

Its deviation from some base case x_0 can be described using a power series expansions of its derivatives as shown in 3.2, if and only if f has derivatives of all orders at the point x_0.

$$y(x_0 + \Delta x) = f(x_0) + f'(x_0)\Delta x + \frac{1}{2!}f''(x_0)\Delta x^2 + \cdots + \frac{1}{n!}f^n(x_0)\Delta x^n \tag{3.2}$$

Although not shown, a similar power series expansion for a multi-variable system can be written.

Small signal analysis makes use of Taylor's theorem and assumes that the function is sufficiently linear that its behavior can be approximated by its first derivative, the other terms are considered too small to have an effect. The small signal model is definied in definition Further, if the disturbance is infinitesimally small then the behavior of the function can be described exactly by the first derivative. This is shown in Theorem 3.1 for the multi-variable case.

Definition 3.1 (Small Signal Response) *If a multi-variable system of the form $y_n = f_n(x_1, x_2, ..., x_m)$ is subjected to an infinitesimally small disturbance then the effect of the disturbance can be described by equation 3.3.*

$$\begin{bmatrix} \Delta y_1 \\ \Delta y_2 \\ \vdots \\ \Delta y_n \end{bmatrix} \cong \begin{bmatrix} \frac{\partial f_1}{\partial x_1} & \frac{\partial f_1}{\partial x_2} & \cdots & \frac{\partial f_1}{\partial x_m} \\ \frac{\partial f_2}{\partial x_1} & \frac{\partial f_2}{\partial x_2} & \cdots & \frac{\partial f_2}{\partial x_m} \\ \vdots & \vdots & \ddots & \vdots \\ \frac{\partial f_n}{\partial x_1} & \frac{\partial f_n}{\partial x_2} & \cdots & \frac{\partial f_n}{\partial x_m} \end{bmatrix} \begin{bmatrix} \Delta x_1 \\ \Delta x_2 \\ \vdots \\ \Delta x_m \end{bmatrix} \tag{3.3}$$

If a function is already linear then its small signal and large signal models are identical. This is an important observation, as for systems that are composed mainly of linear parts

[1] The term small signal analysis is interchangeable with the term linearized analysis

it is only the non-linear parts that need be *linearized*. This is particularly relevant to power electronic systems that are often interfaced with completely linear systems and only occasionally act non-linearly themselves.

3.3 SMALL SIGNAL MODEL OF A POWER ELECTRONIC CONVERTER

The small signal hybrid model of the power electronic converter incorporates the large signal continuous dynamics of the hybrid system. In contrast the discrete dynamics are linearized. One consequence of linearization is that the switching instants and the stage order are assumed to be solved *a-priori* and form part of the operating point. The effect of SIVs, as will be shown and proved, is included at the unmodified switching instant by injecting (or removing) energy into the state using a difference equation and adding an impulse to the output.

Simplification of the system to the linearized equivalent is not without its cost. Fixing the stage order and fixing the switching instants degrades the ability of the small signal model to model the exact behavior of the system. However, it is a potentially useful trade off as although accuracy is lost, great gains are made in producing a model whose form is amenable to analysis, gains that are exploited by later chapters.

3.4 BASE OPERATING POINT

The base operating point around which the small signal model is built is the response of the large signal model over some time interval $\alpha < t < \beta$. Normally the system is assumed to be operating periodically over this interval, however, this is not a necessary requirement, and in general any response can be considered.

To construct the small signal model of the hybrid power electronic model the information needed is the stage order, the switching instants, the base case inputs at the switching instants, the base case initial state, and the base case states at the end of each stage. It is not necessary to define the states at the start of each stage as these states can be exactly determined using the transition maps. The inverse, i.e trying to determine the pre-jump state from the post-jump state, is not always possible as the projection matrices are not necessarily invertible. These variables along with the DEs of each relevant stage, and the jump destination maps between them form the minimum information set needed to form a small signal model. This information is summarized in Table 3.1

3.5 SMALL SIGNAL MODEL DURING A STAGE

The small signal model during a stage is trivial to form as the continuous dynamics of the hybrid system are completely linear, so they also govern the behavior of the small signal

Stage Order	$[1, 2, 3, ...n....N]$	
Switching Instants	$\{t_{\theta_n}\}$	$\forall\, n \in 1, 2, ..N+1$
Inputs at SI	$\{u_{elec}(t_{\theta_n})\}$	$\forall\, n \in 1, 2, ..N$
States at end of stage	$\left\{x_n\left(t^-_{\theta_{n+1}}\right)\right\}$	$\forall\, n \in 1, 2, ..N$
Initial state of the first stage	$x_1(t_{\theta_1})$	
Stage DE	$\{A_n, B_n, C_n, D_n\}$	$\forall\, n \in 1, 2, ..N$
Jump Destination maps	$\{G[n]\}$	$\forall\, n \in 2, ..N$
Jump Sets	$\{V[n], F[n]\}$	$\forall\, n \in 2, ..N$

Table 3.1 The base case operating point and other information needed to form the small signal model. Note that the switching point $t_{\theta_{N+1}}$ is the end of the last stage, if the base case is T periodic then $t_{\theta_{N+1}} = T$. The only jump destination maps and sets that are needed are those that describe how the system evolves across the base case stage order, a notational change for the Jump destination maps is included where $\{G[n]\}$ is associated with the n^{th} switching instant.

model. Formally the small signal model of the n^{th} stage at time t is that given by equation 3.4.

$$\begin{aligned}\begin{bmatrix}\Delta\dot{x}(t)\\ \Delta y(t)\end{bmatrix} &= \begin{bmatrix}\frac{\partial\dot{x}(t)}{\partial x(t)} & \frac{\partial\dot{x}(t)}{\partial u_{elec}(t)}\\ \frac{\partial y(t)}{\partial x(t)} & \frac{\partial y(t)}{\partial u_{elec}(t)}\end{bmatrix}\begin{bmatrix}\Delta x(t)\\ \Delta u_{elec}(t)\end{bmatrix} \quad \forall t^+_{\theta_n} < t \leq t_{\theta_{n+1}}\\ &= \begin{bmatrix}A_n & B_n\\ C_n & D_n\end{bmatrix}\begin{bmatrix}\Delta x(t)\\ \Delta u_{elec}(t)\end{bmatrix}\end{aligned} \tag{3.4}$$

Alternatively the integral form of this equation is

$$\Delta x(t - t_{\theta_n}) = e^{A_i(t-t_{\theta_n})}x(t^+_{\theta_n}) + \int_{t^+_{\theta_n}}^{t} e^{A_i\tau}Bu_{elec}(\tau)d\tau \tag{3.5}$$

The interval which each stage governs the continuous dynamics have been written so that the stage proceeding a switching instant governs the continuous dynamics at the switching instant. This is necessary to specify if an impulse in the input is present at the switching instant. For a small signal model this is highly likely if its inputs are the outputs of other small signal devices.

3.6 SMALL SIGNAL MODEL AT A SWITCHING INSTANT

If there is no SIV across a stage then the small signal model that describes the state after a switching instant is simply the difference equation of the base case jump destination map. Here the projection and injection matrices are written so that they are associated with the switching instant, rather than with the stages that are jumped between as was done in the hybrid model.

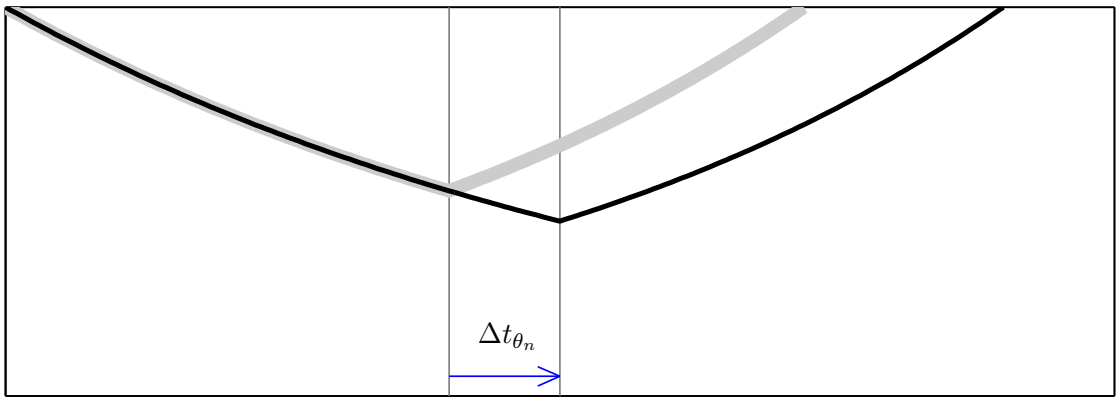

Figure 3.1 Large signal effect of SIV. **thick** base case trajectory **thin** large signal trajectory when the switching instant is delayed

$$\Delta x_n(t_{\theta_n}^+) = P[n]\Delta x_{n-1}(t_{\theta_n}^-) + Q[n]\Delta u_{elec}(t_{\theta_n})$$

If a SIV occurs, and assuming the stage order is unaffected, the point where the new stage is active is delayed or advanced. For a large signal model the effect is that of Figure 3.1. In this figure two trajectories of a two stage system are shown. The first trajectory called the base case is shown as a thick grey line. This trajectory is compared with a second trajectory in which the switching instant between the two stages is delayed. This second trajectory was found using a large signal model.

A delay in the instant where one set of dynamics takes over from the next is a non-linear effect. For the small signal model, the entire effect of the SIV is applied at the original switching instant as a step change in the state and an impulse in the output. Each of these effects are studied in turn.

3.6.1 Small signal effect of switching instant variation on the state

An example of the small signal step change in state caused by a variation in switching instant is depicted in Figure 3.2. The size of the step change is found in two steps.

- The base-case of the pre-switching stage is extrapolated to the new SI using the *pre*-switching gradient $\frac{dx_{n-1}(t_{\theta_n}^-)}{dt}$.
- This value is then extrapolated back to the old SI using the *post* switching gradient $\frac{dx_n(t_{\theta_n}^+)}{dt}$.

The size of the step change is then equal to $\left(\frac{dx_{n-1}(t_{\theta_n}^-)}{dt} - \frac{dx_n(t_{\theta_n}^+)}{dt}\right)\Delta t_{\theta_n}$

The error between the small signal trajectory of Figure 3.2 and the large signal trajectory of Figure 3.1 is greatest during the switching instant variation Δt_{θ_n}.

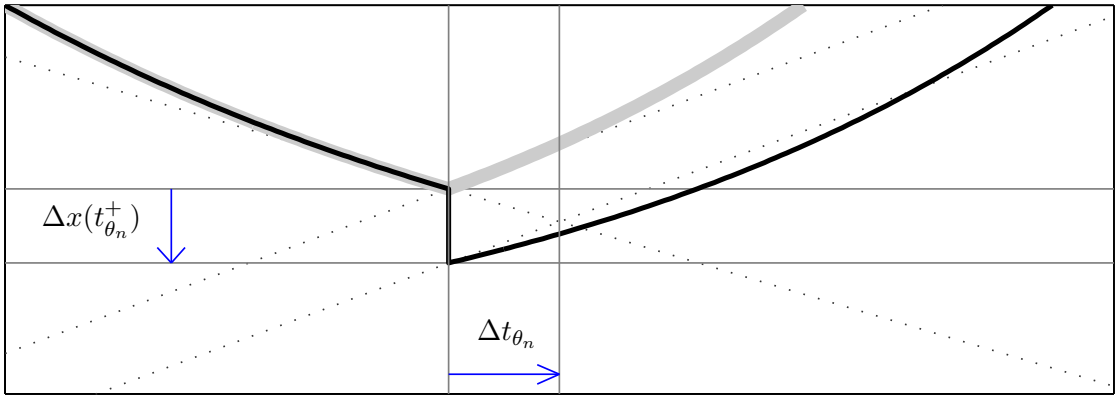

Figure 3.2 Small signal effect of SIV. The deviation in the state in the post switching state is given for a switching advance of Δt_{θ_n}. The base-case is given as the **thick grey** line, whilst the small signal case is given as the **thin/black** line. The construction lines for determining the switching instant variation are given as dotted lines. These construction lines are the gradient of the base case.

Formally the small signal effect on the state is described using the difference equation, equation 3.6.

Theorem 3.2 (Small Signal effect of a SIV on the state) *If a system switches from stage $n-1$ to stage n at the point t_{θ_n}, then the effect of an infinitesimal increase in the switching instant Δt_{θ_n} on the state tends to that of difference equation 3.6.*

$$\begin{aligned}\Delta x_n(t_\theta^+) &= \frac{dx_n(t_{\theta_n})}{dt_{\theta_n}}\Delta t_{\theta_n} \\ &= \left(-\frac{dx_n(t_{\theta_n}^+)}{dt} + P[n]\frac{dx_{n-1}(t_{\theta_n}^-)}{dt} + Q[n]\frac{du_{elec}(t_{\theta_n})}{dt}\right)\Delta t_{\theta_n} \qquad (3.6)\end{aligned}$$

Proof The proof for the small signal effect can be found by examining the large signal forced evolution across a switching instant from within the pre switching stage $(n-1)$, to the post switching stage (n), assuming a known stage order ($[n-1 \to n]$), and a known switching instant t_{θ_n}. The state at the beginning of the evolution is given by $x_{n-1}(t_0)$, which is evolved, along with the forced component, up to the switching instant. The value of the state, before switching, is given by equation 3.7. In equation 3.7 the term, $\Phi(t_2, t_1)$ is the state transition matrix from the point t_1 to the point t_2. If both points are within the same stage then $\Phi(t_2, t_1) = e^{A_n(t_2-t_1)}$. For a large signal model the state transition matrix across a switching instant is the projection matrix, i.e. $\Phi(t_n^+, t_n^-) = P[n]$

$$x_{n-1}\left(t_{\theta_n}^-\right) = \Phi(t_{\theta_n}, t_0)x_{n-1}(t_0) + \int_{t_0}^{t_{\theta_n}} \Phi(t_{\theta_n}, \tau)B_{n-1}u_{elec}(\tau)d\tau \qquad (3.7)$$

The value just before switching, $x_{n-1}\left(t_{\theta_n}^-\right)$, is transformed at the switching instant to the

new stage using the n^{th} jump destination map.

$$x_n\left(t_{\theta_n}^+\right) = P[n]x_{n-1}\left(t_{\theta_n}^-\right) + Q[n]u_{elec}\left(t_{\theta_n}\right) \tag{3.8}$$

This state is then evolved to point t using the state transition matrix of the new stage. The forced contribution that occurs within this new stage is also included.

$$x_n(t) = \Phi(t, t_{\theta_n}^+)x_n\left(t_{\theta_n}^+\right) + \int_{t_{\theta_n}^+}^{t} \Phi(t, t_{\theta_n}^+)B_n u_{elec}(\tau)d\tau \tag{3.9}$$

The total evolution between t_0 and t can be described by firstly evaluating 3.7 into 3.8 and then evaluating into 3.9, the result is equation 3.10.

$$x_n(t) = \Phi(t, t_{\theta_n}^+)\left\{P[n]\left\{\Phi(t_{\theta_n}, t_0)x_{n-1}(t_0) + \int_{t_0}^{t_{\theta_n}} \Phi(t_{\theta_n}, \tau)B_{n-1}u_{elec}(\tau)d\tau\right\} + Q[n]u_{elec}(t_{\theta_n})\right\} + \int_{t_{\theta_n}^+}^{t} \Phi(t, \tau)B_n u_{elec}(\tau)d\tau \tag{3.10}$$

The small signal effect of a switching instant change can be found by differentiating equation 3.10 with respect to t_{θ_n} to find the derivative $\frac{dx_n(t)}{dt_{\theta_n}}$ as shown in equation 3.11.

$$\frac{dx_n(t)}{dt_{\theta_n}} = \frac{d\Phi(t, t_{\theta_n}^+)}{dt_{\theta_n}}x_n(t_{\theta_n}^+) + \Phi(t, t_{\theta_n}^+)\left\{P[n]\left\{\frac{d\Phi(t_{\theta_n}, t_0)}{dt_{\theta_n}}x_{n-1}(t_0) + \frac{d\int_{t_0}^{t_{\theta_n}} \Phi(t_{\theta_n}, \tau)B_{n-1}u_{elec}(\tau)d\tau}{dt_{\theta_n}}\right\} + Q[n]\frac{du_{elec}(t_{\theta_n})}{dt_{\theta_n}}\right\} + \frac{d\int_{t_{\theta_n}^+}^{t} \Phi(t, t_{\theta_n}^+)B_n u_{elec}(\tau)d\tau}{dt_{\theta_n}} \tag{3.11}$$

Then by using the following identities

$$\frac{d\Phi(t,t_{\theta_n}^+)}{dt_{\theta_n}} = -\Phi(t,t_{\theta_n}^+)A_n \tag{3.12}$$

$$\begin{aligned}\frac{d\int_{t_0}^{t_{\theta_n}}\Phi(t_{\theta_n},\tau)B_{n-1}u_{elec}(\tau)d\tau}{dt_{\theta_n}} &= \frac{d\Phi(t_{\theta_n},t_0)\int_{t_0}^{t_{\theta_n}}\Phi(t_0,\tau)B_{n-1}u_{elec}(\tau)d\tau}{dt_{\theta_n}} \\ &= A_{n-1}\Big(x_{n-1}(t_{\theta_n})-\Phi(t_{\theta_n},t_0)x_{n-1}(t_0)\Big) \\ &\quad +B_{n-1}u_{elec}(t_{\theta_n})\end{aligned} \tag{3.13}$$

$$\frac{d\int_{t_{\theta_n}^+}^{t}\Phi(t,t_{\theta_n}^+)B_nu_{elec}(\tau)d\tau}{dt_{\theta_n}} = -\Phi(t,t_{\theta_n}^+)B_nu_{elec}(t_{\theta_n}^+) \tag{3.14}$$

equation 3.11 can be reduced to

$$\begin{aligned}\frac{dx_n(t)}{dt_{\theta_n}} = &-\Phi(t,t_{\theta_n}^+)A_nx_n(t_{\theta_n}^+)+\Phi(t,t_{\theta_n}^+)\Bigg\{P[n]\Big\{A_{n-1}\Phi(t_{\theta_n},t_0)x_{n-1}(t_0) \\ &+A_{n-1}\Big(x_{n-1}(t_{\theta_n})-\Phi(t_{\theta_n},t_0)x_{n-1}(t_0)\Big) \\ &+B_{n-1}u_{elec}(t_{\theta_n})\Big\}+Q[n]\frac{du_{elec}(t_{\theta_n})}{dt}\Bigg\}-\Phi(t,t_{\theta_n}^+)B_nu_{elec}(t_{\theta_n}^+)\end{aligned}$$

which can be further reduced by collecting terms to 3.15.

$$\begin{aligned}\frac{dx_n(t)}{dt_{\theta_n}} &= -\Phi(t,t_{\theta_n}^+)A_nx_n(t_{\theta_n}^+)-\Phi(t,t_{\theta_n}^+)\Bigg\{P[n]\Big\{A_{n-1}x_{n-1}(t_{\theta_n})+B_{n-1}u_{elec}(t_{\theta_n})\Big\} \\ &\quad + \quad Q[n]\frac{du_{elec}(t_{\theta_n})}{dt}\Bigg\}+\Phi(t,t_{\theta_n}^+)B_nu_{elec}(t_{\theta_n}^+) \\ &= \Phi(t,t_{\theta_n}^+)\Bigg\{-\frac{dx_n(t_{\theta_n}^+)}{dt}+P[n]\frac{dx_{n-1}(t_{\theta_n})}{dt}+Q[n]\frac{du_{elec}(t_{\theta_n})}{dt}\Bigg\}\end{aligned} \tag{3.15}$$

When the limit $t \to t_{\theta_n}^+$ is approached then the state transition matrix $\Phi(t,t_{\theta_n}^+)$ becomes an identity matrix, and equation 3.15 reduces to equation 3.6. ∎

Remark A SIV only has an effect on those states whose gradient is discontinuous across the switching instant.

Remark The effect of SIV can be added to the base case jump destination map to form a

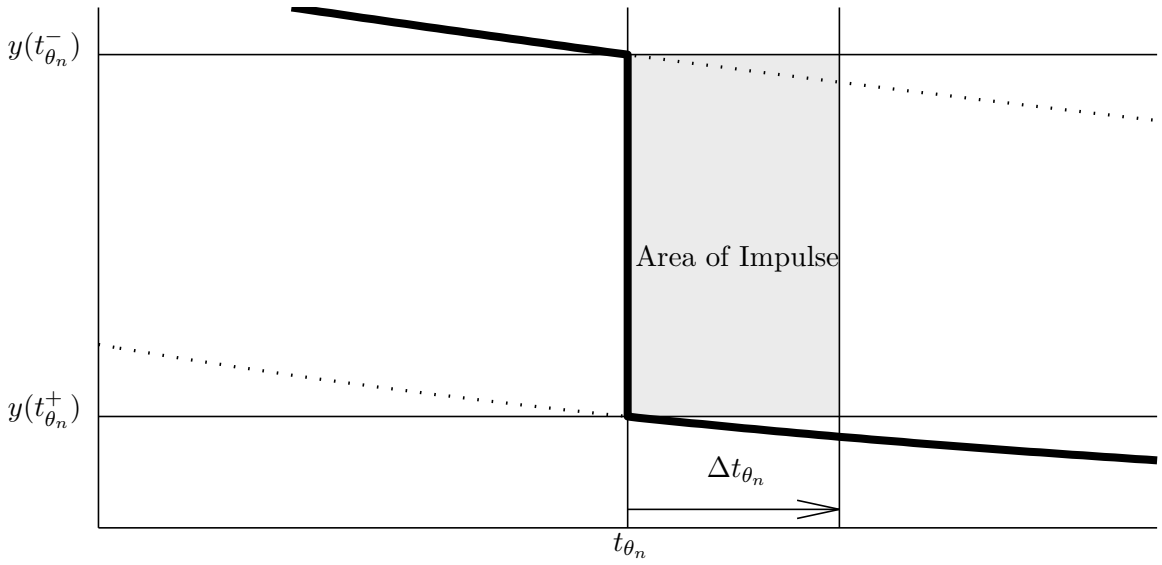

Figure 3.3 Area of impulse injected to an output for the small signal effect of a switching instant variation of t_{θ_n}. The base-case is given as the **thick black** line.

small signal destination map as written in equation 3.16, which shows that the small signal change in the post switching instant state $\Delta x_n(t_{\theta_n^+})$ is a function of the small signal change in the pre switching state $\Delta x_{n-1}(t^-_{\theta_n})$, and the small signal change in the the electrical input at the switching instant $\Delta u_{elec}(t_{\theta_n})$, and any SIV Δt_{θ_n}.

$$\Delta x_n(t^+_{\theta_n}) = P\Delta x_{n-1}(t^-_{\theta_n}) + Q[n]\Delta u_{elec}(t_{\theta_n}) + \left(-\frac{dx_n(t^+_{\theta_n})}{dt} + P[n]\frac{dx_{n-1}(t^-_{\theta_n})}{dt} + Q[n]\frac{du_{elec}(t_{\theta_n})}{dt}\right)\Delta t_{\theta_n} \quad (3.16)$$

3.6.2 Small signal effect of switching instant variation on the output

Switching instant variations only affect the base case output if the output is discontinuous at the switching instant. The effect is a modulated impulse centered at the base case switching instant. If the output is continuous across the switching instant there is no effect of SIV on the output. In the case when the output is discontinuous the area of the impulse is the difference between the post and pre-switching outputs of the base case multiplied by the size of the variation, as shown in Figure 3.3.

Theorem 3.3 (Small Signal effect of a SIV on the output) *If a system switches from stage $n-1$ to stage n at the point t_{θ_n}, then the effect of an infinitesimal increase in the switching instant, Δt_{θ_n} on the output tends to that of the impulse of equation 3.17.*

$$\begin{aligned}\Delta y(t_{\theta_n}) &= \frac{dy_n(t_{\theta_n})}{dt_{\theta_n}}\Delta t_{\theta_n} \\ &= \left\{ y(t_{\theta_n}^-) - y(t_{\theta_n}^+) \right\} \delta\left(t - t_{\theta_n}\right) \Delta t_{\theta_n}\end{aligned} \tag{3.17}$$

Proof Equation 3.18 describes the evolution of the output from t_0 within stage $n-1$ to t within stage n. The jump between the stages occurs at t_{θ_n}. The use of Heaviside functions [26], (where $u(t-t_{\theta_n})$ in this formula is a Heaviside function that steps at t_{θ_n}), controls which stage dictates the output. The terms multiplied by the $u(t-t_{\theta_n})$ Heaviside function are the contribution from the $n-1^{th}$ stage, whilst the terms multiplied by $(1-u(t-t_{\theta_n}))$ are the contributions from the n^{th} stage.

$$\begin{aligned}y(t) = C_n x_n(t) u(t-t_{\theta_n}) + C_{n-1} x_{n-1}(t)\Big(1-u(t-t_{\theta_n})\Big) \\ + \left(D_n u(t-t_{\theta_n}) + D_{n-1}\Big(1-u(t-t_{\theta_n})\Big)\right) u_{elec}(t)\end{aligned} \tag{3.18}$$

The derivative $\frac{dy_n(t)}{dt_{\theta_n}}$ can be found by differentiating $y(t)$ with t_{θ_n}. Note that $\frac{du(t-t_{\theta_n})}{dt_{\theta_n}} = -\delta(t-t_\theta)$.

$$\begin{aligned}\frac{dy_n(t)}{dt_{\theta_n}} &= \left(C_{n-1}x_{n-1}(t_{\theta_n}^-) - C_n x_n(t_{\theta_n}^+) + \big(D_{n-1}-D_n\big)u_{elec}(t_{\theta_n})\right)\delta\left(t-t_{\theta_n}\right) \\ &= \left\{ y(t_{\theta_n}^-) - y(t_{\theta_n}^+) \right\} \delta\left(t - t_{\theta_n}\right)\end{aligned}$$

This derivative is zero valued everywhere except at the switching instant t_θ where it is an impulse. ∎

In Wood[27], Hume [5], and Laird [28] this same result is found using Schwartz's analysis of the pulse duration modulator [29].

3.6.3 Magnitude of the switching instant variations

There are two types of SIVs, those originating from a controller, and those that are autonomously determined by variables within the electric circuit.

Controlled Switching Instant Variation The control switching instant variations are determined by the vector $\Delta u_{ctrl}(t)$. This vector has a different form to its hybrid system large signal equivalent $u_{ctrl}(t)$. Instead of being a set of discrete control orders, one for every controllable switch, the small signal version contains one element for every controlled switching instant of the base base. For example the buck-boost converter operating in discontinuous stage for one cycle as illustrated in the previous chapter in Figure 2.8, will have small signal control signal with two elements one for the turn on firing signal at t_{θ_1} and one for the turn off signal at t_{θ_2}, i.e.

$$\Delta u_{ctrl}(t) = \begin{bmatrix} \Delta t_{\theta_1}(t) \\ \Delta t_{\theta_2}(t) \end{bmatrix} \tag{3.19}$$

Each element of the small signal control vector is the small signal delay (or advance if negative) of the control switching instant. Potentially these elements are time varying due to the controller dynamics, but it is the value at the base case switching instant that determines the size of the delay (or advance). If a controller is included then it is likely that it would need to be linearized to produce the small signal control vector. It is suspect that in most cases a technique similar to finding the autonomous switching instant variation of the power electronic converter would be employed.

Autonomous Switching Instant Variation Autonomous switching instant variations are the result of some disturbance in the system space, $x_{n-1}(t)$, or the electrical input, $u_{elec}(t)$, at the base case switching instant. Their linearization is detailed below.

Recall that a jump set in the hybrid power electronic model is a function of the input $u_{elec}(t)$, and the state, which for a small signal model will be that of the stage before the switching instant, $x_{n-1}(t)$. As the stage order is fixed, the jump set that was satisfied in the base case is the same jump inequality to be satisfied in the small signal model. The general form of such an autonomous jump set inequality is,

$$\begin{aligned} V_n(t) &\leq g1_n x_{n-1}(t) + g2_n u_{elec}(t) \quad or \\ &< g1_n x_{n-1}(t) + g2_n u_{elec}(t) \end{aligned}$$

The small signal variation is expressed in equation 3.20, and given the term $\Delta V_n(t)$.

$$\Delta V_n(t) = g1_n \Delta x_{n-1}(t) + g2_n \Delta u_{elec}(t) \tag{3.20}$$

An autonomous jump occurs the moment the system enters the set. If a system is disturbed then the location of the jump is delayed or advanced. The linearized prediction of this

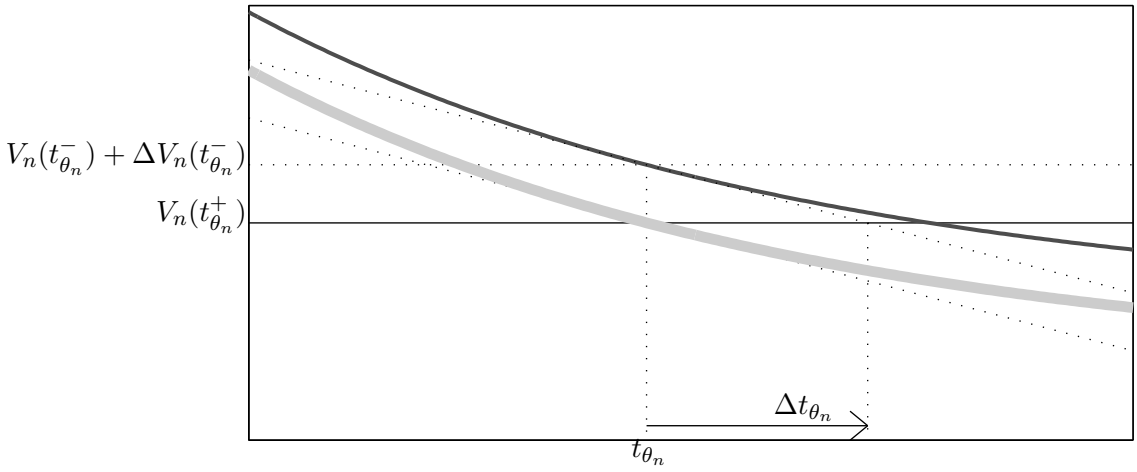

Figure 3.4 The linearized prediction, Δt_n, of an autonomous switching instant variation resulting from a $\Delta V_n(t_{\theta_n})$ increase in the right hand side of the jump set inequality. **Solid/Grey** Base Case **Black** Large signal Jump inequality right hand side distortion. **Thin/Dotted** Construction lines used to find the linearized SIV.

variation is depicted in Figure 3.4, where the gradient of the base case trajectory, and the small signal variation in the right hand side of the autonomous jump set inequality are used to determine the size of the SIV. Formally the linearized prediction of SIV is given by Theorem 3.4.

Theorem 3.4 (Small signal variation of an Autonomous Switching instant) *If a system autonomously switches from stage $n-1$ to stage n at the point t_{θ_n}, then the effect of infinitesimal deviations in the state $\Delta x_{n-1}(t)$ and/or input $\Delta u_{elec}(t)$ on the switching instant tends to that of 3.21, if and only if the base case of the jump set inequality $V_n(t)$ is continuous at the base case switching instant.*

$$\Delta t_{\theta_n} = -\frac{1}{\frac{dV_n(t^-_{\theta_n})}{dt}} \left\{ g1_n \Delta x_{n-1}(t^-_{\theta_n}) + g2_n \Delta u_{elec}(t_{\theta_n}) \right\} \tag{3.21}$$

Remark If the base case $V_n(t)$ is discontinuous at the switching instant, then small signal changes in the right hand side of the jump set inequality have no linear effect on the location of the switching instant.

Remark In cases where a controlled jump set is *primed* to jump as soon as the jump set is entered then it is treated in the same manner as an autonomous jump set.

3.7 COMPLETE SMALL SIGNAL MODEL OF AN IDEAL POWER ELECTRONIC SYSTEM

The complete small signal response is the enumeration of a base case operating point, a set of differential equations describing the small signal response during the stages, a set of difference equations that describe how the state jumps between stages, a set of dependent impulses that describes the output at the switching instants, and finally a set of difference equations that describe the size of autonomous SIVs. Formally the small signal response is defined below in Definition 3.2.

Definition 3.2 (Small Signal Response) *The small signal response of a power electronic system is described by the following five equations. The first two describe the output and state during the n^{th} stage's evolution. The third and the fourth describe the output and state at the n^{th} switching instant . The final equation determines the magnitude of SIV if the n^{th} switching instant is autonomous.*

$$\begin{aligned}
\Delta\dot{x_n}(t) &= A_n\Delta x_n(t) + B_n\Delta u_{elec}(t) \\
\Delta y(t) &= C_n\Delta x_n(t) + D_n\Delta u_{elec}(t) \\
\Delta x_n(t_{\theta_n}^+) &= \left(-\frac{dx_n(t_{\theta_n}^+)}{dt} + P[n]\frac{dx_{n-1}(t_{\theta_n}^-)}{dt} + Q[n]\frac{du_{elec}(t_{\theta_n})}{dt}\right)\Delta t_{\theta_n} \\
\Delta y(t_{\theta_n}) &= \left\{y(t_{\theta_n}^-) - y(t_{\theta_n}^+)\right\}\delta\left(t - t_{\theta_n}\right)\Delta t_{\theta_n} \\
\Delta t_{\theta_n} &= -\frac{1}{\frac{dV_n(t_{\theta_n})}{dt}}\left\{g1_n\Delta x_{n-1}(t_{\theta_n}) + g2_n\Delta u_{elec}(t_{\theta_n})\right\}
\end{aligned}$$

3.8 S-DOMAIN

No restriction on the input waveforms have so far been applied and they have been assumed to be of any form, including discontinuous signals, and they have been assumed easily integrated. Unfortunately the solvability of some integrals is not certain or at best extremely difficult. To remove this uncertainty the input signals are restricted to a set of signals that have known integrals, collectively this set is called the s-domain and is the set of complex exponentials of the form shown in equation 3.22.

$$u(t) = u_0 e^{st} \quad \forall\, u \in \Re^{n\times 1} \quad \text{and} \quad \forall\, s \in C \tag{3.22}$$

The vector u_0 is a real vector of length $n \times 1$ and s is any complex number.

At first glance this may seem a restrictive set of signals, however, thanks to the Fourier Transform all signals which are physically realizable [30] can be expressed as a set of

complex time dependent (s-domain) exponentials. Restricting inputs to this set is common in modern LTI control theory [31] [32], and besides being readily integratable their use also facilitates advanced system and control analysis. The evolutions of LTI systems disturbed by s-domain signals is described in Table 3.2.

LTI System Description	symbol	formula
Steady State	$x_{ss}(t)$	$T_{ns}(sI-\lambda_{ns})^{-1}T_{ns}^{+}Bu_0e^{st}$
Transient response	$x_{tr}(t)$	$e^{At}x(t_0)-T_{ns}e^{\lambda_{ns}t}(sI-\lambda_{ns})^{-1}T_{ns}^{+}Bu(t_0)$
Resonant response	$x_{rr}(t)$	$T_stT_s^{+}Be^{\lambda_st}u_0$
Output response	$y(t)$	$C\left(x_{ss}(t)+x_{tr}(t)+x_{rr}(t)\right)+Du_0e^{st}$

Table 3.2 The LTI systems responses when the input is restricted to signals from the s-domain, including where s is an Eigenvalue of the dynamics matrix A

.

The equations of this table are different to those found in most references [31] [32]as they include the response that occurs when s is an Eigenvalue of A. This response is called here the resonant response. Including resonance is performed by partitioning the system in two; the first part is associated with Eigenvalues equal to s, λ_s, and the second part is associated with the other Eigenvalues λ_{ns}. These parts are called the singular and non-singular parts respectively, and their segregation is performed by the non-square transforms T_s, T_{ns}, and their pseudo-inverses T_s^{+}, T_{ns}^{+}. Those transformations and the proof for the correct evolution of a resonating LTI system are given in Appendix A. An example of when the resonant response occurs is during the charging stage of the buck-boost converter where the inductor is excited by the DC voltage source.

For a PWL system, each stage has its own steady state, transient and resonant responses. To explicitly identify that a response is for a particular stage they are called within this thesis a stage's *partial steady state* (PSS), *partial transient* (PT), and *partial resonance* (PR)[2]. As they are of central importance to the analysis of the following chapters their formal definitions are included below in definitions 3.3, 3.4, and 3.5.

Definition 3.3 (Partial Steady State (PSS)) *Each stage in an N stage system when excited by an input of the form $u_{elec}(t)=u_0e^{st}$ will have a resonant response which contains the partial steady state as given by equation 3.23.*

$$x_{PSS_n}(t)=T_{ns_n}(sI-\lambda_{ns_n})^{-1}T_{ns_n}^{+}B_nu_{elec_0}e^{s(t-t_{\theta_n})} \tag{3.23}$$

Definition 3.4 (Partial Transient (PT)) *Each stage in an N stage system has a response related to the relaxation of the stage's states. This relaxation is called the partial transient, and for the n^{th} stage, starting at t_{θ_n} the PT is given by equation 3.24.*

$$x_{PT_n}(t)=e^{A_n(t-t_{\theta_n})}x_n(t_{\theta_n}^{+})-T_{ns_n}e^{\lambda_{ns_n}t}(sI-\lambda_{ns_n})^{-1}T_{ns_n}^{+}B_nu_{elec}(t_{\theta_n^{+}}) \tag{3.24}$$

[2]The PSS and PT are terms that have been previously used by [15] [5]

Variable	Value
Stage order	$\{4, 2, 1\}$
C	$50\mu F$
R	1Ω
L	$9\mu H$
f_s	$20000Hz$
Duty Cycle	10%
t_{θ_1}	0
t_{θ_2}	5.00×10^{-6}
t_{θ_3}	3.30×10^{-5}
t_{θ_4}	5.00×10^{-5}
v_{dc}	15V
$x_1(t_{\theta_1}^-) = x_1(T^-)$	$-1.9346V$
$x_4(t_{\theta_2}^-)$	$[8.3333A - 1.7505V]$
$x_2(t_{\theta_3}^-)$	$[0.0000A - 2.7191V]$

Table 3.3 Buck-Boost operating point

Definition 3.5 (Partial Resonance (PR)) *When each stage in a N stage system is subjected to a s-domain signal whose s component is equal to an Eigenvalue of the stages dynamics matrix, A_n, then the system will have a partial resonance that evolves according to equation 3.25.*

$$x_{PR}(t) = T_{s_n}(t - t_{\theta_n})T_{s_n}^{+}B_n e^{s(t-t_{\theta_n})}u_0 \tag{3.25}$$

3.9 BUCK-BOOST CONVERTER EXAMPLE

The linearization of a converter is demonstrated using the discontinuous buck-boost converter to solve an initial value problem of a converter deviated from its operating point. The base case is described in Table 3.3. In this case the base case is T-periodic so the length of the base case can easily be extended by the appending additional cycles.

The converter is subjected to the electrical source disturbance of 1V, 0Hz, and a control disturbance of 1% increase in duty cycle or $\Delta t_{\theta_2} = 5 \times 10^{-7}$. The small signal deviation from the operating point is shown in Figures 3.5, and 3.6 respectively. For comparison with the large signal effect each figure also shows the effect of the disturbances as modelled by PSCAD.

The inductor current does not exist as a state during stage 1 which exists between t_{θ_3} and t_{θ_4}. In Figures 3.5 and 3.6 the inductor current during this interval is shown as zero valued. Strictly speaking the inductor current should not exist during the interval, and the current waveform should be discontinuous.

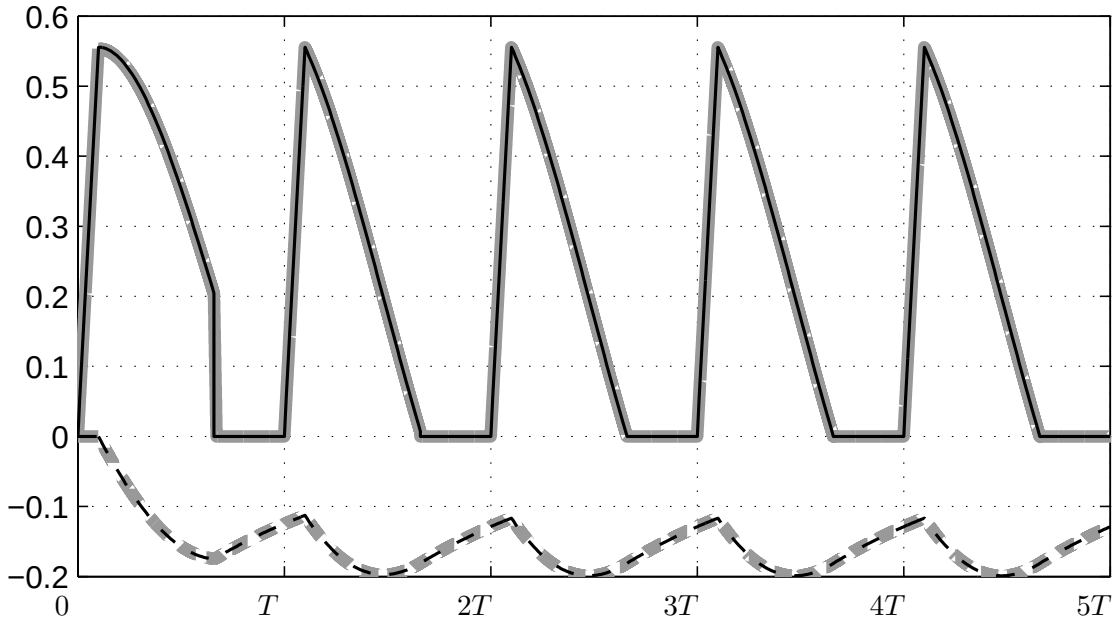

(a) Inductor Current **solid** and Capacitor Voltage **dashed**

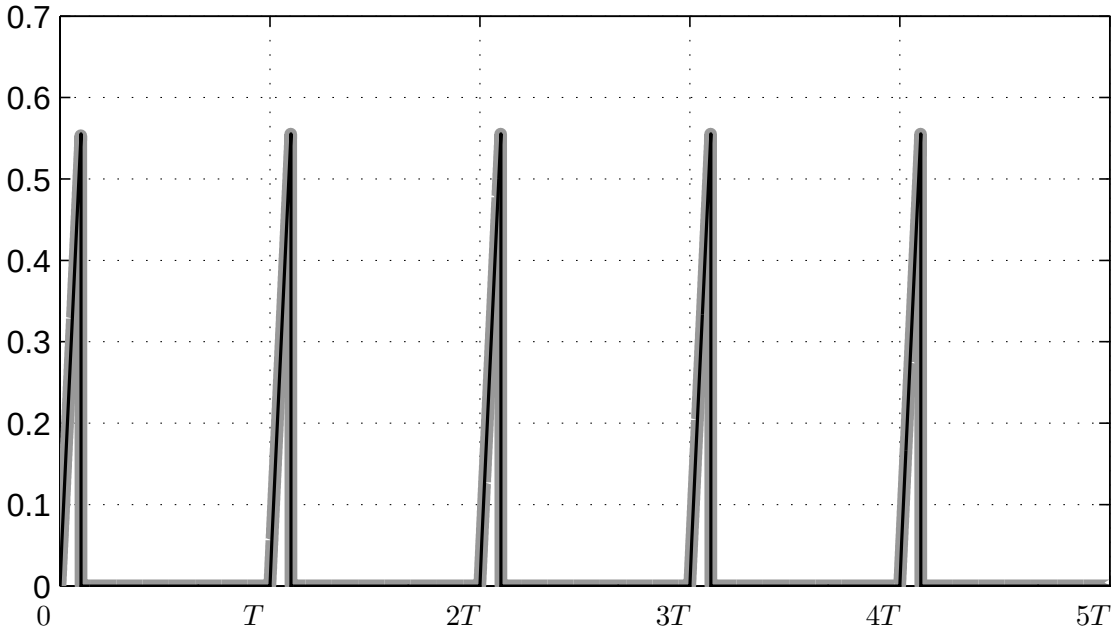

(b) DC source current

Figure 3.5 1 Volt step change change in DC source voltage **thick** Large signal (PSCAD), **thin** small signal response.

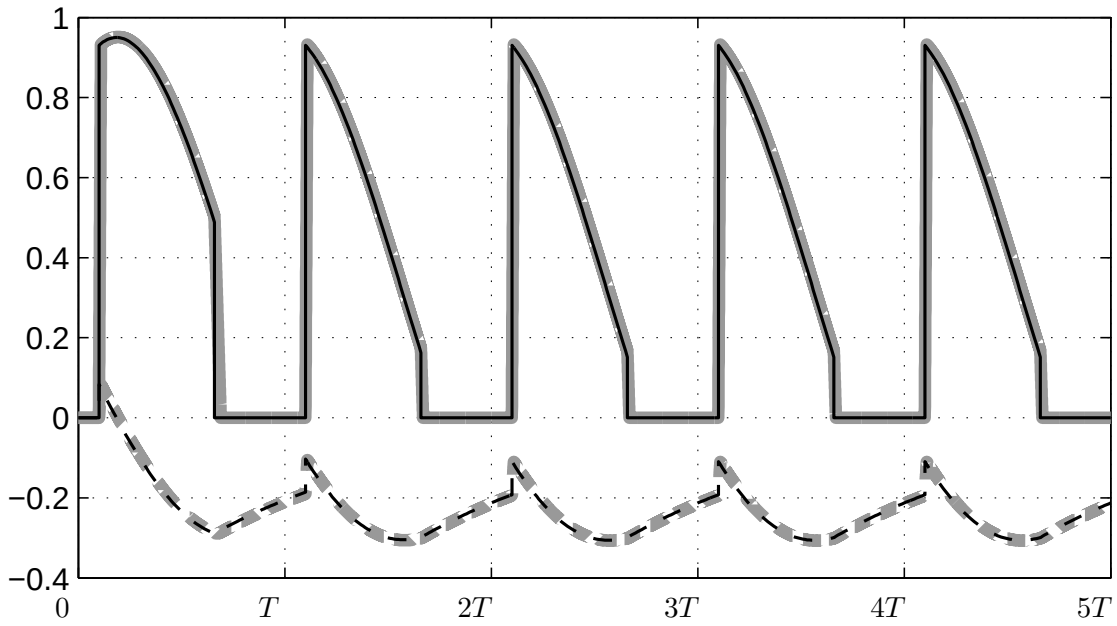

(a) Inductor Current **solid** and Capacitor Voltage **dashed**

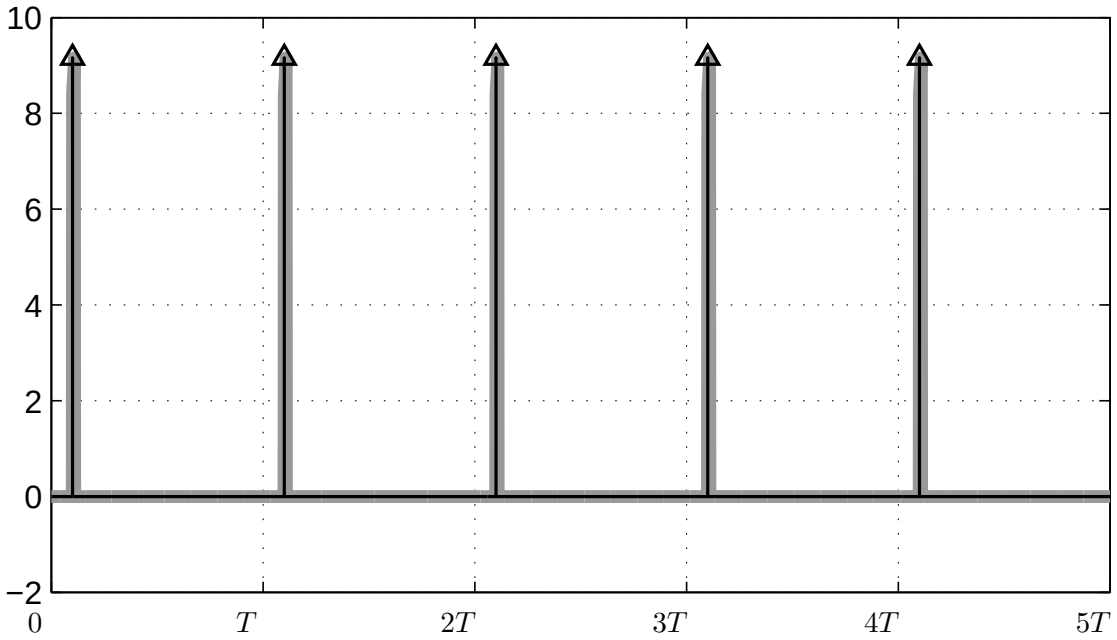

(b) DC source current

Figure 3.6 1% duty cycle increase **thick** Large signal (PSCAD), **thin** small signal response NOTE: The impulses of the small signal model have been artificially scaled to be the same height as the PSCAD *pseudo-impulses*, however, both the PSCAD and small signal impulses have the same time area

3.10 DISCUSSION

The comparison between the small signal and the PSCAD simulations are remarkably similar, and the buck-boost can be deemed highly linear. This conforms to similar observations made by Hume [5] who observed that the Graetz Bridge was also highly linear. It would be premature to suggest that all power electronic devices exhibit this linearity; however, it is at least a good basis for pursuing the linear modelling of power electronic converters.

An interesting feature of the buck-boost converter in discontinuous operation is that although it has an autonomous switching instant, its variation has no linear effect on either of the states. This can be shown by the evaluation of equation 3.6 for the buck-boost converter across the autonomous switching instant t_{θ_3}, as shown in 3.26 (remembering that the stage order is 4,2,1).

$$\begin{aligned}
\Delta x_1(t_{\theta_3}^+) &= \frac{\partial x_n(t_{\theta_3})}{\partial t_{\theta_3}} \Delta t_{\theta_3} \\
&= \left(-\frac{\partial x_1(t_{\theta_3}^+)}{\partial t} + P[3]\frac{\partial x_2(t_{\theta_3}^-)}{\partial t} + Q[3]\frac{\partial u_{elec}(t_{\theta_3}^-)}{\partial t} \right) \Delta t_{\theta_3} \\
&= \left(-\left[5.4383 \times 10^4\right] + \begin{bmatrix} 0 & 1 \end{bmatrix} \begin{bmatrix} -3.0213 \times 10^5 \\ 5.4383 \times 10^4 \end{bmatrix} + \begin{bmatrix} 0 \end{bmatrix} \begin{bmatrix} 0 \end{bmatrix} \right) \Delta t_{\theta_3} \\
&= \begin{bmatrix} 0 & \Delta t_{\theta_3} \end{bmatrix}
\end{aligned} \tag{3.26}$$

The interpretation of the above evaluation is that the base case capacitor voltage is continuous across the switching instant, whilst the inductor current is non-existent in the post switching stage.

3.11 CONCLUSIONS

A small signal time-domain model of the hybrid power electronic system is derived in this chapter. The resulting model is a mix of both differential and difference equations. The differential equations describe the continuous dynamics of the small signal model using the same equations found in the hybrid model. The discrete dynamics of the hybrid system are frozen by the linearization and their small signal remains are modeled using difference equations, and an injected impulse. The s-domain was introduced to ensure the stage integrals are easily solvable. The resulting model was implemented for a buck-boost converter operating discontinuously and it was shown that the buck-boost converter's behavior is very linear.

Chapter 4

SMALL SIGNAL SOLUTION TO THE CYCLIC STEADY STATE

The first application of the small signal model explored in this thesis is solving the cyclic steady state [1] (CSS) problem of a power electronic converter subjected to periodic excitation and control. In the formulation studied here it is assumed that the stage sequence is known *a-priori*. The problem that remains is finding the switching instants and the states. These two interdependent parts are solved congruently using a numerical method. The first part, the so called two point boundary value (TPBV) problem, solves for the state so that its evolution does not deviate across a cycle, i.e. $x(\alpha) = x(T + \alpha)$. The second part, called here the switching problem, solves for the steady state autonomous switching instants. It is this latter part that makes the CSS problem non-linear and requires its solution to be found using a numerical technique.

Solving the CSS can be achieved with a transient simulation such as PSCAD-EMTDC, EMTP, SPICE. With a simulator the solution is obtained by running until the simulation has reached a cyclic steady state. This method is called contraction mapping [33] [34], or more simply the *brute-force* method. This method of solving the CSS is essentially an initial value interpretation of the TPBV problem, where the switching instants are solved as a by-product. Although not tremendously fast the technique does have the additional benefits of solving the stage sequence problem.

An alternative technique that has received some attention in power electronic literature and circuits and systems literature, is the shooting method. The shooting method is a technique developed for solving TPBV problems of non-linear equations [35] [36]. Like most numerical techniques it begins with an initial estimate, or candidate solution, of the unknowns at each boundary point. This guess is then used to construct a trajectory to *shoot* the known and unknown variables of the other boundary. The magnitude of the trajectories' *miss* of the *target* is used to update the solution. The technique almost exclusively used for calculating this update is to use a sensitivity matrix (also called the

[1] It would be more usual to call this the periodic steady state, however it is called the cyclic steady state in this thesis to avoid an acronym conflict with the partial steady state

Jacobian, or the partial derivative) of the trajectory. This method of updating is a Newton method and is much faster than contraction mapping.

The shooting method was first reported for the solution of circuits and systems by Aprille and Trick [33]. In their analysis the shooting method was used to solve the TPBV of non-linear models. Their emphasis was not on the piece-wise linear power electronic circuits, which are the focus of this thesis, but rather on more exotic oscillatory style circuits or naturally commutating circuits with non-ideal switch models. In [37] Aprille and Trick extended their algorithm to circuits whose period is not known *a-priori*. Their work has been expanded by many others included but not limited to [38] and [39]. In both these works the algorithm is extended to multi-point boundary value problems where the system is solved at multiple points along the periodic solution. This method increases the number of solution variables, and consequently increases the amount of computation required in each iteration. However it is reported to offer better convergence [39] than a classic TPBV algorithm.

Armanazi [40] used the shooting method of Aprille and Trick to solve for piece-wise linear circuits. In Armanazi's treatment, the switching instants, the sensitivity matrices, and the stage sequence are discovered during a time domain simulation of the trajectory using a finite difference method developed in Armanazi's dissertation [41].

In [34] El-Bidweihy and Al-Badwaihy solved both the autonomous switching instants and the state using two Newton algorithms iterated consecutively. The algorithm is limited to solving those circuits with either one autonomous switching instant per cycle, or several that are switched equally distant from each other.

In [42], Kato used a shooting method whose TPBV sensitivity matrix accounted for SIVs, but as was mentioned in the previous chapter only for systems where the state is continuous across the switching instant. Independently, Bedrosian and Vlach [43] used a shooting method that also contained a sensitivity matrix that accounted for switching instant variation, but unlike Kato's analysis, Bedrosian and Vlach's was able to model states that were discontinuous across the switching instant, using a complicated *two-step* approach [20].

Contreras-Sampayo *et al.* [44] recognized that as the algorithm neared the correct solution (typically after the first iteration) the stage sequence of the system would often not alter in subsequent iterations. This was taken advantage of by appending the shooting method with a switching instant problem, where the autonomous switching instants became part of the Newton solution. Evolution and sensitivity across each stage were calculated with PT and PSS s-domain evolutions of the type advanced in Section 3.1 of the last chapter. Another novel aspect of the work is that the algorithm is the form of MPBV solution where the states were solved at each switching instant. The shortcoming of their analysis is that discontinuous states at switching instants were not solved.

In this chapter a Newton shooting method is developed directly from the small signal

model of the previous chapter. Two special cases of the algorithm are discussed. The first special case is when the state transition matrix across a cycle contains only zeros. This occurs when no transient energy is retained across a cycle of the system, in this case only the switching problem is solved. The second special case is when every switching instant is fixed by the controller. In this case the system is linear, and a single iteration is sufficient to solve the system. The algorithm is demonstrated by finding the CSS of the now familiar buck-boost converter, and to another converter, the Graetz Bridge, whose simplified hybrid model is also introduced.

The contribution of this chapter is the demonstration of the small signal model as a core component of a common power electronic analysis technique. The minor contributions of the chapter include modelling of states that are discontinuous at switching instants, calculating the sensitivities across the switching instants analytically, and calculating the evolution and sensitivities between switching instants analytically (including resonating stages).

4.1 TIME DOMAIN CYCLIC STEADY STATE ALGORITHM

Before the full algorithm is examined, both the TPBV problem and the switching instant problem are stated.

4.1.1 Switching instant problem

The switching instant problem (SI) is the problem of determining when the autonomous jumps are satisfied. As the stage order is known *a-priori* it is already known which autonomous jump sets will be satisfied. Formally the switching instant (given for the n^{th} switching instant) problem is that of Definition 4.1.

Definition 4.1 (Switching Instant Problem) *Given an autonomous jump set $V_n \geq g1_n x_{n-1}(t) + g2_n u(t)$ (or $V_n > g1_n x_{n-1}(t) + g2_n u(t)$) the switching instant problem is solved when t is found such that the jump set is satisfied at its boundary. This t is the n^{th} switching instant t_{θ_n}.*

4.1.2 Two Point Boundary Value Problem

A two point boundary value problem, as the name suggests, differs from an initial value problem in that the conditions are specified at two points, typically the end points of an interval. Formally the TPBV problem is specified in Definition 4.2. The problem is solved by determining the unknown variables at each end point. Although seemingly a simple modification to the initial value problem, the TPBV problem has far more complicated uniqueness and existence properties than the initial value problem. The details of the

existence and uniqueness are beyond the scope of this thesis, but any interested reader should begin by consulting [26] or [35].

Definition 4.2 (Two point Boundary Value problem) *Given a function (or system) of order N and of the form $x(t+\tau) = f(x(t), u(t))$, where $x(t)$ is a vector of elements $\left[x_1(t), x_2(t)\ , ..., x_i(t), ..., x_N(t)\right]$. Then the two point boundary value problem is determining $x(t)\ \forall\ t$ over the interval $\gamma < t < \delta$, that satisfies the K boundary conditions of the form $c_k = g_k(x(\alpha), x(\beta))$ defined at the points α and β within the interval.*

For the CSS problem the boundaries of interest are the implicit boundaries known as the periodic boundary value conditions [36]. For these boundaries, the system is defined over the complete time domain interval(i.e. $-\infty < t < \infty$)and the boundary conditions at α and $T + \alpha$ are defined in Definition 4.3 using a similar form to that suggested by Aprille [33].

Definition 4.3 (Periodic Boundary Conditions) *The periodic two point boundary conditions are of the form of equation 4.1.*

$$x(\alpha) - x(T + \alpha) = 0 \tag{4.1}$$

Typically α is replaced with $t = 0$.

As stated in the introduction the method advanced here to solve the TPBV problem is via the shooting method using a Newton algorithm. The Newton algorithm also simultaneously solves the switching instant problem in parallel. The details of this parallel solution are outlined in the following section.

4.1.3 Newton Method

The Newton method is a numerical method for finding the roots of a function by using its gradient to update successive candidate solutions. For the cyclic steady state problem the solution variables are the initial state that satisfies the periodic TPBV problem, and the autonomous switching instants, as shown equation 4.2.

$$\begin{bmatrix} x_1(t_{\theta_1}^+) \\ \{t_{\theta_n}\}_{n\in\{a\}} \end{bmatrix} \tag{4.2}$$

The set $\{a\}$ is the set of autonomous switching indices, $\{t_{\theta_n}\}_{n\in\{a\}}$ is the set of autonomous switching instants, and $x_1(t_{\theta_1}^+)$ is the initial state at the start of the very first stage. Similarly although not in the above equation $\{c\}$ is the set of controlled switching indices and $\{t_{\theta_k}\}_{k\in\{c\}}$ is the set of controlled switching instants.

The mismatch equation set for the CSS problem has contributions from both the TPBV and the SI parts of the CSS problem. The TPBV problem contributes a single equation which is the initial condition compared to the summation of the forced contribution of each stage evolved to the end of the cycle and the initial conditioned multiplied by the cyclic length state transition matrix, as shown in equation 4.3.

$$M\left[x_1\right] = f\Big(x_1(t_{\theta_1}^+), \{t_{\theta_n}\}_{n\in\{a\}}, \{t_{\theta_n}\}_{n\in\{c\}}, u_{elec}(t)\Big) \tag{4.3}$$

When evaluated, the homogenous function is equal to the difference of the initial condition, $x_1(t_{\theta_1}^+)$ and the initial condition evolved across a cycle, $\Phi(T + t_{\theta_1}^+, t_{\theta_1}^+)x_1(t_{\theta_1}^+)$. The contribution from the forced response is the summation of the forced responses at the end of each stage evolved to the end of cycle, as shown below.

$$\begin{aligned} M\left[x_1\right] \;=\; & \Phi(T + t_{\theta_1}^+, t_{\theta_1}^+)x_1(t_{\theta_1}^+) - \quad x_1(t_{\theta_1}^+) \\ & + \sum_{n=2}^{N} \Phi(T + t_{\theta_1}^+, t_{\theta_n}^+)\Big(P[n]\left[x_{PSS_{n-1}}(t_{\theta_n}^-) + x_{PR_{n-1}}(t_{\theta_n}^-)\right] \\ & + Q[n]u_{elec}(t_{\theta_n}) - x_{PSS_n}(t_{\theta_n}^+)\Big) \end{aligned}$$

The switching instant problem contributes one equation for every autonomous switching instant as shown in equation 4.4.

$$\begin{aligned} \{M\left[t_{\theta_n}\right]\}_{\forall\, n\in\{a\}} &= g\Big(x(t_{\theta_1}^+), \{t_{\theta_n}\}_{n\in\{a\}}, u_{ctrl}, u_{elec}(t)\Big) \\ &= g1_n\; x_{n-1}(t_{\theta_n}^-) + g2_n\; u(t_{\theta_n}) \end{aligned} \tag{4.4}$$

The switching instant mismatch is a function of the state just before the switching instant, $x_{n-1}(t_{\theta_n}^-)$. This state is the candidate initial state evolved from the first stage to $t_{\theta_n}^-$, summed with the effect of the forced responses of those stages before the switching instant, also evolved to the point $t_{\theta_n}^-$. Increased efficiency of the algorithm can be gained by obtaining these values during the calculation of equation 4.3.

The location of the switching instants in equations 4.3 and 4.4 are either specified by the controller in the case of a control switching instant, or are taken from the candidate solutions of the autonomous switching instants. It is also assumed that the electrical input contains only harmonics of the pumping frequency. Consequently the evolutions across each stage are governed by the equations of Table 3.2.

To solve the mismatch equations using a Newton algorithm, the gradient (or Jacobian) of

the mismatches with respect to the solution variables is required. This Jacobian can be broken down into four sections as shown in equation 4.5.

$$J = \begin{bmatrix} \frac{\partial M[x_1]}{\partial x_1(t_{\theta_1}^+)} & \left\{ \frac{\partial M[x_1]}{\partial t_{\theta_k}} \right\} \\ \left\{ \frac{\partial M[t_{\theta_n}]}{\partial x_1(t_{\theta_1}^+)} \right\} & \left\{ \frac{\partial \{M[t_{\theta_n}]\}}{\partial t_{\theta_n}} \right\} \end{bmatrix} \tag{4.5}$$

The partial derivatives that form the Jacobian can be obtained from the small signal model of the previous chapter, the elements of each of the partial derivatives are shown below in equation set 4.6.

$$\begin{aligned}
\frac{\partial M[x_1]}{\partial x(t_{\theta_1}^+)} &= \Phi(T + t_{\theta_1}^+, t_{\theta_1}^+) - 1 \\
\frac{\partial M[x]}{\partial t_{\theta_n}} &= \Phi(T + t_{\theta_1}^+, t_{\theta_n}^+) \Bigg(- \frac{\partial x_n}{\partial t}\left(t_{\theta_n}^+\right) \\
&\quad + P[n] \frac{\partial x_{n-1}}{\partial t}\left(t_{\theta_n}^-\right) + Q[n] \frac{\partial u_{elec}(t_{\theta_n})}{\partial t} \Bigg) \quad \forall\, n \in \{a\} \\
\frac{\partial M[t_{\theta_n}]}{\partial x_1(t_{\theta_1}^+)} &= g1_n \Phi(t_{\theta_n}^-, t_{\theta_1}^+) \qquad when\ n \in \{a\} \\
\frac{\partial M[t_{\theta_n}]}{\partial t_{\theta_n}} &= g1_n \frac{\partial x_{n-1}}{\partial t}(t_{\theta_n}^-) + g2_n \frac{\partial u}{\partial t}(t_{\theta_n}) \qquad \forall\, n \in \{a\}
\end{aligned} \tag{4.6}$$

To increase efficiency of an implementation the state transition matrixes of the Jacobian can be scavenged from their prior calculation during the evaluation of the mismatch equations.

4.2 SIMPLIFIED CYCLIC STEADY STATE PROBLEM

No autonomous switching instants Two simplifications to the CSS problem can be made for two classes of systems. The first class of systems are those in which all switching instants are specified by the controller. In this class there are no autonomous switching instants to be solved and finding the CSS is reduced to solving the TPBV problem. Additionally solving this TPBV problem can be achieved in a single iteration from any candidate solution as the problem is now completely linear. The mismatch equation for this special case is that of equation 4.7, whilst the Jacobian is that of equation 4.8.

$$
\begin{aligned}
M\left[x\right] &= f\Big(x_1(t_{\theta_1}^+), \{t_{\theta_n}\}_{n\in\{c\}}, u_{elec}(t)\Big) \\
&= \Phi(T + t_{\theta_1}^+, t_{\theta_1}^+)x_1(t_{\theta_1}^+) - x_1(t_{\theta_1}^+) \quad + \sum_{n=1}^{N} \Phi(T + t_{\theta_1}^+, t_{\theta_n}^+)\Bigg(P[n]\left[x_{PSS_{n-1}}(t_{\theta_n}^-) + x_{PR_{n-1}}(t_{\theta_n}^-)\right] \\
&\quad + Q[n]u_{elec}(t_{\theta_n}) - x_{PSS_n}(t_{\theta_n}^+)\Bigg) \qquad (4.7)
\end{aligned}
$$

$$
\frac{\partial M\left[x\right]}{\partial x(t_{\theta_1}^+)} = \quad \Phi(T + t_{\theta_1}^+, t_{\theta_1}^+) - 1 \qquad (4.8)
$$

No cyclic length transients The second class of systems that can be simplified are those where the transient evolutions do not completely span the length of the cycle. Typically this occurs when there is a stage with no independent energy. An example system of this class is the Graetz Bridge, and the solution to its CSS is the focus of Section 4.4. In all such systems there is at least one jump destination map where the projection matrix is either null or zero valued[2]. At the associated switching instant no independent energy is projected across to the states of the next stage. In these systems the solution variables are reduced to just the autonomous switching instants. The mismatch equations used to find the solution of these systems are of the form of equation 4.9. The partial derivative, $\left\{\frac{\partial M[t_{\theta_k}]}{\partial t_{\theta_k}}\right\}$, that is used in the Newton update of this class is diagonal. The diagonal elements are of the form of equation 4.10.

$$
\{M\left[t_{\theta_n}\right]\} = g1_n x_{n-1}(t_{\theta_n}^-) + g2_n u(t_{\theta_n}) \qquad \forall\, n \in \{a\} \qquad (4.9)
$$

$$
\left\{\frac{\partial M\left[t_{\theta_n}\right]}{\partial t_{\theta_n}}\right\} = g1_n \frac{\partial x_{n-1}^-(t_{\theta_n})}{\partial t} + g2_n \frac{\partial u}{\partial t}(t_{\theta_n}) \qquad \forall\, n \in \{a\} \qquad (4.10)
$$

The mismatch equation of this special case, like that of the general TPBV of Section 4.1, requires the state to be known at each autonomous switching instant. However, due to their being no cyclic length transient evolution, the state is obtained not by evolving from a candidate solution of the state, but by evolving from the closest preceding switching instant that has a jump destination map with a null (or zero valued) projection matrix.

[2]In a multi-variable systems this may not be quite true. If a system has several independent states that have a section of evolution where they do not interact with each other, then each state could be *nullified* at different switching instants during that section of evolution.

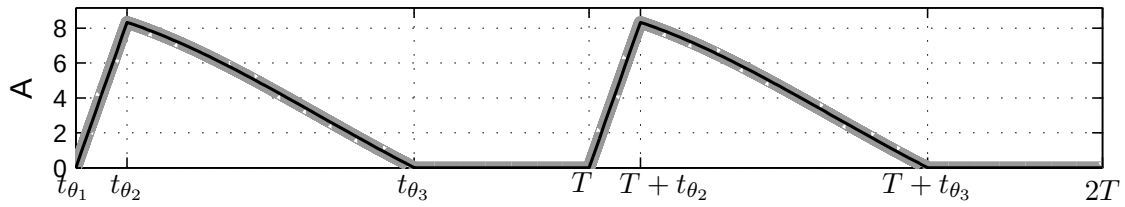

(a) Inductor Current

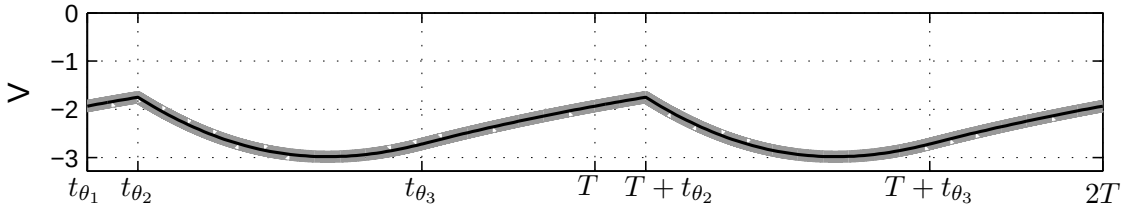

(b) Capacitor Voltage

Figure 4.1 Comparison between the PSCAD solution to the CSS of a discontinous buck-boost converer, and the Newton solution. **thick** PSCAD **Black/Thin** Newton Method.

4.3 BUCK-BOOST EXAMPLE

The discontinuous buck-boost converter's cyclic steady state is solved using the TPBV Newton technique outlined in this chapter. The assumed stage sequence, electrical inputs, and control switching orders are summarized in Table 3.3 of Chapter 3. The initial states are all set to zero, whilst the initial estimate of t_{θ_3} was 0.01ms. The solved CSS is shown in Figure 4.1, and is compared to that found using a PSCAD Simulation. The Newton's method converged in 7 iterations, the initial state and the autonomous switching instant at the start of ever every iteration is summarized in Table 4.1. As the converter is operating in discontinuous mode, the inductor current is always zero at t_{θ_1}, so only the capacitor voltage need be recorded. As can be seen from this table the autonomous switching instant was only updated after the second iteration, in the experience of this author this method converges more readily than allowing the autonomous switching instance to be updated at the very first iteration.

The system was also solved by reusing the second iteration's Jacobian in subsequent iterations. This method, as discussed in [36], still converges to the solution, but after a greater number of iterations, in this case 22 iterations instead of 6. Although the method uses more iterations, it can be quicker as computational time is saved as the Jacobian is not formed or inverted in each iteration. Actual speed comparisons are not given in this thesis, as the code used to generate the result is not optimized enough to produce any meaningful comparison.

iteration	t_{θ_3} (ms)	$v_c(t_{\theta_1})$
1	0.01000	0
2	0.01000	-0.3530
3	0.01731	-4.3147
4	0.03033	-1.0921
5	0.03181	-2.0993
6	0.03297	-1.9435
7	0.03298	-1.9345

Table 4.1 The candidate solutions before each iteration of the Buck-Boost converter

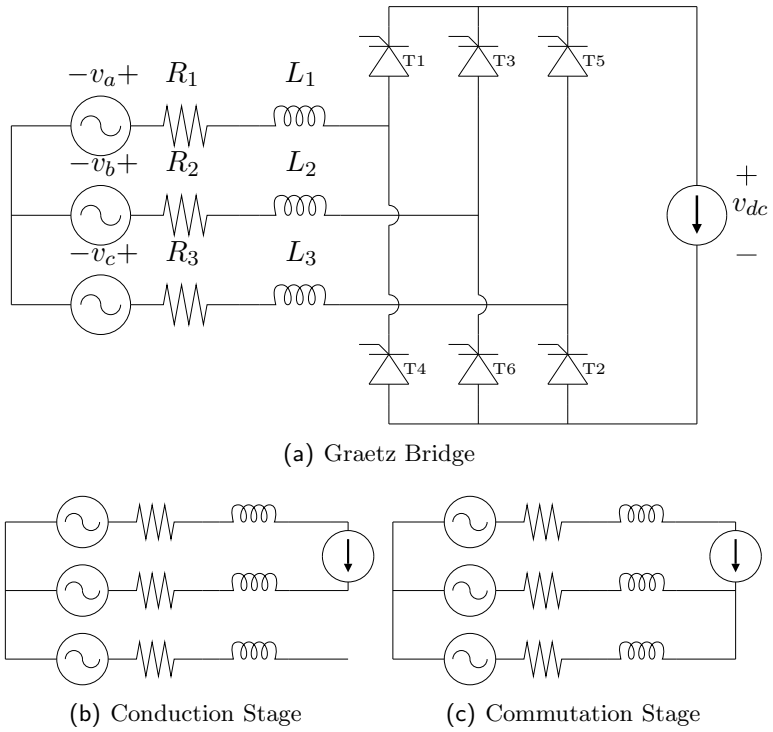

(a) Graetz Bridge

(b) Conduction Stage

(c) Commutation Stage

Figure 4.2 Graetz bridge, with AC side connected in a floating neutral star configuration, DC side connected to a current source, and resistance in each transformer limb.

4.4 GRAETZ BRIDGE EXAMPLE

The second example used to demonstrate and validate the CSS algorithm is the Graetz Bridge. The hybrid model of the Graetz bridge is presented in sufficient detail for finding the CSS under normal operating conditions.

4.4.1 Hybrid model

The Graetz Bridge is modelled here using the same system boundaries used by [5], [45], [46] and [15], and depicted in Figure 4.2. These boundaries are used in this thesis to be consistent with this past literature. Other boundaries, such as including a DC side inductor, could easily be used.

One consequence of the configuration of Figure 4.2 is that during conduction those inductors of the conducting phases are dependent on the DC current source. This source dependent inductor requires the gradient of the current source to determine the voltage drop across it. Fortunately if the system is only subjected to s-domain signals then the gradient can be easily found.

I/O This model's electrical input on the AC side is three star connected voltage sources, whilst on the DC side the input is a single current source. The control input is modelled here as six individual signals, one for each type II switch (Thyristor). The vector input and output vectors are listed below.

$$y(t) = \begin{bmatrix} i_a(t) \\ i_b(t) \\ i_c(t) \\ v_{dc}(t) \end{bmatrix} \quad u_{elec}(t) = \begin{bmatrix} v_a(t) \\ v_b(t) \\ v_c(t) \\ i_{dc}(t) \\ \frac{di_{dc}(t)}{dt} \end{bmatrix} \quad u_{ctrl}(t) = \begin{bmatrix} gate_1(t) \\ gate_2(t) \\ gate_3(t) \\ gate_4(t) \\ gate_5(t) \\ gate_6(t) \end{bmatrix}$$

The gate signals can be rewritten in terms of, α, as shown in equation 4.11.

$$\begin{bmatrix} gate_1(t) \\ gate_2(t) \\ gate_3(t) \\ gate_4(t) \\ gate_5(t) \\ gate_6(t) \end{bmatrix} = \begin{bmatrix} 1 \\ 1 \\ 1 \\ 1 \\ 1 \\ 1 \end{bmatrix} \Big[\alpha(t)\Big] + \begin{bmatrix} 0 \\ \frac{T}{6} \\ \frac{T}{3} \\ \frac{T}{2} \\ \frac{2T}{3} \\ \frac{5T}{6} \end{bmatrix} \tag{4.11}$$

Stages Although this model has 6 switches, and potentially 2^6 stages, only twelve are considered here; the six commutation stages, and the six conduction stages. Examples of both a commutation stage and a conduction stage are depicted in Figures 4.2(b) and 4.2(c) respectively. The switching arrangement for all 12 stages are shown in Table 4.2.

The base-case stage sequence assumed in the Graetz Bridge is that of its normal operation and shown in equation 4.12.

$$[12, 1, 7, 2, 8, 3, 9, 4, 10, 5, 11, 6] \tag{4.12}$$

Governing equations Examples of the equations that govern the dynamics of each stage are shown in equation 4.13, and equation 4.14. As there are no independent states in the conduction circuit, the governing equations' only non-zero matrix is the D feed-forward matrix.

Stage	T1	T2	T3	T4	T5	T6
1	•					•
2	•	•				
3		•	•			
4			•	•		
5				•	•	
6					•	•
7	•	•				•
8	•	•	•			
9		•	•	•		
10			•	•	•	
11				•	•	•
12	•				•	•

Table 4.2 Graetz Bridge Stages Switching topologies, the first 6 stages are conduction stages, and the last 6 are commutation stages

The governing equation for stage 7 of the Graetz Bridge is that of equation 4.13. The state of the system is called the *commutation* state and is the current flowing through the thyristor that is commutating on. In the case of stage 7 this is the current in thyristor 2. Similar equations can be written for the other 5 commutating stages.

$$\begin{aligned}
\left[\dot{i_{com}}(t)\right] &= \left[-\tfrac{R_2+R_3}{L_2+L_3}\right]\left[i_{com}(t)\right] + \begin{bmatrix} 0 & \frac{1}{L_2+L_3} & -\frac{1}{L_2+L_3} & \frac{R_2}{L_2+L_3} & \frac{L_2}{L_2+L_3}\end{bmatrix}\begin{bmatrix} v_a(t)\\ v_b(t)\\ v_c(t)\\ i_{dc}(t)\\ \frac{di_{dc}(t)}{dt}\end{bmatrix} \\
\begin{bmatrix} i_a(t)\\ i_b(t)\\ i_c(t)\\ v_{dc}(t)\end{bmatrix} &= \begin{bmatrix} 0\\ 1\\ -1\\ -R_3 + L_3\frac{(R_3+R_2)}{L_2+L_3}\end{bmatrix}\left[i_{com}(t)\right] \\
&+ \begin{bmatrix} 0 & 0 & 0 & 1 & 0\\ 0 & 0 & 0 & -1 & 0\\ 0 & 0 & 0 & 0 & 0\\ 1 & -\frac{L_3}{L_2+L_3} & \frac{L_3}{L_2+L_3}-1 & -R_1-\frac{L_2R_2}{L2+L3} & -L_1-\frac{L_2L_3}{L_2+L_3}\end{bmatrix}\begin{bmatrix} v_a(t)\\ v_b(t)\\ v_c(t)\\ i_{dc}(t)\\ \frac{di_{dc}(t)}{dt}\end{bmatrix}
\end{aligned} \tag{4.13}$$

The governing equation for stage 1 of the Graetz bridge is that of equation 4.14. Similar equations can be formed for the other five conducting stages.

$$\begin{bmatrix} i_a(t) \\ i_b(t) \\ i_c(t) \\ v_{dc}(t) \end{bmatrix} = \begin{bmatrix} 0 & 0 & 0 & 1 & 0 \\ 0 & 0 & 0 & -1 & 0 \\ 0 & 0 & 0 & 0 & 0 \\ 1 & -1 & 0 & -(R_1+R_2) & -(L_1+L_2) \end{bmatrix} \begin{bmatrix} v_a(t) \\ v_b(t) \\ v_c(t) \\ i_{dc}(t) \\ \frac{di_{dc}(t)}{dt} \end{bmatrix} \tag{4.14}$$

Jump Sets The jumps from conduction stages to commutation stages are controlled jumps, whilst the jumps from commutation to conduction stages are autonomous. Each of the autonomous jumps occur when the current in the commutating off thyristor reaches zero. The inequalities that describe the areas of the autonomous jump sets are summarized in equation set 4.15.

$$\begin{aligned} i_{dc} - i_{com} &\leq 0 \quad \text{Rectifier Positive rail} \\ i_{dc} + i_{com} &\leq 0 \quad \text{Rectifier Negative rail} \\ -i_{dc} + i_{com} &\leq 0 \quad \text{Inverter Positive rail} \\ -i_{dc} - i_{com} &\leq 0 \quad \text{Inverter Negative rail} \end{aligned} \tag{4.15}$$

Jump Destination Maps The projection maps are non-square matrices, either $\mathbb{R}^{1\times 0}$ for conduction to commutation or $\mathbb{R}^{0\times 1}$ for commutation to conduction. The injection maps are zero valued.

This completes the hybrid model of the Graetz Bridge in sufficient detail to find the cyclic steady solution of a bridge under normal operation.

Model Parameters The inputs, the switching regime, and the transformer inductance are from the Y connected rectifier bridge of the CIGRE Benchmark [47] ($R = 1\Omega$ and $L = 0.0428H$), subjected to a 375.36kV peak 3-phase AC side voltages, and a 2kA DC current.

4.4.2 Solution to the CSS problem

The Graetz bridge cyclic steady state is solved using the algorithm outlined in this chapter. As transients only occur in the commutation stages the simplified CSS method is used and the solutions are the autonomous switching instants. Although not presented in this thesis, the model has been verified for a range of different resistance values, and unbalanced inputs. The solved CSS is shown in Figure 4.4.2, and is compared to that found using a PSCAD Simulation. The candidate solutions after each iterative step are summarized in Table 4.3.

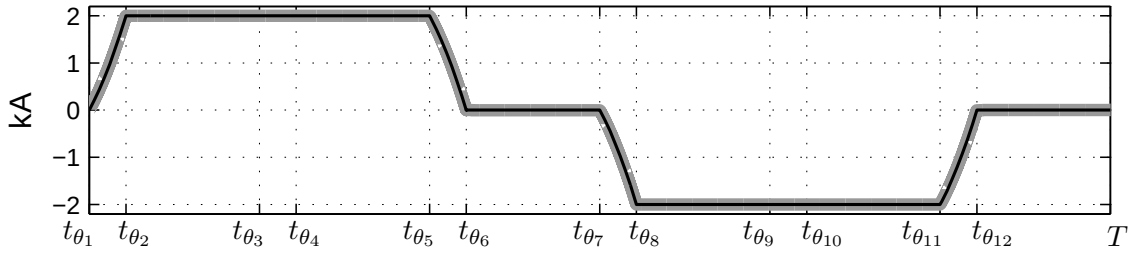

(a) AC side phase currents

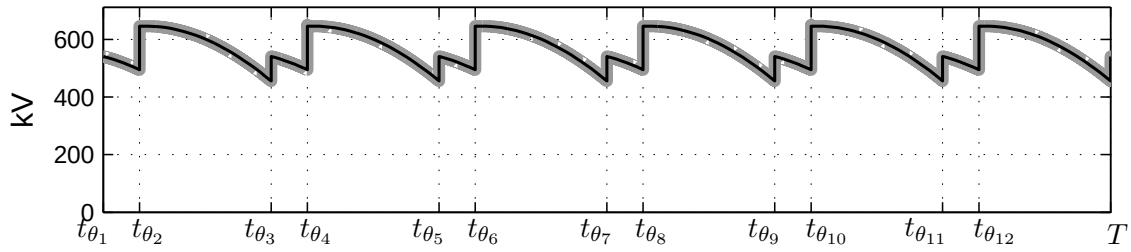

(b) DC side voltage

Figure 4.3 Comparison between a PSCAD solution to the CSS of a Graetz Bridge, and a Newton solution. **grey/thick** PSCAD, **black/thin** Newton.

iteration	t_{θ_2} (ms)	t_{θ_4} (ms)	t_{θ_6} (ms)	t_{θ_8} (ms)	$t_{\theta_{10}}$ (ms)	$t_{\theta_{12}}$ (ms)
1	3.3599	6.6932	10.0265	13.3599	16.6932	20.0265
2	3.2252	6.5585	9.8918	13.2252	16.5585	19.8918
3	3.2201	6.5534	9.8867	13.2201	16.5534	19.8867
4	3.2201	6.5534	9.8867	13.2201	16.5534	19.8867
5	3.2201	6.5534	9.8867	13.2201	16.5534	19.8867

Table 4.3 The candidate solutions after each iteration of the Graetz Bridge converter

4.5 DISCUSSION

The algorithms presented can only solve the cyclic steady state of a converter if the stage sequence is known. In general this assumption can't be made and in practice a transient simulator would need to be used in tandem with the shooting method. Even relatively simply DC:DC converters using "on","off" duty cycle control are reported to have four unique stage sequences[48]. A further example is a Graetz bridge with $\mu > 60^o$, in which case simultaneous commutations occur on the upper and lower rails. It is envisaged that initially a transient simulator would simulate the circuit until a correct stage sequence is suspected, at that point the shooting method would then be used to quickly find the exact cyclic steady state. It is expected that in most cases only a single cycle of simulation would need to be performed to reach this point. Additionally the shooting method should stop iterating if it starts to diverge or the switching instants become inconsistent in which case the simulator should be restarted to find a new stage sequence, and using this new stage sequence a further attempt could be made to solve the CSS with the shooting method.

4.6 CONCLUSION

The small signal model was used to form a general solution to the cyclic steady state of a power electronic converter subjected to a periodic excitation and control. The algorithm developed used a Newton technique to solve a boundary value problem. Two simplifications were made for two special classes of system. The first class had no autonomous switching instants and was completely linear. The second class had no transient states and its CSS was solved using only switching instant variations. The algorithms were then successfully applied to find the CSS of a discontinuously operated buck-boost converter and a Graetz bridge.

Chapter 5

HARMONIC SENSITIVITY MATRICES: BUILT WITH PARTIAL WAVEFORMS

5.1 INTRODUCTION

Chapter 3 describes a time-domain small signal model of a periodically switching power electronic converter. In Chapter 4, the small signal model is used to formulate a general CSS problem. In this chapter, the small signal model is extended to the harmonic domain to model the small signal transfers from harmonics injected into the input (both electrical and control) to the state and the output (both electrical and control). The form of these transfers is that of equation 5.1 and in this thesis these transfers are called Harmonic Sensitivity Matrices (HSM).

$$\begin{bmatrix} \vdots \\ i(-j1\omega_1) \\ i(j0\omega_1) \\ i(j1\omega_1) \\ \vdots \end{bmatrix} = \begin{bmatrix} \ddots & \vdots & \vdots & \vdots & \\ \dots & Y(1,1) & Y(1,0) & Y(1,-1) & \dots \\ \dots & Y(0,1) & Y(0,0) & Y(0,-1) & \dots \\ \dots & Y(-1,1) & Y(-1,0) & Y(-1,-1) & \dots \\ & \vdots & \vdots & \vdots & \ddots \end{bmatrix} \begin{bmatrix} \vdots \\ v(-j1\omega_1) \\ v(j0\omega_1) \\ v(j1\omega_1) \\ \vdots \end{bmatrix} \tag{5.1}$$

The approach advanced in this thesis for determining the elements of the HSM of a power electronic circuit is to use a partial waveform technique similar to that advanced by Hume in [5] and Osusukas *et al* in [15].

The partial waveform technique calculates the HSM by finding the small signal change in each stage's response broken down into its PT, PSS, and PR portions. Their harmonic components are found and then summed together to form the complete waveforms of the system.

5.1.1 Literature review of HSMs

Constructing HSMs has received attention in the past literature. The summary given below breaks the literature into three groups; those who constructed them numerically, those who have constructed them directly in the harmonic domain for inclusion in a Newton

Harmonic Domain Analysis (NHDA)[1]; and finally those who constructed frequency domain models that can be used to form a HSM. In this last group not all authors have gone to the final step of creating a HSM, but using a frequency domain model to produce a HSM is largely a trivial operation. Most of the literature is focused on the modelling of high voltage direct current (HVDC) links that employ Graetz bridge converters.

Large systems can be broken down into subsystems as was done by Carbone *et al* in [49]. In this work Carbone broke an PWM adjustable speed drive into subsystems, found their HSMs and combined to produce an overall description of the system. The details of the HSM of each subsystem are not given, although it is mentioned that either an analytic technique or a numerical technique can be used.

Newton Harmonic Domain Analysis In [6] and also in [50], Smith built a converter model for use in a Newton Harmonic Domain technique, the modeled converter was a Graetz bridge, connected on the AC side to a Y connected transformer whose impedance was modeled as a pure inductance with no resistance. The model completely and accurately modeled that configuration including unbalanced sources, unbalanced impedances, control SIVs and autonomous SIVs. The model was formed in the HD using *phasor equations* and the HSMs were found by differentiating the phasor equations. The aim of the model was not just to describe the sensitivity of harmonics across the bridge, but to build a model for inclusion in a Newton solution to the harmonic steady state of a power electronic circuit and the connected electrical system. In the case of Smith the system was a HVDC link based upon the CIGRE link [47]. Although the Greatz bridge did not include resistance it was included in a connected subsystem. This work was later extended by Bathurst [46] for a fuller set of HVDC link configurations.

Numerical methods Larsen [12] constructed harmonic sensitivity matrices using a numerical simulation technique. The analysis was applied to the five terminal Hydro-Quebec → New England HVDC link and was used for studying low-order harmonic interactions.

In [13], Hume *et. al.* used PSCAD-EMTDC to create harmonic sensitivity matrices for an HVDC link. Later Hume would use this data to verify the much more computationally efficient frequency domain method used in [5].

Frequency domain methods The frequency domain methods of interest are those that model the transfer from an input distortion to a complete set of harmonics. Of the literature reviewed here the bulk is for the modelling of the Graetz bridge. Crucial requirements of the Graetz bridge operation are including the commutation stage, sometimes referred to as the commutation overlap, and including the effect of distortions that alter

[1]The authors of NHDA analysis normally refer to their technique as Harmonic Domain Analysis, however in the opinion of this author that label is too broad, and so is relabeled Newton Harmonic Domain Analysis

the start of the commutation period (a controlled SIV) and those that alter the end of the commutation period.

An early significant contribution was that of Persson [51] who modeled a Graetz bridge of the same style as Smith. Persson's model included the commutation stage, and importantly for an early paper approximated the effects of distortions on the commutation period.

In [52], Hu and Yacamini created a frequency domain model of a Graetz bridge simplified as a modulator.

Wood in [53] constructed a frequency domain model of a Graetz bridge converter. The model included the effects of commutation and switching instant variations. The effect of switching instant variation was found using a modulated spectra from Schwarz[29]. Laird, in [28] used a similar analysis for the single phase diode rectifier. Woods' model was later used by Todd [2] to form an s-domain model of a HVDC link, and by Chen [54] to study a core saturation instability problem.

In [15] and in [55] Osauskas, Hume, and Wood built a more accurate small signal frequency domain model of the Graetz Bridge. The model was directly obtained from a time domain description of the small signal model where the partial transient and partial steady state responses were constructed for each stage before each contribution was sampled to form the complete frequency domain model. This technique is described here as the partial waveform method. In addition the model correctly accounted for the small signal effect of both controlled SIVs (turn on of the bridge's thyristors) and autonomous SIVs (turn off the bridge's thyristors). The only small signal transfer not modeled was the effect of zero frequency harmonic disturbances, which is not included as a partial resonance analysis was not included.

The Graetz Bridge modelled in [15] and in [55] has two features that simplifies its modelling using partial waveforms, both features are related to the partial transients (PT) waveforms. The first feature is there is only a PT during the commutation stages, which occur every 2nd stage. This restricts the PT to a single stage which are not projected to subsequent stages to influence the partial transients within those stages. The second advantageous feature of the PTs of the non-resistive Graetz Bridge is that it's PT relaxation is at DC as the pole of the commutation stages is at the s-plane's origin. In a general circuit neither of these features are present, which complicates the analysis.

Several authors have constructed HSMs for fully controllable converters, [14], [49], [16], of the PWM style. The PWM converter in the circuits presented can be modelled as a modulator. Möllerstedt *et. al.* [16] modelled a voltage source converter for a light rail locomotive in the harmonic state space (HSS). This technique is very powerful and is the subject of Chapter 6.

5.1.2 Chapter Outline

To date there has been no general analytic method for determining the HSM of a converter - all analytic techniques have been developed for specific devices. Constructed in this chapter, heavily influenced by the work in [15] and [55], is one such general technique. The developed general technique can model circuits that do not have the modelling simplifications of the non-resistive Graetz Bridge.

The model described in [15] and [55] is a frequency domain model; the general technique advanced here is applicable only to the harmonic domain disturbances – i.e the frequency of the disturbances is restricted to harmonics of the fundamental. This additional constraint on the frequency of the input signal is required for states that persist across a cycle.

The outline of the construction of the general model is as follows.

- HSM, and HD signals, and their notation, are introduced. Fundamental HSM operations such as LTI systems, multiplication and interactions with time domain signals are included.

- The transfer between the electrical input and the state of a general power electronic model are described. This can be considered the core component of the model.

- The input to state transfer is extended to include electrical outputs, observers of autonomous switching instants, and control inputs.

- The extended model is used to find the small signal estimate of the harmonic steady state of both a discontinuously operating buck-boost converter and a Graetz Bridge with transformer resistance.

5.2 HARMONIC DOMAIN MODELS

In both the large and the small signal sense a harmonic domain model is always restricted to the determination of the periodic steady state of a system. The large signal model has the form of equation 5.2, where in this case the state of a system, $\hat{x}$, is some function of the input $\hat{u}$.

$$\hat{x} = f(\hat{u}) \tag{5.2}$$

The use of the hat, $\hat{x}$, denotes a signal as being in the harmonic domain and contains one element for every harmonic of the pumping frequency. If a single element is required the notation $\hat{x}(jk\omega_1)$ is used, where k is an integer.

Using Taylor's theorem, the small signal linearization of a harmonic domain function has the form of equation 5.3.

$$\begin{aligned} \Delta\hat{x} &= \frac{\partial f(\hat{u})}{\partial \hat{u}}\Delta\hat{u} \\ &= \frac{\partial \hat{x}}{\partial \hat{u}}\Delta\hat{u} \end{aligned} \tag{5.3}$$

5.2.1 Harmonic Sensitivity Matrix of a power electronic converter

Equation 5.3 can be thought of as the linearized prediction of a new steady state of the system subjected to a periodic distortion. This prediction of the new steady state is determined by the partial derivative $\frac{\partial \hat{x}}{\partial \hat{u}}$, which is of the form of a Harmonic Sensitivity Matrix (HSM). In the harmonic domain, the HSM couples small signal changes in the input spectrum $\Delta\hat{u}$ to small signal changes in the output $\Delta\hat{x}$, and has the form of equation 5.4.

$$\begin{bmatrix} \vdots \\ \Delta\hat{x}(-j1\omega_1) \\ \Delta\hat{x}(j0\omega_1) \\ \Delta\hat{x}(j1\omega_1) \\ \vdots \end{bmatrix} = \begin{bmatrix} \ddots & \vdots & \vdots & \vdots & \\ \dots & HSM(1,1) & HSM(1,0) & HSM(1,-1) & \dots \\ \dots & HSM(0,1) & HSM(0,0) & HSM(0,-1) & \dots \\ \dots & HSM(-1,1) & HSM(-1,0) & HSM(-1,-1) & \dots \\ & \vdots & \vdots & \vdots & \ddots \end{bmatrix} \begin{bmatrix} \vdots \\ \Delta\hat{u}(-j1\omega_1) \\ \Delta\hat{u}(j0\omega_1) \\ \Delta\hat{u}(j1\omega_1) \\ \vdots \end{bmatrix} \tag{5.4}$$

HSM(g,k) is shorthand for the transfer from the k^{th} harmonic input disturbance $\Delta\hat{u}_{elec}(jk\omega_1)$ to the g^{th} harmonic state disturbance $\Delta x(jg\omega_1)$, and is described as the $(g,k)^{th}$ element of the Harmonic Sensitivity Matrix.

In general, the HSM is neither a frequency domain multiplication nor is it a convolution. Instead it is a combination of both these operations. The elements of the HSM are unique between every harmonic frequency of the input and every harmonic of the state (or output) as is shown in the general form of equation 5.4.

5.2.2 Simple Harmonic Sensitivity Matrices

Before constructing the elements of the HSM for a general power electronic model several simple Harmonic Sensitivity Matrices are introduced.

HSM of a constant multiplier One simple HSM commonly used in this thesis, that does not have harmonic cross coupling is the constant multiplier.

For the constant, K, the elements of its HSM, $\mathcal{K}$, are described via equation 5.5.

$$\mathcal{K}(g,k) = \begin{cases} K & g = k \\ 0 & g \neq k \end{cases} \tag{5.5}$$

This produces the HSM of equation 5.6.

$$\begin{bmatrix} \vdots \\ \hat{x}(-j1\omega_1) \\ \hat{x}(j0\omega_1) \\ \hat{x}(j1\omega_1) \\ \vdots \end{bmatrix} = \begin{bmatrix} \ddots & \vdots & \vdots & \vdots & \\ \dots & K & 0 & 0 & \dots \\ \dots & 0 & K & 0 & \dots \\ \dots & 0 & 0 & K & \dots \\ & \vdots & \vdots & \vdots & \ddots \end{bmatrix} \begin{bmatrix} \vdots \\ \hat{u}(-j1\omega_1) \\ \hat{u}(j0\omega_1) \\ \hat{u}(j1\omega_1) \\ \vdots \end{bmatrix} \tag{5.6}$$

As equation 5.5 shows constants are readily interchangeable between the time and harmonic domains.

LTI response Another commonly used HSM transfer that has no frequency cross coupling is the HSM of an LTI system – $H(j\omega_1)$. The elements of its HSM, $\mathcal{H}$, are described by equation 5.7. It should be noted that if $jk\omega_1$ falls on a resonant frequency then there is no mapping between the harmonics of the input and the harmonics of the output.

$$\mathcal{H}(g,k) = \begin{cases} H(jk\omega_1) & g = k \text{ if } jk\omega_1 \notin \{\lambda_n\} \\ 0 & g \neq k \\ 0 & g \in \{\lambda_n\} \end{cases} \tag{5.7}$$

This produces the HSM of equation 5.6.

$$\begin{bmatrix} \vdots \\ \hat{x}(-j1\omega_1) \\ \hat{x}(j0\omega_1) \\ \hat{x}(j1\omega_1) \\ \vdots \end{bmatrix} = \begin{bmatrix} \ddots & \vdots & \vdots & \vdots & \\ \dots & H(-j\omega_1) & 0 & 0 & \dots \\ \dots & 0 & H(0) & 0 & \dots \\ \dots & 0 & 0 & H(j\omega_1) & \dots \\ & \vdots & \vdots & \vdots & \ddots \end{bmatrix} \begin{bmatrix} \vdots \\ \hat{u}(-j1\omega_1) \\ \hat{u}(j0\omega_1) \\ \hat{u}(j1\omega_1) \\ \vdots \end{bmatrix} \tag{5.8}$$

Gradient relationship A particularly useful HSM for systems with input dependent states is the HSM that relates a signal to its gradient – $\frac{d}{dt}$. The elements of the gradient function HSM are described via equation 5.9.

$$\frac{d}{dt}(g,k) = \begin{cases} jk\omega_1 & g = k \\ 0 & g \neq k \end{cases} \tag{5.9}$$

This produces the HSM of equation 5.10.

$$\begin{bmatrix} \vdots \\ \hat{\hat{u}}(-j1\omega_1) \\ \hat{\hat{u}}(j0\omega_1) \\ \hat{\hat{u}}(j1\omega_1) \\ \vdots \end{bmatrix} = \begin{bmatrix} \ddots & \vdots & \vdots & \vdots & \\ \dots & -j\omega_1 & 0 & 0 & \dots \\ \dots & 0 & 0 & 0 & \dots \\ \dots & 0 & 0 & j\omega_1 & \dots \\ & \vdots & \vdots & \vdots & \ddots \end{bmatrix} \begin{bmatrix} \vdots \\ \hat{u}(-j1\omega_1) \\ \hat{u}(j0\omega_1) \\ \hat{u}(j1\omega_1) \\ \vdots \end{bmatrix} \tag{5.10}$$

Convolution relationship The last HSM defined here is that of the convolution operator. If a signal is to be multiplied by another signal in the time domain, then the equivalent operation in the harmonic domain is convolution. For example, suppose in the time domain the function $y(t) = a(t) \times u(t)$ is required, then if all three signals are T-periodic, and $a(t)$ acts in the role of a transfer the harmonic domain equivalent is $\hat{y} = \hat{a} * \hat{u}$. As a HSM the convolution of $\hat{u}$ with $\hat{a}$ is the form of the Toeplitz matrix of equation 5.11.

$$\begin{bmatrix} \vdots \\ \hat{y}(-j\omega_1) \\ \hat{y}(0) \\ \hat{y}(j\omega_1) \\ \vdots \end{bmatrix} = \begin{bmatrix} \ddots & \vdots & \vdots & \vdots & \\ \dots & \hat{a}(0) & \hat{a}(-1) & \hat{a}(-2) & \dots \\ \dots & \hat{a}(1) & \hat{a}(0) & \hat{a}(-1) & \dots \\ \dots & \hat{a}(2) & \hat{a}(1) & \hat{a}(0) & \dots \\ & \vdots & \vdots & \vdots & \ddots \end{bmatrix} \begin{bmatrix} \vdots \\ \hat{u}(-j\omega_1) \\ \hat{u}(0) \\ \hat{u}(j\omega_1) \\ \vdots \end{bmatrix} \tag{5.11}$$

Time domain to harmonic domain relationships In the analytical description of the power electronic converter's HSM, time domain signals are related to harmonic domain signals. The transfers of these relationships are in the form of a row vector, and have one element for each harmonic of the HD signal.

One common transfer of this style that is frequently used in this chapter, is the *point sampling function*. The point sampling function samples a harmonic domain signal, $\hat{u}$, to find its time domain value at a point as shown in equation 5.12.

$$u(t_\theta) = \Psi[t_\theta]\hat{u} \tag{5.12}$$

The coefficients of the point sampling function's vector $\Psi[t_\theta]$, are defined in equation 5.13.

$$\Psi[t_\theta](k) = e^{jk\omega_1 t_\theta} \quad \forall\, k \ \in I \tag{5.13}$$

Conversely if a harmonic domain signal is dependent on a time domain signal, the transfer between the two signals is with a column vector, where a single time domain element is used to form a harmonic domain signal with potentially a double infinite number of elements.

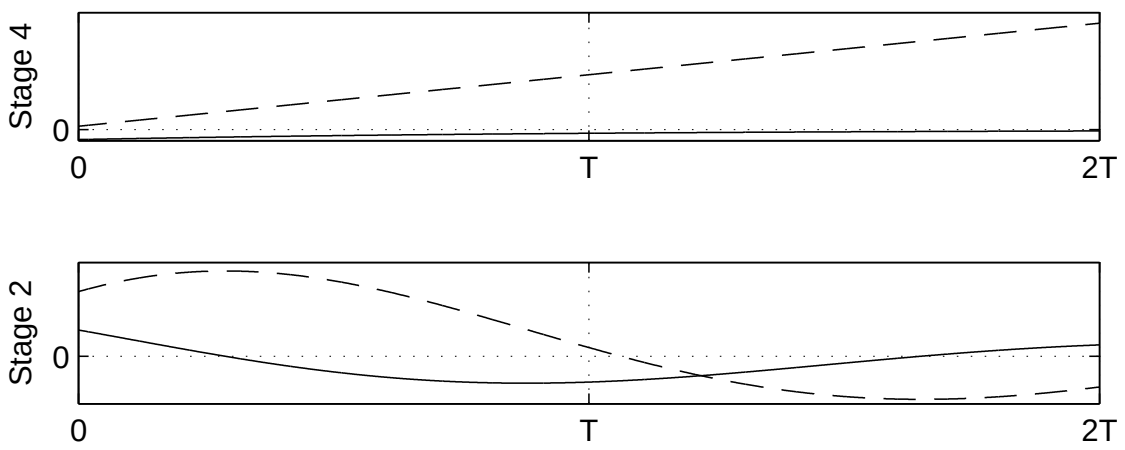

Figure 5.1 The time domain response of the buck-boost converter. In each plot the Dashed lines are the inductor currents, whilst the solid lines are the capacitor voltages

5.3 SMALL SIGNAL ANALYTICAL HSM OF A POWER ELECTRONIC CONVERTER

The small signal HSM for a power electronic converter is derived analytically using the three step derivation outlined below. The aim of this chapter is to describe and combine these steps into a single analytically described HSM.

Step 1: Form Partial Responses of Each Stage The time domain responses of each stage are formed using the s-domain evolution functions of Chapter 3.

As defined in Chapter 3, and used in Chapter 4, the partial responses of each stage's LTI system are made from the summation of three waveforms representing the transient, steady state, and resonant responses of the stage. To emphasize that the responses belong to a particular stage rather than the whole system they are given the *partial* qualifier, giving rise to the partial transient (PT) partial steady state (PSS) and the partial resonant (PR) responses. Repeated below are the equations that shape the evolution of each part.

$$x_{PSS_n}(t) = T_{ns_n}(sI - \lambda_{ns_n})^{-1} B_{ns_n} u_{elec} e^{st} \tag{5.14}$$

$$x_{PT_n}(t) = e^{A_n(t-t_{\theta_n})} \left[x(t_{\theta_n}^+) - T_{ns_n}(sI - \lambda_{ns_n})^{-1} B n s_n u_{elec}(t_{\theta_n}) \right] \tag{5.15}$$

$$x_{PR_n}(t) = T_s(t - t_{\theta_n}) e^{\lambda_s t} B_s u_{elec} \tag{5.16}$$

In Figure 5.1 the summation of these responses are shown for the two stages of a continuously operated buck-boost converter.

The most difficult problem of the three parts of the partial response is finding the initial state of the PT for each stage after the system has reached the cyclic steady state. For

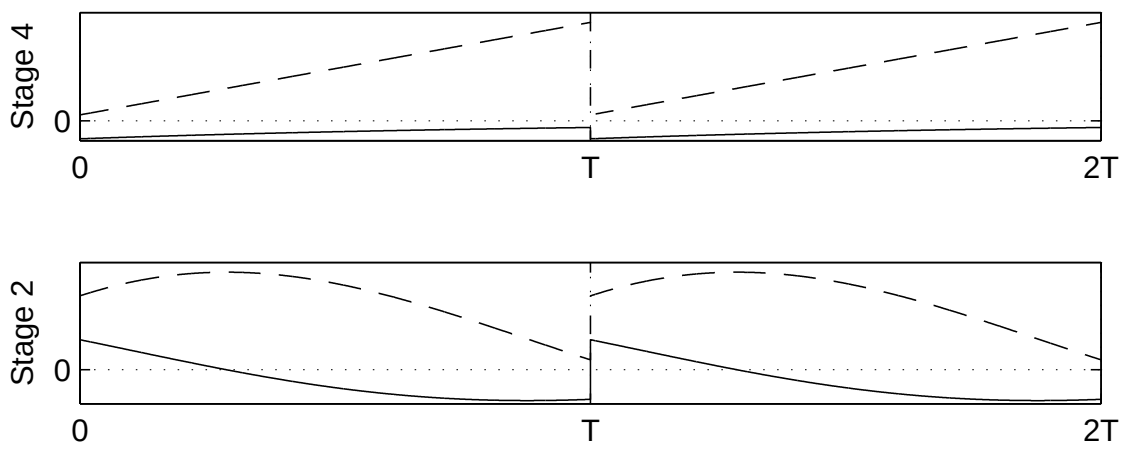

Figure 5.2 The time domain responses of the buck-boost converter after each have been made periodic. In each plot the Dashed lines are the inductor currents, whilst the solid lines are the capacitor voltages

a harmonic domain model the initial state at the start of each stage is a function of the input spectrum. The relationship between the initial state of the partial transient and the input spectrum is derived in section 5.4.3.

Step 2: Periodization of Partial Responses The partial response of each stage are made periodic with the use of the Fourier Series Coefficient Integral. This step assumes that the partial response is the same for each repeated appearance of the stage in subsequent cycles. This assumption is valid if the system has reached a cyclic steady state where the repeating waveform can be described as harmonic domain signal. After they are made periodic the summed partial responses of each stage of the buck-boost converter have the shapes shown in Figure 5.2.

The periodization of each stage's partial steady state response is relatively simple, as the PSS only includes elements of the input spectrum, phase shifted and magnitude changed. Unfortunately, this is not the case for the transient and resonant evolutions which contain frequencies that are in part determined by the stage dynamics. When made periodic, the spectra of the partial transient and partial resonant responses contain a full range of harmonics. This is shown in Figure 5.3 which shows the spectra of the small signal partial responses of stage 4 of the buck-boost converter subjected to the input disturbance with a spectrum of Figure 5.3(a), which is at the 6^{th} harmonic.

In the technique advanced here, the spectra of the PT and PR response are found via a direct implementation of the Fourier series coefficient integral, equation 5.17.

$$C(jg\omega_1) = \frac{1}{T}\int_0^T v(t)e^{-jg\omega_1 t}dt \tag{5.17}$$

Where $v(t)$ is each partial response.

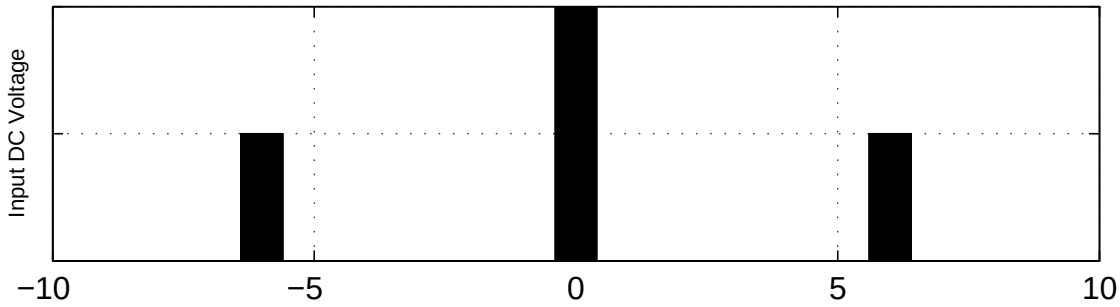

(a) DC current Input Disturbance

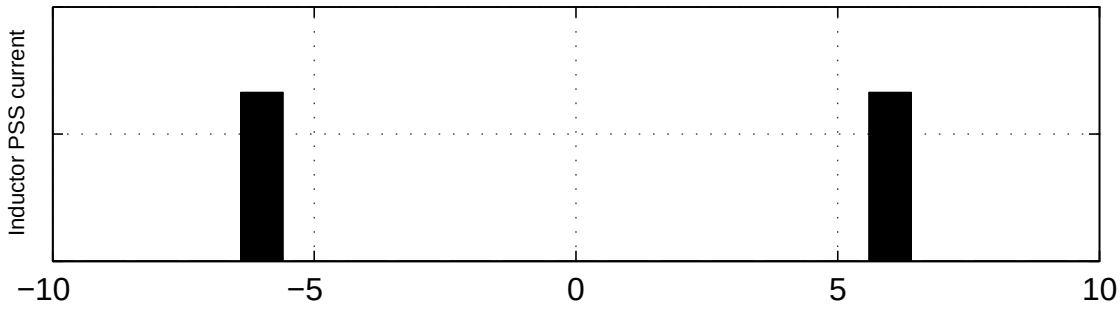

(b) Inductor Current Partial Steady State Spectrum

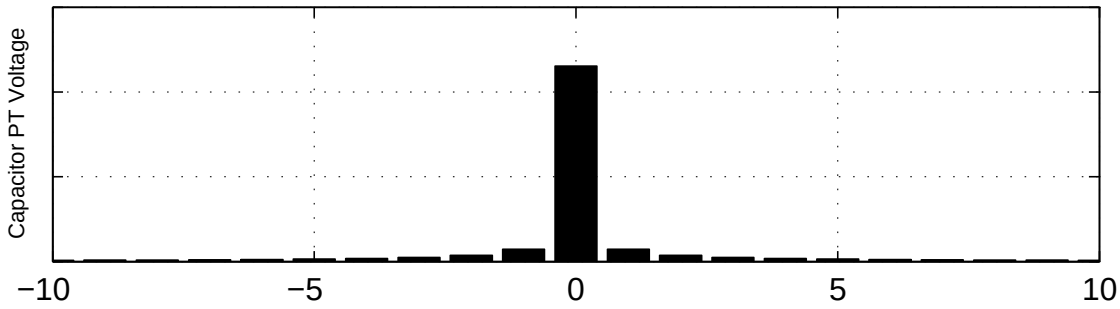

(c) Capacitor Voltage Partial Transient Response

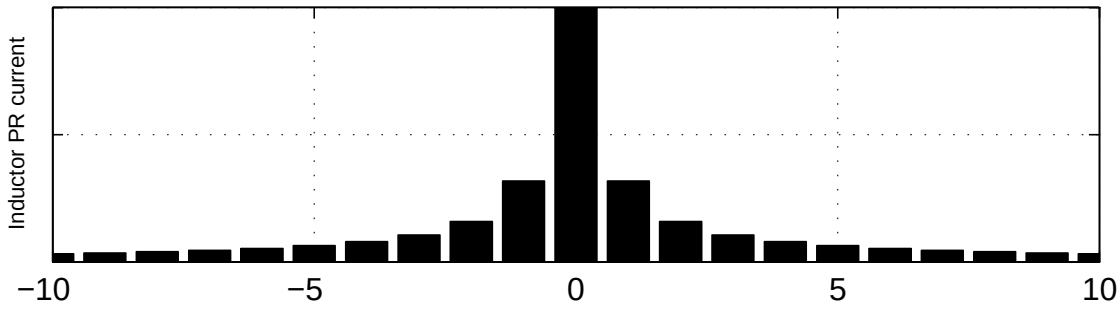

(d) Inductor Current Partial Resonant Response

Figure 5.3 Spectra of the partial responses of stage 4 of a buck-boost converter when subjected to an input disturbance with the spectrum of (a). The PSS and PR responses result in deviations in the inductor current, the spectra of these deviations are shown in (b) and (d) respectively. The capacitor is isolated from the input so it only contains a partial transient response during stage 4, the spectrum of its deviation are shown in (c).

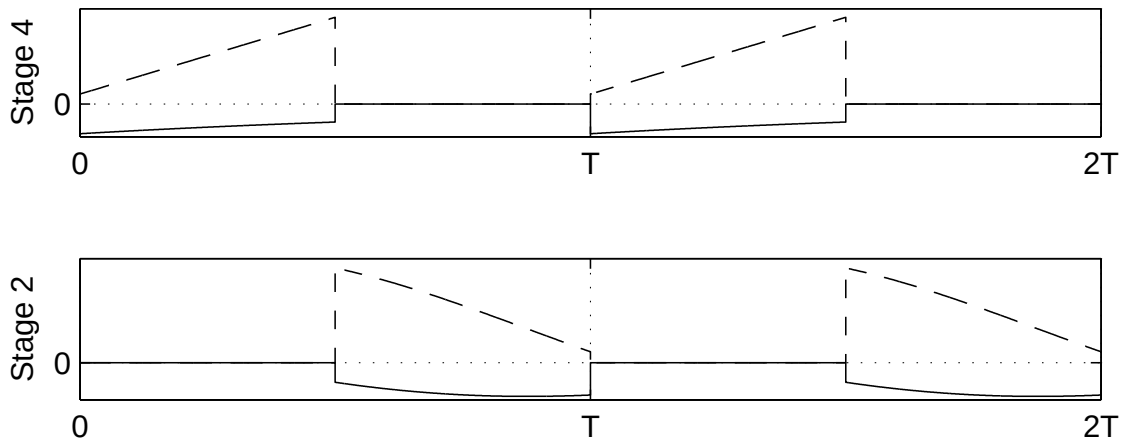

(a) Sampled Partial response of each stage

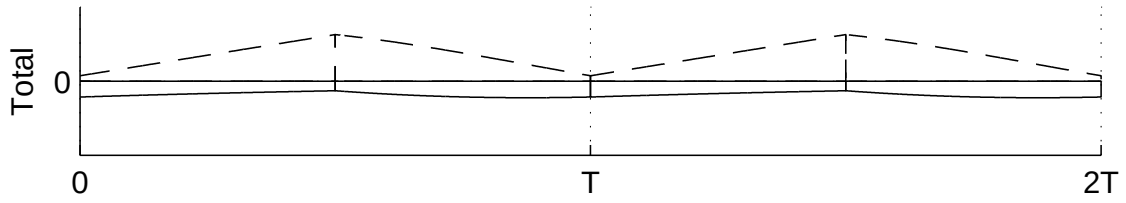

(b) Summation the Partial responses

Figure 5.4 The time domain responses of the buck-boost converter after each have been made periodic. In each plot the Dashed lines are the inductor currents, whilst the solid lines are the capacitor voltages

Step 3: Sampling of Partial Responses The periodic responses are convolved in the harmonic domain by rectangular sampling functions that span the limits of the stage. The sampling function used to apply this restriction is identical for all three partial responses, and in the time domain is a unity, periodically repeating rectangular waveform. The sampled waveforms, (called the sampled partial steady state (SPSS), the sampled partial transient (SPT), and the sampled partial resonant responses (SPR) respectively) from all stages are summed together to find the total response of the system to input disturbances.

The periodic contributions from each stage are summed together to produce the total response of the system to the input disturbance. The time domain description of this sampling is depicted in Figure 5.4.

An alteration to the step described above is instead of sampling the PT and the PR with a rectangular waveform, the same sampling can be achieved by rewriting the limits of equation 5.17 to the beginning and end points of each stage. If this method is used a reduction in the effects of Gibb's Phenomena occurs, and is the method advanced in this thesis.

5.3.1 Buffering of each stage's state vector

One consequence of using the harmonic domain is that it is assumed that all stages have equally dimensioned state matrices, however, as has already been discussed this is not always true. In those cases, the state matrices of each stage are buffered to equal dimensions. For example in the buck-boost example, stage 1 has a single state, whilst stage 2 has two states. By buffering stage 1 to have the same dimensions as stage 2, the state of stage 1 is as described in equation 5.18.

$$\begin{bmatrix} 0 \\ v_c(t) \end{bmatrix} \tag{5.18}$$

In this example, stage 1's states are buffered by an additional state at the start of the state vector. It seems advantageous to keep states that are physically the same identically positioned in all those stages in which they appear. In cases where the states in each stage are physically different, such as in a Graetz bridge, then states either share a position, or have separate unique positions. In the Graetz Bridge this means either one state for each commutating inductor, x_{L_a}, x_{L_b}, x_{Lc} or a single commutating state shared by all commutating stages, $x_{L_{com}}$.

Similarly a stage's A,B,C projection & injection matrixes to and from stage 1 are also buffered, the buffers of those matrixes are made from zero valued elements.

5.4 PARTIAL RESPONSES

As discussed and shown in Figure 5.3 the HD partial response is made from three components, the PT, the PSS and the PR. Each of these components are derived within this section.

5.4.1 Partial Steady State

The partial steady state waveform only contains frequencies of the input distortion. Contributions to other frequencies occur only after sampling. The small signal harmonic change in the PSS from changes in the input has the form of equation 5.19.

$$\Delta\hat{x}_{PSS_n} = \frac{\partial\hat{x}_{PSS_n}}{\partial\hat{u}_{elec}}\Delta\hat{u}_{elec} \tag{5.19}$$

The elements of the partial derivative written in the form of a HSM are defined by equation 5.20 which is of an LTI system.

$$\frac{\partial \hat{x}_{PSS_n}(jg\omega_1)}{\partial \hat{u}_{elec}(jk\omega_1)} = \begin{cases} T_{ns_n}(jk\omega_1 I - \lambda_{ns_n})^{-1} B_{ns_n} & g = k \text{ if } jk\omega_1 \notin \{\lambda_n\} \\ 0 & g \neq k \\ 0 & g = k \text{ if } jk\omega_1 \in \{\lambda_n\} \end{cases} \tag{5.20}$$

Sampled Partial Steady State (SPSS) The PSS spans the entire cycle of the T-periodic system. To produce a response that only spans the length of the stage – described here as the sampled partial steady state (SPSS)– the partial steady state is sampled by a unity valued rectangular sampling function as shown in equation 5.21.

$$\Delta \hat{x}_{SPSS} = \Psi[t_{\theta_{n+1}}, t_{\theta_n}] \Delta \hat{x}_{PSS} \tag{5.21}$$

The coefficients of the sampling function's HSM are described by equation 5.22. The HSM of the sampling function is consistent with a frequency domain convolution and is in the form of a Toeplitz matrix.

$$\Psi[t_{\theta_{n+1}}, t_{\theta_n}](g,k) = \begin{cases} \frac{1}{j2\pi(g-k)} \left(e^{-j(g-k)\omega_1 t_{\theta_n}} - e^{-j(g-k)\omega_1 t_{\theta_{n+1}}} \right) & jg\omega_1 \neq jk\omega_1 \\ \frac{t_{\theta_{n+1}} - t_{\theta_n}}{T} & jg\omega_1 = jk\omega_1 \end{cases} \tag{5.22}$$

5.4.2 Partial Resonant Response

If the input spectrum contains an element at a frequency equal to one of the resonant modes of the stage, $jk\omega_1 \in \{\lambda_n\}$, then during that stage that input component will cause the stage to resonate and evolve according to equation 5.23.

$$\begin{aligned} x_{PR_n}(t) &= T_{s_n}(t - t_{\theta_n}) e^{\lambda_{s_n} t} B_{s_n} u_{elec} \\ &= T_{s_n}(t - t_{\theta_n}) e^{jk\omega_1 t} B_{s_n} u_{elec} \end{aligned} \tag{5.23}$$

For a LTP system, this will produce a resonant response every time the system enters that stage as shown in Figure 5.5. In this figure a dc voltage excites an inductor. The inductor contributes a pole at zero frequency. This pole resonates at zero frequency and the current rises linearly. When this stage is active in the next cycle, the resonant condition occurs again and the current again builds linearly.

As can been seen from equation 5.23 the partial resonant response contains frequencies other than those of the input. Further, the response is only describable at all in the harmonic domain if the resonance is only excited for a portion of the cycle. Assumed this requirement is satisfied the partial resonant response can be described as a spectrum - the

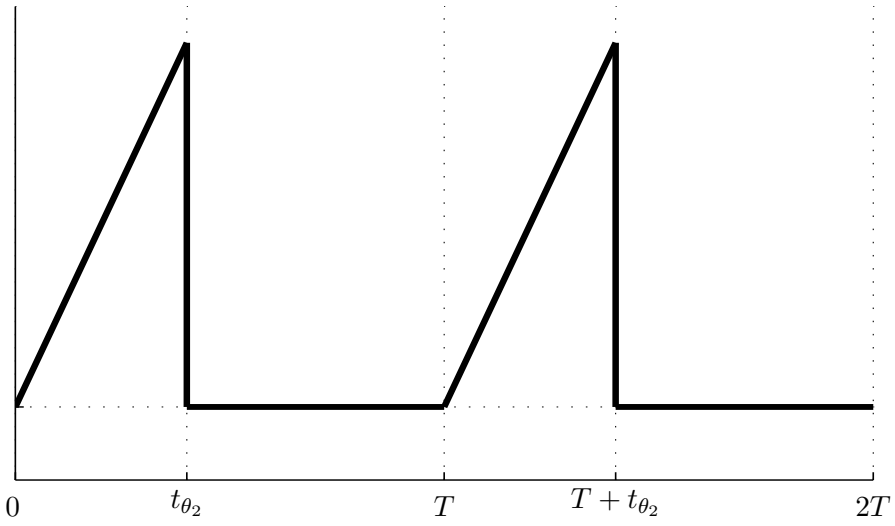

Figure 5.5 Partial resonance response of an inductor subjected to DC voltage between t_{θ_1} and t_{θ_2}, every cycle

spectrum's coefficients can be found directly with the use of the Fourier Series Coefficient Integral(FSCI) as shown in equation 5.24.

$$\begin{aligned}
\hat{x}_{PR_n}(jg\omega_1) &= \frac{1}{T}\int_0^T T_{s_n}(t-t_{\theta_n})e^{j(k-g)\omega_1 t}B_{s_n}\hat{u}_{elec}(jk\omega_1)dt \\
&= \begin{cases}
\frac{T_{sn}}{T(j(k-g)\omega_1)^2}\Big\{1 + j(k-g)\omega_1 t_{\theta_n} + & \\
j(k-g)\omega_1(T-t_{\theta_n})e^{j(k-g)\omega_1 T}\Big\}B_{s_n}\hat{u}_{elec}(jk\omega_1) & jg\omega_1 \neq jk\omega_1 \\
T_{s_n}\left(\frac{1}{2}T - t_{\theta_n}\right)B_{s_n}\hat{u}_{elec}(jk\omega_1) & jg\omega_1 = jk\omega_1
\end{cases}
\end{aligned} \tag{5.24}$$

The HSM that this result forms is described by equation 5.25.

$$\Delta\hat{x}_{PR_n} = \frac{\partial\hat{x}_{PR_n}}{\partial\hat{u}_{elec}}\Delta\hat{u}_{elec} \tag{5.25}$$

Its elements are described by equation 5.28

$$\frac{\partial \hat{x}_{PR_n}(jg\omega_1)}{\partial \hat{u}_{elec}(jk\omega_1)} = \begin{cases} \frac{T_{s_n}}{T(j(k-g)\omega_1)^2}\Big\{1 + j(k-g)\omega_1 t_{\theta_n} + & \\ \quad j(k-g)\omega_1(T - t_{\theta_n})e^{j(k-g)\omega_1 T}\Big\}B_{s_n} & jg\omega_1 \neq jk\omega_1, jk\omega_1 \in \{\lambda_n\} \\ T_{s_n}\left(\frac{1}{2}T - t_{\theta_n}\right)B_{s_n} & jg\omega_1 = jk\omega_1, jk\omega_1 \in \{\lambda_n\} \\ 0 & jk\omega_1 \notin \{\lambda_n\} \end{cases} \tag{5.26}$$

Sampled Partial Resonant (SPR) The sampled partial resonant response could be found in a similar manner to the SPSS. However, an alternative to using an explicit sampling function is simply to adjust the limits of the FSCI used in equations 5.24, to t_{θ_n} and $t_{\theta_{n+1}}$. This effectively samples the PR without the use of a rectangular sampling function. The HSM that this result forms is described by equation 5.27.

$$\Delta\hat{x}_{SPR_n} = \frac{\partial \hat{x}_{SPR_n}}{\partial \hat{u}_{elec}}\Delta\hat{u}_{elec} \tag{5.27}$$

Its elements are described by equation 5.28

$$\frac{\partial \hat{x}_{SPR_n}(jg\omega_1)}{\partial \hat{u}_{elec}(jk\omega_1)} = \begin{cases} \frac{T_{sn}}{T(j(k-g)\omega_1)^2}\Big\{\Big\{j(k-g)\omega_1 t_{\theta_{n+1}} - 1 & \\ + \quad j(g-k)\omega_1 t_{\theta_n}\Big\}e^{j(k-g)\omega_1 t_{\theta_{n+1}}} & jg\omega_1 = jk\omega_1, jk\omega_1 \in \{\lambda_n\} \\ + \quad e^{j(k-g)\omega_0 t_{\theta_{n+1}}}\Big\}B_{s_n} & \\ \frac{T_{sn}}{T}\left\{\frac{t_{\theta_{n+1}}^2}{2} + \frac{t_{\theta_n}^2}{2} - t_{\theta_{n+1}}t_{\theta_n}\right\}B_{sn} & g\omega_1 \neq jk\omega_1, jk\omega_1 \in \{\lambda_n\} \\ 0 & jk\omega_1 \notin \{\lambda_n\} \end{cases} \tag{5.28}$$

This alternative formulation has been found to reduce the effect of ringing (or Gibbs Phenomenon) in the derived waveforms. Reducing Gibb's Phenomenon reduces harmonic truncation errors.

5.4.3 Partial Transient Response

The partial transient responses, as declared in Definition 5.15, are the relaxation of each stage's modes. Their trajectory is determined by equation 5.29. An example trajectory is shown in Figure 5.6.

$$\begin{aligned} x_{PT_n}(t) &= e^{A_n(t-t_{\theta_n})}\left[x(t_{\theta_n}^+) - T_{ns_n}(sI-\lambda_{ns_n})^{-1}B_{ns_n}u_{elec}(t_{\theta_n})\right] \\ &= e^{A_n(t-t_{\theta_n})}\left[x(t_{\theta_n}^+) - x_{PSS_n}(t_{\theta_n}^+)\right] \\ &= e^{A_n(t-t_{\theta_n})}\left[\varepsilon_n(t_{\theta_n})\right] \end{aligned} \tag{5.29}$$

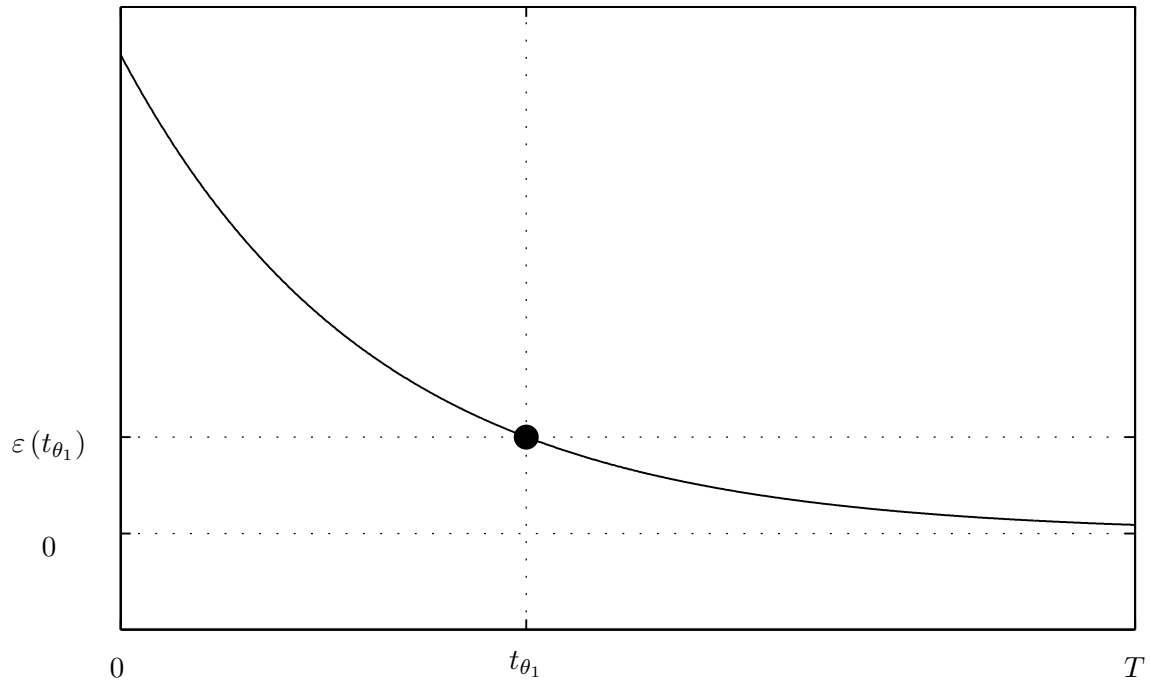

Figure 5.6 Partial transient response of a stage, showing the start of stage mismatch, $\varepsilon(t_{\theta_1})$, and its trajectory.

The shape of the relaxation is described by the exponential, $e^{A_n(t-t_{\theta_n})}$, whilst the mismatch between a stage's initial condition and its PSS is given by the time domain vector $\varepsilon_n(t_{\theta_n})$. Expressions for both the shape of the PT and the size for the mismatch are combined using the chain rule to form a single expression for the PT.

$$\Delta\hat{x}_{PT_n} = \frac{\partial\hat{x}_{PT_n}}{\partial\varepsilon_n(t_{\theta_n}^+)}\frac{\partial\varepsilon_n(t_{\theta_n}^+)}{\partial\hat{u}_{elec}}\Delta\hat{u}_{elec} \tag{5.30}$$

In the chain rule a mix of both time domain and harmonic domain variables are present.

Partial Transient Mismatch

The time domain mismatch variable, $\varepsilon_n(t_{\theta_n}^+)$, is equal to the initial value of the state, $x(t_{\theta_n}^+)$, minus the partial steady state value at the start of each stage $x_{PSS_n}(t_{\theta_n}^+)$. If at the start of a stage the steady state and the initial value agree then there is no transient during that stage. If there is a mismatch then relaxation occurs. The sensitivity of the mismatch to the input disturbance is described in equation 5.32.

$$\begin{aligned} \Delta\varepsilon_n(t_{\theta_n}^+) &= \frac{\partial\varepsilon_n(t_{\theta_n}^+)}{\partial\hat{u}_{elec}}\Delta\hat{u}_{elec} \\ &= \left(\frac{\partial x_n(t_{\theta_n}^+)}{\partial\hat{u}_{elec}} - \frac{\partial x_{PSS_n}(t_{\theta_n}^+)}{\partial\hat{u}_{elec}}\right)\Delta\hat{u}_{elec} \end{aligned} \tag{5.31}$$

$$\tag{5.32}$$

Equation 5.32 that shows the mismatch's sensitivity is a function of the harmonic domain input disturbance $\hat{u}_{elec}$. Detailed derivations of the two partial derivatives that describe this relationship are described below.

Sensitivity of the Partial Steady State at the start of a stage to input disturbances The relationship between the PSS and the input spectrum was previously covered in the section on the PSS response, Section 5.4.1. Here the whole PSS response is not required, only the PSS at the point t_{θ_n} is needed. The PSS at this point with the use of the *point sampling function* $\Psi[t_{\theta_n}]$ is as shown in equation 5.33.

$$\begin{aligned} \Delta x_{PSS_n}(t_{\theta_n}^+) &= \frac{\partial x_{PSS_n}(t_{\theta_n}^+)}{\partial\hat{u}_{elec}}\Delta\hat{u}_{elec} \\ &= \Psi[t_{\theta_n}]\frac{\partial\hat{x}_{PSS_n}}{\partial\hat{u}_{elec}}\Delta\hat{u}_{elec} \end{aligned} \tag{5.33}$$

State at the start of a stage: $x(t_{\theta_n}^+)$ The time domain quantity $x(t_{\theta_n}^+)$ is the initial value of the state at the start of the n^{th} stage and includes the residue of partial transient evolutions caused by past mismatches between the initial state and the steady state value from all previous stages. For a (stable) periodic system these partial transients settle to a constant periodically varying waveform as shown in the example of Figure 5.7(b). When the system's partial transients have become periodic the initial state and consequently the mismatch between the initial state, and the steady state, also converge to a constant. Depicted in Figure 5.7 is the evolution of a LTP system at a periodic steady state. After every cycle, the state returns to the value it had at the beginning of the cycle, which is expected when the TPBV equality has been satisfied. Using this TPBV argument an

expression for the state at the start of a stage, in terms of the partial steady state, partial resonant and input waveforms can be expressed as shown in Theorem 5.1.

The TPBV requirement restricts the input disturbances to harmonics of the pumping frequency and makes the general power electronic HSM constructed here a harmonic domain model. This is in contrast to the model constructed in [15] and [55] which is a frequency domain model, however the Graetz Bridge modeled is a simpler example as it has no persistent states, so the mismatch at the start of each stage is never a function of the transient response evolved across a cycle.

Theorem 5.1 *For a Piece wise linear time periodic system with N piece-wise linear stages per period of length T the initial state at the start of the n^{th} stage will at the periodic steady state have the value given by equation 5.34, if and only if $\|\Phi(T + t^+_{\theta_n}, t^+_{\theta_n})\| < 1$ for any t.*

$$\begin{aligned}\Delta x_n(t^+_{\theta_n}) = \left(I - \Phi\left(T + t^+_{\theta_n}, t^+_{\theta_n}\right)\right)^{-1} \Bigg\{ & \sum_{m=2}^{n} \Phi\left(t^+_{\theta_n}, t^+_{\theta_m}\right) \Big\{ P[m] \left\{ \Delta x_{PSS_{m-1}}(t^-_{\theta_m}) + \Delta x_{PR_{m-1}}(t^-_{\theta_m}) \right\} \\ & + Q[m]\Delta u_{elec}(t_{\theta_m}) - \Delta x_{PSS_m}(t^+_{\theta_m}) \Big\} \\ + \sum_{m=n+1}^{N} & \Phi\left(T + t^+_{\theta_n}, t^+_{\theta_m}\right) \Big\{ P[m] \left\{ \Delta x_{PSS_{m-1}}(t^-_{\theta_m}) + \Delta x_{PR_{m-1}}(t^-_{\theta_m}) \right\} \\ & + Q[m]\Delta u_{elec}(t_{\theta_m}) - \Delta x_{PSS_m}(t^+_{\theta_m}) \Big\} \Bigg\} \end{aligned} \quad (5.34)$$

Proof The magnitude of the relaxation term at the start of the m^{th} stage can be expressed as a function of the remnant effects of relaxation that occurred in the previous stage, the PSS and PR at the end of the previous stage, the electrical input at the switching instant, and the PSS of the current stage.

$$\begin{aligned}\varepsilon_m(t^+_{\theta_m}) = P[m] & \left\{ x_{PSS_{m-1}}(t^-_{\theta_m}) + x_{PR_{m-1}}(t^-_{\theta_m}) \right\} \\ & + \quad Q[m]u_{elec}(t_{\theta_m}) \\ & \quad - x_{PSS_m}(t^+_{\theta_m}) + \Phi(t^+_{\theta_m}, t^+_{\theta_{m-1}})\varepsilon_{m-1}(t^+_{\theta_{m-1}}) \end{aligned} \quad (5.35)$$

If the switching instant is controlled then $P[m]$ and $Q[m]$ are the projection and injection matrices of the hybrid model. If the switching instant is autonomous then $P[m]$ and $Q[m]$ must also take account of the effect of autonomous switching instants. These switching instances can be gained from equation 3.6 and equation 3.21.

An expression for the N^{th} stage's relaxation in terms of the $N-1$ previous stages can be written by $N-1$ successive substitutions of equation 5.35.

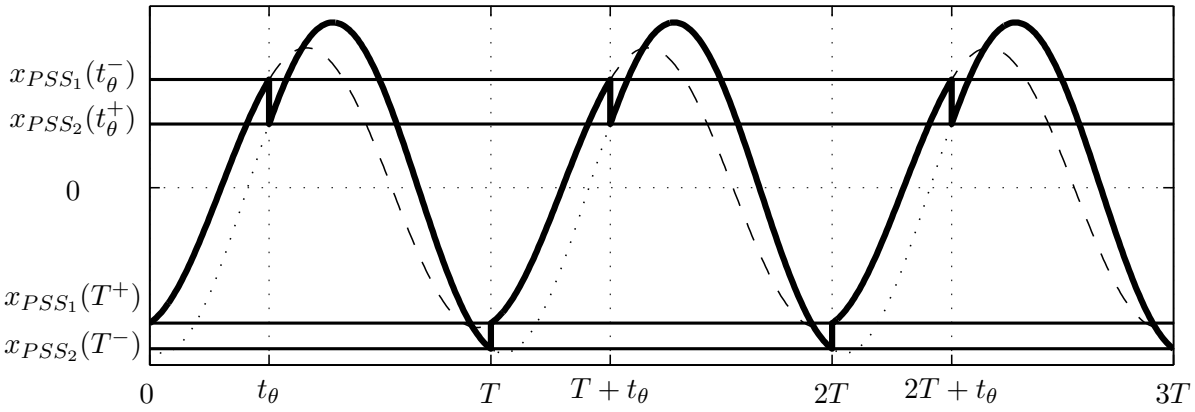

(a) Partial Steady state waveforms

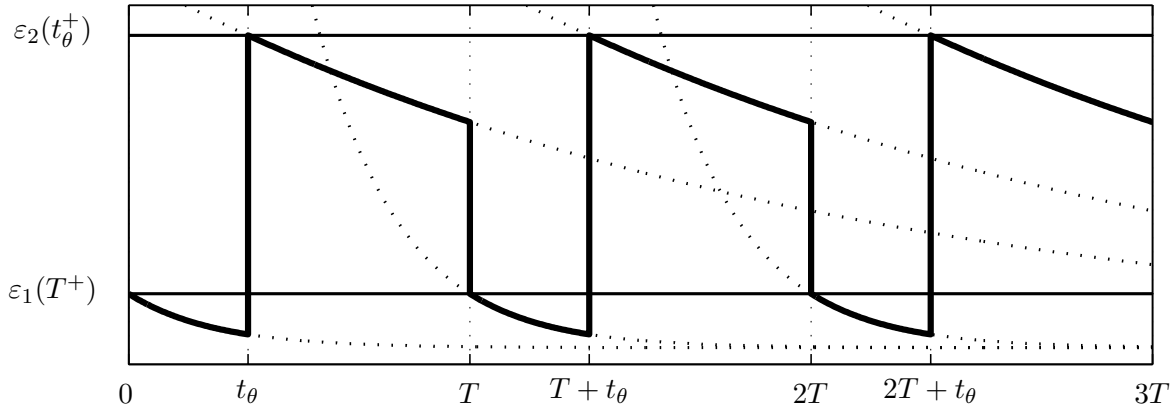

(b) Partial Transient waveforms

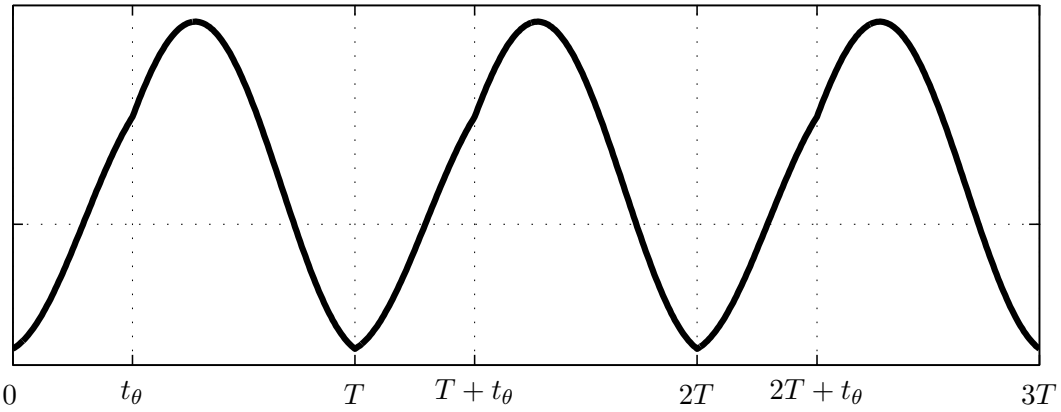

(c) Total Response Waveforms

Figure 5.7 Time domain response of a LTP system with two stages that has reached the periodic steady state. It is assumed that there is no resonant response. The switch between the stages occurs at $t = t_\theta$.

$$\varepsilon_N(t^+_{\theta_N}) = \sum_{m=2}^{N} \Phi\left(t^+_{\theta_N}, t^+_{\theta_m}\right) \Big\{ P[m] \left\{ x_{PSS_{m-1}}(t^-_{\theta_m}) + x_{PR_{m-1}}(t^-_{\theta_m}) \right\} + Q[m] u_{elec}(t_{\theta_m}) - x_{PSS_m}(t^+_{\theta_m}) \Big\} + \Phi\left(t^+_{\theta_N}, t^+_{\theta_1}\right) \varepsilon_1(t^+_{\theta_1}) - x_{PSS_N}(t^+_{\theta_N}) \quad (5.36)$$

When a system reaches the steady state then after a cycle with N stages the relaxation term at the start of the $N^{th}+1$ stage, $\varepsilon_{N+1}(t^+_{\theta_{N+1}})$, should be the same as that of the first, $\varepsilon_1(t^+_{\theta_1})$. By extension the states at the start and end of a cycle should also be the same, giving rise to the following identities.

$$\begin{aligned} \varepsilon_{N+1}(t^+_{\theta_N}) &= \varepsilon_1(t^+_{\theta_1}) \\ &= x_1(t^+_{\theta_n}) + x_{PSS_1}(t^+_{\theta_1}) \\ &= x_{N+1}(t^+_{\theta_N}) + x_{PSS_{N+1}}(t^+_{\theta_{N+1}}) \end{aligned} \quad (5.37)$$

By substituting the mismatch variables as functions of the initial state $x_1(t^+_{\theta_n})$ into equation 5.36, equation 5.38 can be derived after collecting terms.

$$x_1(t^+_{\theta_N}) = \left(I - \Phi\left(T + t^+_{\theta_1}, t^+_{\theta_1}\right)\right)^{-1} \Bigg\{ \sum_{m=2}^{N} \Phi\left(t^+_{\theta_N}, t^+_{\theta_m}\right) \Big\{ P[m] \left\{ x_{PSS_{m-1}}(t^-_{\theta_m}) + x_{PR_{m-1}}(t^-_{\theta_m}) \right\} + Q[m] u_{elec}(t_{\theta_m}) - x_{PSS_m}(t^+_{\theta_m}) \Big\} \Bigg\} \quad (5.38)$$

Equation 5.34 is the equivalent equation written more generally for the initial value of the n^{th} stage rather than just the 1^{st} stage. ∎

Remark If the m^{th} switching instant is autonomous then $P[m]$ and $Q[m]$ are the small signal injection and projection matrices of equation 3.6 and equation 3.21.

In equation 5.34, the initial state of the n^{th} stage $x_n(t_{\theta_n})$ is a function of the time domain signals, $u_{elec}(t)$, $x_{PSS_n}(t)$ and $x_{PR_n}(t)$. Ultimately these signals are functions of the harmonic domain input signal, $\hat{u}_{elec}$. The sensitivity of $x_n(t^+_{\theta_n})$ to small changes in $\hat{u}_{elec}$ is expressed in the partial derivative of equation 5.39.

$$\frac{\partial x_n(t_{\theta_n}^+)}{\partial \hat{u}_{elec}(jk\omega_1)} = \left(I - \Phi\left(T + t_{\theta_n}^+, t_{\theta_n^+}\right)\right)^{-1} \Bigg\{ \sum_{m=1}^{n} \Phi\left(t_{\theta_n}^+, t_{\theta_m}^+\right) \Psi[t_{\theta_m}] \Bigg\{ P[m] \Bigg(\frac{\partial x_{PSS_{m-1}}(t_{\theta_m}^-)}{\partial \hat{u}_{elec}} + \frac{\partial x_{PR_{m-1}}(t_{\theta_m}^-)}{\partial \hat{u}_{elec}} \Bigg) + Q[m] - \frac{\partial x_{PSS_m}(t_{\theta_m}^-)}{\partial \hat{u}_{elec}} \Bigg\} + \sum_{m=n+1}^{N} \Phi\left(t_{\theta_n}^+, t_{\theta_m}^+\right) \Psi[t_{\theta_m}] \Bigg\{ P[m] \Bigg(\frac{\partial x_{PSS_{m-1}}(t_{\theta_m}^-)}{\partial \hat{u}_{elec}} + \frac{\partial x_{PR_{m-1}}(t_{\theta_m}^-)}{\partial \hat{u}_{elec}} \Bigg) + Q[m] - \frac{\partial x_{PSS_n}(t_{\theta_m}^-)}{\partial \hat{u}_{elec}} \Bigg\} \Bigg\} \quad (5.39)$$

The relationship between the time domain PSS and the harmonic domain input is that of equation 5.33 which used the point sampling function. A similar relationship between the PR and the harmonic domain input could also be described using the point sampling function, however, this causes truncation errors due to Gibb's Phenomenon if the PR is sampled at the end of a cycle where it is discontinuous. Instead the elements $\frac{\partial x_{PR_{m-1}}(t_{\theta_m}^-)}{\partial \hat{u}_{elec}}$ which is in the form of a row vector, can be directly obtained from equation 5.40, which describes the k^{th} element of the vector.

$$\frac{\partial x_{PR_{m-1}}(t_{\theta_m}^-)}{\partial \hat{u}_{elec}}(jk\omega_1) = \begin{cases} T_{s_n}(t_{\theta_m} - t_{\theta_{m-1}}) e^{jk\omega_1(t_{\theta_m} - t_{\theta_{m-1}})} T_{s_n}^+ & \forall\, jk\omega_1 \in \{\lambda_{m-1}\} \\ 0 & \forall\, jk\omega_1 \notin \{\lambda_{m-1}\} \end{cases} \quad (5.40)$$

Partial Transient Shape

The harmonics needed to build the shape of the partial transient are found via a direct evaluation of the FSCI, as shown in equation 5.41.

$$\begin{aligned} x_{PT_n}(jg\omega_1) &= \frac{1}{T}\int_0^T e^{(A_n - jgI\omega_1)t - A_n t_{\theta_n}} \varepsilon_n(t_{\theta_n}) dt \\ &= \begin{cases} \frac{(A_n - jg\omega_1)^{-1}}{T}\left\{ e^{(A_n - jgI\omega_1)T - A_n t_{\theta_n}} - e^{-A_n t_{\theta_n}} \right\} \varepsilon_n(t_{\theta_n}) & jg\omega_1 \notin \{\lambda_n\} \\ \left\{ \left\{ \frac{T_{ns_n}}{T}\left\{ \lambda_{ns_n} - jgI\omega_1 \right\} \times \right. \right. & \\ \left. \left\{ e^{(\lambda_{ns_n} - jgI\omega_1)T} - I \right\} T_{ns_n}^+ \right\} + T_{s_n} T_{s_n}^+ \Bigg\} e^{-A_n t_0} \varepsilon_n(t_{\theta_n}) & jg\omega_1 \in \{\lambda_n\} \end{cases} \end{aligned} \quad (5.41)$$

The second solution occurs when the output frequency falls on an Eigenvalue of the dynamics matrix, when this occurs $A_n - jg\omega_1$ is singular, and not invertible. A solution in this case is found by first decomposing A_n into a diagonal form $T_n\lambda_n T_n^{-1}$, where λ_n is a diagonal matrix containing the Eigenvalues of A_n. The part of λ_n, with diagonal elements equal to $jg\omega_1$ is partitioned into the *singular* portion λ_{s_n}, whilst the rest is partitioned into the *non-singular* portion λ_{ns_n}. Each portion inside the FSCI is then evaluated separately. In Appendix A a similar technique is used to find the evolution of a LTI system subjected to a resonant source.

The form of a transfer between the time domain mismatch variable and the harmonic domain partial transient response is that of equation 5.42, the elements of this transfer can be gained from equation 5.41.

$$\Delta\hat{x}_{PT_n} = \frac{\partial\hat{x}_{PT_n}}{\partial\varepsilon_n(t_{\theta_n})}\Delta\varepsilon_n(t_{\theta_n}) \tag{5.42}$$

Final Partial Transient Response

By combining equations 5.42, 5.33 and 5.39 a single HSM transfer for the partial transient response can be formed as shown in equation 5.43.

$$\begin{aligned}\Delta\hat{x}_{PT_n} &= \frac{\partial\hat{x}_{PT_n}}{\partial\varepsilon_n(t^+_{\theta_n})}\left(\frac{\partial x_n(t^+_{\theta_n})}{\partial\hat{u}_{elec}} - \frac{\partial x_{PSS_n}(t^+_{\theta_n})}{\partial\hat{u}_{elec}}\right)\Delta\hat{u}_{elec} \\ &= \frac{\partial\hat{x}_{PT_n}}{\partial\hat{u}_{elec}}\Delta\hat{u}_{elec}\end{aligned} \tag{5.43}$$

Sampled Partial Transient (SPT) In a similar manner as was done for the SPR the SPT harmonics can be found by altering the limits of the integral 5.41 to t_{θ_n} and $t_{\theta_{n+1}}$. For the sake of brevity this is not done here.

5.4.4 Total response

Using superposition, the total response of the system is derived from the summation of each stage's SPSS, SPT, and SPR responses as expressed in equation 5.44.

$$\begin{aligned}\Delta\hat{x} &= \sum_{n=1}^{N}\hat{x}_{SPT_n}+\sum_{n=1}^{N}\hat{x}_{SPR_n}+\sum_{n=1}^{N}\hat{x}_{SPSS_n}\\ &= \left\{\sum_{n=1}^{N}\Delta\frac{\partial\hat{x}_{SPT_n}}{\partial\hat{u}_{elec}}+\sum_{n=1}^{N}\Delta\frac{\partial\hat{x}_{SPR_n}}{\partial\hat{u}_{elec}}\right.\\ &+ \left.\sum_{n=1}^{N}\Delta\frac{\partial\hat{x}_{SPSS_n}}{\partial\hat{u}_{elec}}\right\}\Delta\hat{u}_{elec}\end{aligned} \tag{5.44}$$

5.5 CONTROLLED SWITCHES

In this section, the effect of delays and advances in the firing signal sent to controlled switches is included.

When control inputs are included the HD model of the general power electronic converter has the form of equation 5.45.

$$\hat{x} = f(\hat{u}_{elec}, \hat{u}_{ctrl}) \tag{5.45}$$

The small signal linearized equivalent of this model is that of equation 5.46.

$$\Delta\hat{x} = \frac{\partial\hat{x}}{\partial\hat{u}_{elec}}\Delta\hat{u}_{elec}+\frac{\partial\hat{x}}{\partial\hat{u}_{ctrl}}\Delta\hat{u}_{ctrl} \tag{5.46}$$

The first partial derivative is the equation 5.44, derived in the previous sections. The second partial derivative is the small signal effect of control disturbances on the state of the system. The derivation of this PD is the subject of this section and its formulation has similarities to the partial transient of equation 5.43.

The control vector $\Delta\hat{u}_{ctrl}$ has one element, $\Delta\hat{u}_{ctrl_n}$, for every controlled switching instant of the base case. Each element is expressed here as a harmonic domain signal. The effect of a controlled SIV is to advance or delay the change from one stage's dynamic equations to the next. The size of the delay for the n^{th} switching instant is a direct evaluation of the $\Delta\hat{u}_{ctrl_n}$ at the switching instant, t_{θ_n}. This can be easily found using the point sampling function

$$\Delta u_{ctrl_n}(t_{\theta_n}) = \Psi[t_{\theta_n}]\Delta\hat{u}_{ctrl_n} \tag{5.47}$$

The small signal effect of this delay is to step change the state at the start of the new stage by the amount given in equation 3.6, is repeated below.

$$\Delta x(t_{\theta_n}^+) = \left\{ P[n]\frac{\partial x(t_{\theta_n}^-)}{\partial t} + Q[n]\frac{\partial u_{elec}(t_{\theta_n})}{\partial t} - \frac{\partial x(t_{\theta_n}^+)}{\partial t} \right\} \Delta u_{ctrl_n}(t_{\theta_n})$$

The step change in state occurs every time that stage is visited. Using a similar TPBV argument as was used in formulating the PT contributions, the effect on the initial state of the n^{th} stage from the m^{th} controlled switching instant is that of equation 5.48.

$$\begin{aligned} \Delta x_n(t_{\theta_n}^+) &= \frac{\partial x_n(t_{\theta_n}^+)}{\partial \hat{u}_{ctrl_m}} \Delta \hat{u}_{ctrl_m} \\ &= \left(I - \Phi\left(T + t_{\theta_n}^+, t_{\theta_n}^+\right)\right)^{-1} \Phi\left(t_{\theta_n}^+, t_{\theta_m}^+\right) \left\{ P[n]\frac{\partial x(t_{\theta_m}^-)}{\partial t} \right. \\ &\quad \left. + Q[n]\frac{\partial u_{elec}(t_{\theta_n})}{\partial t} - \frac{\partial x(t_{\theta_m}^+)}{\partial t} \right\} \Psi[t_{\theta_m}] \Delta \hat{u}_{ctrl_m} \end{aligned} \tag{5.48}$$

This equation is valid only when $m < n$. If $m \geq n$ then the term $\Phi\left(t_{\theta_n}^+, t_{\theta_m}^+\right)$ is replaced with $\Phi\left(T + t_{\theta_n}^+, t_{\theta_m}^+\right)$.

The change in evolution of each stage is shaped by the same function as the PT and the harmonic content of each evolution is given by the same HSM, defined in equation 5.42, where the change in mismatch is $x_n(t_{\theta_n}^+)$.

$$\Delta \hat{x}_{PT_n} = \frac{\partial \hat{x}_{PT_n}}{\partial \varepsilon_n(t_{\theta_n}^+)} \frac{\partial x_n(t_{\theta_n}^+)}{\partial \hat{u}_{elec}} \Delta \hat{u}_{elec} \tag{5.49}$$

The total effect of the controlled SIVs (the second PD of equation 5.46) can be then be found by the summation of the control induced PT from each stages.

5.6 SWITCHING INSTANT VARIATION OF AUTONOMOUS SWITCHES

In the PT transfer the effect of autonomous switching instants was embedded in the partial transient response of equation 5.34. The terms $P[m]$ and $Q[m]$ included the effect of SIV of autonomous switches. In cases where the SIV is required for observation, the SIV can be described by equation 5.50 which shows the autonomous SIV, Δt_{θ_n}, as a function of the electrical inputs, and the controlled SIV inputs.

$$\Delta t_{\theta_n} = \frac{-1}{\frac{\partial V(t_{\theta_n})}{\partial t}} \Bigg\{ g1_n \Bigg\{ \frac{\partial x_{PT_{n-1}}(t_{\theta_n})}{\partial \hat{u}_{elec}} + \frac{\partial x_{PR_{n-1}}(t_{\theta_n})}{\partial \hat{u}_{elec}} + \frac{\partial x_{PSS_{n-1}}(t_{\theta_n})}{\partial \hat{u}_{elec}} \Bigg\} + g2_n \Psi[t_{\theta_n}] \Bigg\} \Delta \hat{u}_{elec} + \Bigg\{ g1_n \frac{\partial x_{PT_{n-1}}(t_{\theta_n})}{\partial \hat{u}_{ctrl}} \Bigg\} \Delta \hat{u}_{ctrl} \quad (5.50)$$

All the partial derivatives terms of the right of this equation can be found from previously presented expressions in this chapter.

5.7 TRANSFERS TO SOURCE OUTPUTS

Transfers to outputs of each stage are of a similar form to the transfers to the states, where the outputs are a linear combination of the state and the input as per the output equation of equation 5.51.

$$y(t) = Cx(t) + Du_{elec}(t) \quad (5.51)$$

Most of the time, as was discussed in Section 13, the small signal output linearly follows the state and the input. In the harmonic domain this following of the state and the input is achieved by multiplying 5.44 by the appropriate state observation matrix, C_n, and the input by the appropriate input feed-forward matrix, D_n, and rectangular sampling function, as shown in equation 5.52.

$$\Delta \hat{y} = \Bigg\{ \sum_{n=1}^{N} C_n \frac{\partial \hat{x}_{SPT_n}}{\partial \hat{u}_{elec}} + \sum_{n=1}^{N} C_n \frac{\partial \hat{x}_{SPR_n}}{\partial \hat{u}_{elec}} + \sum_{n=1}^{N} C_n \frac{\partial \hat{x}_{SPSS_n}}{\partial \hat{u}_{elec}} + \sum_{n=1}^{N} \Psi[t_{\theta_{n+1}}, t_{\theta_n}] D_n \Bigg\} \Delta \hat{u}_{elec} + \Bigg\{ \sum_{n=1}^{N} C_n \frac{\partial \hat{x}_{SPT_n}}{\partial \hat{u}_{ctrl}} \Bigg\} \Delta \hat{u}_{ctrl} \quad (5.52)$$

This holds true at all points except at variable switching instants where the output is described by the impulse of equation 3.17 which is repeated below.

$$\begin{aligned}\Delta y(t_{\theta_n}) &= \frac{\partial y_n(t_{\theta_n})}{\partial t_{\theta_n}}\Delta t_{\theta_n} \\ &= \lim_{t\to t_{\theta_n}}\left\{y(t_{\theta_n}^-) - y(t_{\theta_n}^+)\right\}\delta\left(t - t_{\theta_n}\right)\Delta t_{\theta_n} \\ &= \left\{y(t_{\theta_n}^-) - y(t_{\theta_n}^+)\right\}\delta\left(0\right)\Delta t_{\theta_n}\end{aligned}$$

Using this partial derivative a complete expression for the HD output transfer can be formed, and is written in equation 5.54, remembering that there are two sources of SIV; autonomous and controlled, where autonomous SIVs are ultimately functions either of the electrical inputs or the control inputs.

$$\begin{aligned}\Delta\hat{y} &= \left\{\sum_{n=1}^{N} C_n\frac{\partial\hat{x}_{SPT_n}}{\partial\hat{u}_{elec}} + \sum_{n=1}^{N} C_n\frac{\partial\hat{x}_{SPR_n}}{\partial\hat{u}_{elec}} + \sum_{n=1}^{N} C_n\frac{\partial\hat{x}_{SPSS_n}}{\partial\hat{u}_{elec}}\right. \\ &\quad \left. + \sum_{n=1}^{N}\Psi[t_{\theta_{n+1}}, t_{\theta_n}]D_n\sum_{n=1}^{N}\frac{\partial\hat{y}}{\partial t_{\theta_n}}\frac{\partial t_{\theta_n}}{\partial\hat{u}_{elec}}\right\}\Delta\hat{u}_{elec} \qquad (5.53) \\ &\quad + \left\{\sum_{n=1}^{N}\frac{\partial\hat{y}}{\partial t_{\theta_n}}\frac{\partial t_{\theta_n}}{\partial\hat{u}_{ctrl}} + C_n\frac{\partial\hat{x}_{SPT_n}}{\partial\hat{u}_{ctrl}}\right\}\Delta\hat{u}_{ctrl} \qquad (5.54)\end{aligned}$$

Where $\frac{\partial\hat{y}}{\partial t_{\theta_n}}$ is a column vector whose coefficients are the Fourier coefficients of an impulse centered at t_{θ_n} multiplied by the constant $\left(y(t_{\theta_n}^-) - y(t_{\theta_n}^+)\right)$.

$$\frac{\partial\hat{y}}{\partial t_{\theta_n}}(jk\omega_1) = \left(y(t_{\theta_n}^-) - y(t_{\theta_n}^+)\right)\frac{1}{T}e^{-jk\omega_1 t_{\theta_n}} \qquad (5.55)$$

5.8 EXAMPLE: BUCK-BOOST CONVERTER

In this section the buck-boost converter studied previously in Chapters 2,3,4 is analyzed with the use of the analytically derived HSM. The base case is that described in Table 3.3.

The discontinuous operated buck-boost example demonstrates the ability of the technique to model converters with transients projected across stages, and to converters with stages that resonate. In the next section the Graetz Bridge is modelled. The Graetz Bridge is included to demonstrate the technique on a device that has received a large focus in the literature. As will be seen despite the greater complexity of the Graetz Bridge schematic, the buck-boost is a more difficult circuit to model.

The the HSMs produced for the buck-boost converter have the structures depicted in Figure 5.8, which were created using MATLAB's *imagesc* imaging function. These images

show the magnitude of the HSM elements in the form of a 2D image, where the cooler colours (blues) are elements of relatively small transfers, the hotter colours (red) are of elements of relatively large transfers.

In studying these images, it is important to note that applied harmonic disturbances are in conjugate frequency pairs. The resulting output disturbance from each conjugate is summed. This summation can result in some cancelling that can't be predicted by the images. However, despite this limitation of the images, they are still useful in giving a rough prediction of the harmonic transfers of the converters inputs, outputs and states. A summarized description of these coupling predictions is presented in the following itemized list.

- **Voltage source distortion.** In plot a) the effect of a low frequency voltage source distortion will predominantly affect only the low frequency components of the inductor current. In plot d) the effect on the disturbance on the capacitor voltage is even more biased to the DC component. In plot g) the effect on the source current is strongly diagonal, where the largest affected harmonic of the source current has an identical frequency to the disturbance. The spectrum of the source current will also include a large spread of harmonics centered around the disturbance frequency, this is in contrast to the narrower bands of the inductor current and capacitor voltage. To electrical disturbances the buck-boost effectively operates as a low pass filter, this is shown in all three of the voltage source distortion transfers where attenuation at high frequencies occurs.

- **Switching distortion** Unsurprisingly the effect of a control disturbance is not attenuated with increased frequency. The only thing of importance is the size of the control disturbance at the base case SI. This is shown in graphs b), c) e) f) and h) which all show that the effect of a control distortion as a step change on the appropriate state or output, as shown by the narrow band of resultant frequencies centered around DC in each of these graphs. In graph i) a similar independence on control disturbance frequency is shown, however in this transfer the result is an impulse. This impulse is evident from the complete spectrum of harmonics resulting from each input disturbance. This is consistent with the remark of Theory 3.3 which states that an impulse only occurs if the base case were discontinuous at a switching instant.

5.8.1 Verification of Harmonic domain model

The accuracy of the HSM's prediction of the periodic steady state of the buck-boost converter is examined by the application of two distortions, the first is a 1V DC voltage source distortion, and the second is a 1% increase in duty cycle which causes a control ordered delay of 5×10^{-7} off time of the type III controllable switch. The results produced by the

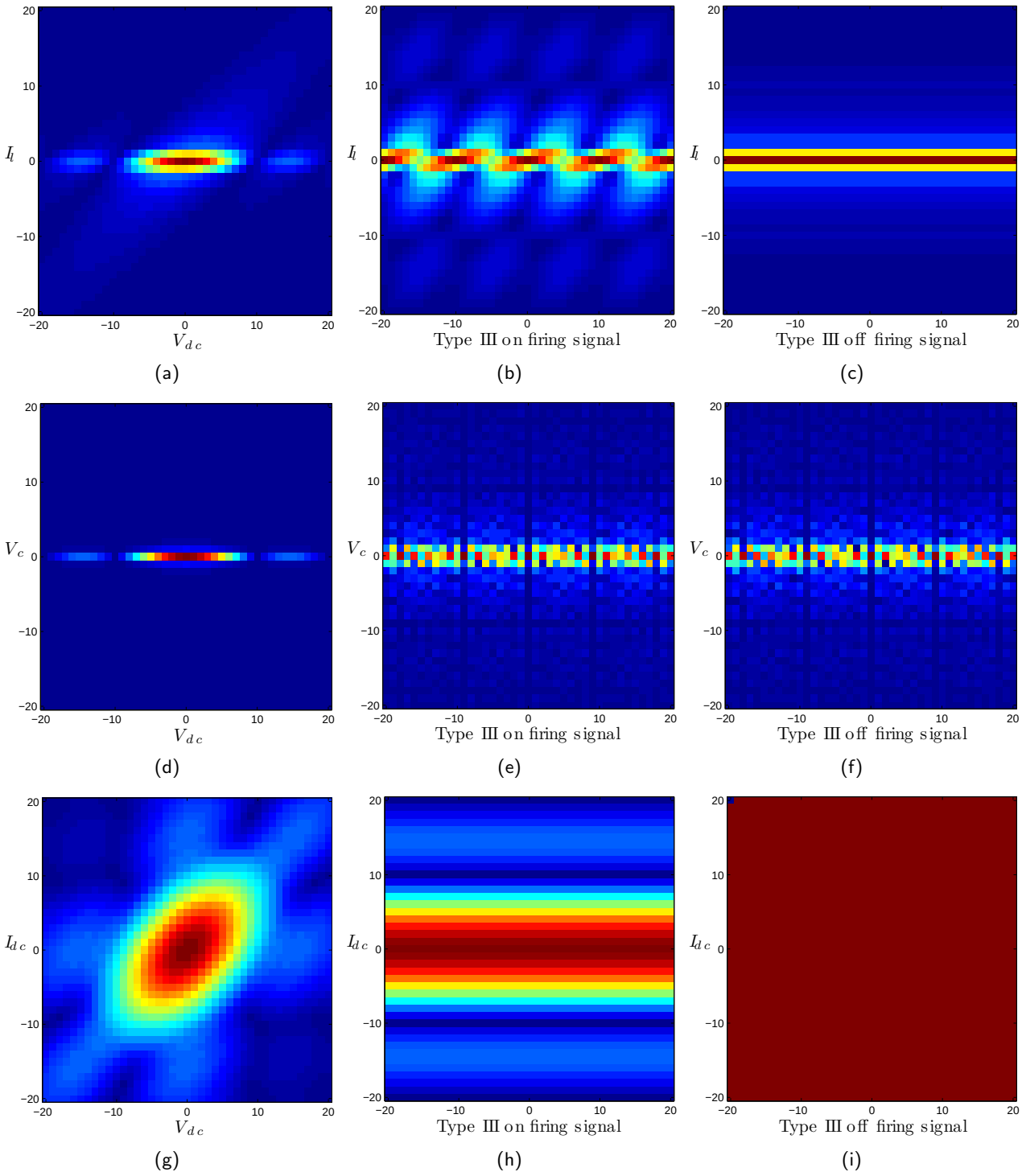

Figure 5.8 Buck-boost HSM, the input of each HSM is shown on the bottom axis, and the output is shown on the left-hand side axis. Each axis contains the set of harmonics from the -20^{th} harmonic to the 20^{th}.

HSM for both of these distortions were compared against PSCAD-EMTDC simulations in Figures 5.9 and 5.10. In each case the resulting state and output spectra are depicted using a magnitude, angle representation of the Fourier series, as opposed to the complex Fourier representation predominantly used in this thesis.

For the voltage distortion, the PSCAD-EMTDC and HSM show an almost exact match. This is not surprising as the discontinuous buck-boost converter's response to voltage disturbances is linear, and no voltage disturbance of any frequency or any magnitude will change the switching instants of the converter.

For the firing order delay, the match although not perfect is still close. The major feature of interest is the output current spectra; both the PSCAD-EMTDC and the HSM spectra are heavily dominated by an impulse. However, the PSCAD-EMTDC has a non impulsive distortion super-imposed on top, it is suspected that this part of the PSCAD-EMTDC distortion is non-linear. This suspicion is confirmed by examining a smaller, 0.1% increase in duty cycle, as shown in Figure 5.11. In this figure the impulse spectrum is retained, but the suspect non-linear contribution to the PSCAD-EMTDC spectrum is greatly reduced. In addition, the phases of the higher frequency components have a much better match for this smaller increase in the switching signal.

5.9 EXAMPLE: GRAETZ BRIDGE

The second example used to demonstrate and validate the HSM is the Graetz Bridge. The operating point of the Graetz Bridge is solved in Chapter 4.

5.9.1 Harmonic Domain HSM

Using the process outlined in this Chapter the electrical and control input partial derivative of the Graetz Bridge are constructed. Visually the transfers of these partial derivatives are depicted in the MATLAB *imagesc* plots of Figures 5.12.

The most obvious difference between the HSM of the Graetz Bridge and the buck-boost is sparsity. The Graetz Bridge HTs are highly sparse compared to the much more continuous nature of most transfers of the single-phase buck-boost converter. Another obvious difference in the Graetz transfers is frequency shifting. In the two terminal transfers between the AC and DC sides the largest elements are frequency transforms to sum and difference terms, these are shown as the double 1st position off diagonals in images e) and g). In the single terminal transforms where frequency shifting does not occur the largest elements are on the main diagonal, as in transfer d), and h). The only transfers that contain impulses are the transfer from the firing signal to the DC voltage, transfer i), and the transfer from the DC current to the DC voltage, transfer h). This is again consistent with the remark of Theory 3.3 that stated that an impulse would only occur if the base case was discontinuous at a switching instant.

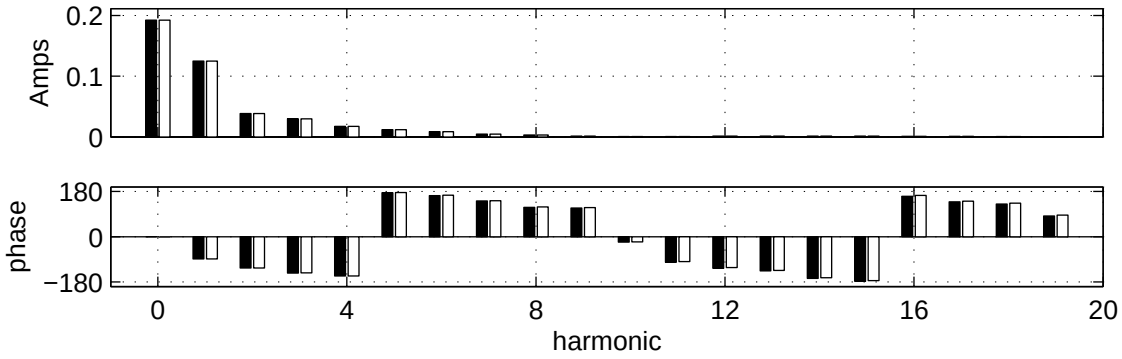

(a) Inductor Current I_l

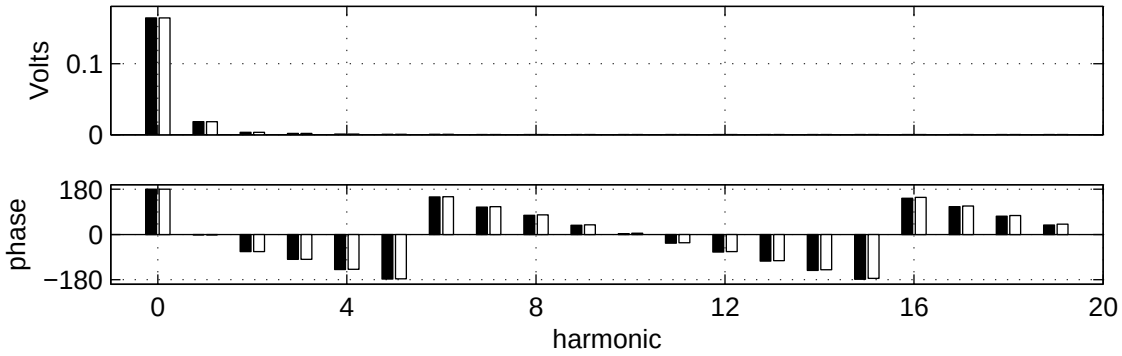

(b) Capacitor Voltage V_c

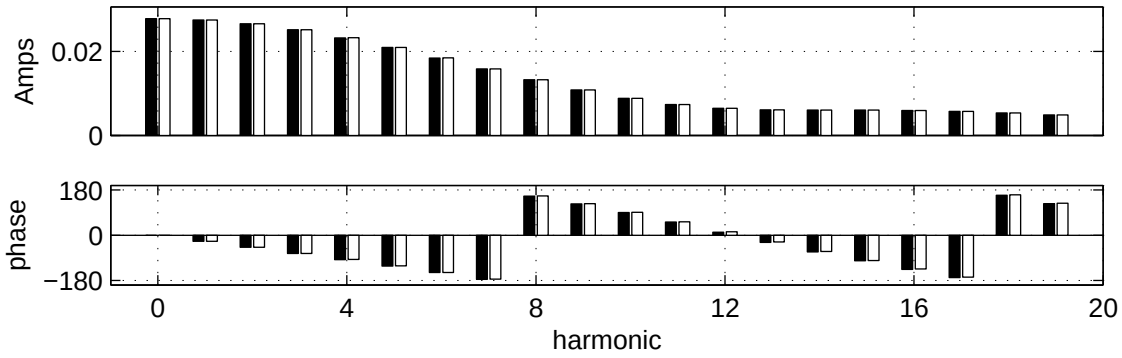

(c) Source Current I_{dc}

Figure 5.9 Comparison between distortions obtained by the HSM and PSCAD-EMTDC to a 1V DC voltage source disturbance for the buck-boost converter. **black** HSM, **white** PSCAD

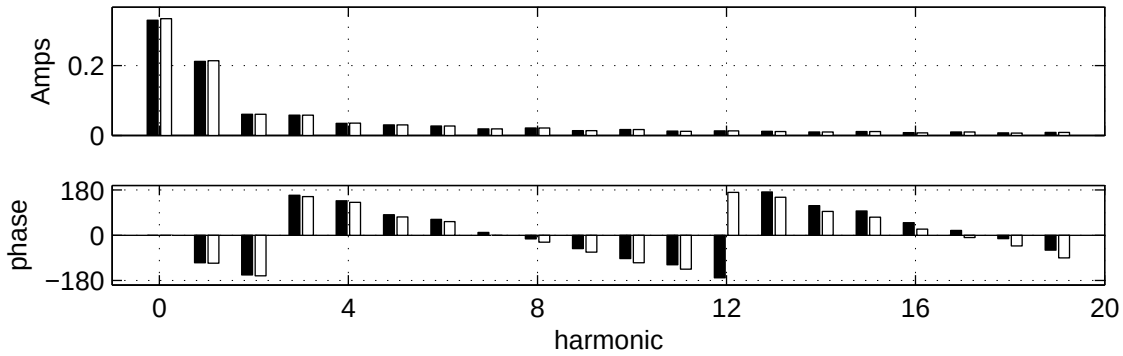

(a) Inductor Current I_l

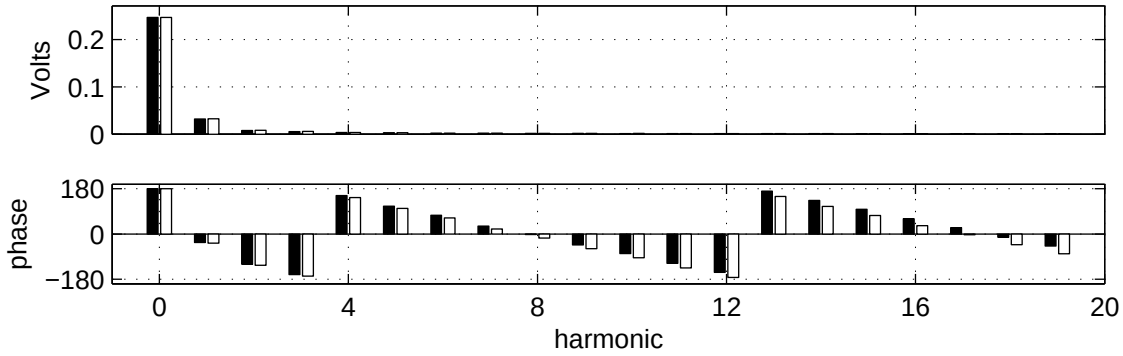

(b) Capacitor Voltage V_c

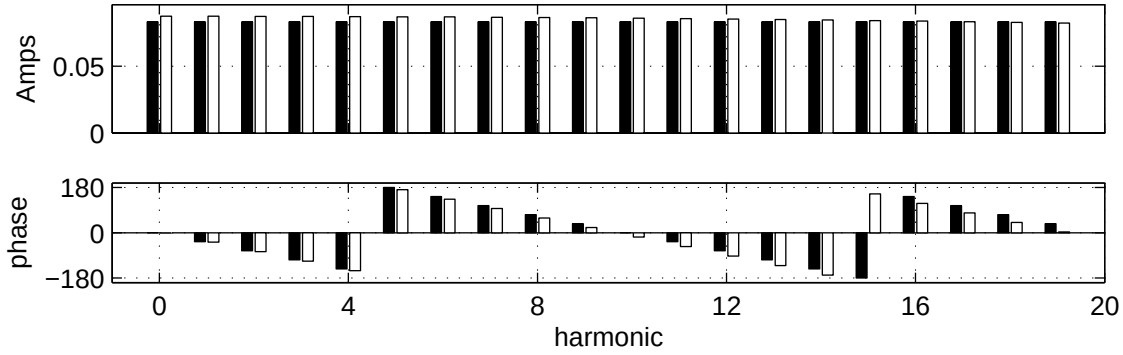

(c) Source Current I_{dc}

Figure 5.10 Comparison between distortions obtained by the HSM and PSCAD-EMTDC to a 1% increase in duty cycle for the buck-boost converter. **black** HSM, **white** PSCAD

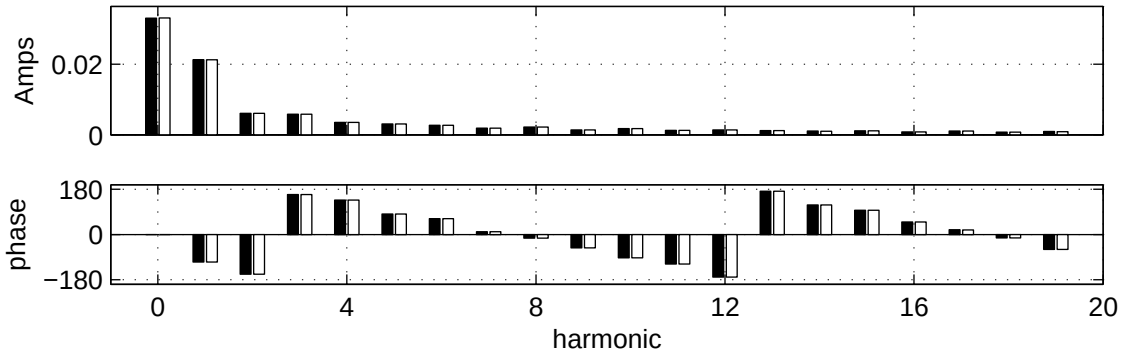

(a) Inductor Current I_l

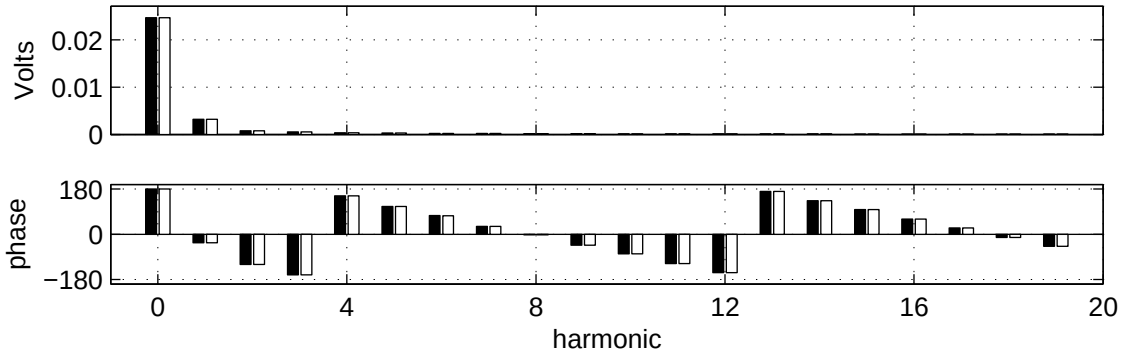

(b) Capacitor Voltage V_c

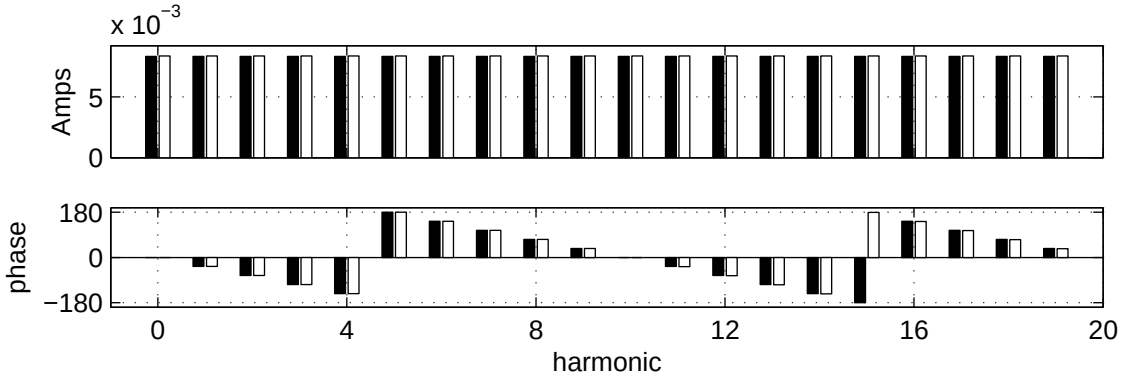

(c) Source Current I_{dc}

Figure 5.11 Comparison between distortions obtained by the HSM and PSCAD-EMTDC to a 0.1% increase in duty cycle for the buck-boost converter. **black** HSM, **white** PSCAD

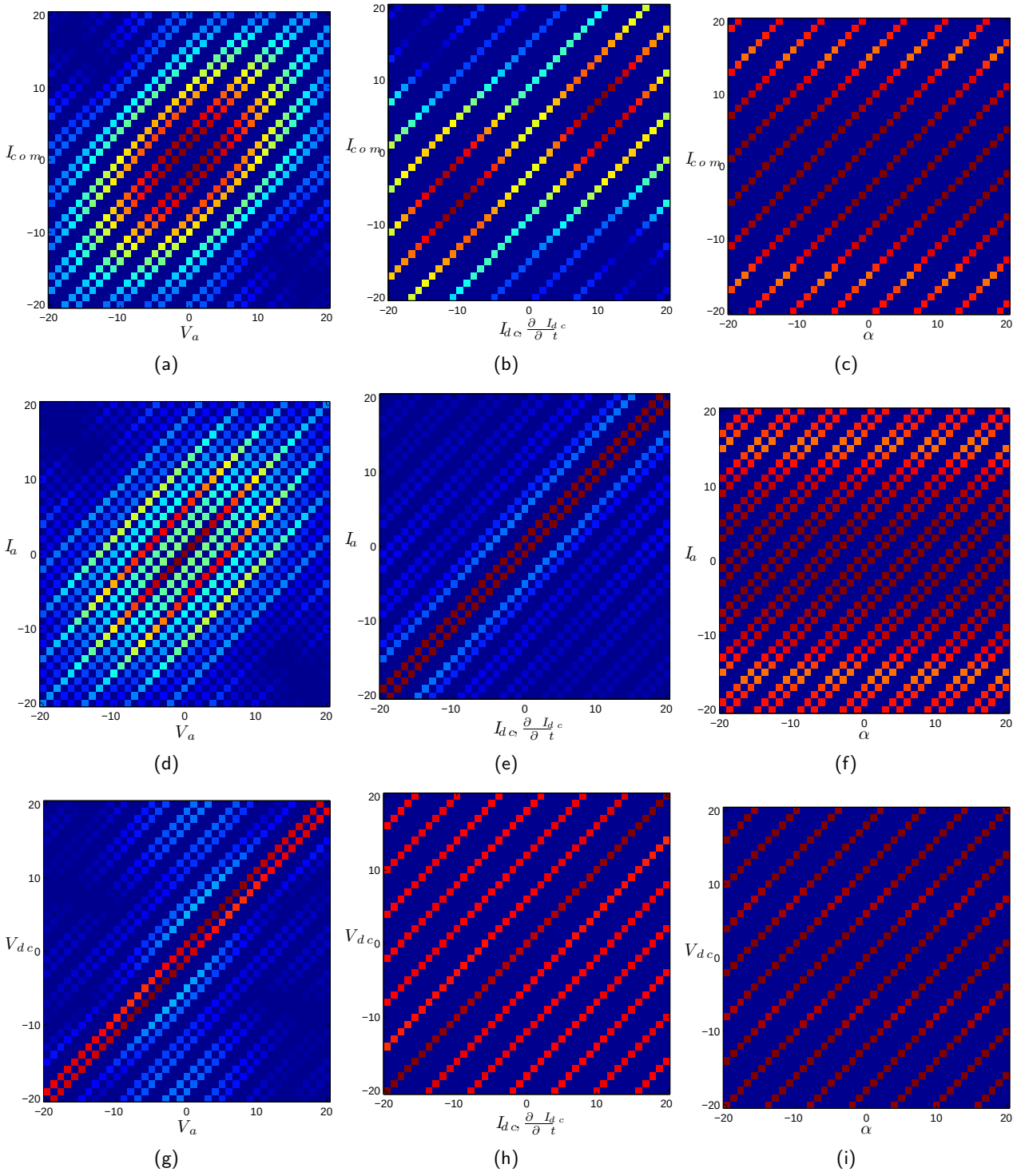

Figure 5.12 Graetz Bridge HSM, the input of each HSM is shown on the bottom axis, and the output is shown on the left-hand side axis.

5.9.2 Verification of Harmonic domain model

The harmonic domain model of the Graetz Bridge is verified for 4 disturbances; a 0.25(p.u.) and a 0.05(p.u.) in the DC component of the DC current source I_{dc}, a 0.05(p.u), 150HZ phase A voltage source distortion V_a, and a 1 degree delay in the firing signal α. Two DC distortions have been chosen to show the linearity of the converter.

As can be seen from the figures the HSM model of the Graetz Bridge and the PSCAD model are in close agreement, similar agreements were found for a range of other disturbances. This is in agreement with the observation made by Hume [5], that the Graetz Bridge is highly linear.

5.10 DISCUSSION

Although the Graetz Bridge seems like a more complicated example than the buck-boost, with its greater passive component count (6 vs 3), its greater switch count (6 vs 2) and its higher number of visited stages (12 vs 3), the buck-boost converter is a much harder device to model as a HSM. Not only does the buck-boost contain complex transient responses that leak across cycles, but it also contains a resonant mode, and has a higher independent state count (2 vs 1). Despite this, due the Graetz bridge's importance in power systems, harmonic modelling of it has been the focus of a large amount of research. However, in the author's opinion this narrow focus, and the exploitation of its simplicity, has resulted (until now) in the lack of a general technique and the greater understanding such a general technique brings. It is believed that the general description contained in this chapter, should be able to produce analytically derived HSM for any of today's and the future's PE devices[2].

Re-arranging the IO The IO of the state space description may not be of the form desired, especially in HDA algorithm that requires the HSM to be in the form of an admittance matrix. Once formed as a HSM the inputs and outputs can easily be arranged, an example of such a rearrangement is shown below in equation 5.56 and equation 5.57. In equation 5.56 the original arrangement is shown with the HTs HSM_1,HSM_2,HSM_3 and HSM_4. In equation 5.57 the IO is re-arranged to with terminal 1's IO ($\hat{I}_1$ and $\hat{O}_1$) swapped.

$$\begin{bmatrix} \hat{O}_1(\{jk\omega_1\}) \\ \hat{O} - 2(\{jk\omega_1\}) \end{bmatrix} = \begin{bmatrix} HSM_1 & HSM_2 \\ HSM_3 & HSM_4 \end{bmatrix} \begin{bmatrix} \hat{I}_1(\{jk\omega_1\}) \\ \hat{I}_2(\{jk\omega_1\}) \end{bmatrix} \tag{5.56}$$

[2]As long as they are able to be described ideally using the hybrid model of Chapter 2

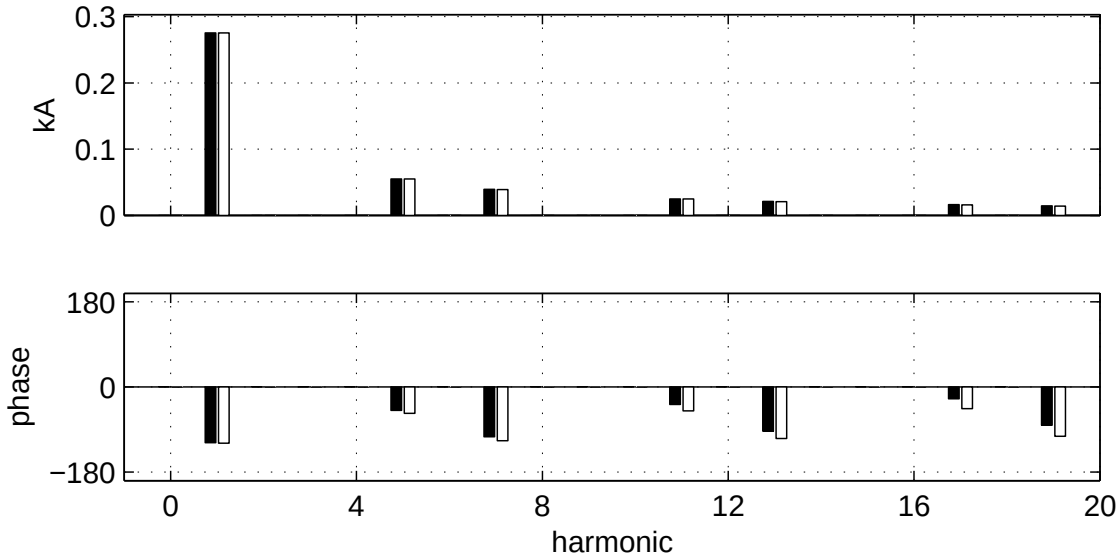

(a) Phase A Current I_a

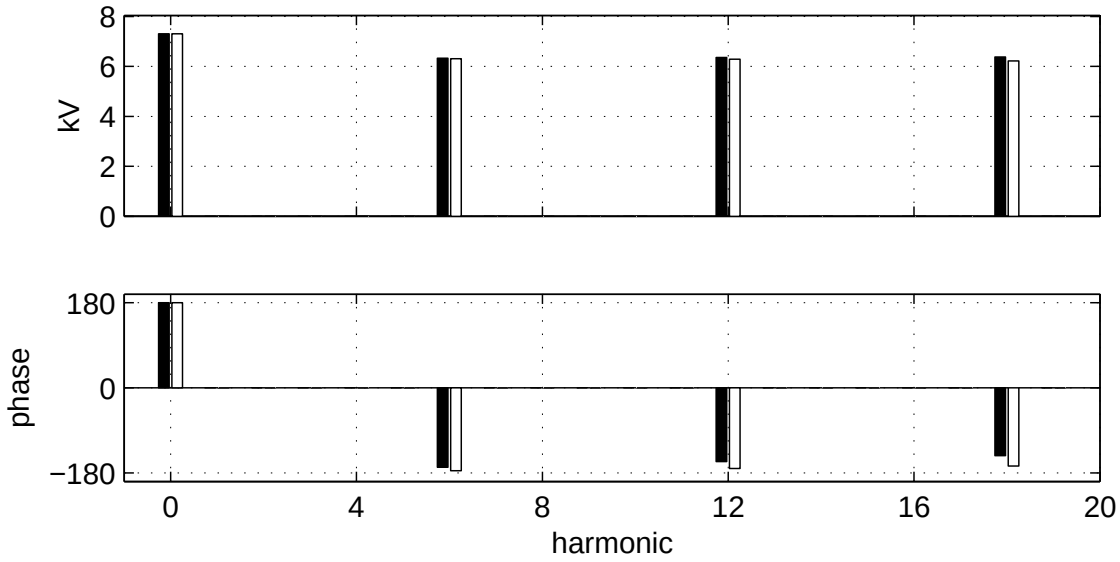

(b) DC Side voltage V_{dc}

Figure 5.13 Comparison between distortions obtained by the HSM and PSCAD-EMTDC to a 0.25 (p.u.) increase in DC current. **black** HSM, **white** PSCAD

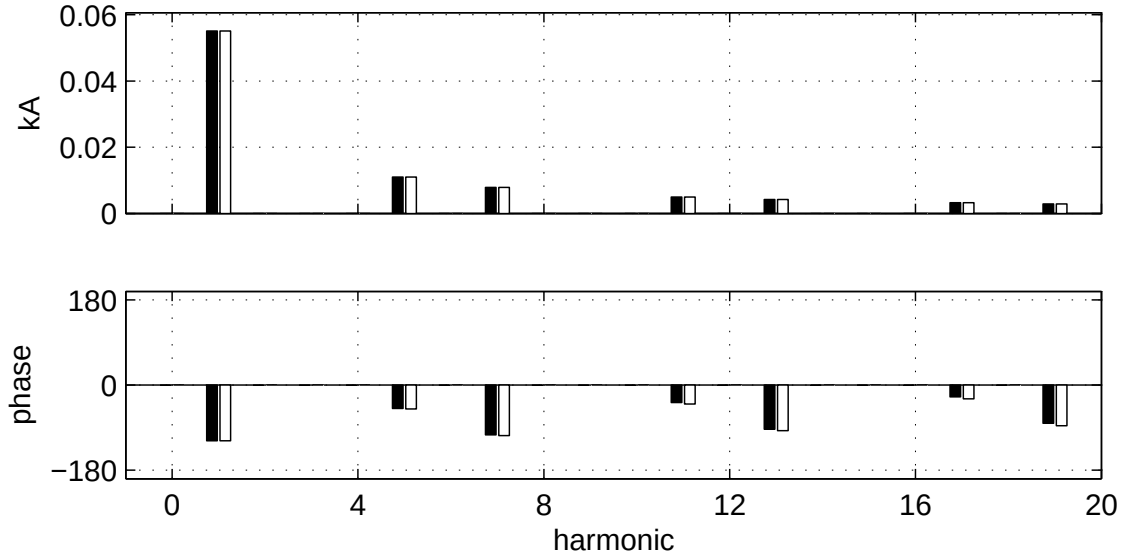

(a) Phase A Current I_a

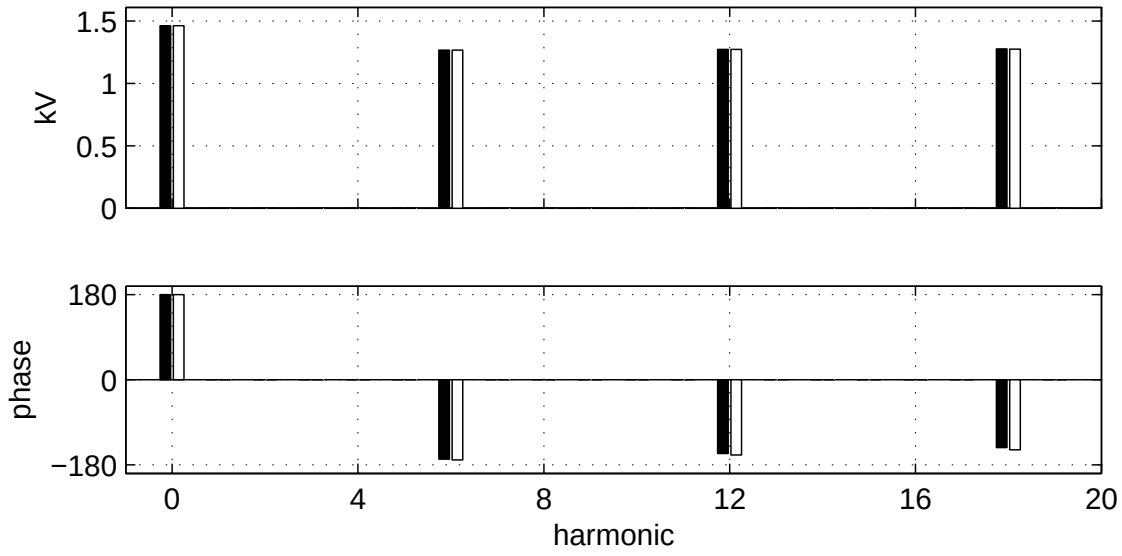

(b) DC Side voltage V_{dc}

Figure 5.14 Comparison between distortions obtained by the HSM and PSCAD-EMTDC to a 0.05 (p.u.) increase in DC current. **black** HSM, **white** PSCAD

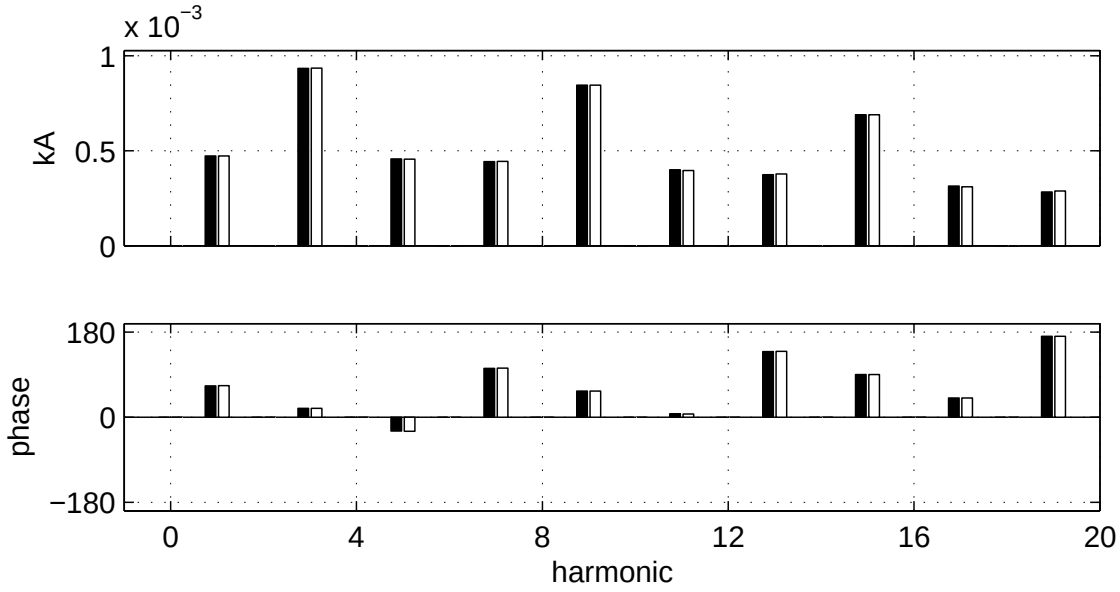

(a) Phase A Current I_a

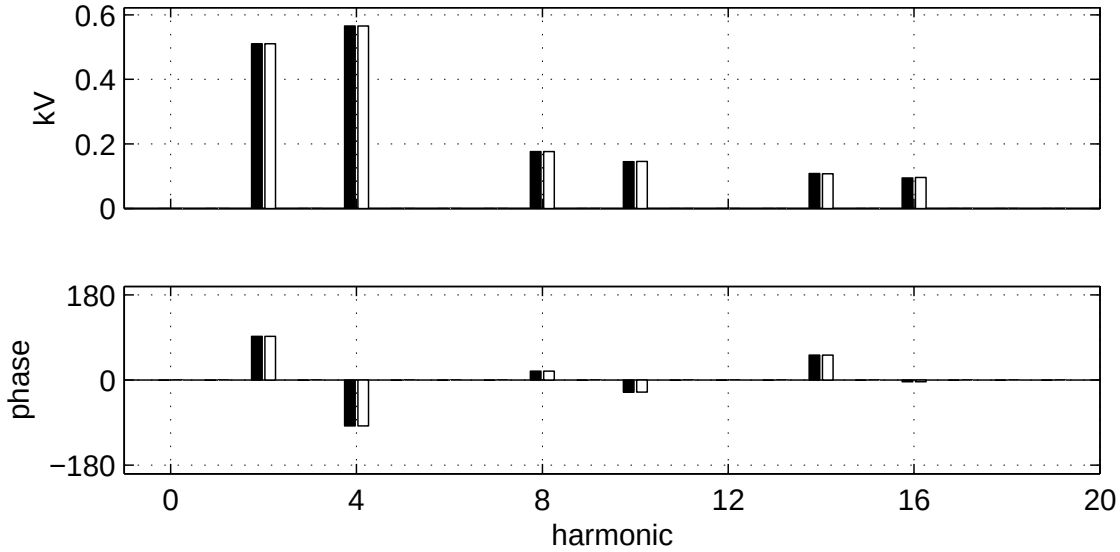

(b) DC Side voltage V_{dc}

Figure 5.15 Comparison between distortions obtained by the HSM and PSCAD-EMTDC to a 0.05 (p.u.) 150 (Hz) disturbance in phase A Voltage. **black** HSM, **white** PSCAD

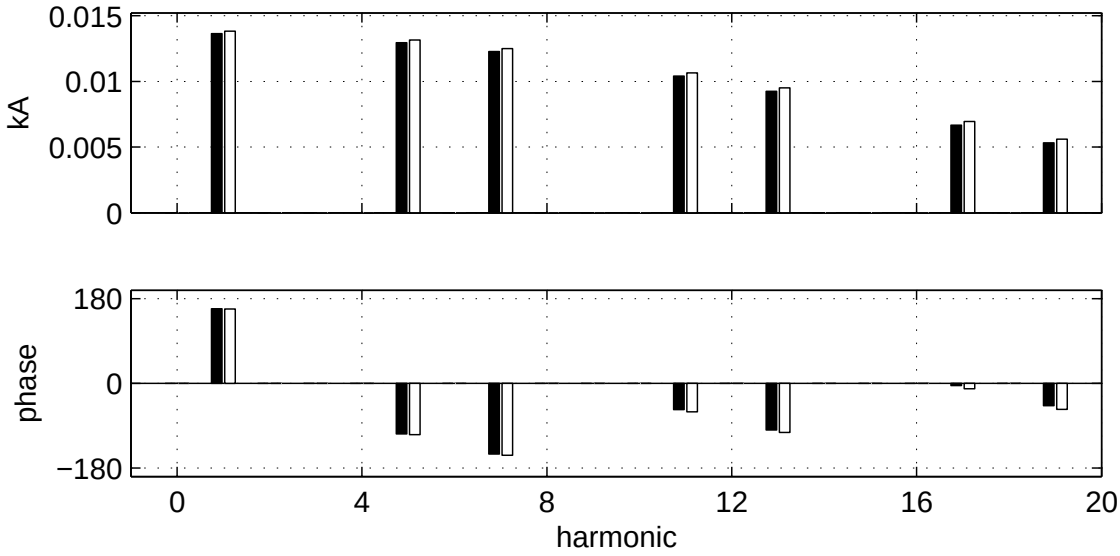

(a) Phase A Current I_a

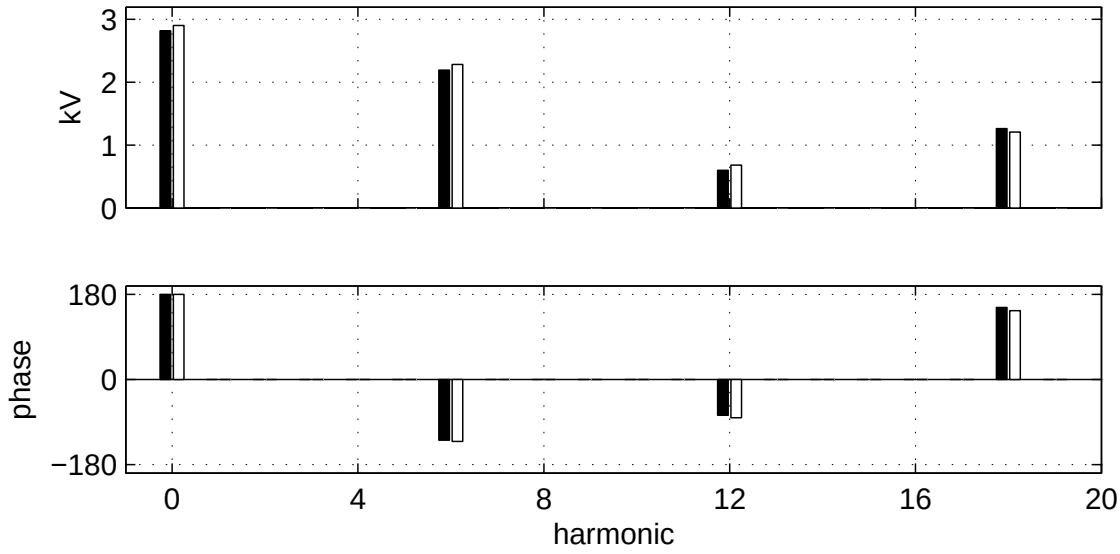

(b) DC Side voltage V_{dc}

Figure 5.16 Comparison between distortions obtained by the HSM and PSCAD-EMTDC to a 1 degree increase in the alpha firing signal. **black** HSM, **white** PSCAD

$$\begin{bmatrix} \hat{I}_1(\{jk\omega_1\}) \\ \hat{O}_2(\{jk\omega_1\}) \end{bmatrix} = \begin{bmatrix} HSM_1^{-1} & HSM_1^{-1}HSM_2 \\ HSM_3HSM_1^{-1} & HSM_4 - HSM_3HSM_1^{-1}HSM_2 \end{bmatrix} \begin{bmatrix} \hat{O}_1(\{jk\omega_1\}) \\ \hat{I}_2(\{jk\omega_1\}) \end{bmatrix} \tag{5.57}$$

Effects of Truncation When the HSM is implemented on a computer truncation of the harmonics is required. Truncated representations lack high frequency components so to some extent results in errors. It was thought (by the author) that lower frequencies transfers may also contain errors as higher frequencies could be *wrapped* back to the lower frequency transfers during their formulation, and their absence due to truncation may result in an error. However, this did not prove to be the case, and the elements in the center of the HSM are unaffected by the truncation of higher frequency components. In the next chapter, Chapter 6, an alternative technique is used to derive the HSM using the harmonic state space. This alternative technique, as will be shown, is susceptible to harmonic truncation.

5.11 CONCLUSION

In this chapter, a general technique for producing the harmonic domain model of a power electronic converter was described. Compared to previous harmonic domain models of power electronic converters the general technique has the made the following advances.

- The technique is general and should be amenable to all converter topologies that can be defined using the hybrid model of Chapter 2.
- The technique is able to model partial transients that evolve at any complex frequency.
- The technique can model harmonic distortion that excites a mode of a stage, i,e. the partial resonant response.
- The technique is successfully able to model transients and the effects of resonance across stage boundaries and across cycles.

The harmonic domain model was verified for a range of distortions for two common converters; the buck-boost converter, and the Graetz bridge. The DC:DC buck-boost converter represented a converter with Partial Transients that lasted a complete cycle, and included both autonomous and controlled switches. The Graetz bridge was modeled as it is a converter that has received considerable modelling effort. In both examples, the technique was verified, and the converters were shown both to be highly linear.

Chapter 6

HARMONIC STATE SPACE MODEL OF A POWER ELECTRONIC CONVERTER

6.1 INTRODUCTION

The small signal model of a piece wise linear system linearized over a cyclic steady state falls within the LTP class of systems. An LTP system is described formally in definition 6.1.

Definition 6.1 (Linear Time Periodic) *A linear time periodic system is described by a set of first order linear equations of the form of equation 6.1.*

$$\begin{aligned} \frac{\partial x(t)}{\partial t} &= A(t)x(t) + B(t)u_{elec}(t) \\ y(t) &= C(t)x(t) + D(t)u_{elec}(t) \end{aligned} \tag{6.1}$$

Where $A(t)$,$B(t)$,$C(t)$ and $D(t)$ are all T-periodic, i.e. $A(T+t) = A(t) \quad \forall t$

The clear difference that this description has with the LTI system familiar to most, is that the system coefficients $A(t)$,$B(t)$,$C(t)$,$D(t)$ are time variant and specifically the variance is T-periodic.

Linear Time Periodic systems have engaged researchers for over one hundred years, originally in the study of celestial objects [56], [9]. More recently Wereley [31] developed the Harmonic State Space (HSS) framework for the study of LTP systems. The key advancement of Wereley's work is that it is analogous to the LTI's State Space (LTISS). Instead of using the s-domain to describe signals, a new signal class, the exponentially modulated periodic domain (or EMP-domain) is used.

In the EMP-domain two parts describe signals, a periodic part represented as a vector of Fourier components, and a complex exponential part. The Harmonic State Space is a

description that maps the fourier components to form a linear algebraic description of the dynamics of a linear time periodic system.

Wereley's work was inspired by the modelling of helicopter rotor blades, however it has been used in the study of power electronics, for a voltage source converter [16], [57], and non-linear power systems [58], [59]. In the circuits described in the literature only fully controlled switches have so far been included. A major class of converters not modelled are those with autonomous switching devices and independent states. This class includes both the discontinuous Buck-Boost converter and the Graetz bridge, but also many others including a large number of discontinuously operated DC:DC converters, the Capacitor Commutated Converter [60], and thyristor circuits in FACTS schemes such as the thyristor controlled static compensator [61].

In this chapter, a method for constructing the HSS of a general power electronic converter based upon the small signal model of Chapter 3 is outlined. The HSS is demonstrated and verified by its application to the familiar discontinuous buck-boost and Graetz Bridge converters.

6.2 HARMONIC STATE SPACE

The harmonic state space is an LTP analogue to the (s-domain) LTI state space (LTISS). The important aspects of the LTI state space are outlined next.

6.2.1 LTI State Space

Of central importance to the LTISS is the domain of the signals – the set of complex exponentials or the s-domain. All physically realizable signals of the LTISS; the input, the steady state response, the transient response, and the output are all described within this space [26]. The only signal not describable as a complex exponential in a LTI system is the resonant response. The form and the relationship between the signals are summarized in Table 6.1.

LTI System Description	symbol	formula
Input	u(t)	$u_0 e^{st}$
Steady State	$x_{ss}(t)$	$(sI - A)^{-1}Bu(t)$
Transient response	$x_{tr}(t)$	$e^{At}\left(x(t_0) - x_{ss}(t_0)\right)$
Output Transient response	$y_{tr}(t)$	$Cx_{tr}(t)$
Output Steady State response	$y_{ss}(t)$	$Cx_{ss}(t)$
Transfer Function	$H(s)$	$C(sI - A)^{-1}B$

Table 6.1 LTI system signals and their relationships

.

The steady state and the transient responses are both described using complex exponentials, and although the transient response evolves at the Eigenvalues of the system space,

the steady state response evolves at the frequencies of the input.

If the system is asymptotically stable, then the transient response will vanish as $t \rightarrow \infty$ at which point the system is at the steady state. The steady state is a *one to one* transformation of the input, where both signals have the same frequencies, differing only in magnitude and phase. This mapping between the signals can be described by a transfer function.

As for the actual state space description, of great important is that the LTISS is a linear algebraic set of differential equations. The easy manipulation of these equations for controller design is the key behind the LTISS's popularity.

In summary, the LTP analogue to the LTISS must meet the following requirements,

1. LTP signal space must be able to model all realizable signals
2. The transient response is associated with the relaxation of the system and will vanish as $t \rightarrow \infty$
3. The steady state outputs are at the same frequencies as the inputs.
4. The steady state space must be a one to one map of the input and this map must be able to be described in a transfer function style.
5. LTP state space must be written as a linear algebraic expression.

6.2.2 LTP signal space: Exponentially Modulated Periodic Domain (EMP-domain)

The first three requirements, and part of the fourth requirement, relate to a signal space that is the equivalent to the complex exponential (or s-domain). Wereley gained this signal, the exponentially modulated periodic (EMP) signal, from Floquet theory. Floquet Theory is described below for a LTP system described as a set of first order equations, and is a replication of that presented in [31]. For a classical approach for systems described as second order or n-order then the reader should consult [62] [63].

Theorem 6.1 (Floquet Theory) *Consider the state space model of the linear time periodic system in Definition 6.1. If the state transition matrix $\Phi(T, 0)$, known as the monodromy matrix, is non-defective then the following results hold:*

1. ***State Transition Matrix*** *The state transition matrix can always be expressed as*

$$\Phi(t, \tau) = P(t)e^{Q(t-\tau)}P^{-1}(\tau) \tag{6.2}$$

where $P(t)$ is a nonsingular T-periodic matrix of dimension $n \times n$, and Q is a constant, possibly complex, matrix of $n \times n$ elements.

2. ***Similarity Transformation*** *The state transformation*

$$x(t) = P(t)v(t) \tag{6.3}$$

transforms x(t) into a set of periodically time varying systems of co-ordinates, v(t), such that the dynamics in the new state space is linear time invariant, that is,

$$\begin{aligned} \dot{v}(t) &= Qv(t) + \hat{B}(t)u(t) \\ y(t) &= \hat{C}(t)v(t) + D(t)u(t) \end{aligned} \tag{6.4, 6.5}$$

where,

$$Q = P^{-1}(t)\left\{A(t)P(t) - \dot{P}(t)\right\} \tag{6.6}$$

$$\hat{B}(t) = P^{-1}(t)B(t) \tag{6.7}$$

$$\hat{C}(t) = P^{-1}(t)C(t) \tag{6.8}$$

3. ***Stability*** *A necessary and sufficient condition for stability is that all eigenvalues of the monodromy matrix lie on the open unit disk.*

Proof See Wereley [31]

Central to Floquet's Theory are the time-invariant matrix Q and the time-variant transfer matrices $P(t)$ and $P^{-1}(t)$. Whilst Floquet theory proves the existence of these matrices, it does not reveal how to find them, however in this discussion about the EMP domain as an analogue to the s-domain only knowledge of their existence is required.

The first result of Floquet theory describes the form of the LTP signal space the Exponentially Modulated Periodic signal or (EMP-domain). Its formal definition is described in Definition 6.2.

Definition 6.2 (Exponentially Modulated Periodic Signal) *A Exponential Modulated Periodic signal is the product of a periodic signal and a complex exponential.*

$$u(t) = e^{st} \sum_{n=-\infty}^{\infty} u_n e^{jn\omega_1 t} \tag{6.9}$$

where $s \in C$

Since all s-domain signals can also be described in the EMP-domain[1], although not uniquely, it follows that the EMP-domain can also describe all physically realizable signals. This observation satisfies the first requirement of the analogue that the EMP signal must be able to model all realizable signals.

The second requirement that the transient response is associated with the relaxation of the system can be partially met by looking at the homogenous response of the system. The homogenous response can be described in terms the state transition matrix of Floquet's theorem.

$$\begin{aligned} x_h(t) &= \Phi(t,t_0)x(t_0) \\ &= P(t)e^{Q(t-t_0)}P^{-1}(t_0)x(t_0) \end{aligned} \tag{6.10}$$

Clearly this is an EMP signal, the term $P^{-1}(t_0)x(t_0)$ is a constant, the term $e^{Q(t-t_0)}$ is a matrix exponential, and the term $P(t)$ is T-periodic. In addition, the exponential evolves according to the eigenvalues of Q, which are the poles of the LTP system.

The steady state is also in the form of an EMP-domain signal. This can be shown with the second result of Floquet's theorem, that the LTP system equations can be transformed to a representation where the dynamics matrix is time-invariant.

$$\dot{v}(t) = Qv(t) + \hat{B}(t)u(t) \tag{6.11}$$

The integral of the initial state problem of this equation is, where it is assumed that $t_0 = 0$.

$$v(t) = \Phi(t,0)v(0) + \int_0^t \Phi(t,\tau)\hat{B}(\tau)u(\tau)d\tau \tag{6.12}$$

By noting that $\Phi(t,\tau) = \Phi(t,0)\Phi(0,\tau)$, and evaluating $\Phi(t,0) = e^{Qt}$, and $\Phi(0,\tau) = e^{-Q\tau}$ then the integral can be rewritten as

$$\begin{aligned} v(t) &= \Phi(t,0)v(0) + \Phi(t,0)\int_0^t \Phi(\tau,0)\hat{B}(\tau)u(\tau)d\tau \\ &= e^{Qt}\left(v(0) + \int_0^t e^{-Q\tau}\hat{B}(\tau)u(\tau)d\tau\right) \end{aligned} \tag{6.13}$$

Substituting $u(t)$, $\hat{B}(t)$ in their EMP and periodic forms respectively, 6.13 becomes 6.14.

[1] the reverse is also true, but in general one EMP signal is described by an infinite set of s-domain signals

$$v(t) = e^{Qt}\left\{v(0) + \int_0^t e^{-Q\tau} \sum_{l=-\infty}^{\infty} \hat{B}_l e^{jl\omega_1\tau} \sum_{m=-\infty}^{\infty} u_m e^{s_m\tau} d\tau\right\} \tag{6.14}$$

Where $s_m = jm\omega_1 + s$.

By using the change of index $s_l = jlw_1 + s$, and then rearranging 6.14 can be rewritten as

$$\begin{aligned} v(t) &= e^{Qt}\left\{v(0) + \int_0^t e^{-Q\tau} \sum_{l,m=-\infty}^{\infty} \hat{B}_l u_m e^{(jl\omega_1+s_m)\tau} d\tau\right\} \\ &= e^{Qt}\left\{v(0) + \int_0^t e^{-Q\tau} \sum_{l,m=-\infty}^{\infty} \hat{B}_{l-m} u_m e^{s_l\tau} d\tau\right\} \\ &= e^{Qt}\left\{v(0) + \sum_{l,m=-\infty}^{\infty} \int_0^t e^{(s_lI-Q)\tau} d\tau \hat{B}_{l-m} u_m\right\} \end{aligned} \tag{6.15}$$

When evaluation this integral, assuming s_l is not an Eigenvalue of Q, it can be equated to

$$\begin{aligned} v(t) &= e^{Qt}\left\{v(0) - \sum_{l,m=-\infty}^{\infty} (s_lI - Q)^{-1} \hat{B}_{l-m} u_m\right\} \\ &\quad + \sum_{l,m=-\infty}^{\infty} (s_lI - Q)^{-1} \hat{B}_{l-m} u_m e^{s_l t} \end{aligned} \tag{6.16}$$

The first line of the equation 6.16 is the transient response of the LTP system. When this response is transformed into the $x(t)$ state space, as shown in equation 6.17, the transient response is in the desired form of an EMP-domain signal, where the modulating matrix exponential is the time exponential of Q and is equivalent to the natural relaxation of the system. This fully satisfies the requirement that the transient response of an LTP system be in the form of an EMP signal.

$$x_{tr}(t) = P(t)e^{Qt}\left\{P^{-1}(t)x(0) - \sum_{l,m=-\infty}^{\infty} (s_lI - Q)^{-1} \hat{B}_{l-m} u_m\right\} \tag{6.17}$$

The steady state response can be gained from 6.16 if the initial state of the system is set to

$$v(0) = \sum_{l,m=-\infty}^{\infty} (s_lI - Q)^{-1} \hat{B}_{l-m} u_m$$

Using this condition for $v(0)$, equation 6.16 yields the steady state response. When the equation is expanded it is in the form of a EMP signal, whose modulating exponential is the same as the input and which is multiplied by a periodic portion described as a summation of exponentials, as shown in equation 6.18.

$$\begin{aligned} v_{ss}(t) &= \sum_{l,m=-\infty}^{\infty} \left(s_l I - Q\right)^{-1} \hat{B}_{l-m} u_m e^{s_l t} \\ &= \sum_{l,m=-\infty}^{\infty} \left\{ \left(s_l I - Q\right)^{-1} \hat{B}_{l-m} u_m e^{jl\omega_1 t} \right\} e^{st} \end{aligned} \tag{6.18}$$

Transformed back to the $x(t)$ state space, and by employing another change of index, $x_{ss}(t)$ is also in the form of an EMP signal, with exponential components at the same frequency as the input.

$$x_{ss}(t) = \sum_{n,l,m=-\infty}^{\infty} \left\{ P_{n-l} \left(s_l I - Q\right)^{-1} \hat{B}_{l-m} u_m e^{jn\omega_1 t} \right\} e^{st} \tag{6.19}$$

Together equations 6.17 and 6.19 fully satisfy requirements that the EMP signal be able to describe the transient and steady state response of an LTP system.

6.2.3 Harmonic State Space (HSS)

The aim of this subsection is to write the LTP state space in the desired linear algebraic form called the Harmonic State Space (HSS), from which the map between the input and the output called the harmonic transfer function (HTF) is formed.

If an LTP system is subjected to an input signal of the form,

$$u_{elec}(t) = \sum_{m=-\infty}^{\infty} u_m e^{(jm\omega_1 + s)t} \tag{6.20}$$

Then the steady state and its gradient will be of the form,

$$x(t) = \sum_{n=-\infty}^{\infty} x_n e^{(jn\omega_1 + s)t} \tag{6.21}$$

$$\dot{x}(t) = \sum_{n=-\infty}^{\infty} \left(jn\omega_1 + s\right) x_n e^{(jn\omega_1 + s)t} \tag{6.22}$$

When these signals are substituted into the dynamics line of equation 6.1, along with the Fourier series expansion of the T-periodic matrix $A(t)$ and $B(t)$, equation 6.23 is formed.

$$\begin{aligned}\sum_{n=-\infty}^{\infty}(jn\omega_1+s)\,x_n e^{(jn\omega_1+s)t} &= \sum_{n=-\infty}^{\infty}A_n e^{jn\omega_1 t}\sum_{m=\infty}^{\infty}x_m e^{(jm\omega_1+s)t} \\ &\quad+\sum_{n=-\infty}^{\infty}B_n e^{jn\omega_1 t}\sum_{m=\infty}^{\infty}u_m e^{(jm\omega_1+s)t} \\ &= \sum_{n,m=-\infty}^{\infty}A_n x_m e^{j(n+m)\omega_1}e^{st}+\sum_{n,m=-\infty}^{\infty}B_n u_m e^{j(n+m)\omega_1}e^{st} \\ &= \sum_{n,m=-\infty}^{\infty}A_{n-m} x_m e^{jn\omega_1}e^{st}+\sum_{n,m=-\infty}^{\infty}B_{n-m} u_m e^{jn\omega_1}e^{st}\end{aligned} \tag{6.23}$$

The solution to this equation is the Fourier terms of the state vector, $x_{-\infty},\ldots,x_{-1},x_0,x_1,\ldots,x_\infty$. By using the *principle of the harmonic balance*, which is stated below, equation 6.23 can be rewritten as a set of linear independent equations.

Principle 6.1 (of the harmonic balance) *Every harmonic of the steady state solution of a LTP system is linearly independent.*

Remark If every harmonic of the steady state solution is linearly independent, then every harmonic of the steady state's gradient is also linearly independent.

Using this principle each harmonic of the gradient of x can be written in terms of the RHS components that have the same frequency, as shown in equation 6.24.

$$(jn\omega_1+s)\,x_n e^{(jn\omega_1+s)t}=\sum_{m=-\infty}^{\infty}A_{n-m}x_m e^{(jn\omega_1+s)t}+\sum_{m=-\infty}^{\infty}B_{n-m}u_m e^{(jn\omega_1+s)t} \tag{6.24}$$

With some manipulation and cancellation, equation 6.25 can be derived.

$$sx_n=\sum_{m=-\infty}^{\infty}A_{n-m}x_m+\sum_{m=-\infty}^{\infty}B_{n-m}u_m-jn\omega_1 x_n \tag{6.25}$$

In this equation, the coefficient of the steady state gradient's n^{th} harmonic is written in terms of the coefficients of the steady state and the input. At the steady state all these coefficients are time-invariant.

A similar equation can be written for each harmonic of the output, as shown in equation 6.26.

$$y_n=\sum_{m=-\infty}^{\infty}C_{n-m}x_m+\sum_{m=-\infty}^{\infty}D_{n-m}u_m \tag{6.26}$$

There is one set of these equations for each harmonic. By using Toeplitz matrices the set of equations can be combined into a single first order DE set with linear coefficients. This equation set forms the HSS, and satisfies part 5 of the analogue, that the governing equations of the LTP system must be written in a linear algebraic form. The formal definition of the HSS is given in Definition 6.3.

The first order set of DEs of the HSS describes the time evolution of the harmonic coefficients of the state and the output. It can be treated and manipulated like any first order set of DEs and the same equations that are used to determine the steady state and transient responses of an LTI system can also be used for the HSS differentials. Importantly the periodic variance of each harmonic has been made implicit.

Definition 6.3 (Harmonic State Space (HSS)) *An LTP system of the form of equation 6.1 can be expressed as equation 6.27*

$$\begin{aligned} sx &= (\mathcal{A}-\mathcal{N})x+\mathcal{B}u \\ y &= \mathcal{C}x+\mathcal{D}u \end{aligned} \tag{6.27}$$

Where the signals x,y,u are of the form of infinite dimensioned vectors of harmonic components

$$x = \begin{bmatrix} \vdots \\ x_{-2} \\ x_{-1} \\ x_0 \\ x_1 \\ x_2 \\ \vdots \end{bmatrix} \tag{6.28}$$

The matrices $\mathcal{A}$,$\mathcal{B}$,$\mathcal{C}$, and $\mathcal{D}$ are double infinite Toeplitz matrices expressed in terms of the Fourier coefficients of the LTP coefficients $A(t)$,$B(t)$,$C(t)$ and $D(t)$ respectively.

$$\mathcal{A} = \begin{bmatrix} \ddots & \vdots & \vdots & \vdots & \vdots & \vdots & \\ \cdots & A_0 & A_{-1} & A_{-2} & A_{-3} & A_{-4} & \cdots \\ \cdots & A_1 & A_0 & A_{-1} & A_{-2} & A_{-3} & \cdots \\ \cdots & A_2 & A_1 & A_0 & A_{-1} & A_{-2} & \cdots \\ \cdots & A_3 & A_2 & A_1 & A_0 & A_{-1} & \cdots \\ \cdots & A_4 & A_3 & A_2 & A_1 & A_0 & \cdots \\ & \vdots & \vdots & \vdots & \vdots & \vdots & \ddots \end{bmatrix} \tag{6.29}$$

$\mathcal{N}$ is the block diagonal matrix of the form

$$\mathcal{N} = \begin{bmatrix} \ddots & & & & & & & \\ & -j2\omega_1 & & & & & & \\ & & -j\omega_1 & & & & & \\ & & & 0 & & & & \\ & & & & j\omega_1 & & & \\ & & & & & j2\omega_1 & & \\ & & & & & & \ddots & \end{bmatrix} \tag{6.30}$$

and $s \in C$.

In a similar manner to the LTI state space a transfer function between the input and the output can be written, this transfer is called the HTF is defined below.

Definition 6.4 (Harmonic Transfer Function (HTF)) *The harmonic transfer function is an infinite dimensioned matrix that maps the harmonics of the input to the harmonics of the output.*

$$\mathcal{H}(s) = \mathcal{C}\left[s\mathcal{I} - (\mathcal{A} - \mathcal{N})\right]^{-1}\mathcal{B} + \mathcal{D} \tag{6.31}$$

The HTF fully satisfies part 4 of the analogue that there should be a linear map between the steady state output and the input. Its satisfaction completes the construction of the analogue to the LTI system. When the HTF is evaluated at $H(0)$, the input is purely harmonic and the HTF produced is equivalent to the HSM developed in the previous chapter.

So far in this discussion it has been assumed that the doubly infinite dimensioned matrices and infinite dimensioned vectors can be easily manipulated. In reality however the matrices and vectors need to be truncated. This truncation and the effect it has on accuracy is the focus of an upcoming section.

6.3 LTP MODEL OF THE POWER ELECTRONIC CONVERTER

In this section a description of the general power electronic converter is described in the form of equation 6.1. As the LTP model is linear the LTP model is based around an operating point, and the deviation from this operating point can be described by the small signal model developed in Chapter 3. This observation reduces the problem to finding the LTP description of the small signal model, i.e finding $A(t)$,$B_{elec}(t)$,$B_{ctrl}(t)$,$C(t)$,$D_{elec}(t)$ and $D_{ctrl}(t)$ of equation 6.32.

$$\begin{aligned} \dot{\Delta x}(t) &= A(t)\Delta x(t) + B_{elec}(t)\Delta u_{elec}(t) + B_{ctrl}\Delta u_{ctrl}(t) \\ \Delta y(t) &= C(t)\Delta x(t) + D_{elec}(t)\Delta u_{elec}(t) + D_{ctrl}\Delta u_{ctrl}(t) \end{aligned} \tag{6.32}$$

As was the case in the previous chapter, the LTP description requires that each stage of the converter have commonly dimensioned state spaces.

The coefficients of the LTP system contain three parts; the contribution from evolution within each stage, the effect of autonomous switching instant variations, and the effect of control switching instant variations. As the system is linear, by using the principle of superposition the contributions can be found separately before they are combined together.

Once the LTP description has been found forming the HSS is relatively trivial as the components of the LTP model are either step functions or impulses. Both impulses functions and step functions have Fourier series that are well known [64].

6.3.1 Contribution of stage evolution

The contribution of evolution during a stage is simply the stage's state space matrices multiplied by identical rectangular functions that each spans the stage's base case duration. For example the contribution from the n^{th} stage to the periodic dynamics matrix is given by equation 6.33 where $\mu(t - t_{\theta_{n+1}})$ is a Heaviside function.

$$A_n \left(\mu(t - t_{\theta_n}) - \mu(t - t_{\theta_{n+1}})\right) \tag{6.33}$$

6.3.2 Contribution of an autonomous switching instants

When a system crosses from one stage to another, the state at the start of the stage is found via the jump destination map, which not only project energy from the old state to the new state but also injects energy from the electrical input. Additionally for a small signal model the effects of autonomous switching instant variation are included. In the small signal model described in Chapter 3, the evolution across a switching instant is described by a difference equation for the state.

$$\Delta x_n(t_{\theta_n}^+) = \left(P[n] + \frac{\partial x_n(t_{\theta_n}^+)}{\partial t_{\theta_n}} \frac{\partial t_{\theta_n}}{\partial x_{n-1}(t_{\theta_n}^-)}\right) \Delta x_{n-1}(t_\theta^-) + \left(Q[n] + \frac{\partial x_n(t_{\theta_n}^+)}{\partial t_{\theta_n}} \frac{\partial t_{\theta_n}}{\partial u(t_{\theta_n})}\right) \Delta u(t_\theta)$$

As the LTP system is continuous instead of explicitly using a difference equation for evolving the state across a switching instant, the dynamics equation is altered to include

an impulse in its gradient. This impulse when integrated will produced the desired step change. The size of this impulse has an area equal to the difference between the post and pre switching states as shown in equation 6.34.

$$\begin{aligned}\lim_{t\to t_{\theta_n}} \frac{\partial x(t)}{\partial t} &= \lim_{t\to t_{\theta_n}} \delta(t-t_{\theta_n})\left[x(t_{\theta_n}^+) - x(t_{\theta_n}^-)\right] \\ &= \delta(0)\left[x(t_{\theta_n}^+) - x(t_{\theta_n}^-)\right] \end{aligned} \tag{6.34}$$

To retain $\frac{\partial x(t)}{\partial t}$ as a function of $x(t)$ and $u(t)$ as $t \to t_{\theta_n}$ then it must have the form

$$\begin{aligned}\lim_{t\to t_{\theta_n}} \frac{\partial x(t)}{\partial t} &= \lim_{t\to t_{\theta_n}} \delta(t-t_{\theta_n})\left(K_1[n]x(t) + K_2[n]u(t)\right) \\ &= \delta(0)\left(K_1[n]x(t_{\theta_n}) + K_2[n]u(t_{\theta_n})\right) \end{aligned} \tag{6.35}$$

By recognizing that if $x(t)$ is discontinuous at t_{θ_n} then $x(t_{\theta_n})$ tends towards the mid point of the pre switching and post switching state, i.e.

$$x(t_{\theta_n}) = \frac{1}{2}\left(x(t_{\theta_n}^+) + x(t_{\theta_n}^-)\right) \tag{6.36}$$

Then by equating equation 6.34 with 6.35, and substituting $x(t_{\theta_n})$ for the expression in equation 6.36 equation 6.37 can be formed.

$$x(t_{\theta_n}^+) = \left(I - \frac{K_1[n]}{2}\right)^{-1}\left(I + \frac{K_1[n]}{2}\right)x(t_{\theta_n}^-) + \left(I - \frac{K_1[n]}{2}\right)^{-1} K_2[n]u(t_{\theta_n}) \tag{6.37}$$

Equation 6.37 has a form similar to the jump destination map of the small signal model, by recognizing this similarity identity equations 6.38 and 6.39 can be written.

$$\left(I - \frac{K_1[n]}{2}\right)^{-1}\left(I + \frac{K_1[n]}{2}\right) = \left(P[n] + \frac{\partial x_n(t_{\theta_n}^+)}{\partial t_{\theta_n}}\frac{\partial t_{\theta_n}}{\partial x_n(t_{\theta_n}^-)}\right) \tag{6.38}$$

$$\left(I - \frac{K_1[n]}{2}\right)^{-1} K_2[n] = \left(Q[n] + \frac{\partial x_n(t_{\theta_n}^+)}{\partial t_{\theta_n}}\frac{\partial t_{\theta_n}}{\partial u(t_{\theta_n})}\right) \tag{6.39}$$

It follows that $K_1[n]$ and $K_2[n]$ should be chosen to satisfy these equations, which leads

to equation 6.40 and 6.41.

$$K_1[n] = 2\left(\left(P[n] + \frac{\partial x_n(t_{\theta_n}^+)}{\partial t_{\theta_n}}\frac{\partial t_{\theta_n}}{\partial x_{n-1}(t_{\theta_n}^-)}\right) + I\right)^{-1}\left(\left(P[n] + \frac{\partial x_n(t_{\theta_n}^+)}{\partial t_{\theta_n}}\frac{\partial t_{\theta_n}}{\partial x_{n-1}(t_{\theta_n}^-)}\right) - I\right) \quad (6.40)$$

$$K_2[n] = \left(I - \frac{1}{2}K_1[n]\right)\left(Q[n] + \frac{\partial x_n(t_{\theta_n}^+)}{\partial t_{\theta_n}}\frac{\partial t_{\theta_n}}{\partial u(t_{\theta_n})}\right) \quad (6.41)$$

Choosing $K_1[n]$ and $K_2[n]$ according to equations 6.40 and 6.41 means that the LTP system steps across the autonomous switching instant identically to the difference equation.

From the small signal model, the output equation at a switching instant is described by an impulse of the form

$$\Delta y_{elec}(t_{\theta_n}) = \lim_{t\to t_{\theta_n}} \frac{\partial y_n(t_{\theta_n})}{\partial t_{\theta_n}}\left(\frac{\partial t_{\theta_n}}{\partial x_{n-1}(t_{\theta_n}^-)}\Delta x_{n-1}(t_\theta^-) + \frac{\partial t_{\theta_n}}{\partial u(t_{\theta_n})}\Delta u(t_\theta)\right) \quad (6.42)$$

Where,

$$\begin{aligned}
\frac{\partial y_n(t_{\theta_n})}{\partial t_{\theta_n}} &= \lim_{t\to t_{\theta_n}} \delta(t - t_{\theta_n})\left(y(t_{\theta_n^+}) - y(t_{\theta_n^-})\right) \\
&= \lim_{t\to t_{\theta_n}} \delta(0)\left(y(t_{\theta_n^+}) - y(t_{\theta_n^-})\right) \\
\frac{\partial t_{\theta_n}}{\partial x_n(t_{\theta_n}^-)} &= \frac{-1}{\frac{\partial V_n(t_{\theta_n})}{\partial t}} g1_n \\
\frac{\partial t_{\theta_n}}{\partial u(t_{\theta_n})} &= \frac{-1}{\frac{\partial V_n(t_{\theta_n})}{\partial t}} g2_n
\end{aligned}$$

For the LTP representation the output equation at the autonomous switching instant is expressed as a function of the state and the input in the form of 6.43.

$$\begin{aligned}
\lim_{t\to t_{\theta_n}} y(t_{\theta_n}) &= \lim_{t\to t_{\theta_n}} \delta(t - t_{\theta_n})\left(K_3 x(t) + K_4 u_{elec}(t)\right) \\
&= \delta(0)\left(K_3 x(t_{\theta_n}) + K_4 u_{elec}(t_{\theta_n})\right)
\end{aligned} \quad (6.43)$$

By substituting equation 6.36 into equation 6.43

$$\lim_{t\to t_{\theta_n}} y(t_{\theta_n}) = \delta(0)\left(K_3\frac{1}{2}\left(x(t_{\theta_n}^+) + x(t_{\theta_n}^-)\right) + K_4 u_{elec}(t)\right)$$

and expressing $x(t_{\theta_n}^+)$ using equation 6.37, equation 6.44 can be formed.

$$\lim_{t\to t_{\theta_n}} y(t_{\theta_n}) = \delta(0)\Bigg(K_3\frac{1}{2}\left(\left(I-\frac{K_1[n]}{2}\right)^{-1}\left(I+\frac{K_1[n]}{2}\right)+I\right)x(t_{\theta_n}^-) + \left(\left(I-\frac{K_1[n]}{2}\right)^{-1}K_2[n]+K_4\right)u_{elec}(t)\Bigg) \quad (6.44)$$

This equation has a similar form to equation 6.42 and using a similar argument to the derivation of constants $K_1[n]$ and $K_2[n]$, equations 6.45 and 6.46 can be used to form expressions for constants K_3 and K_4. If these values are chosen then the LTP output equation will contain an impulse of the exactly the same magnitude as the small signal model.

$$K_3 = 2\frac{\partial y_n(t_{\theta_n})}{\partial x_{n-1}(t_{\theta_n}^-)}\left(\left(I-\frac{K_1[n]}{2}\right)^{-1}\left(I+\frac{K_1[n]}{2}\right)+I\right)^{-1} \quad (6.45)$$

$$K_4 = \frac{\partial y_n(t_{\theta_n})}{\partial u(t_{\theta_n})} - \frac{1}{2}K_3\left(I-\frac{K_1[n]}{2}\right)^{-1}K_2[n] \quad (6.46)$$

6.3.3 Contribution of controlled switching instants

Controlled switching instants have a similar contribution as autonomous ones, but instead of the size of the switching variation being dependent on the state and the electrical input, it is directly determined by the appropriate control input. The difference equation that describes this relationship is repeated below, where although the effect of autonomous switching instants are not included, the effects of the base case jump destination maps are.

$$\Delta x_n(t_{\theta_n}^+) = P[n]\Delta x_{n-1}(t_{\theta_n}^-) + Q[n]\Delta u(t_{\theta_n}) + \frac{\partial x_n(t_{\theta_n}^+)}{\partial t_{\theta_n}}\Delta t_{\theta_n} \quad (6.47)$$

The equivalent equation that describes the output at the switching instant is equation 6.48, where since the switching instant is controlled, the impulse at the output is totally dependent on the control order.

$$\Delta y(t_{\theta_n}) = \frac{\partial y(t_{\theta_n})}{\partial t_{\theta_n}}\Delta t_{\theta_n} \quad (6.48)$$

An LTP system at a controlled switching instant tends towards the expressions in equation 6.49 and 6.50.

$$\begin{aligned}\lim_{t\to t_{\theta_n}} \frac{\partial x(t_{\theta_n})}{\partial t} &= \lim_{t\to t_{\theta_n}} \delta(t-t_{\theta_n})\left(K_1[n]x(t)+K_{2elec}[n]u_{elec}(t)+K_{2ctrl}[n]u_{ctrl}(t)\right)\\ &= \lim_{t\to t_{\theta_n}} \delta(0)\left(K_1[n]x(t_{\theta_n})+K_{2elec}[n]u_{elec}(t_{\theta_n})+K_{2ctrl}[n]u_{ctrl}(t_{\theta_n})\right)\end{aligned} \tag{6.49}$$

$$\begin{aligned}\lim_{t\to t_{\theta_n}} y(t_{\theta_n}) &= \lim_{t\to t_{\theta_n}} \delta(t-t_{\theta_n})K_{4ctrl}[n]u_{ctrl}(t)\\ &= \delta(0)K_{4ctrl}[n]u_{ctrl}(t_{\theta_n})\end{aligned} \tag{6.50}$$

Using similar arguments as were given for the autonomous switching instants, the constants $K_1[n]$,K_{2elec},K_{2ctrl}, and K_{4ctrl} are given below.

$$\begin{aligned}K_1[n] &= 2(P[n]+I)^{-1}(P[n]-I)\\ K_{2elec}[n] &= \left(I-\tfrac{K_1[n]}{2}\right)Q[n]\\ K_{2ctrl}[n] &= \left(I-\tfrac{K_1[n]}{2}\right)\tfrac{\partial x_n(t_{\theta_n}^+)}{\partial t_{\theta_n}}\\ K_{4ctrl}[n] &= \tfrac{\partial y(t_\theta^+)}{\partial t_\theta}\end{aligned} \tag{6.51}$$

This completes the HSS model of a power electronic converter. It is now verified by modelling the buck-boost converter and the Graetz Bridge converter.

6.4 EXAMPLE: BUCK-BOOST CONVERTER

The buck-boost converter is used to demonstrate the accuracy of the HSS model. Unlike in the previous chapters the buck-boost converter is operated both discontinuously and continuously. Modelling the converter in continuous operation is used to demonstrate the HSS model against those models and methods found in the literature, in particular this model is compared to a state space averaging model. In this section the model of the discontinuous Buck-Boost converter is examined in detail, before results for the discontinuous buck-boost converter and the continuous buck boost are presented.

6.4.1 Model: Discontinuous Buck-Boost Converter

To form the HSS model of the discontinuous buck-boost converter periodic time varying descriptions of its state space matrices are required. The method for achieving this description was outlined in the previous section. Here a detailed example of how to form the dynamics matrix, $A(t)$, of the discontinuous buck-boost converter is presented.

The dynamics matrix $A(t)$ has contributions from each stage, and the autonomous switching instant t_{θ_3}. The general formulation suggests that it has contributions from the controlled switching instants as well, however as will be seen in this formulation they do not contribute. To start with the general form of the dynamic matrix is that of equation 6.52.

It is important to note that in this formulation the stage order is 4,2,1, whilst the order of switching instants is $t_{\theta_1}, t_{\theta_2}, t_{\theta_3}, T$. This means that the fourth stage exists between the first and second switching instants.

$$\begin{aligned} A(t) = A_4(\mu(t-t_{\theta_1}) - \mu(t-t_{\theta_2})) + A_2(\mu(t-t_{\theta_2}) - \mu(t-t_{\theta_3})) + A_1(\mu(t-t_{\theta_3}) - \mu(t-T)) \\ + K_1[t_{\theta_1}]\delta(t-t_{\theta_1}) + K_1[t_{\theta_2}]\delta(t-t_{\theta_2}) + K_1[t_{\theta_3}]\delta(t-t_{\theta_3}) \end{aligned} \quad (6.52)$$

Each of the coefficients of equation 6.52 are detailed in the following text.

A_4 A_2 A_1: The matrices A_4, A_2 and A_1 are the buffered dynamic stage matrixes, each multiplied by a rectangular sampling function that spans the length of each stage.

$K_1[t_{\theta_3}]$: The sensitivity matrix that models the effect of switching instant variation of the autonomous switching on the post switching state is, as shown in equation 3.26, a non-square matrix with elements that are equal to zero. This occurs as the buck-boost converter capacitor voltage is continuous over the autonomous switching instant, whilst the inductor current does not exist after the autonomous switching instant. The result of an all zero switching instant sensitivity matrix is that the coefficient $K_1[t_{\theta_3}]$ in front of the impulse at the autonomous switching instant is completely determined by the large signal projection matrix. The effect of autonomous switching instant variation has no effect for a linearized model. The projection matrix of the large signal model, that projects the state across the autonomous switching instant is shown below. The bold elements in this projection matrix are the buffered zeros.

$$\begin{aligned} x(t_{\theta_3}^+) &= P[3]x(t_{\theta_3}^-) \\ \begin{bmatrix} 0 \\ V_c(t) \end{bmatrix} &= \begin{bmatrix} \mathbf{0} & \mathbf{0} \\ \mathbf{0} & \mathbf{1} \end{bmatrix} \begin{bmatrix} I_l(t) \\ V_c(t) \end{bmatrix} \end{aligned} \quad (6.53)$$

Using the above projection matrix and equation 6.40 the coefficient $K_1[t_{\theta_3}]$ can be found.

$K_1[t_{\theta_2}]$: The coefficients $K_1[t_{\theta_1}]$ and $K_1[t_{\theta_2}]$ are the magnitudes of the controlled switching instant contributions. These impulses are only present if the projection matrices inject or remove energy from the system between stage transition. The projection matrix across

the second switching instant $P[2]$ is equal to identity matrix as no energy is injected or removed from the system. From equation 6.51 the coefficient $K_1[t_{\theta_2}]$ is then equal to zero.

$K_1[t_{\theta_1}]$**:** The projection matrix across the first switching instant is a buffered matrix as shown below. It projects the capacitor voltage of the last stage to the capacitor voltage and inductor current in the first stage.

$$\begin{bmatrix} I_l(t) \\ v_c(t) \end{bmatrix} = \begin{bmatrix} \mathbf{1} & 0 \\ \mathbf{0} & 1 \end{bmatrix} \begin{bmatrix} \mathbf{0} \\ v_c(t) \end{bmatrix} \tag{6.54}$$

The bold zero in the right hand vector represents the buffered state, whilst the bold zero and bold one in the projection matrix are the projection matrix's buffered elements. In Chapter 5 it was suggested that the buffered elements should be equal to zero. However, if the diagonal element of the buffered section is chosen as a one, then the coefficient $K_1[t_{\theta_1}]$ also becomes zero. It is shown later that impulses in the dynamics matrix increase the effect of truncation, so placing a one here is advantageous as it removes an impulse from the dynamics matrix. Using this observation new rules for what the buffered elements of the projection matrix are stated below:

- If the buffered element is an off-diagonal it should be set to zero
- If the buffered element is an on-diagonal and it is projection from a actual state to a buffered state it should be set to zero.
- If the buffered element is an on-diagonal and it is projection from a buffered state state to an actual state it should be set to one.

Similar formulations can be written for the other HSS matrices $B_{elec}(t)$, $B_{ctrl}(t)$, $C(t)$, $D_{elec}(t)$ and $D_{ctrl}(t)$. The *ctrl* terms are completely described by impulses with the magnitudes of equation 6.51, whilst the C matrix and the *elec* matrices are a mix of stage matrices rectangular sampled, and switching instant variation effects modeled as impulses.

The Toeplitz matrices of the HSS description are formed from the Fourier coefficients of the time-periodic matrices, where each Fourier coefficient is placed along the appropriate diagonal as shown in Definition 6.3.

6.4.2 Results: Discontinuous Buck-boost converter

The HSS model of the converter is built around the operating point described in Table 3.3. The harmonics are truncated to the 21^{st} harmonic. Using this model the converter is subjected to a 1 Volt, zero frequency, voltage source disturbance, a 1% increase in duty cycle. The results of these disturbances are shown in both the time domain for the transient effects, and in the harmonic domain for the steady state in Figures 6.1 and 6.2.

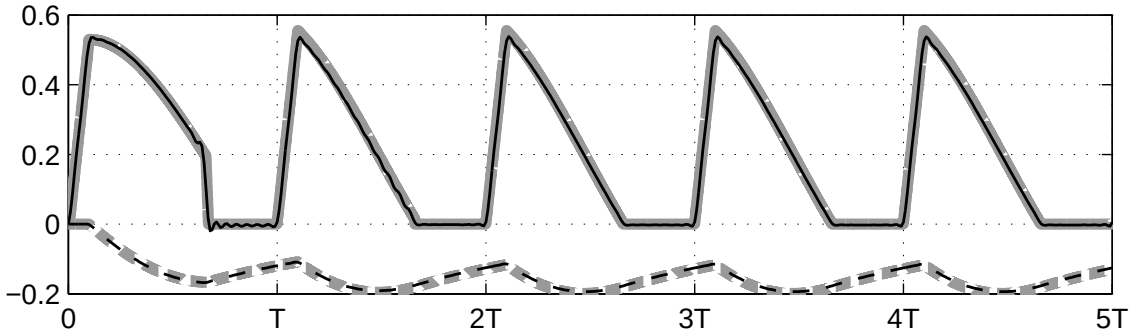

(a) Time domain trajectories of state distortions, upper group are the inductor currents, lower group are the capacitor voltages, **thick** PSCAD, **thin** HSS

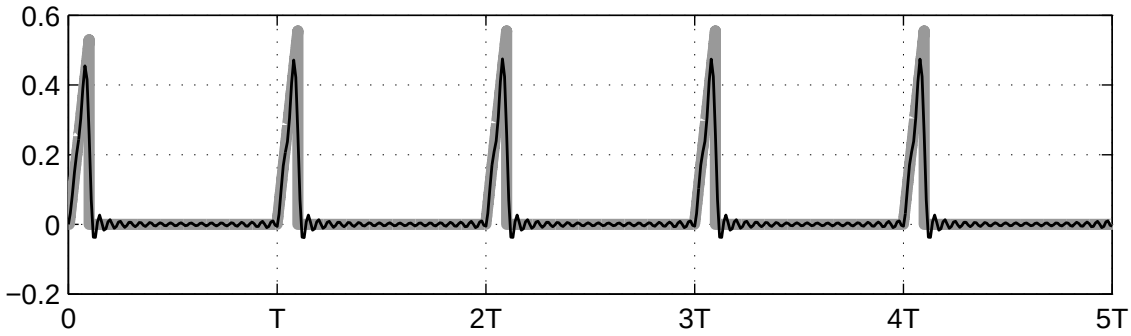

(b) Time domain trajectory of the output current, **thick** PSCAD, **thin** HSS

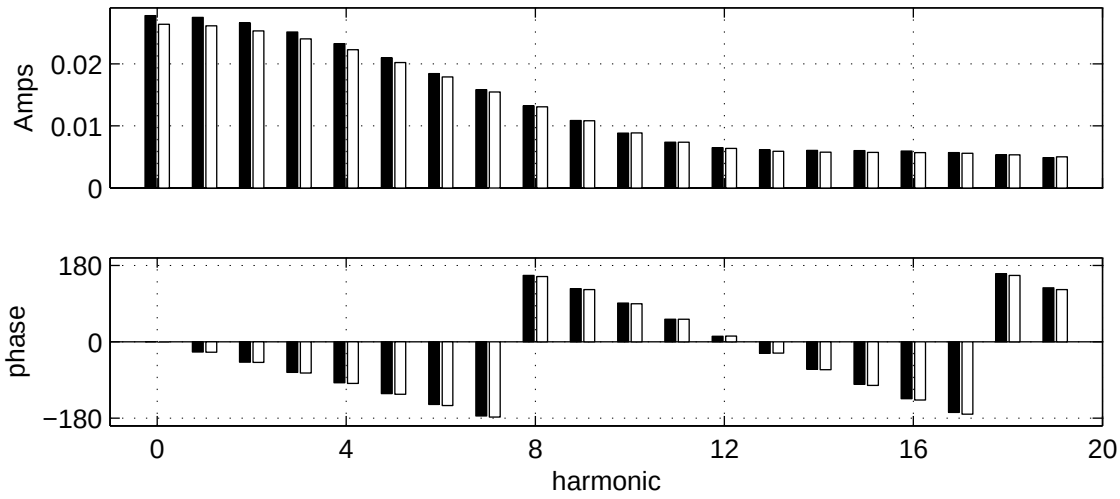

(c) Steady state current output comparison in the Harmonic domain, **black** PSCAD, **white**HSS

Figure 6.1 Comparison between the state and output distortions predicted by a 21 harmonic component HSS model and a PSCAD model of a discontinuous buck-boost converter subjected to a 1 volt source distortion

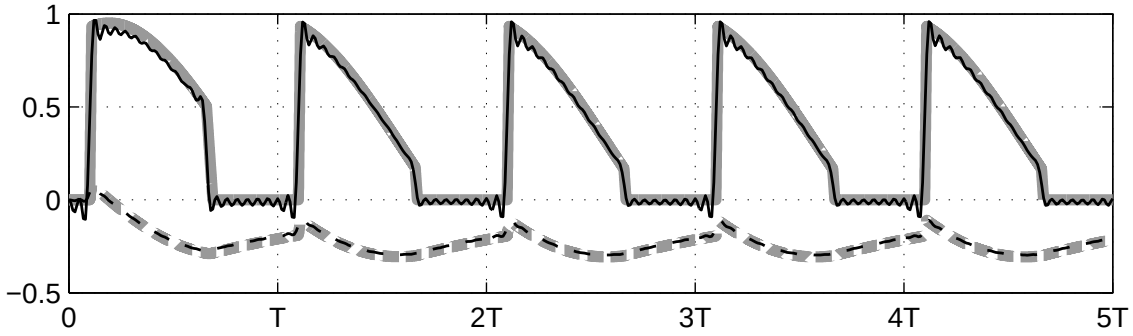

(a) Time domain trajectories of state distortions, upper group are the inductor currents, lower group are the capacitor voltages, **thick** PSCAD, **thin** HSS

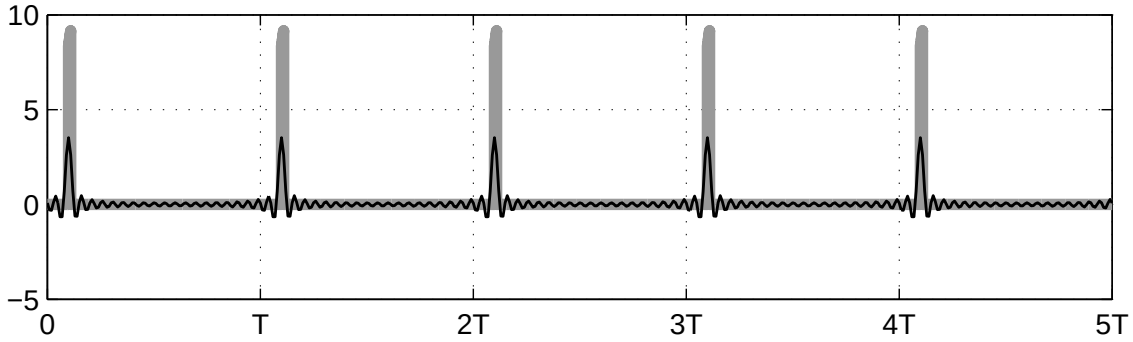

(b) Time domain trajectory of the output current, **thick** PSCAD, **thin** HSS

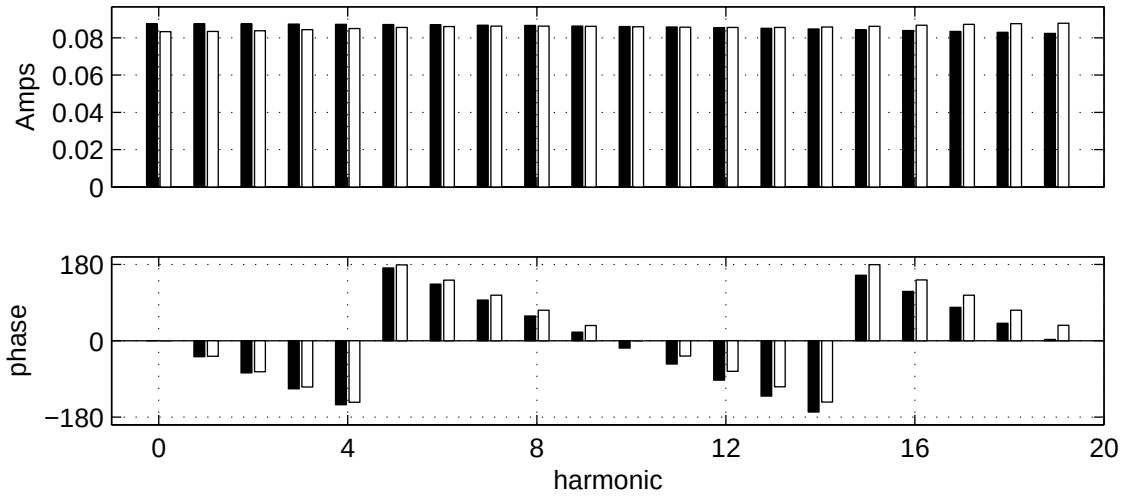

(c) Steady state current output comparison in the Harmonic domain, **black** PSCAD, **white**HSS

Figure 6.2 Comparison between the state and output distortions predicted by a 21 harmonic component HSS model and a PSCAD model of a discontinuous buck-boost converter subjected to a 1% increase in duty cycle (or $\Delta t_{\theta_n} = 5 \times 10^5$)

Variable	Value
Stage order	$\{4, 2, 1\}$
C	$50\mu F$
R	1Ω
L	$9\mu H$
f_s	$20000Hz$
Duty Cycle	50%
t_{θ_1}	0
t_{θ_2}	2.5×10^{-5}
t_{θ_3}	5×10^{-5}
v_{ac}	15V
$x_1(t_{\theta_1}^+)$	$[5.4030A - 16.1270V]$

Table 6.2 Continuous operated Buck-Boost for operating point

The HSS compares well to the PSCAD simulations in these figures. The only exception is in Figure 6.2(b) where the HSS contains truncated impulses, however they do have the same steady state spectra.

6.4.3 Results: Continuous Buck-boost Converter

The same disturbance is applied to a continuous conducting buck-boost converter, whose steady state operating point is described in Table 6.2 in Figures 6.3 and 6.4. A similar match for the continuous case is revealed, where again an impulse in the output, caused by the firing angle delay, is truncated in the time-domain plot of the HSS description. However, when the output of the HSS description is compared with the PSCAD description in the steady state a good match is obtained.

6.4.4 Relationship to State Space Averaging Models and their linearization

A popular technique for producing an LTI state space equivalent of a power electronic system is state space averaging [1], [65] and [66]. Although it has been used in systems with autonomous switched converters [65] [48] the modelled systems are linearly unaffected, such as the buck-boost converter, by switching instant variation. Most literature for state space averaging is very case specific, with the majority of papers centered around the modelling of DC:DC converters. State space averaging lacks the systematic approach presented in this thesis.

The basic principle behind state space averaging is to average the coefficients of each LTI stage to produce a single continuous coefficient instead of a set of coefficients each valid for only a portion of the evolution. The general expressions of these coefficients is that of equation set 6.55. This expression differs from most in the literature as it is expressed in terms of switching instants. Most references express these coefficients in terms of the

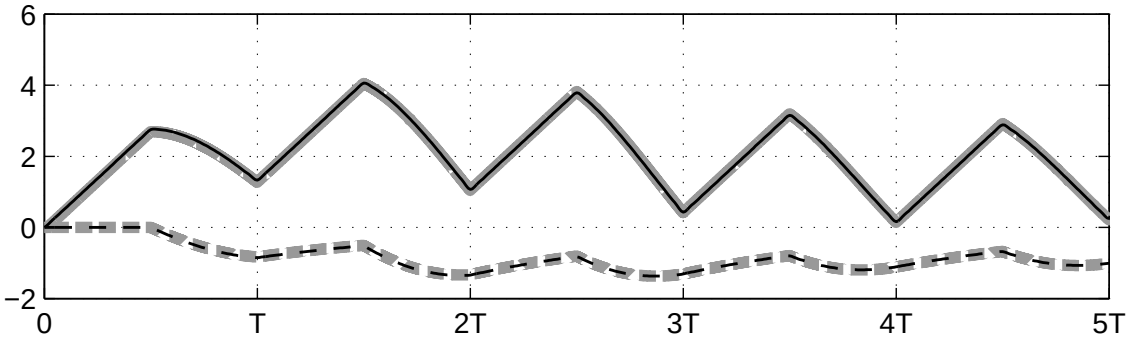

(a) Time domain trajectories of state distortions, upper group are the inductor currents, lower group are the capacitor voltages, **thick** PSCAD, **thin** HSS

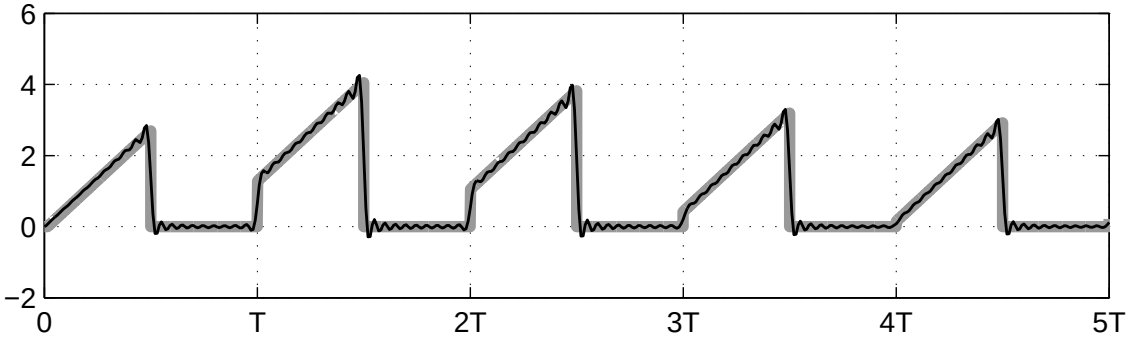

(b) Time domain trajectory of the output current, **thick** PSCAD, **thin** HSS

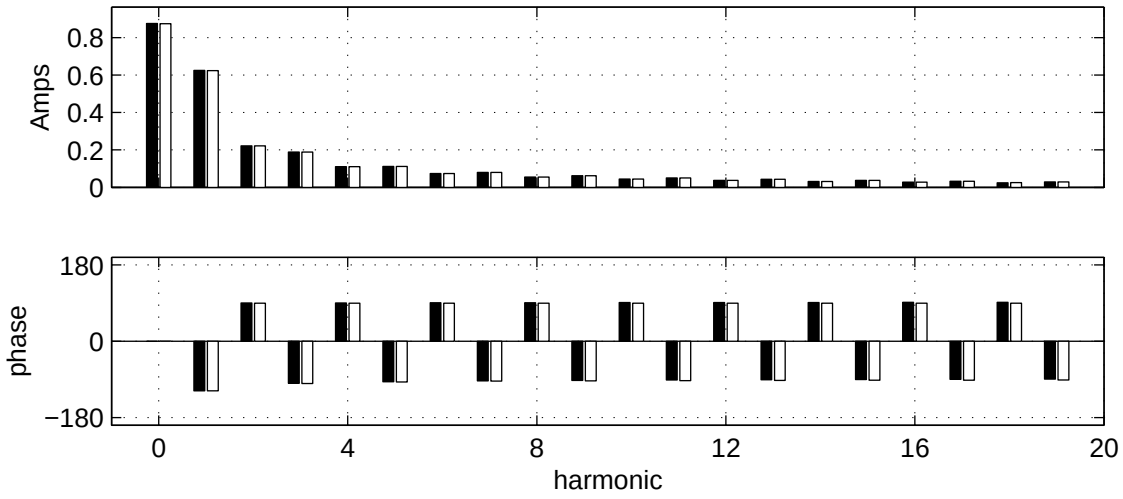

(c) Steady state current output comparison in the Harmonic domain, **black** PSCAD, **white**HSS

Figure 6.3 Comparison between the state and output distortions predicted by a 21 harmonic component HSS model and a PSCAD model of a continuous buck-boost converter subjected to a 1 volt increase in DC source voltage

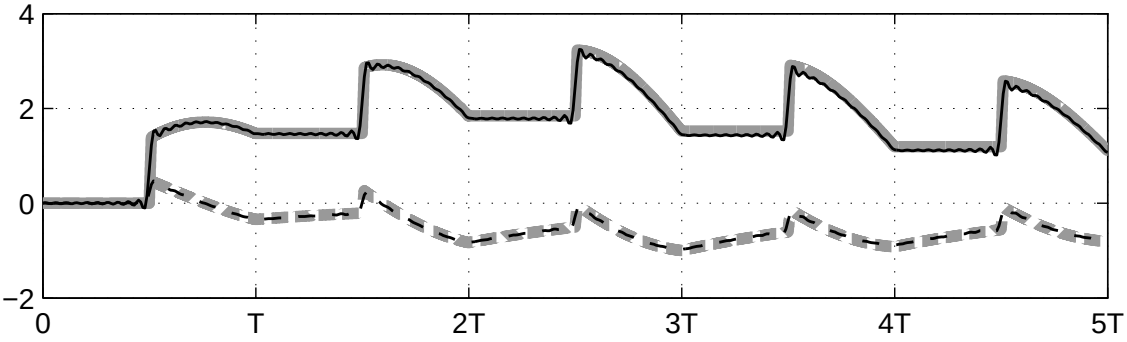

(a) Time domain trajectories of state distortions, upper group are the inductor currents, lower group are the capacitor voltages, **thick** PSCAD, **thin** HSS

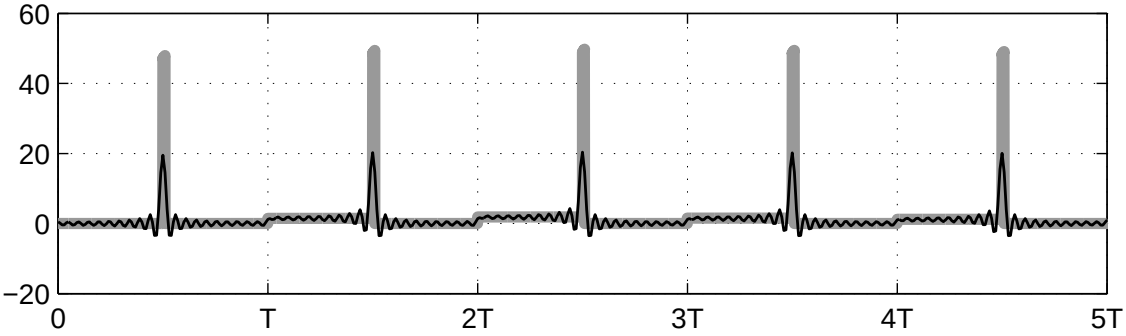

(b) Time domain trajectory of the output current, **thick** PSCAD, **thin** HSS

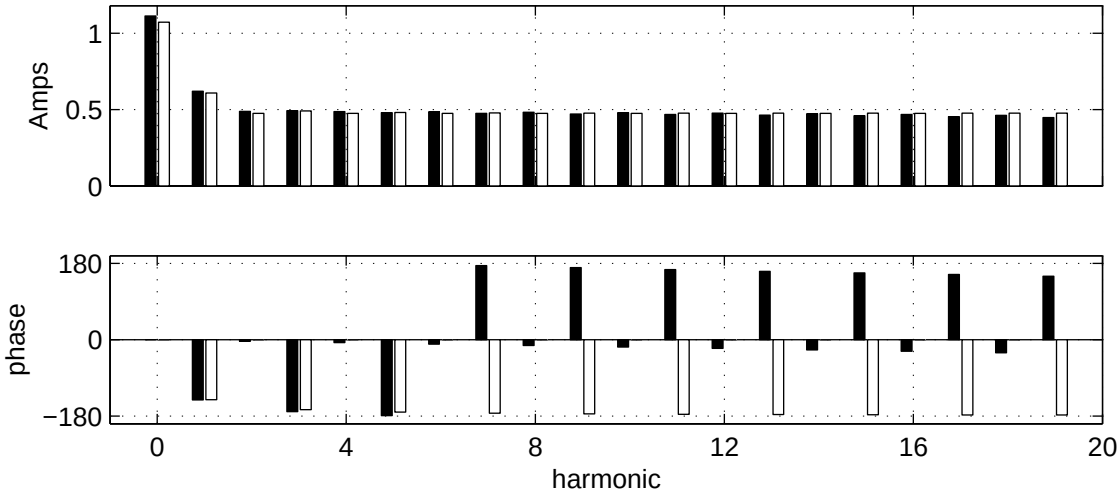

(c) Steady state current output comparison in the Harmonic domain, **black** PSCAD, **white**HSS

Figure 6.4 Comparison between the state and output distortions predicted by a 21 harmonic component HSS model and a PSCAD model of a continuous buck-boost converter subjected to a 1% increase in duty cycle (or $\Delta t_{\theta_n} = 5 \times 10^5$)

intervals the stages are active [1], [65] and [66], but the expressions presented here are equivalent.

$$\begin{aligned}
A_{ave} &= \frac{1}{T}\left(A_1(t_{\theta_2}-t_{\theta_1})+\cdots+A_n(t_{\theta_{n+1}}-t_{\theta_n})+\cdots+A_N(t_{\theta_N}-t_{\theta_{N-1}})\right) \\
&= \\
B_{ave} &= \frac{1}{T}\left(B_1(t_{\theta_2}-t_{\theta_1})+\cdots+B_n(t_{\theta_{n+1}}-t_{\theta_n})+\cdots+B_N(t_{\theta_N}-t_{\theta_{N-1}})\right) \\
&= \\
C_{ave} &= \frac{1}{T}\left(C_1(t_{\theta_2}-t_{\theta_1})+\cdots+C_n(t_{\theta_{n+1}}-t_{\theta_n})+\cdots+C_N(t_{\theta_N}-t_{\theta_{N-1}})\right) \\
&= \\
D_{ave} &= \frac{1}{T}\left(D_1(t_{\theta_2}-t_{\theta_1})+\cdots+D_n(t_{\theta_{n+1}}-t_{\theta_n})+\cdots+D_N(t_{\theta_N}-t_{\theta_{N-1}})\right)
\end{aligned} \tag{6.55}$$

The expressions of equation set 6.55 are used to form the averaged state space equations.

$$\begin{aligned}
\frac{\partial x(t)}{\partial t} &= A_{ave}(t_{\theta_1},\ldots,t_{\theta_n},\ldots,t_{\theta_N})\,x(t)+B_{ave}(t_{\theta_1},\ldots,t_{\theta_n},\ldots,t_{\theta_N})\,u(t) \\
y(t) &= C_{ave}(t_{\theta_1},\ldots,t_{\theta_n},\ldots,t_{\theta_N})\,x(t)+D_{ave}(t_{\theta_1},\ldots,t_{\theta_n},\ldots,t_{\theta_N})\,u(t)
\end{aligned} \tag{6.56}$$

For the continuously operated Buck-Boost converter the state space averaged model is...

$$\begin{aligned}
\begin{bmatrix}\dot{i}_l(t)\\ \dot{v}_c(t)\end{bmatrix} &= \begin{bmatrix}0 & \frac{1}{L}\frac{t_{\theta_3}-t_{\theta_2}}{T}\\ -\frac{1}{C}\frac{t_{\theta_3}-t_{\theta_2}}{T} & -\frac{1}{CR}\end{bmatrix}\begin{bmatrix}i_l(t)\\ v_c(t)\end{bmatrix}+\begin{bmatrix}\frac{1}{L}\frac{t_{\theta_2}-t_{\theta_1}}{T}\\ 0\end{bmatrix}\begin{bmatrix}u_{elec}(t)\end{bmatrix} \\
\begin{bmatrix}y(t)\end{bmatrix} &= \begin{bmatrix}\frac{t_{\theta_2}-t_{\theta_1}}{T}\\ 0\end{bmatrix}\begin{bmatrix}i_l(t)\\ v_c(t)\end{bmatrix}+\begin{bmatrix}0\end{bmatrix}\begin{bmatrix}u_{elec}(t)\end{bmatrix}
\end{aligned} \tag{6.57}$$

The averaged model is a non-linear large signal model, albeit one with reduced accuracy, as the averaged coefficients are still functions of the switching instants.

Typically the averaged model is linearized to form a LTI equation set [1], [65] and [66]. The linearization is carried out below in a similar manner to Chapter 3, to form an LTI state space equation of the form shown in equation 6.58, where all switching instants are assumed to be controlled. The base case for this linearization is carried out around the base case switching instants, and the averaged state $\widehat{x_0}$, and the averaged input $\widehat{u_0}$.

$$\begin{aligned}
\Delta\dot{x}(t) &= A_{ave}\Delta x(t) + B_{ave}\Delta u(t) + \left[\frac{\partial A_{ave}}{\partial t_{\theta_1}}\hat{x} + \frac{\partial B_{ave}}{\partial t_{\theta_1}}\hat{u}\right]\Delta t_{\theta_1} + \left[\frac{\partial A_{ave}}{\partial t_{\theta_2}}\hat{x} + \frac{\partial B_{ave}}{\partial t_{\theta_2}}\hat{u}\right]\Delta t_{\theta_2} \\
&\quad + \cdots + \left[\frac{\partial A_{ave}}{\partial t_{theta_n}}\hat{x} + \frac{\partial B_{ave}}{\partial t_{\theta_n}}\hat{u}\right]\Delta t_{\theta_n} \\
\Delta y(t) &= C_{ave}\Delta x(t) + B_{ave}\Delta u(t) + \left[\frac{\partial C_{ave}}{\partial t_{\theta_1}}\hat{x} + \frac{\partial D_{ave}}{\partial t_{\theta_1}}\hat{u}\right]\Delta t_{\theta_1} + \left[\frac{\partial C_{ave}}{\partial t_{\theta_2}}\hat{x} + \frac{\partial D_{ave}}{\partial t_{\theta_2}}\hat{u}\right]\Delta t_{\theta_2} \\
&\quad + \cdots + \left[\frac{\partial C_{ave}}{\partial t_{\theta_n}}\hat{x} + \frac{\partial D_{ave}}{\partial t_{\theta_n}}\hat{u}\right]\Delta t_{\theta_n}
\end{aligned} \tag{6.58}$$

The linearized state space averaged model of the buck-boost converter is

$$\begin{aligned}
\begin{bmatrix}\Delta\dot{i}_l(t)\\ \Delta\dot{v}_c(t)\end{bmatrix} &= \begin{bmatrix}0 & \frac{1}{L}\frac{t_{\theta_{3_0}} - t_{\theta_{2_0}}}{T} \\ -\frac{1}{C}\frac{t_{\theta_{3_0}} - t_{\theta_{2_0}}}{T} & -\frac{1}{CR}\end{bmatrix}\begin{bmatrix}\Delta i_l(t)\\ \Delta v_c(t)\end{bmatrix} + \begin{bmatrix}\frac{1}{L}\frac{t_{\theta_{2_0}} - t_{\theta_{1_0}}}{T}\\ 0\end{bmatrix}\left[\Delta u_{elec}(t)\right] \\
&\quad + \begin{bmatrix}\frac{1}{L}\left(\frac{\widehat{u_{elec_0}}}{T} - \frac{\widehat{v_{c_0}}}{T}\right) & \frac{1}{L}\left(\frac{\widehat{v_{c_0}}}{T} - \frac{\widehat{u_{elec_0}}}{T}\right) \\ \frac{1}{C}\frac{\widehat{i_{l_0}}}{T} & -\frac{1}{C}\frac{\widehat{i_{l_0}}}{T}\end{bmatrix}\begin{bmatrix}\Delta t_{\theta_2}\\ \Delta t_{\theta_3}\end{bmatrix}
\end{aligned} \tag{6.59}$$

$$\left[\Delta y(t)\right] = \begin{bmatrix}\frac{t_{\theta_{2_0}} - t_{\theta_{1_0}}}{T}\\ 0\end{bmatrix}\begin{bmatrix}\Delta i_l(t)\\ \Delta v_c(t)\end{bmatrix} + \left[0\right]\left[\Delta u_{elec}(t)\right] + \begin{bmatrix}\frac{\widehat{i_{l_0}}}{T} & -\frac{\widehat{i_{l_0}}}{T}\end{bmatrix}\begin{bmatrix}\Delta t_{\theta_2}\\ \Delta t_{\theta_3}\end{bmatrix}$$

The variables with the widehat, i.e $\widehat{i_{l_0}}$ are the averaged (or D.C.) values of the base case state, and inputs.

Although initially equation set 6.58 appears to have many similarities to the HSS model advanced in this thesis truncated to only a 0 frequency harmonic, it has a crucial difference. Instead of the linear model being constructed around the actual piece wise linear power electronic circuit, it is constructed around its averaged equivalent. This difference can be highlighted by examining the HSS model of the continuous buck-boost converter described with single (zero-frequency) harmonic truncated vectors.

$$\begin{bmatrix}\Delta\dot{i}_l(t)\\ \Delta\dot{v}_c(t)\end{bmatrix} = \begin{bmatrix}0 & \frac{1}{L}\frac{t_{\theta_{3_0}}-t_{\theta_{2_0}}}{T}\\ -\frac{1}{C}\frac{t_{\theta_{3_0}}-t_{\theta_{2_0}}}{T} & -\frac{1}{CR}\end{bmatrix}\begin{bmatrix}\Delta i_l(t)\\ \Delta v_c(t)\end{bmatrix} + \begin{bmatrix}\frac{1}{L}\frac{t_{\theta_{2_0}}-t_{\theta_{1_0}}}{T}\\ 0\end{bmatrix}\begin{bmatrix}\Delta u_{elec}(t)\end{bmatrix} + \begin{bmatrix}\frac{\frac{\partial i_{l_0}(t_{\theta_2}^-)}{\partial t}-\frac{\partial i_{l_0}(t_{\theta_2}^+)}{\partial t}}{T} & \frac{\frac{\partial i_{l_0}(t_{\theta_3}^-)}{\partial t}-\frac{\partial i_{l_0}(t_{\theta_3}^+)}{\partial t}}{T}\\ \frac{\frac{\partial v_{c_0}(t_{\theta_2}^-)}{\partial t}-\frac{\partial v_{c_0}(t_{\theta_2}^+)}{\partial t}}{T} & \frac{\frac{\partial v_{c_0}(t_{\theta_3}^-)}{\partial t}-\frac{\partial v_{c_0}(t_{\theta_3}^+)}{\partial t}}{T}\end{bmatrix}\begin{bmatrix}\Delta t_{\theta_2}\\ \Delta t_{\theta_3}\end{bmatrix} \tag{6.60}$$

$$\begin{bmatrix}\Delta y(t)\end{bmatrix} = \begin{bmatrix}\frac{t_{\theta_{2_0}}-t_{\theta_{1_0}}}{T}\\ 0\end{bmatrix}\begin{bmatrix}\Delta i_l(t)\\ \Delta v_c(t)\end{bmatrix} + \begin{bmatrix}0\end{bmatrix}\begin{bmatrix}\Delta u_{elec}(t)\end{bmatrix} + \begin{bmatrix}\frac{i_{l_0}(t_{\theta_2}^-)}{T} & -\frac{i_{l_0}(t_{\theta_3}^+)}{T}\end{bmatrix}\begin{bmatrix}\Delta t_{\theta_2}\\ \Delta t_{\theta_3}\end{bmatrix}$$

Where the vector $\begin{bmatrix}\Delta t_{\theta_2}\\ \Delta t_{\theta_3}\end{bmatrix}$ is the control input u_{ctrl}.

As can be seen there are many similarities between the expressions, in particular the electrical parts are identical. The difference between the two models is the contribution from the controlled switching instant variation. In the linearized state space averaged model the control effect is described in terms of the averaged state and input, whilst in the truncated HSS model it is described in terms of the state at the switching instant. The difference between the controlled switching instance effects is especially true in cases with a large amount of ripple – where the value of the base case state trajectory at the switching instants are far from the average values.

A comparison between the evolution of the HSS at various levels of truncation and the linearized state space averaging model are depicted in Figures 6.5, for a DC input voltage increase and a 1% increase in duty cycle respectively. To make for a fair comparison both the HSS and State space averaging model are based around the same operating point obtained by small signal solution to the TPBV problem described in Chapter 4.

As Figure 6.5(a) shows, and was predicted from the examination of equations 6.59 and 6.60, the effect of a DC current increase is identically modeled by the linearized state space average model and the truncated HSS model. The truncated HSS model is a much better match than the linearized state space averaging model when modelling the effects of a duty cycle increase.

An extension to state space averaging theory, variously called generalized state space averaging [66], and later by the some of same author's Dynamic Phasors, has been developed in the literature for the study of DC:DC converters, electric machines and also FACTS. In these models the vectors of the system are implicitly described as harmonics of the pumping frequency, this enables the modelling of AC:DC converters, and machines with a mix of AC and DC terminals. In later papers [67] frequency coupling occurs, where

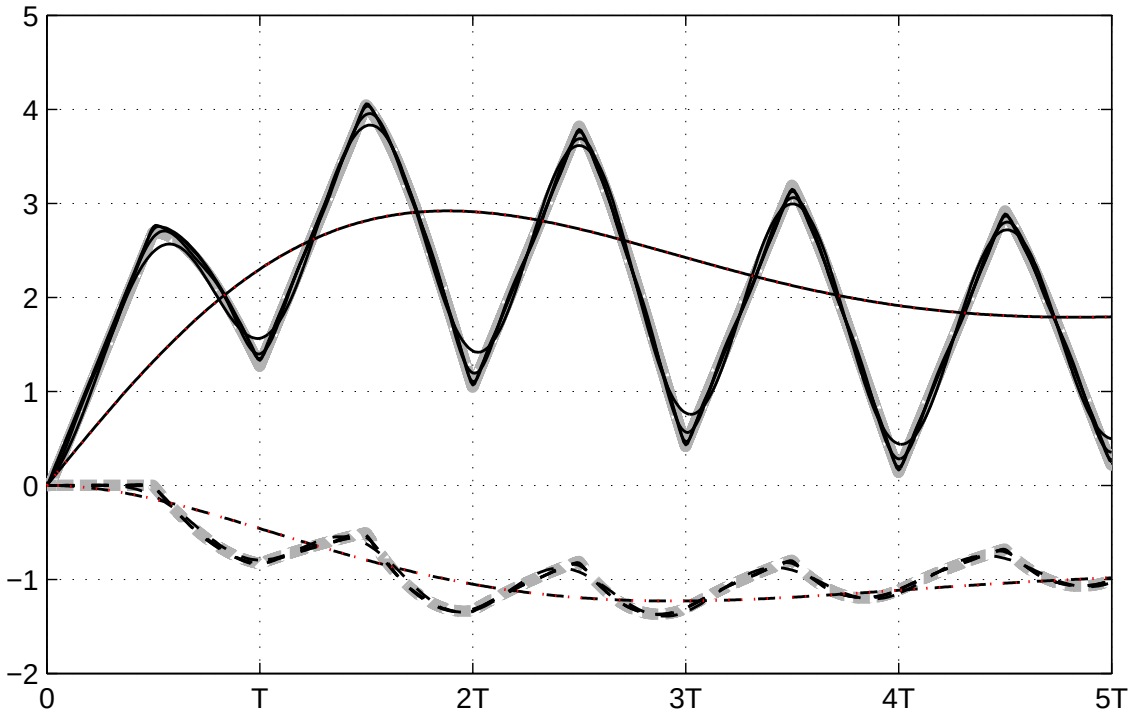

(a) 1 Volt, 0 frequency, voltage source distortion.

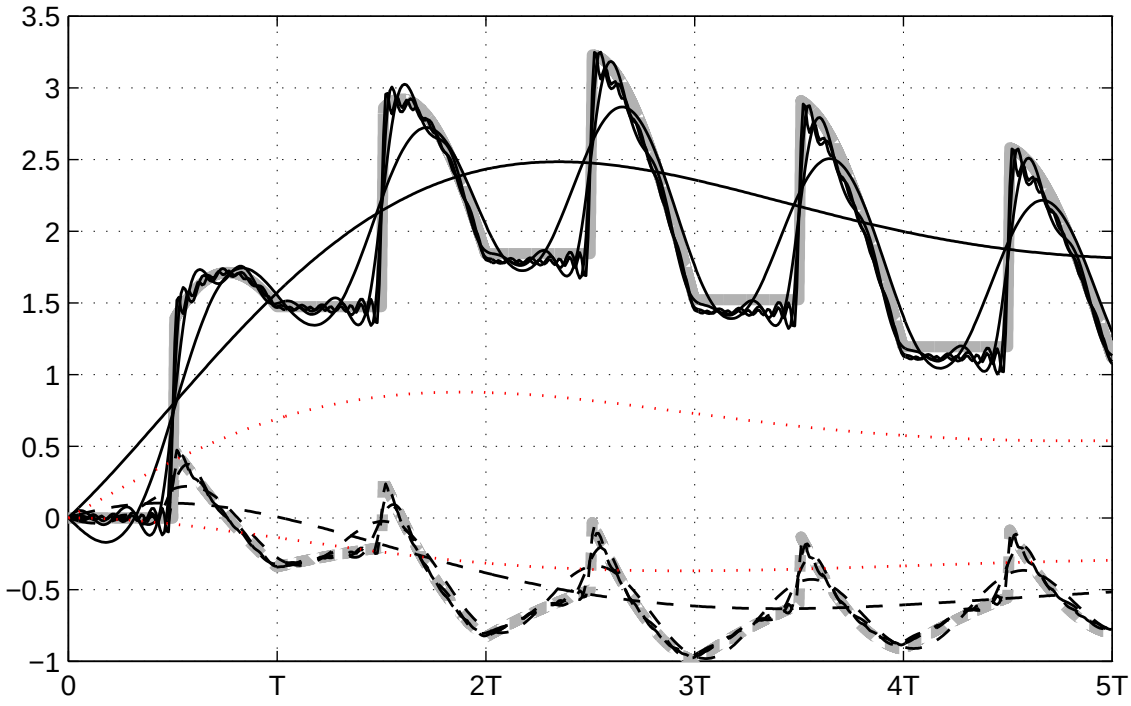

(b) 1% increase in duty cycle

Figure 6.5 Comparison between the evolutions of several HSS models of different harmonic truncations (**thin black** line), a linearized state space averaging model (**dotted red** line), and PSCAD (**thick grey** line) for a buck boost converter subjected to a 1 Volt, 0 frequency, voltage source distortion, and a 1% increase in duty cycle. In each graph the upper group are inductor currents, whilst the lower group are capacitor voltages.

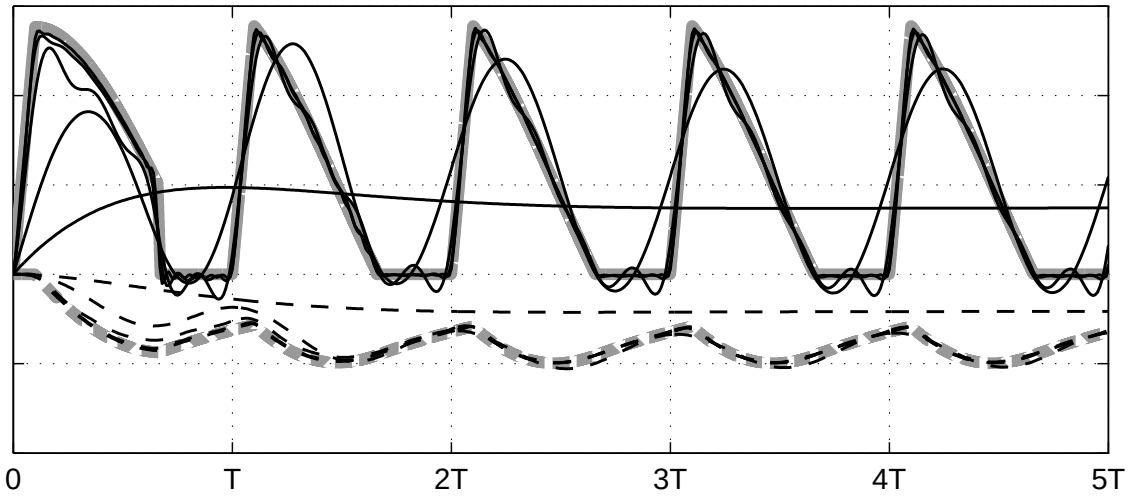

Figure 6.6 HSS models of different harmonic truncations modelling a discontinuous buck-boost converter subjected to a 1 Volt increase in source voltage. The upper group is inductor current, and the lower group is capacitor voltage. The differently truncated HSS are the **thin black** lines, whilst the PSCAD comparison is a **thick grey** line.

states are split into a set of elements each at an different frequency. It is assumed that a linearized dynamic phasor model will also differ from the HSS model as it too is based on averaged base case values.

6.4.5 Truncation

Truncation of the Fourier components can effect the accuracy of the HSS trajectories. This was hinted at in Figure 6.5 for the continuous operated buck-boost converter. However for a discontinuously operated buck-boost converter the effect is even larger for both increase in DC voltage and increase in firing order. Figure 6.6 shows this effect for a set of HSS with signals truncated to a vector with only a DC component up to a vector with 21 components when subjected to a 1 Volt step change in source voltage.

Importantly it isn't only high frequency transfers which are affected by truncation but also low frequency transfers. During the manipulation of the truncated HSS system coefficients, for the calculation of the transient and steady state responses an inverse operation is performed when calculating the kernel, $(sI - (\mathcal{A} - \mathcal{N}))^{-1}$. This inverse results in high frequency components being *wrapped* back to the low frequency transfers, and if the high frequency components are missing then errors in the low frequency transfers appear. Similar truncation errors are likely to occur when calculating the matrix exponential $e^{\mathcal{A}t}$ during the transient response.

Truncation effects are largest when a system contains an impulse in its dynamics matrix $A(t)$. The Fourier components of an impulse don't roll off and it is this lack roll off that results in significant truncation errors. Wereley [31] suggests that the number of harmonic

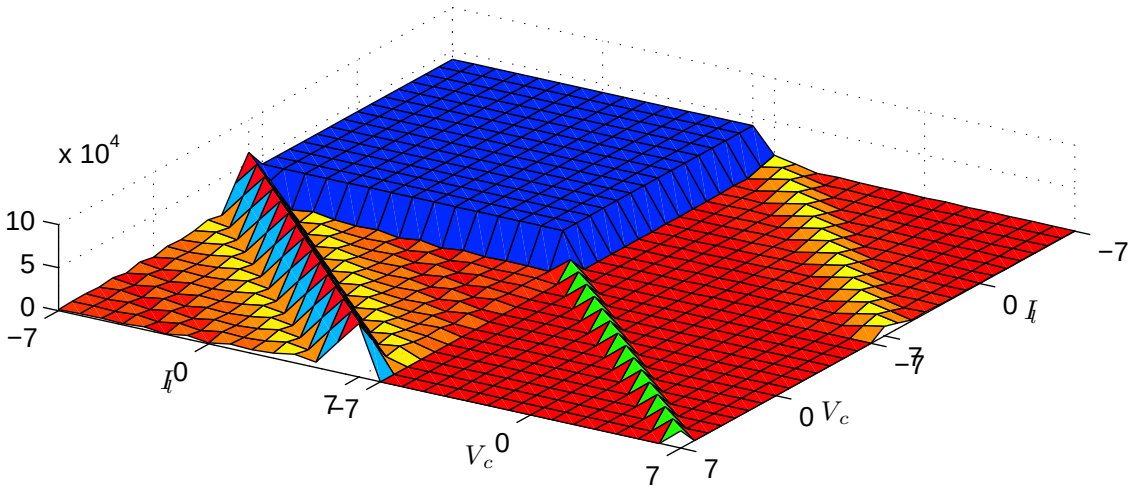

(a) Discontinuous buck-boost Dynamics matrix.

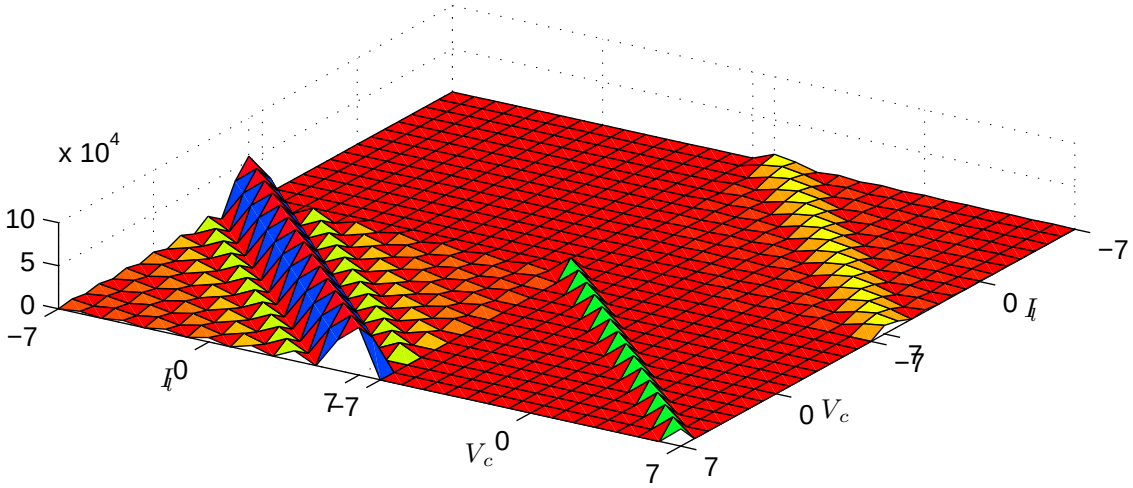

(b) Continuous buck-boost Dynamics matrix.

Figure 6.7 The magnitude plots of LTP dynamics matrixes A(t) of a continuous buck-boost converter (a) and a discontinuous buck-boost converter (b) expressed as doubly infinite Toeplitz matrixes of the HSS.

components needed to produce a good match is larger for systems with discontinuous dynamics equations.

The effects that a switching instant impulse has on the HSS dynamics matrices is shown in Figure 6.7. In the figure are shown the dynamics matrices of the HSS descriptions of the continuous and discontinuous buck-boost converters. In a) the continuous buck-boost converter the dynamics matrix has no contributions from switching instant impulses and its terms roll off completely. In b) the discontinuous converter dynamics matrix contains the effect of impulse. The cause of this impulse is the non-identity projection matrix (equation 6.53)across the autonomous switching instant. The terms of the impulse do not role off instead they remain at constant magnitude.

Truncation is a crucial weakness of the HSS, a weakness not shared by HSMs found using

	Continuous		Discontinuous	
Transfer	u_{elec}	$u_{ctrl}\ 10^6$	u_{elec}	$u_{ctrl}\ 10^5$
HSS Dc only	1.0000	2.8740	0.0149	2.3029
HSS 1 component	0.8774	2.3030	0.0294	2.2819
HSS 4 component	0.8748	2.1935	0.0268	1.8213
HSS 10 component	0.8746	2.1582	0.0273	1.7610
HSS 20 component	0.8745	2.1454.	0.0275	1.6909
Partial waveform	0.8745	2.1320	0.02780	1.6667
State Space Averaged	1.0000	0.6016	N \ A	N \ A

Table 6.3 The electrical and control DC:DC transfer of the buck-boost converter for both discontinuous and continuous operation of several differently truncated HSS representations. Also are included are the transfers using the partial waveform approach of Chapter 5, and the linearized state space averaging approach (for the continuous case only)

the partial waveform method developed in the previous chapter. In the partial waveform method low frequency components are unaffected by the absence of the higher frequency components. In Table 6.3 the effects of truncation on the electrical and control DC:DC transfer of the buck-boost converter in both discontinuous and continuous modes. The Table reinforces that the discontinuous buck-boost is much more susceptible to truncation error than a continuously operated one. In the table's second to last line the value of this transfer for a HSM found using the partial waveform shaping method is also included for comparison. It is the partial waveform value that the HSS tend towards as the number of harmonics in the truncated signals is increased. The last line of the Table shows the values obtained from the continuous state space averaging model.

6.5 EXAMPLE: GRAETZ BRIDGE

Modelling of the Graetz Bridge dynamics in the s-domain has recently been focus of several authors.

In [2], Todd *et al* constructed an s-domain model for a converter bridging an AC and DC system using System Identification. Todd's model was the first to model the converter in this domain and showed that the converter, and its system, could be described in the s-domain accurately. The s-domain model was constructed by first finding the closed loop inverter voltage to rectifier current transfer in the frequency domain using Wood's describing function [68] for the converter, and s-domain models for the DC systems. This transfer is then curved fitted with a rational function with as many poles and zeros as needed to form a sufficient match

Jovcic *et al* [3] constructed an analytical model of a HVDC-HVAC converter system built up from subsystems. The AC side is referred to the DC side using a $dq0$ frequency transformation. The converters are lumped with the DC system and the converter controllers.

The actual dynamics of the bridge are taken directly from the basic equations of HVDC theory [69].

In [4], Osauskas *et al* produced a small signal (s-domain) dynamic model of the Graetz bridge based on the small signal analytic frequency domain model of [15] [5]. The transfers of the frequency domain method, which are described analytically in terms of the converter operating point are reduced to their dominant components. This reduction produces transfers with no frequency coupling. In all but one case the transfers reduce to a single complex constant with no frequency dependence. The case which isn't described as a constant (the transfer from dc current to dc voltage) is linearly dependent on frequency and dictates that the state space description of the converter includes a single state. The converter model was included in an HVDC link, with a DC system, rectifier and inverter AC systems, and a PLL closed loop PI controller. To account for the AC:DC frequency shift of the converter, the AC sides, described in positive negative sequence pairs were shifted to the DC side. When verified against PSCAD this model produced an excellent match.

In summary a dynamic converter models within a system have needed to overcome four obstacles.

- Including the 50Hz $\rightarrow$ 0Hz frequency transformation between the DC and AC sides.
- Accounting for the effects of controlled and autonomous switching instant variations.
- Determining the state dimensions
- Forming a description of the converter governing equations.

For a HSS model built upon the small signal model of Chapter 3, using the method outlined in this chapter, all of the outlined obstacles are overcome. The frequency transformation is intrinsically part of the HSS, where a DC distortion will couple to the $+50Hz$ and $-50Hz$ components on the AC side. Autonomous and controlled switching instants are included through the HSS model being built upon the small signal model of Chapter 3. The state dimension is dictated by the DEs of the stage equations. The governing equations are obtained directly from the hybrid model.

Whilst Jovcic's and Osauskas's models are arguably more elegant solutions than that presented by Todd, they are both methods that require an intimate knowledge of the converter. The strength of Todd's system identification method is that it is more readily applicable to other converter topologies as less knowledge of the converter's operation is needed. It is advanced here that the HSS description of the small signal power electronic model is the best of both worlds. The method is elegant and systematic as there are clear steps in going from the small signal model to the HSS model, yet it also requires a minimum of knowledge about the system. All that is needed are the stage DE equations,

the jump sets of each stage, the jump destination map that tie the stages together, and the base case operating point.

Using the same operating point solved for in chapter 4, a HSS converter model was constructed for 41 harmonic components. Its validation for a 0.05(p.u.) increase in DC side current, a 0.05(p.u.) 150HZ phase A voltage disturbance, and 1 degree increase in firing angle are shown in Figures 6.8, 6.9 and 6.10.

As there are no states that persist over the entire cycle the transient response at most only lasts the length of a commutating stage and so the results are shown only in the steady state in the harmonic domain.

For both distortions the HSS and PSCAD models have good matches. The only slight exception is the transfer from firing angle distortions to AC current distortion. The mismatch in this transfer is solely due to truncation errors, and if the number of harmonics are increased an almost perfect match is obtained.

6.6 DISCUSSION

In comparing the model produced in the last chapter to the model produced here, each have similar advantages in that both techniques are accurate, but are also systematic and can easily be applied to other converter topologies. The weakness of the partial waveform method of the previous chapter is that it was described in the harmonic domain, and subsequently could only model the effect of harmonics. The weakness of the HSS method is its susceptibility to truncations errors.

One comparison not presented here is a comparison of the computational effort required to build each model. Such a comparison is not available to the author of this thesis, as the code used to produce the results is far from optimized. Producing optimized code is a task for the future.

6.7 CONCLUSION

In this chapter a systematic method for producing a HSS small signal model of a power electronic converter was presented. It is suggested that the models are analogues to the LTI state space, and this was backed up in a discussion of the similarities between the LTISS and the HSS.

HSS models were produced for the buck-boost converter and the Graetz Bridge. For the former an analysis of truncation effect was presented that showed for some operating points and disturbances the effects of truncation can be large. The HSS description of a continuously operated buck-boost converter was compared against a state space averaged model, and showed comparable performance for electrical inputs, and arguably better

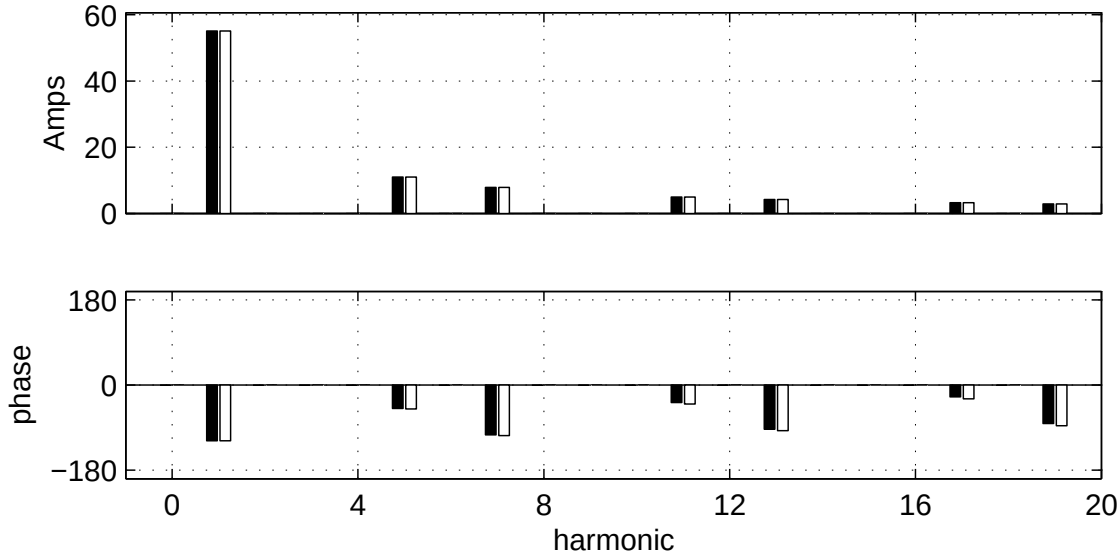

(a) Phase A Current I_a

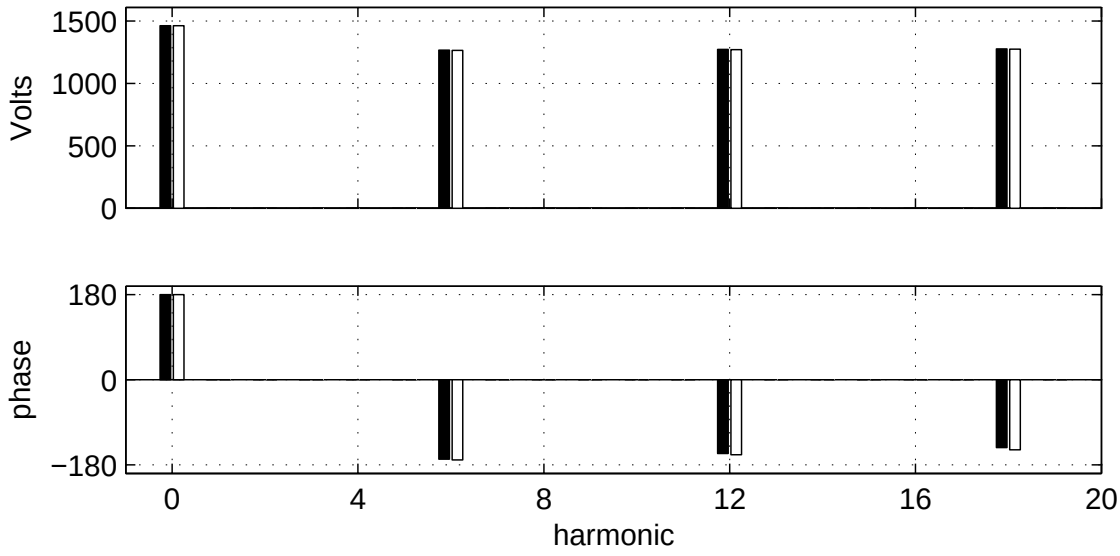

(b) DC Side voltage V_{dc}

Figure 6.8 Comparison between distortions obtained by the HSS and PSCAD-EMTDC to a 0.05 (p.u.) increase in DC current. **black** PSCAD, **white** HSS

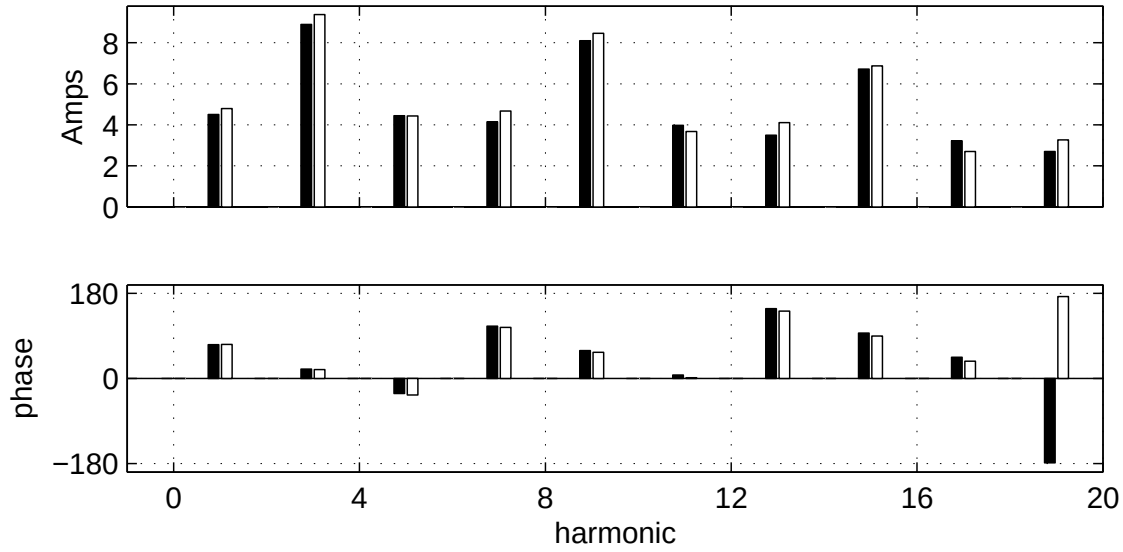

(a) Phase A Current I_a

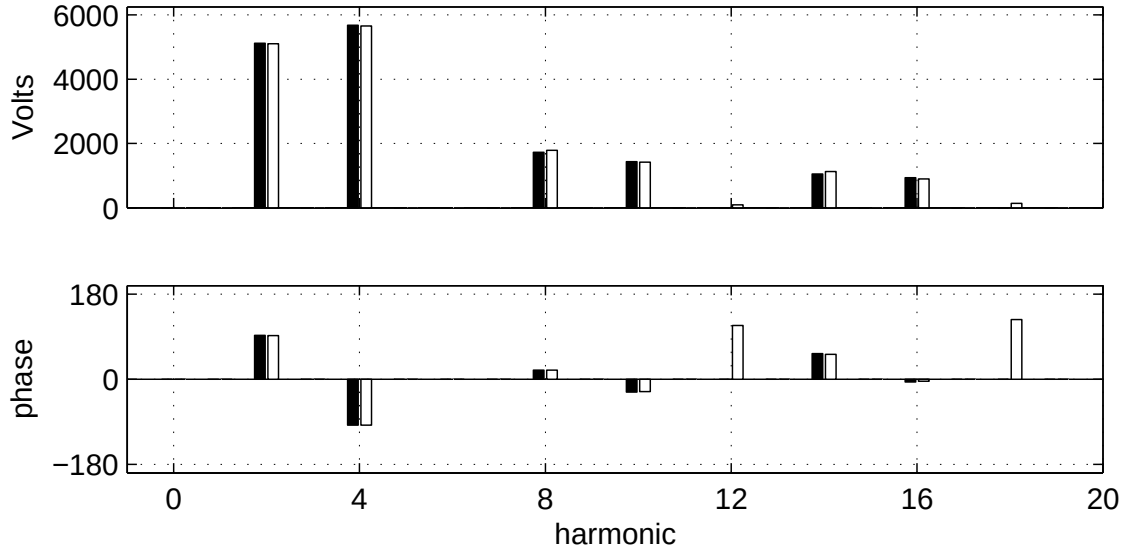

(b) DC Side voltage V_{dc}

Figure 6.9 Comparison between distortions obtained by the HSS and PSCAD-EMTDC to a 0.05 (p.u.) phase A voltage distortion. **black** PSCAD, **white** HSS

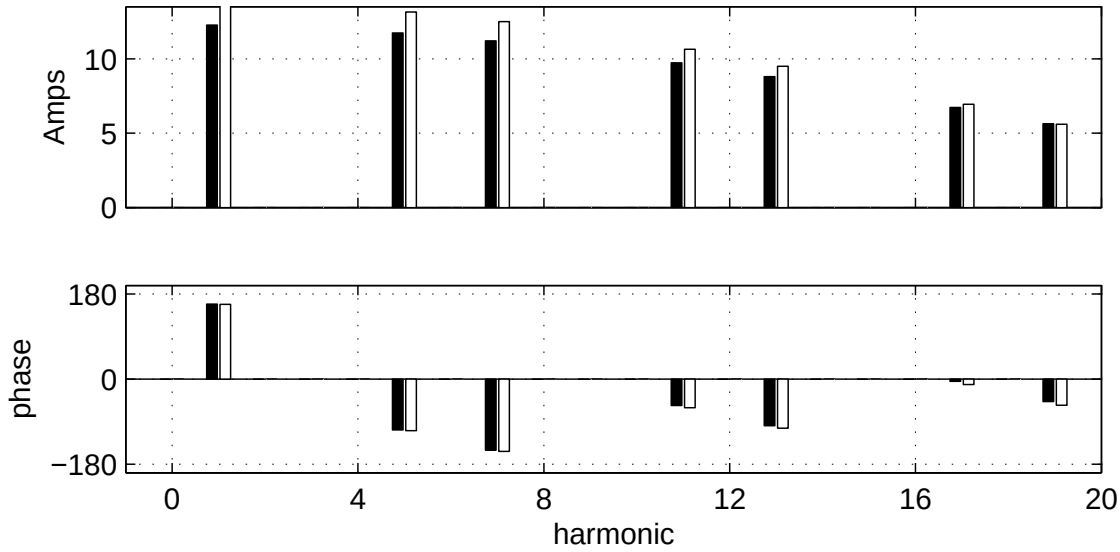

(a) Phase A Current I_a

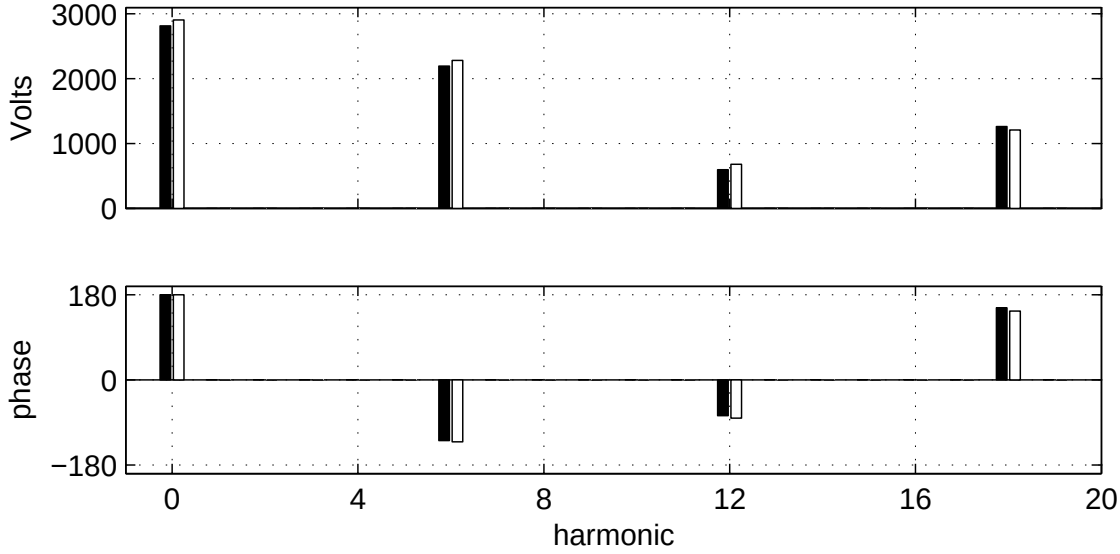

(b) DC Side voltage V_{dc}

Figure 6.10 Comparison between distortions obtained by the HSS and PSCAD-EMTDC to a 1 degree firing angle increase in DC current. **black** PSCAD, **white** HSS

performance for control inputs. The Graetz model was compared against PSCAD and showed good agreement.

Chapter 7

CAPACITOR COMMUTATED CONVERTER

7.1 INTRODUCTION

A capacitor commutated converter (CCC) is a modified Graetz bridge with capacitors placed within each AC phase, as shown in Figure 7.1. In some cases the capacitors are controlled [70] [71], [72] but in the CCC studied here it is assumed that it is static. The capacitors are included to provide an additional voltage to help drive the commutation between thyristors. In terms of operation, the CCC has several advantages over traditional Graetz bridges, summarized below; these advantages offer either a transient or a steady state benefit.

Transient Advantages

- Improved performance against remote 3-phase AC faults [73] [70] [74]. The CCC inverter is able to withstand a more severe 3-phase fault before commutation failure of the inverter occurs.
- Improved recovery from close in 3-phase AC faults [74] [70]. For the CCC both the recovery time and the stress placed on the valves following a 3-phase close in fault is less than that of a conventional Gratez bridge.

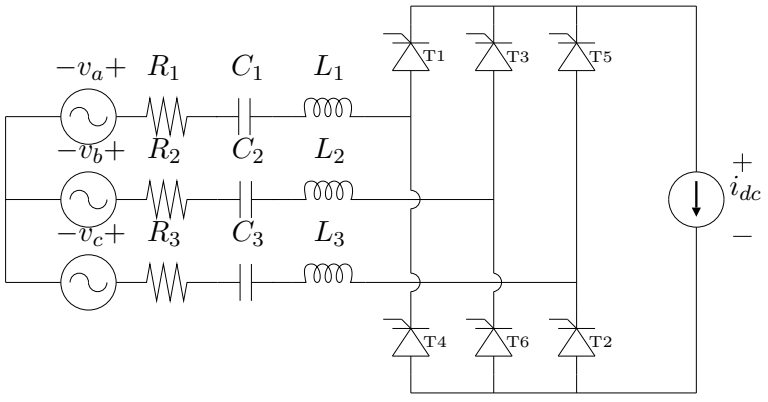

Figure 7.1 Capacitor Commutated Converter, with AC side connected in a star configuration, DC side connected to a current source, and resistance in each transformer limb.

- Improved Inverter load rejection over-voltage [74] [70]. The voltage of the CCC following a step change in inverter load, is far less than that of the conventional Gratez bridge.

- Increased allowable step change in the set point variable of the controller before commutation failure occurs [74].

- Reduced Valve short circuit overcurrent [70].

Steady State Advantages

- Reduced VAR consumption. The reduction in the VAR requirements is a direct result of the increased firing angle range and the smaller extinction angle afforded to the CCC by the commutating capacitor [73], [70], [74] [60].

- A consequence of the reduced VAR requirements of the CCC is that smaller filters can be used with narrow passbands, as the filters are only required for harmonic elimination not VAR support. [70] This narrow band filtering can be provided by a continuously tuned filter [60].

- Lower operational Short Circuit Ratio (SCR) of inverter side AC system [73],[70] enables HVdc link to be connected to *weak* AC systems or *weak* points of an otherwise strong AC system. The SCR is a measure of the strength of the AC system versus the DC Transmission system and is given by formula 7.1[25].

$$SCR = \frac{\text{Short Circuit MVA of AC system}}{\text{DC converter MW rating}} \tag{7.1}$$

.

A SCR of less than two is considered very low [75], however, there is at least one operational CCC with a worst case short circuit ratio of 1.5 [76], and simulations have found the CCC to be able to operate at SCRs of below 1[60].

A related measure for the strength of the AC:DC interaction is called the maximum available power (MAP) [70], [73] and [74]. This measure presents the interaction in the form a voltage stability PV curve from classical power systems analysis [25]. Using this measure the CCC increases the amount of power that can be transmitted to the inverter AC system before voltage instability occurs.

- The variations in an inverter's AC system voltage from its rated voltage for different converter powers is smaller for an CCC inverter than a traditional converter [70]. This lack of variation is another symptom of increased voltage stability.

- In addition to low variations in the inverter AC system voltage, the DC system also has smaller voltage variations across a range of power set points [74].

Despite these advantages the CCC also has some operational disadvantages, these are summarized below.

Transient Disadvantages

- Reduced performance against remote 1-phase faults [74]. The conventional Graetz converter is able to withstand more severe single phase faults than the CCC before commutation failure occurs.
- The recovery time of the CCC from a single phase close in fault is greater than that of a conventional Graetz bridge [74], however the valve stress during this recovery is almost identical for both conventional converters and the CCC.
- Sub-synchronous oscillations have been predicted for the operation of the CCC when connected to a weak AC system [77]. Similar oscillations are also predicted for conventional converters, however, since CCCs are able to be connected to weaker systems these oscillations are particularly relevant for CCCs.

Steady State Disadvantages

- The voltage across a converter valve is increased for a CCC due to the addition of the voltage across the commutating capacitor [60] [70]. This increase in valve voltage is the limiting factor used to determine the commutating capacitor size, typically an increase in voltage of 10% over the traditional converter valves has been proposed [70].
- The CCC under normal operation produces a higher level of harmonics than traditional Graetz bridge [60].

In addition to the CCC becoming the subject of increasing amounts of literature, it has also seen use in a real commercial system with the construction of the first commercially operating CCC at Garabi in Brazil. This station connects the Brazilian and Argentinean power systems via a 2000MW back-to-back link with the use of Asea Brown and Boveri CCC stations, as shown in Figure 7.1. Phase 1 of this station (1000MW) has been operational since June 2000, and the full 2000MW station has been fully operational since 2002 [76]. The CCCs were chosen as although the Brazilian and Argentinean systems are strong, with a combined installed capacity of 81GW, the link is sited at a weak point in both power systems, culminating in worst case SCRs of 1.5 and 2.5 in the Argentinean and Brazilian sides respectively.

In this chapter, the small signal model of the CCC is constructed, and the techniques developed for small signal models in the previous Chapters 4-6 are applied to this model. The CCC is considered a good example for an indepth analysis, as its analysis by anything other than a EMTDC/EMTP style simulation is scarce. The only non-EMTDC analysis of the CCC that the author is aware is for steady state analysis of the major frequency

Figure 7.2 2000MW Garabi back-to-back converter station cited in Brazil, and linking the Brazilian power system to the Argentinean

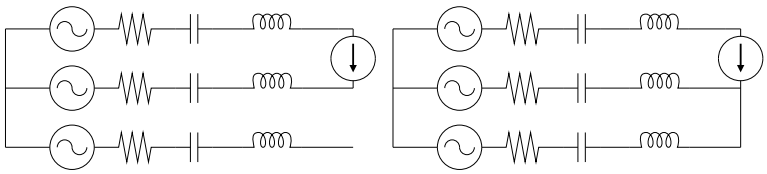

(a) Conduction Stage (b) Commutation Stage

Figure 7.3 Capacitor Commutated Converter commutation and conduction stages

components [78]. The CCC is complicated to model as not only do the states of each stage have a different phsyical meaning in each stage, it has both autonomous and controlled switching instants and it also has transients that persist across each cycle. All these aspects make the CCC a difficult modelling prospect but well within the capabilities of the modelling techniques developed in this thesis.

7.2 HYBRID MODEL

The circuit for the CCC in that depicted in Figure 7.1. With the exception of the Commutating Capacitors the circuit is identical to the Graetz bridge and the hybrid model of the Graetz bridge and the CCC have many similarities. Both have the same I/O, the same switch conditions, and under normal operation, the same stage sequence. Their differences are chiefly the differential equations that describe the continuous operation of each stage and the continuous component of the jump destination maps. As was the case with the Graetz bridge under normal operation the CCC is restricted to commutation and conduction stages, an example of each is depicted in Figure 7.3.

Governing equations Examples of the equations that govern the dynamics of each stage are shown in equations 7.2 and 7.3 for a conducting stage, and in equations 7.4 and 7.5 for a commutating stage.

The governing equations for stage 1 of the CCC are those of Equations 7.2 and 7.3, which have the same current convention as the Graetz Bridge. For a conduction stage of the CCC there are 3 elements in each state vector one for every capacitor of the bridge. During conduction there will always be one capacitor which is left floating whose voltage is maintained across the stage. In stage 1, a conduction stage, this is the voltage across capacitor $C3$. In practice there is always a large resistance in parallel with this capacitor however for the model developed here an assumption is made that the discharge into this capacitor during a typical conduction period is small enough that it isn't necessary to model it. If it is necessary to model this resistance then its damping effect can be included fairly easily by modification to the stage DEs.

$$\begin{bmatrix} \dot{vcap_a}(t) \\ \dot{vcap_b}(t) \\ \dot{vcap_c}(t) \end{bmatrix} = \begin{bmatrix} 0 & 0 & 0 \\ 0 & 0 & 0 \\ 0 & 0 & 0 \end{bmatrix} \begin{bmatrix} vcap_a(t) \\ vcap_b(t) \\ vcap_c(t) \end{bmatrix} + \begin{bmatrix} 0 & 0 & 0 & \frac{1}{C_1} & 0 \\ 0 & 0 & 0 & -\frac{1}{C_2} & 0 \\ 0 & 0 & 0 & 0 & 0 \end{bmatrix} \begin{bmatrix} v_a(t) \\ v_b(t) \\ v_c(t) \\ i_{dc}(t) \\ \frac{di_{dc}(t)}{dt} \end{bmatrix} \tag{7.2}$$

$$\begin{bmatrix} i_a(t) \\ i_b(t) \\ i_c(t) \\ v_{dc}(t) \end{bmatrix} = \begin{bmatrix} 0 & 0 & 0 \\ 0 & 0 & 0 \\ 0 & 0 & 0 \\ -1 & 1 & 0 \end{bmatrix} \begin{bmatrix} vcap_a(t) \\ vcap_b(t) \\ vcap_c(t) \end{bmatrix} + \begin{bmatrix} 0 & 0 & 0 & 1 & 0 \\ 0 & 0 & 0 & -1 & 0 \\ 0 & 0 & 0 & 0 & 0 \\ 1 & -1 & 0 & -(R_1+R_2) & -(L_1+L_2) \end{bmatrix} \begin{bmatrix} v_a(t) \\ v_b(t) \\ v_c(t) \\ i_{dc}(t) \\ \frac{di_{dc}(t)}{dt} \end{bmatrix} \tag{7.3}$$

The governing equations for stage 7 of the CCC are those of Equations 7.4 and 7.5. The elements of the state vector are the current in the commutating "on" phase (the same as the Graetz Bridge) and two states for the three capacitors. Only two states are needed as the capacitors form a loop in which the voltage across any two capacitors can determine the voltage across the remaining capacitor. In the description given here the states chosen are the voltage across the the commutating "on" capacitor, $v_{com}(t)$, and the voltage across the capacitor of whichever phase is connected to the rail that is not commutating, $v_{cond}(t)$. Similar equations can be written for the other 5 commutating stages.

$$\begin{bmatrix} \dot{v_{cond}}(t) \\ \dot{v_{com}}(t) \\ \dot{i_{com}}(t) \end{bmatrix} = \begin{bmatrix} 0 & 0 & 0 \\ 0 & 0 & -\frac{1}{C_3} \\ \frac{1}{L_2+L_3} & \frac{2}{L_2+L_3} & -\frac{R2+R3}{L_2+L_3} \end{bmatrix} \begin{bmatrix} v_{cond}(t) \\ v_{com}(t) \\ i_{com}(t) \end{bmatrix} + \begin{bmatrix} 0 & 0 & 0 & \frac{1}{C_1} & 0 \\ 0 & 0 & 0 & 0 & 0 \\ 0 & \frac{1}{L_2+L_3} & -\frac{1}{L_2+L_3} & \frac{R_2}{L_2+L_3} & \frac{L_2}{L_2+L_3} \end{bmatrix} \begin{bmatrix} v_a(t) \\ v_b(t) \\ v_c(t) \\ i_{dc}(t) \\ \frac{di_{dc}(t)}{dt} \end{bmatrix} \tag{7.4}$$

$$\begin{bmatrix} i_a(t) \\ i_b(t) \\ i_c(t) \\ v_{dc}(t) \end{bmatrix} = \begin{bmatrix} 0 & 0 & 0 \\ 0 & 0 & 1 \\ 0 & 0 & -1 \\ -1-\frac{L_3}{L_2+L_3} & 1-2\frac{L_3}{L_2+L_3} & -R_3+L_3\frac{(R_3+R_2)}{L_2+L_3} \end{bmatrix} \begin{bmatrix} v_{cond}(t) \\ v_{com}(t) \\ i_{com}(t) \end{bmatrix} + \begin{bmatrix} 0 & 0 & 0 & 1 & 0 \\ 0 & 0 & 0 & -1 & 0 \\ 0 & 0 & 0 & 0 & 0 \\ 1 & -\frac{L_3}{L_2+L_3} & \frac{L_3}{L_2+L_3}-1 & -R_1-\frac{L_2R_2}{L_2+L_3} & -L_1-\frac{L_2L_3}{L_2+L_3} \end{bmatrix} \begin{bmatrix} v_a(t) \\ v_b(t) \\ v_c(t) \\ i_{dc}(t) \\ \frac{di_{dc}(t)}{dt} \end{bmatrix} \tag{7.5}$$

Jump destination Maps The discrete parts of the CCC's destination maps are the same as those of the Graetz bridge, the difference lie in the continuous maps. Under normal operation there are two types of map, those that map the states of a conduction stage to a commutation stage, and the reverse, those that map the states of a commutating stage to a conducting stage. An example of each is shown below.

Equation 7.6 shows the continuous portion of the jump destination map of stage 7 (commutating stage) to stage 2 (conduction stage). In this map there is no contribution from the input, so the map only has a projection matrix.

$$\begin{bmatrix} vcap_a(t) \\ vcap_b(t) \\ vcap_c(t) \end{bmatrix} = \begin{bmatrix} 1 & 0 & 0 \\ -1 & -1 & 0 \\ 0 & 1 & 0 \end{bmatrix} \begin{bmatrix} v_{cond}(t) \\ v_{com}(t) \\ i_{com}(t) \end{bmatrix} \tag{7.6}$$

Equation 7.7 shows the continuous portion of the jump destination map of stage 1 (conduction stage) to stage 7 (commutation stage).

$$\begin{bmatrix} v_{cond}(t) \\ v_{com}(t) \\ i_{com}(t) \end{bmatrix} = \begin{bmatrix} 1 & 0 & 0 \\ 0 & 0 & 1 \\ 0 & 0 & 0 \end{bmatrix} \begin{bmatrix} vcap_a(t) \\ vcap_b(t) \\ vcap_c(t) \end{bmatrix} \tag{7.7}$$

iteration	$v_{cond}(t^+_{\theta_1})$	$v_{com}(t^+_{\theta_1})$	$i_{com}(t^+_{\theta_1})$	t_{θ_2} (ms)	t_{θ_4} (ms)	t_{θ_6} (ms)	t_{θ_8} (ms)	$t_{\theta_{10}}$ (ms)	$t_{\theta_{12}}$ (ms)
0	0.0	0	0	0.0028	0.0061	0.0094	0.0128	0.0161	0.0194
1	5396.3	-64527	0	0.0028	0.0061	0.0094	0.0128	0.0161	0.0194
2	3283.8	-38562	0	0.0031	0.0064	0.0097	0.0131	0.0164	0.0197
3	3914.9	-45789	0	0.0031	0.0064	0.0097	0.0130	0.0164	0.0197
4	4022.8	-46297	0	0.0030	0.0064	0.0097	0.0130	0.0164	0.0197
5	4022.7	-46296	0	0.0030	0.0064	0.0097	0.0130	0.0164	0.0197
6	4022.7	-46296	0	0.0030	0.0064	0.0097	0.0130	0.0164	0.0197

Table 7.1 The candidate solutions after each iteration for the Capacitor Commutated Converter

7.3 SMALL SIGNAL MODEL

7.3.1 Shooting method

As was done in Chapter 4 for the Buck-Boost converter, the small signal model of the CCC is used to find the cyclic steady state (CSS) of a CCC subjected to periodic inputs of 375.36kV peak 3-phase AC side voltages, a 2kA DC current, and a 15^o firing angle. The passive components of the CCC in each phase have the following values, $R = 1\Omega$, $L = 0.0428H$, and $C = 144\mu F$.

The CCC has transients that persist over the length of each cycle so the two point boundary value problem is solved for the initial state at the start of each cycle, in parallel with a set of switching instant problems for each of the autonomous switching instants. The output waveforms of the CSS are shown in Figure 7.4 and compared to those waveforms found using PSCAD. The candidate solution after each iterative step is summarized in Table 7.1. The first candidate solution has all electrical states at zero, and all autonomous switching angles 5 degrees delayed from the preceding controlled switching instant.

When compared to the Graetz bridge that was solved in Chapter 4 the CCC has a shortened commutation angle as expected by the use of the commutation capacitors ($\mu_{CCC} = 9.8880^o$, $\mu_{Graetz} = 12.9614^o$).

7.3.2 Small Signal Model: Time-domain transient evolution

Using the base case defined in Table 7.1, the small signal time domain evolutions of the CCC are depicted in Figures 7.5 and 7.6 for a CCC subjected to a 10kV, 150Hz phase a voltage disturbance, and a 1 degree increase in firing angle. Both disturbances are applied as step changes, and their effects are studied by looking at the voltages across the commutating capacitors.

As can be seen in both these figures the small signal model produces results which have a good match with PSCAD.

7.3.3 Harmonic Sensitivity Matrix derived using partial waveforms

The HSM of the CCC is constructed from its small signal model using the partial waveform techniques outlined in Chapter 5 around the base-case operating point found in the

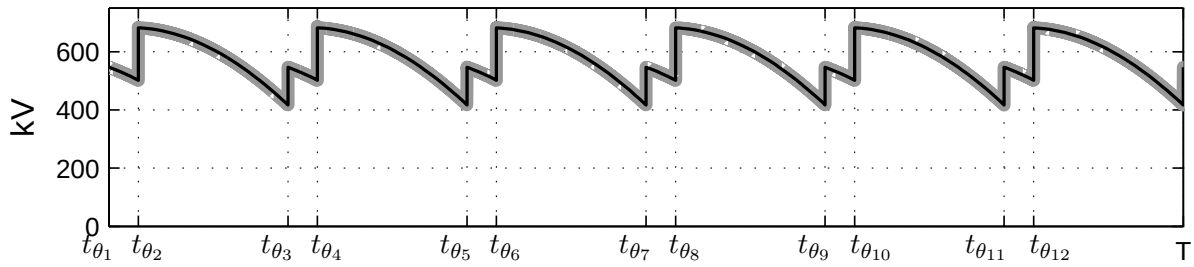

(a) DC side voltage

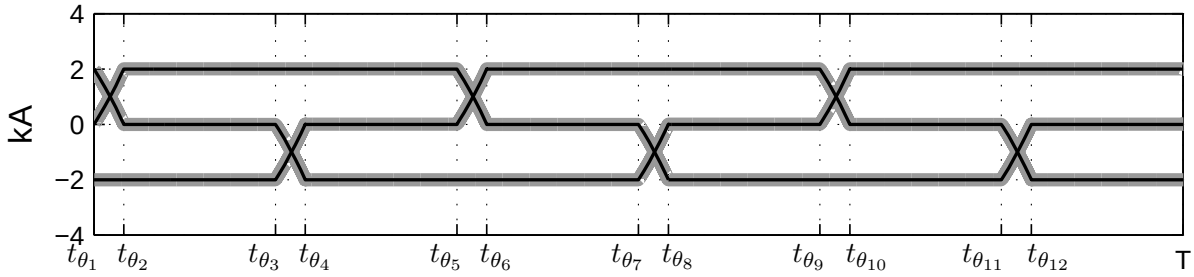

(b) AC side phase currents

Figure 7.4 Comparison between a PSCAD solution to the CSS of a Capacitor Commutated Converter and a Newton solution. **grey/thick** PSCAD, **black/thin** Newton.

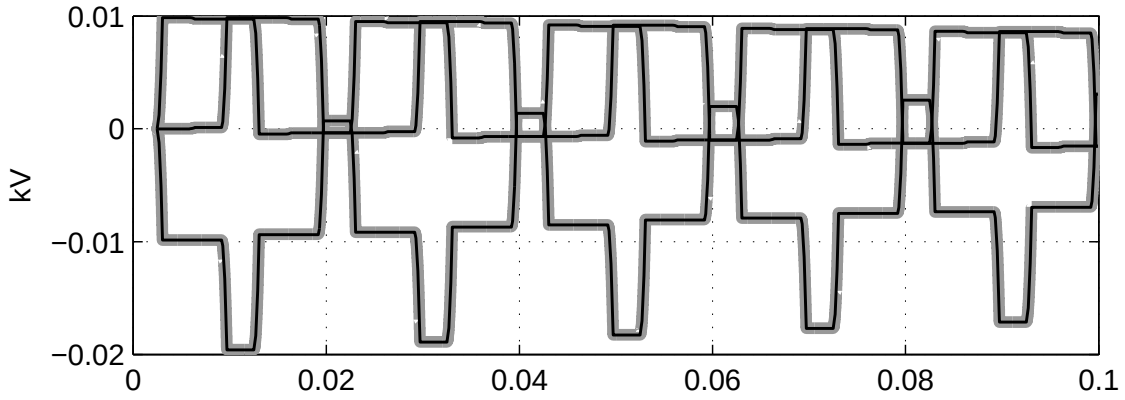

Figure 7.5 Comparison between distortions obtained by the HSS and PSCAD-EMTDC for a capacitor commutated converter subjected to a 10kV, 150Hz, disturbance in phas A voltage. **thick** PSCAD, **thin** Small Signal

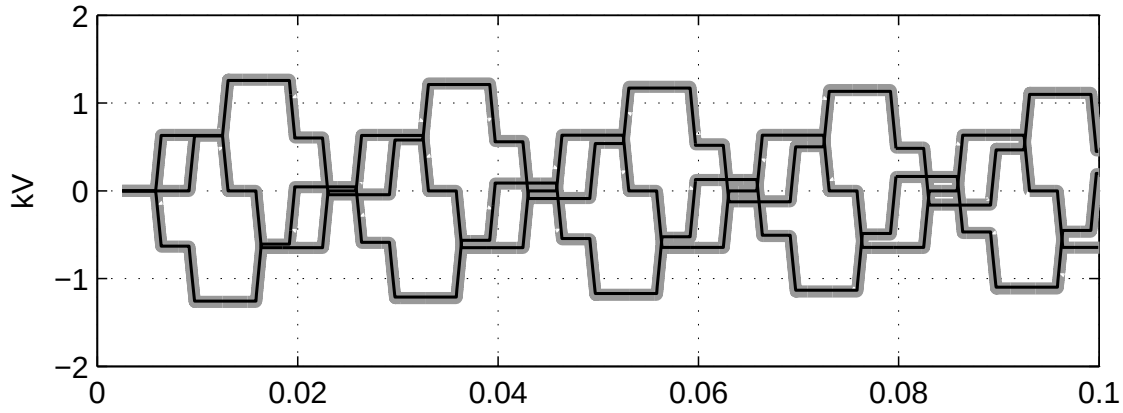

Figure 7.6 Comparison between distortions obtained by the HSS and PSCAD-EMTDC for a capacitor commutated converter subjected to a 1 degree increase in firing angle. **thick** PSCAD, **thin** Small Signal

previous section. The HSM is truncated to 41 components, and verified against PSCAD in Figures 7.7 and 7.8 for a 10kV 150Hz phase-a voltage disturbance, and a 1 degree increase in firing angle.

7.4 HARMONIC STATE SPACE

7.4.1 Harmonic Sensitivity Matrices

The alternative technique to finding the HSM is by using a HSS model. The HSS model is used to find the HSM of the CCC and is subjected to the same disturbances as the HSM derived in the previous chapter as shown in Figures 7.9 and Figures 7.10. In this case the HSM is derived for 41 harmonic components. The HSM has a good match with the PSCAD data, the mismatch that is present is largely due to harmonic truncation, if the harmonic components are increased the size of the mismatches effectively vanishes.

For this analysis the DEs of the CCC are transformed to an expanded new state space with four elements, one for each of the three capacitors and one for the commutating inductor. This new state space is used to reduce truncation errors present when capacitor C_3 and the commutating stage inductor L_{com} share the same position in the state vector.

7.4.2 Transient Evolution

The transient evolution of the CCC is modeled here by the HSS for the 10kV, 150Hz, step change in the phase A voltage. The most evident effect of the transient evolution of the CCC is the voltage across the commutation capacitors. This voltage is shown in Figure 7.11 for all three phases for several HSS models truncated to 6,21,41 and 81 harmonic components. As was the case with the HSM produced by the HSS, the transient evolution is also affected by truncation of the harmonic vector.

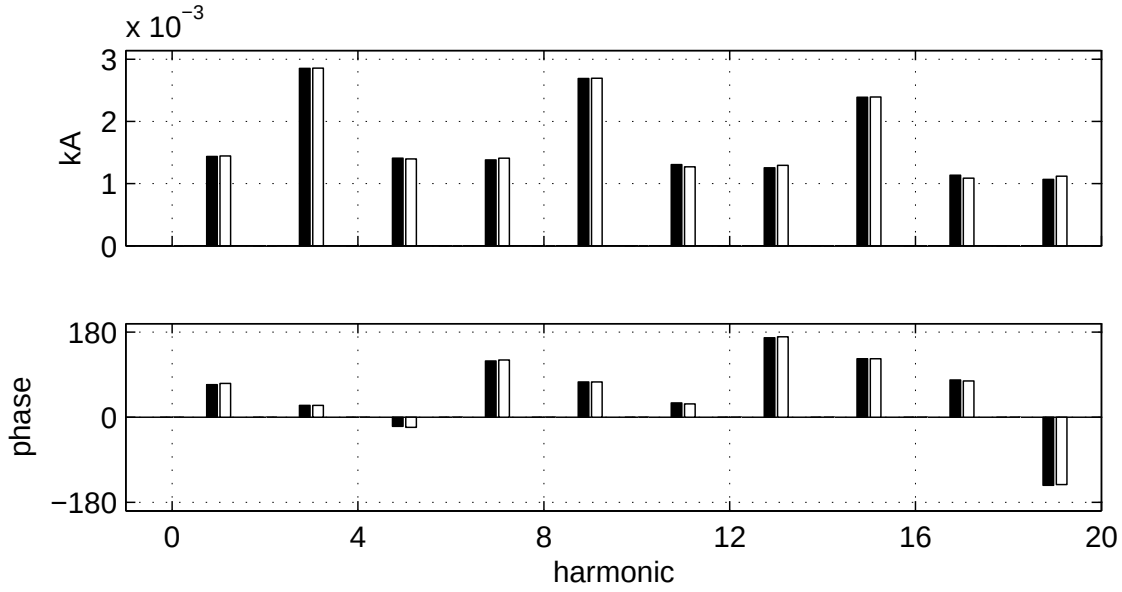

(a) Phase A Current I_a

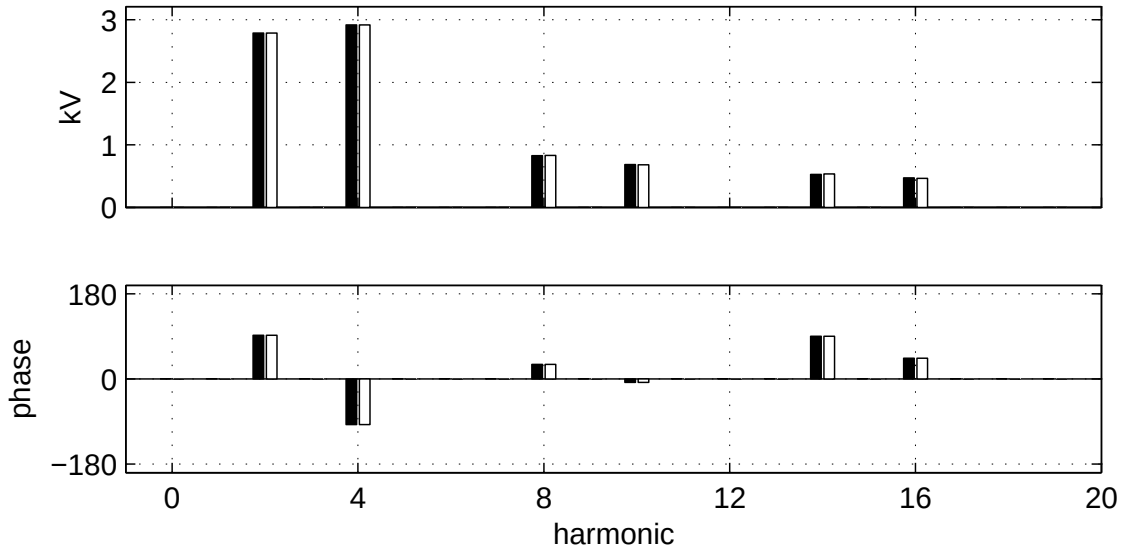

(b) DC Side voltage V_{dc}

Figure 7.7 Comparison between distortions obtained by the piecewise formation of a HSM and PSCAD-EMTDC for a capacitor commutated converter subjected to a 10kV, 150Hz phase a voltage disortion. **black** Partial Waveform HSM**white** PSCAD

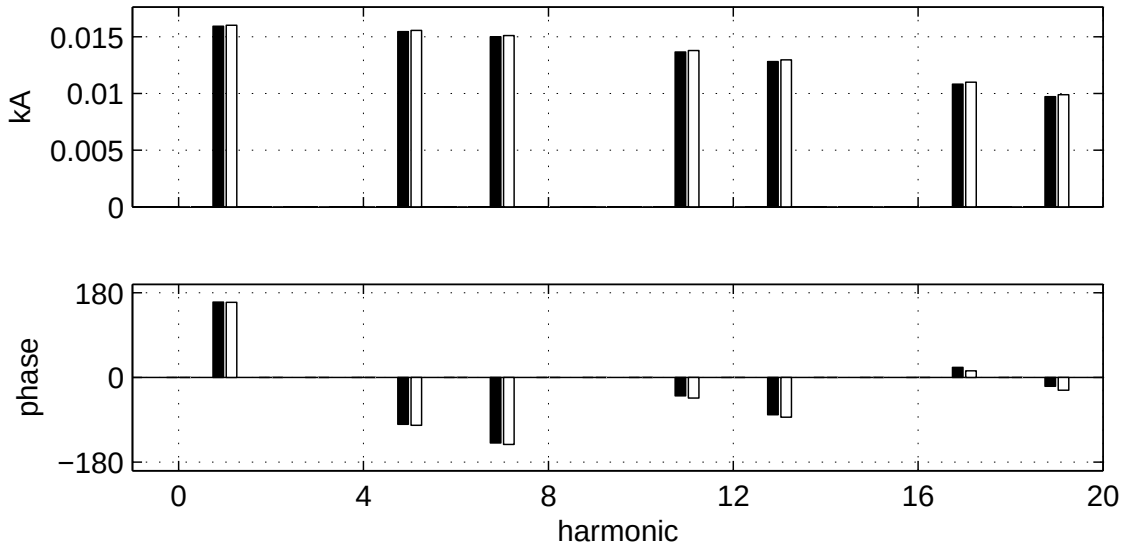

(a) Phase A Current I_a

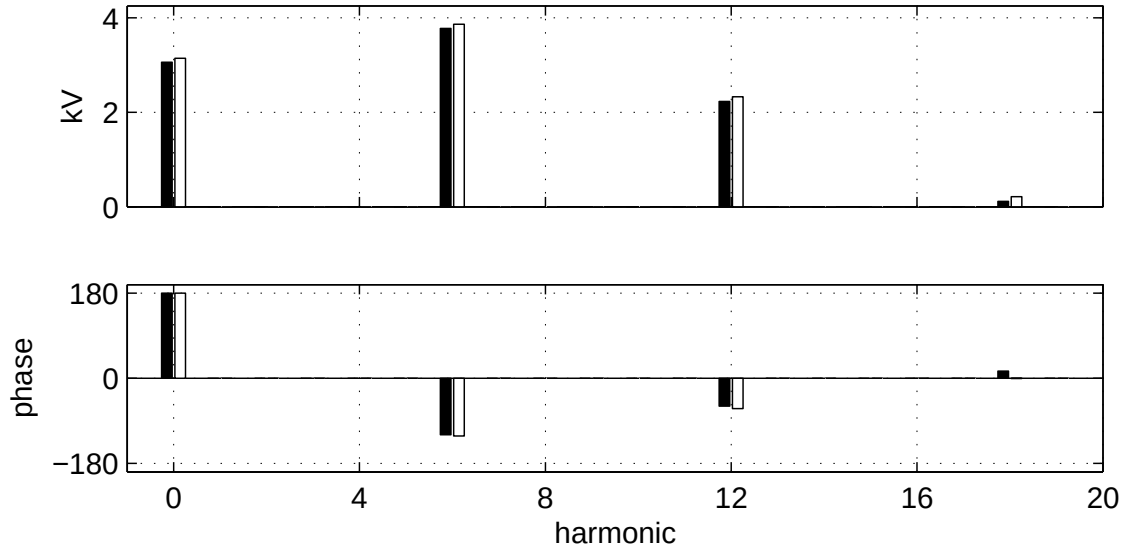

(b) DC Side voltage V_{dc}

Figure 7.8 Comparison between distortions obtained by the piecewise formation of a HSM and PSCAD-EMTDC for a capacitor commutated converter subjected to a 1 degree increases in firing angle. **black** Partial Waveform HSM**white** PSCAD

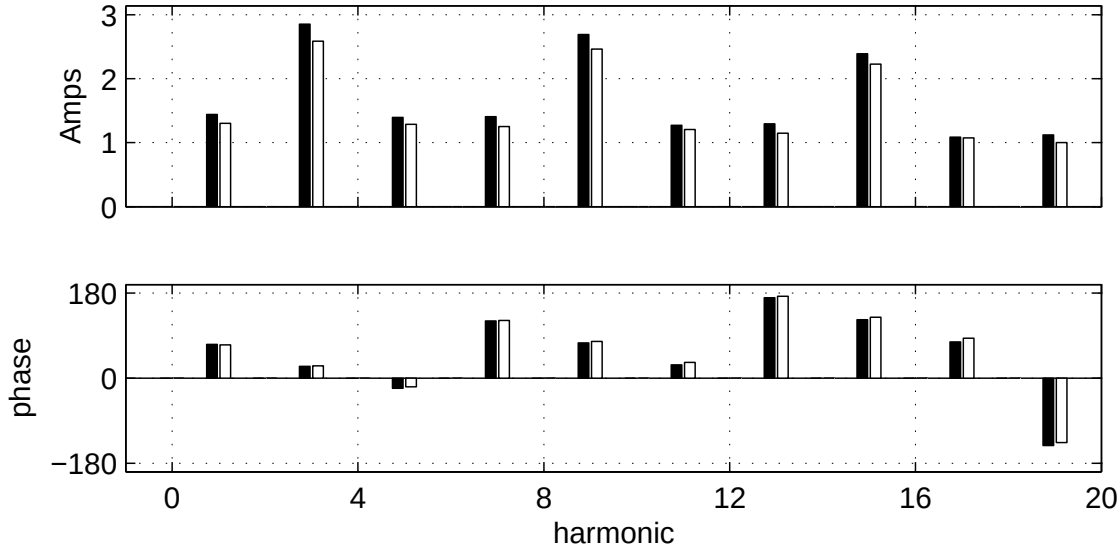

(a) Phase A Current I_a

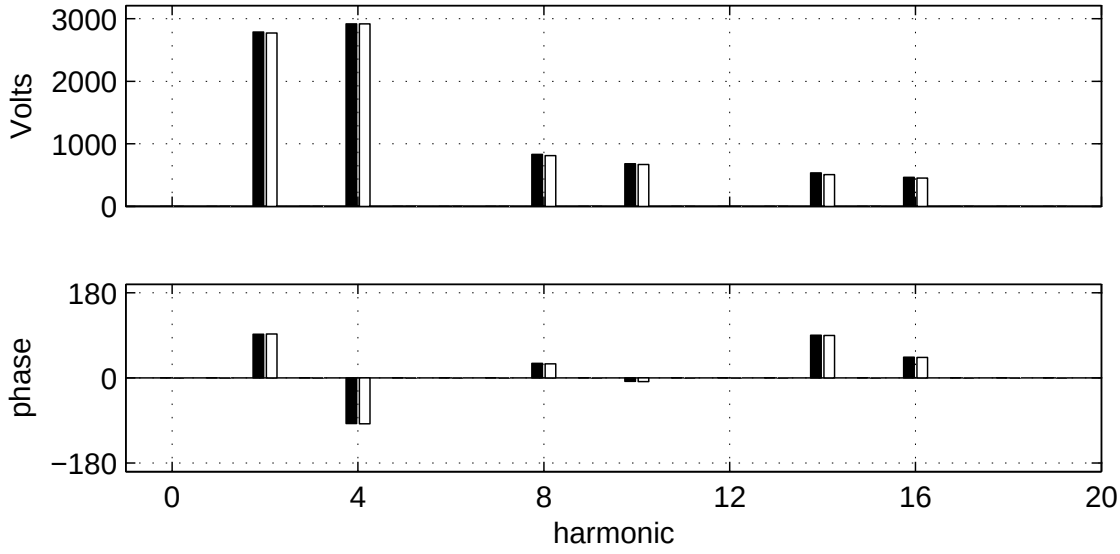

(b) DC Side voltage V_{dc}

Figure 7.9 Comparison between distortions obtained by the HSS and PSCAD-EMTDC for a capacitor commutated converter subjected to a 10kV, 150Hz phase a voltage disortion. **black** HSS, **white** PSCAD

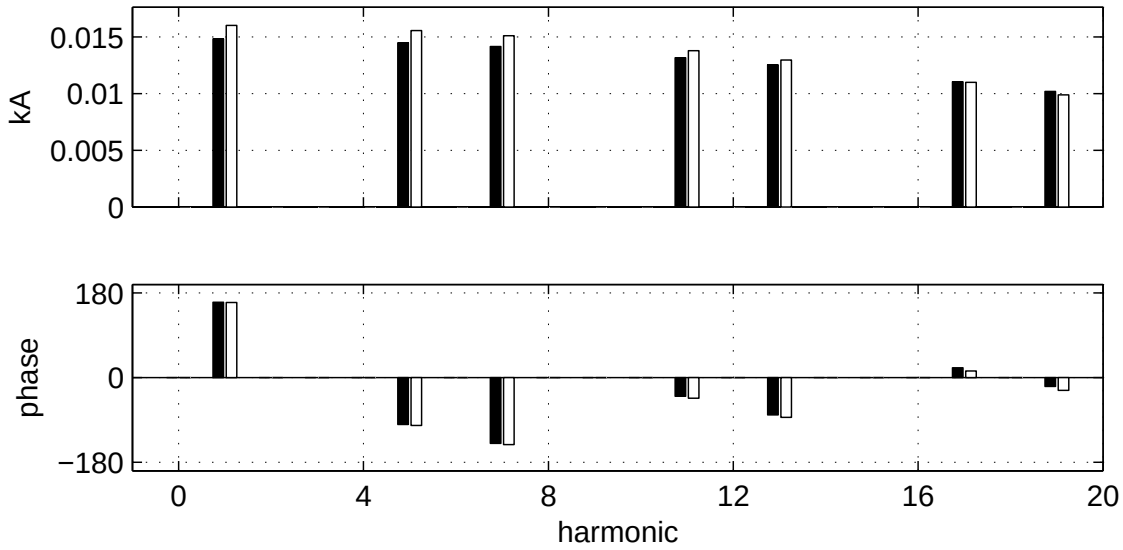

(a) Phase A Current I_a

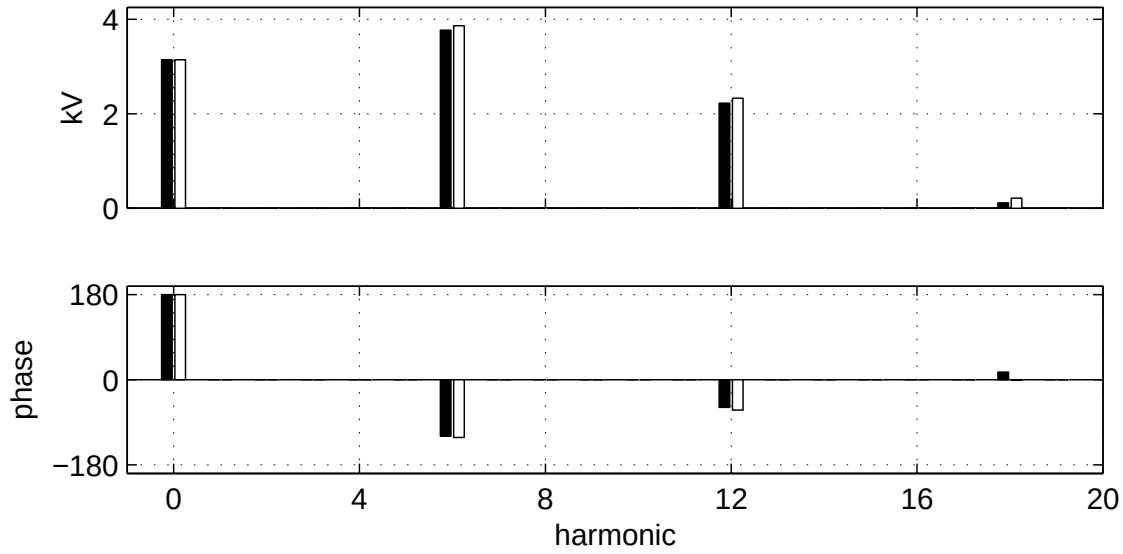

(b) DC Side voltage V_{dc}

Figure 7.10 Comparison between distortions obtained by the HSS of and PSCAD-EMTDC for a capacitor commutated converter subjected to a 1 degree increases in firing angle. **black** HSS, **white** PSCAD

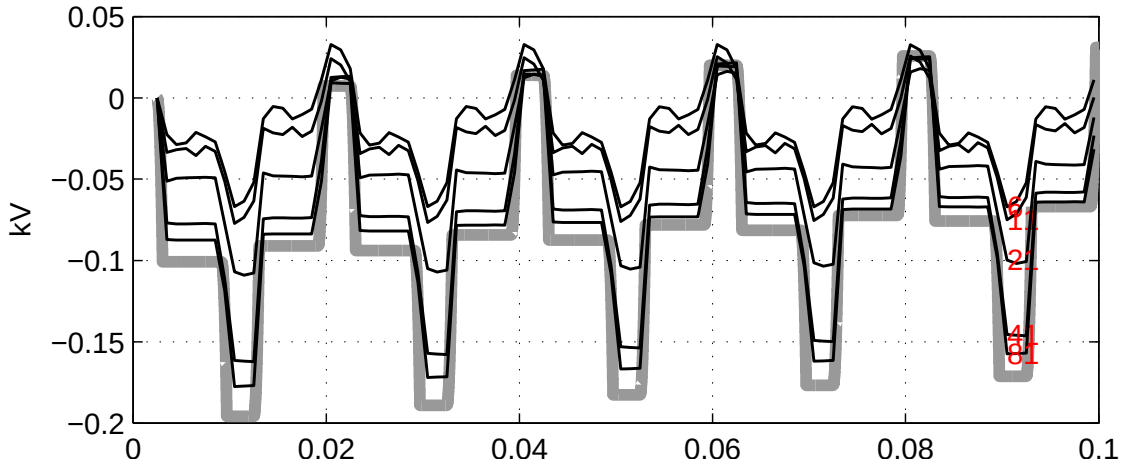

(a) Phase A Capacitor Voltage

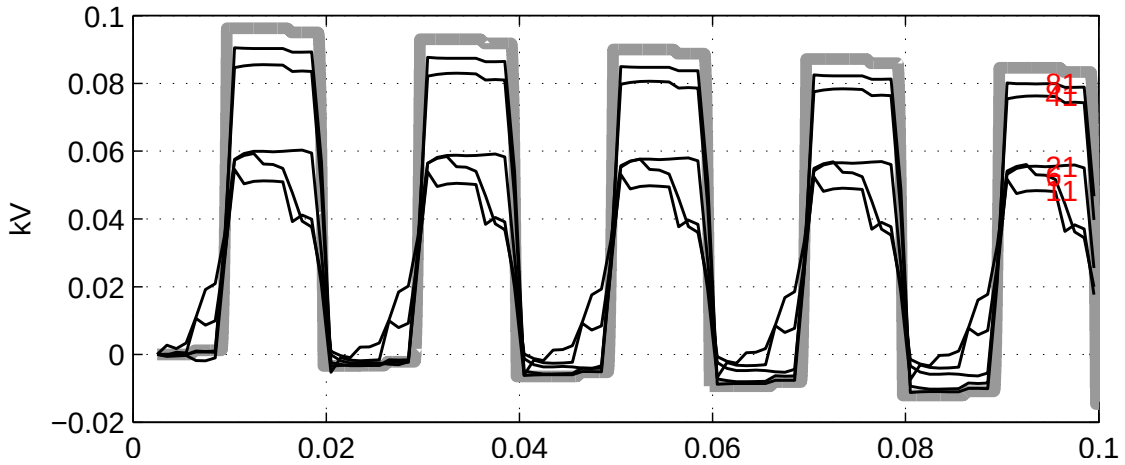

(b) Phase B Capacitor Voltage

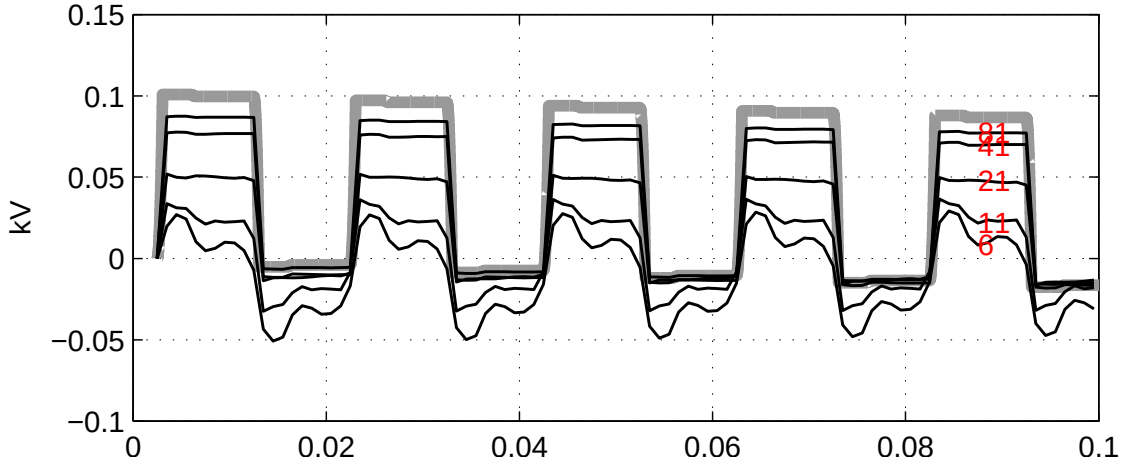

(c) Phase C Capacitor Voltage

Figure 7.11 Comparison between the transient evolutions of a HSS model reduced to its major energy components with scaling and PSCAD-EMTDC for a capacitor commutated converter subjected to a 10kV, 150Hz phase A voltage disortion. **grey** PSCAD, **black** HSS

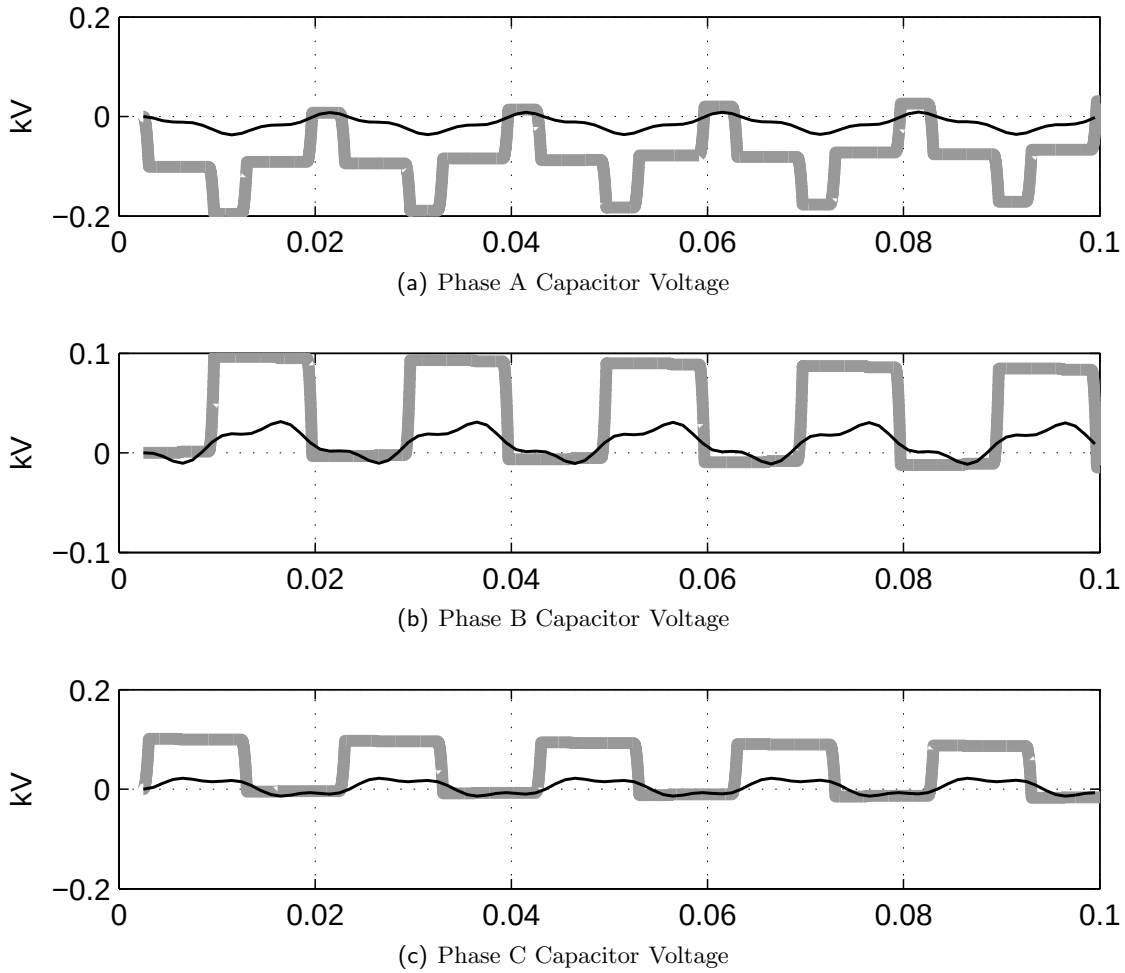

(a) Phase A Capacitor Voltage

(b) Phase B Capacitor Voltage

(c) Phase C Capacitor Voltage

Figure 7.12 Comparison between the transient evolutions of a HSS model reduced to its major energy components with scaling and PSCAD-EMTDC for a capacitor commutated converter subjected to a 10kV, 150Hz phase A voltage disortion. **grey** PSCAD, **black** HSS

One very useful model to have is the HSS of a CCC, with vectors reduced to just the main energy harmonics, the harmonic of the main energy component is the largest harmonic of the base case operating point. This truncates the AC electrical inputs (V_a, V_b, V_c), AC electrical outputs, (I_a, I_b, I_c), and the capacitor states the first (50Hz) harmonic, i.e. $\{-1, 1\}$. The DC electrical input (I_{dc}) the DC electrical output (V_{dc}), and the control components to the 0Hz harmonic, $\{0\}$. Lastly the commutating state is truncated to the (150Hz) harmonic i.e. $\{-3, 3\}$. This truncated state space model is compared to the PSCAD model for a 10kV, 150Hz step change in AC voltage Figure 7.12.

As can be seen from Figure 7.12 the HSS model of the CCC reduced to just its main energy components and is extremely effected by truncation errors. This is not unexpected when looking at Figure 7.11 which shows that even a HSS with 6 harmonic components per electrical input is susceptible to truncation errors.

7.5 DISCUSSION

Once the hybrid model of the CCC is defined, the general techniques of the rest of the thesis were applied without alteration. Being able to apply techniques generally without alteration was a major objective of this thesis, and their application to modelling a CCC shows that this objective has been meet.

Despite successful modelling of the CCC, this chapter showed there is still some work needed to produce a general algorithm for the systematic creation of harmonic state space models that are not so heavily affected by harmonic truncation. As was discussed in the previous chapter the main cause of the truncation errors are impulses in the system dynamics matrix. There are two sources of these impulses, autonomous switching variations, and basis changes between stages. For the Buck-Boost converter the effect is completely due to basis changes caused when a stage went from having two states to one state. For the capacitor commutated converter both the effects of autonomous switching instant variations and changing of basis between each stage have contributed to the truncation errors.

The scale of the basis changes can be found by examining the projection matrixes of equation 7.6 and 7.7. If no change in basis were to occur then these matrixes would be identity matrixes, which as these equations show they clearly aren't. A potential method for alleviating the truncation errors caused by basis changes is to construct the system descriptions, and choose the states of each stage, in such a way to produce projection matrices between neighboring stages that are as close to identity matrices as possible. Ideally an algorithm would transform physically meaningful state descriptions for each stage, like the states of the CCC description modelled in this chapter, to the potentially physically meaningless description used to reduce the number of impulses in the periodic dynamics matrix. One method of achieving this for projection matrixes that are diagonalizable is to find the matrix LDR transform [79]. The pre switching state is multiplied on the right by the *Left* and *Diagonal* matrixes of the transform, whilst the post switching state is multiplied on the left by the *right* hand matrix of the transform. The new projection matrix between the two transformed states would then become the desired identity matrix.

The effects of autonomous switching instant variation on the capacitor voltages are apparent from Figure 7.11 where large changes in capacitor voltages occur at the switching instants. A potential method for alleviating the effects of truncation due to switching instant variations is to split a system into subsystems so that the switches are isolated from the passive energy components. For the capacitor commutated converter a good split would be to separate the system into two between the capacitors, and the inductors. This would split the capacitors and AC voltages sources into one subsystem, whilst the inductors, resistors and thyristors would form the other subsystem. The HSS of each subsystem could be formed in isolation, before they are connected together to form a complete system description. Further discussion on splitting large subsystems into subsystems is discussed in the remaining chapter of this thesis, Chapter 8.

7.6 CONCLUSION

The small signal techniques developed else-where in this thesis were applied and verified for the Capacitor Commutated Converter. The partial waveform technique was able to produce Harmonic Sensitivity Matrices that accurately modelled the sensitivity of the CCC to small signal harmonic disturbances. The HSS is also able to model both the effect of harmonic disturbances on the steady state and the effect of step changes in the input on the transient evolution. The HSS however did require a disappointingly high number of harmonics to produce an accurate response.

Chapter 8

CONCLUSIONS AND FUTURE WORK

The study of power electronic devices within power systems has traditionally been via time domain simulation using commercial programs such as PSCAD-EMTDC or PSPICE. Time domain simulation is a powerful and mature technique that can model unusual circuit topologies with ease. However, time domain simulation is not always ideal for tasks such as controller design, filter design or stability analysis. Additionally time domain simulation is too computationally intensive to be used in large scale contingency analysis. Unfortunately alternatives to time-domain simulation for power electronic devices are lacking, especially for rare or new topologies such as the capacitor commutated converter. In this thesis a set of such techniques were developed – all techniques that exploit the small-signal linearity of converters.

The first step in the development of a small signal description was defining the operation of an ideal power electronic circuit containing passive devices and ideal switches. In this thesis this was achieved with a hybrid model. The hybrid model described the circuit as a set of stages, described as sets of 1st order differential equation sets (or state space equations), and a set of rules for jumping between them. These rules were of three parts; jump sets which determine when to switch, discrete jump destination maps that determine which stage to switch too, and continuous jump destination maps that determine the initial state of the new stage.

To produce a small signal model of the hybrid converter the effect of distortions was detailed. Of crucial importance was the effect of switching instant variations from both controlled and autonomous switches. The effect was shown to be a step change in the initial state of the stage following the switching instant variation, and an impulse in the output.

The first application of the small signal model was developing a general technique for obtaining the cyclic steady state solution of a converter subjected to periodic oscillating electrical inputs and periodic control orders. This technique used a Newton based solution in two parts, a TPBV portion and a switching instant problem. The small signal model was used to describe the sensitivities between solution variables and mismatch equations in the form of a Jacobian. Although this technique was not novel it did demonstrate the

usefulness of a small signal model.

The second technique developed was the *analytically described* formation of a harmonic sensitivity matrix (HSM). The construction of a general non-numerical technique for constructing a HSM is a major advance of this thesis. The HSM was built using a partial waveform technique, where the partial transient, steady state and resonant response of each stage was calculated and summed together. The greatest difficulty to be overcome in the development of this technique was finding the initial state at the start of each stage, which is needed for determining the magnitude of the relaxations of each partial transients. In this thesis a TPBV argument was used to form an expression for calculating these states.

The final model developed was the harmonic state space model of a power electronic converter. The HSS model is a LTP analogue of a LTI state space description and can be used to describe a power electronic converter operating around a periodic base case. The HSS can be used as an alternative technique for finding the harmonic sensitivity of a converter, it also can be used to describe the dynamic behavior of the converter as well. It was found that systems with state dependent autonomous switches required large number of harmonics in their description to minimize truncation errors.

Finally the techniques were applied to the capacitor commutated converter. The techniques all performed well when verified against PSCAD simulations. However as was predicted the HSS performed poorly when it was truncated to just a few harmonics.

8.1 FUTURE WORK

In this thesis, the focus has been upon the modelling of a single power electronic topology. Despite this the intention has always been that the derived models will be included in a larger system divided into subsystems. Two styles of system descriptions that are in mind are a dynamic s-domain description, and a harmonic domain description used for finding the harmonic steady state of a system.

Dynamic system description Algorithms for reducing two subsystems written as LTI state space descriptions to a single state space equation are well known and in common use. For a HSS similar reduction of subsystems could easily be achieved, with care needed to ensure that the EMP signals between connecting subsystems be truncated to the same harmonic components. By writing control systems as HSS subsystems, remembering that any LTI system (such as a PI controller) can easily be written as a HSS system, including the effects of control on a power electronic device could be achieved.

Harmonic Steady State of a system Finding the harmonic steady state of a power electronic circuit has a long history in the literature. The most extensive and compre-

hensive work on the subject to date is that contained in the thesis of Bathurst [46]. In this work systems are divided into subsystems whose interactions with one another is described using harmonic domain signals. The complete solution to the system is solved using a Newton's method. The mismatch equations of the Newton's method are typically busbar signals described in the harmonic domain. For example at an AC busbar, the three phase voltages are used as solution variables, and the currents that feed into the busbar are arranged using Kirchoff's current law to form the mismatch equations. For power electronic and other non-linear devices, additional solution and control variables are included – including switching instants. As a Newton's method is used, a Jacobian is needed that relates the sensitivity of the solution variables to the mismatches; in the implementation of Bathurst and others this Jacobian is largely in the form of a harmonic sensitivity matrix.

The work in this thesis enables the modelling of any power electronic topology in the HD iterative method framework. Like all subsystems included in the framework, two routines are needed. The first routine is used to find the power electronic subsystem's contribution to the busbar mismatch equations. Essentially this routine can be described as the problem of finding the steady state output of a device subjected to an input. The second routine describes the harmonic domain sensitivity of the device in the form of a matrix.

The solution to the steady state output of a power electronic device can be broken down to finding three pieces of information; the stage sequence of the device, the autonomous switching instants of the device, and if at least part of the device's state persists across an entire period of evolution, the state somewhere within the period. This last piece of information has not been necessary for converters so far modelled in the iterative HD literature. The best way to achieve the three pieces of information is with a combination of simulation and shooting methods, as outlined by [44], and already discussed in Chapter 4. To describe the contribution to the mismatch equation in the harmonic domain, each stage's contribution would be described using their partial forms before being convolved by a sampling function.

The second necessary routine is an algorithm for finding the harmonic sensitivity between the input and the output of a device. This is easily found using either the partial waveform technique of Chapter 5 or the HSS technique of the Chapter 6. Further work is needed to discover which technique is fastest.

As the implementation used by Bathurst [46] is modular in nature, it should be a simple task to add a general power electronic model. The modularity of the overall system is particularly useful for its implementation in a parallel computer, and is a particularly fortuitus aspect of the technique, considering that most PCs are soon predicted to have multi-core processors [80]. A future development of the implementation of Bathurst would be to apply threading to the algorithm.

Other LTP systems Many other non-linear devices, including controller elements such as phase locked loops, and electrical elements, in particular Transformers, found in electric powers system are well suited for approximation as LTP systems written in the HSS. Their inclusion would be important for studies of power systems containing power electronics.

Harmonic resonance A system of connected HSS models is clearly a promising tool for determining harmonic resonant problems associated with power electronics. A classic and much studied example is the so called core-saturation instability of Ainsworth [81]. Two recent examples of such a resonance are; Harmonic resonance resulting in failure of the Swiss rail system [16], and Turbine-Generator shaft vibrations in a Norwegian oil platform that is believed to have been caused by harmonics of variable speed drives [82]. A HSS model is prefectly suited for the study of these kinds of harmonic resonances. It is expected that in some cases the resonance will be found by truncating the HSS to those harmonics central to the energy transfer of the systems, whilst in others the resonance might be caused by harmonics being cross coupled to a resonant close to a resonating mode of the system.

Asynchronous links and systems In the discussion presented on connecting systems, it was assumed that the connected systems were synchronized with each other and had a common pumping frequency. In many cases this is not true, and connected subsystems could have vastly different pumping frequencies. In cases where the asynchronous components are both integer multiplies of another common frequency, (i.e. a 50Hz 60Hz asynchronous link has a common base of 10HZ), then it is a simple task of writing the HSS or HSM of each system using the common base frequency and period. This was done by Hume for an asynchronous HVDC link [83]. In general however, there is no guarantee of a common base, in these cases a different approach is needed, one such approach that may prove fruitful is outlined here, and may warrant further investigation.

In the HSS a domain of signals called the EMP domain was constructed to allow for the frequency transformation that can occur in LTP systems. It is proposed here that for asynchronous systems a new type of signal is needed. The form of this new signal is an exponential that instead of modulating a set of harmonics, modulates the set of all frequencies. As an analogue this new signal is to EMP signals, what the Fourier transform is to Fourier series. This new signal space is described here as a Exponentially modulated Frequency Spectrum, or (EFS-domain) and is defined below.

Definition 8.1 (Exponential modulated Frequency Spectrum(EFS-domain)) *The EFS-domain has a form that is described by equation 8.1.*

$$u(t) = \left[\sum_{k=-\infty}^{\infty} e^{j2\pi f_k t} \right] e^{st} \tag{8.1}$$

where the set of all $\{f_k\}$ *is equal to the set of real numbers* $\Re$ *(i.e not just the integers)*

This signal space can be used to from a state space called here the Frequency Spectrum State Space (FSSS), which is similar to the HSS except with the obvious difference that EFS-domain signals instead of HSS signals are used.

Just as was the case of the HSS the vector of the EFS-domain signals will need to be truncated for implementation. Determining how best to truncate the vector, and how to form the transfers of the FS state space are all tasks that will need to be overcome.

Creating the subsystem descriptions An extremely useful piece of code to write would an algorithm that can form a hybrid model description including all of the necessary jump destination maps, jump sets, and stage differential equations. Ideally for compatibility with other programs it should be formed from a net-list style description. This piece of code would enable any of the small signal techniques discussed above to be easily applied to any arbitrary circuit.

A related coding project would also be to produce a time-stepping simulation tool for the hybrid system. This would require expanding the hybrid model to allow for switching cascades.

Truncation A greater understanding of truncation, and how it affects the HSS is required. A large body of mathematics literature exists for the truncation of infinite Toeplitz matrices and a possible future avenue for understanding and mitigating truncation could lie within them.

Appendix A

SOLUTION TO A SET OF DES SUBJECTED TO A RESONANT SOURCE

If the DE of equation A.1 is subjected to an s-domain signal of the form of equation A.2 then the evolution can be described using formula A.3 for all s not equal to an eigenvalue of the dynamics matrix A.

Set of single order DEs:

$$\dot{x}(t) = Ax(t) + Bu(t) \tag{A.1}$$

Exponential Signal:

$$u(t) = u_0 e^{st} \tag{A.2}$$

Response of system to set of Exponential Signals:

$$\begin{aligned} x(t) &= x_{ss}(t) + x_{tr}(t) \\ &= (sI - A)^{-1} B u_0 e^{st} + e^{At}\left(x_0(t_0) - (sI - A)^{-1} B u_0\right) \end{aligned} \tag{A.3}$$

When s is an eigenvalue of the A then the kernel, $(sI - A)^{-1}$, is non-invertible and a different approach is needed. The approach advanced here begins by partition the system into two – one partition contains the modes of the system with Eigenvalues not equal s whilst the other contains modes with Eigenvalues that are equal to s . These partitions are called the singular and non-singular partitions respectively and their partitioning is performed using the similarity transformation $x(t) = Tz(t)$. Where T is invertible and is chosen such that $T^{-1}AT$ is a diagonal matrix consisting of the eigenvalues of A and is of the form of equation A.4.

$$\begin{bmatrix} \lambda_s & \\ & \lambda_{\neq s} \end{bmatrix} \tag{A.4}$$

Where λ_s are the eigenvalues equal to s, and $\lambda_{\neq s}$ are the eigenvalues that are not equal to s.

One necessary requirement of this partitioning is for the matrix A to be diagonalizable. Formal requirements for a diagonalizable matrix are defined in [79], but here it is assumed that the A matrix of interest is a member of the set of diagonalizable matrixes.

By splitting T into the non-square transforms T_s & T_{ns} and finding their pseudoinverses T_s^+ , T_{ns}^+, then the state $z(t)$ can be split into its singular and nonsingular parts, i.e. $z_s = T_s^+ x(t)$ and $z_{ns} = T_{ns}^+ x(t)$. Using these transforms form separate DEs for the singular and non-singular partitions can be written as shown in equations A.5 and A.6.

$$\begin{aligned} \dot{z}_s(t) &= T_s^+ A T_s x(t_0) + T_s^+ B u(t) \\ &= \lambda_s z_s(t_0) + B_s u(t) \qquad \text{(A.5)} \\ \dot{z}_{ns}(t) &= T_{ns}^+ A T_{ns} x(t_0) + T_{ns}^+ B u(t) \\ &= \lambda_{ns} z_{ns}(t_0) + B_{ns} u(t) \qquad \text{(A.6)} \end{aligned}$$

Each state of the system is now linearly independent, as the λ matrixes are diagonal, and the dynamics in one state evolves independent to the evolutions of the other states. This independence means the evolution of each state can be solved in isolation, where the non-singular states can be solved using equation A.3, but the singular states are solved via the alternative solution of theorem A.1.

Theorem A.1 *A single state, differential of the form $\dot{z}(t) = \lambda z(t) + B_s u(t)$, when subjected to an exponential input of the form $u_0 e^{\lambda t}$ evolves according to equation A.7.*

$$z(t) = e^{\lambda t} \left(z(t_0) + B_s u_0 t \right) \qquad \text{(A.7)}$$

Proof: This result can be proved using several techniques, a general technique that could be used for multi dimensional systems would be to use the method of variation of parameters, [26]. However, for the simple one state case, it is sufficient to use Laplace transforms, and is the technique used in this proof.

By taking the laplace transform of both side of the system equation, equation A.8 is formed.

$$sZ(s) - z(t_0) = \lambda Z(s) + \frac{B_s u_0}{s - \lambda} \qquad \text{(A.8)}$$

With some simple manipulation this becomes.

$$Z(s) = \frac{B_s u_0}{(s - \lambda)^2} + \frac{z(t_0)}{s - \lambda} \qquad \text{(A.9)}$$

Which when the inverse Laplace transform is used produces equation A.7.

$$\begin{aligned} z(t) &= \mathscr{L}^{-1}\left[\frac{B_s u_0}{(s-\lambda)^2} + \frac{z(t_0)}{s-\lambda}\right] \\ &= e^{\lambda t}\left(z(t_0) + B_s u_0 t\right) \end{aligned} \tag{A.10}$$

This concludes the proof.

Remark: Although equation A.7 doesn't have a steady state response in the tradition of a damped system, it does have a transient response , $e^{\lambda t}z(t_0)$, the remaining part of the response, $e^{\lambda t}B_s u_0 t$, is know here as the resonant response.

Remark: Although each mode of a system can only contribute either a transient and a steady steady response, or a transient and a resonance response, combined, a system of DEs can have all three responses. A system of this kind yields a response of the form shown in equation A.11.

$$\begin{aligned} x(t) &= \underbrace{\left[T_s e^{\lambda_s t} T_s^{+} + T_{ns} e^{\lambda_{ns} t} T_{ns}^{+}\right] x(t_0) - T_{ns} e^{\lambda_{ns} t}(sI - \lambda_{ns})^{-1} B_{ns} u(t_0)}_{\text{Transient Response}} \\ &\quad + \underbrace{T_{ns}(sI - \lambda_{ns})^{-1} B_{ns} u_0 e^{st}}_{\text{Steady State Response}} + \underbrace{T_s t B_s e^{\lambda_s t} u_0}_{\text{Resonant Response}} \end{aligned} \tag{A.11}$$

Remembering that for the resonant part $e^{\lambda_s t} = e^{st}$.

REFERENCES

[1] R.D. Middlebrook and S. Cuk. A general unified approach to modeling of switching-converter power stages. *IEEE Power Electronics Specialist conference*, pages 18–34, 1976.

[2] S. Todd and A.R. Wood. An s-domain model of an HVdc converter. *IEEE Transactions on Power Delivery*, 12(4):1723 to 1729, October 1997.

[3] D. Jovcic and N. Pahalawaththa M. Zavahir. Analytic modelling of HVdc-HVAC systems. *IEEE Transactions on Power Delivery*, 14(2):506–511, April 1999.

[4] C. Osauskas and A. Wood. Small signal dynamic modeling of HVdc systems. *IEEE Transactions on Power Delivery*, 18(2):506–511, January 2003.

[5] D.J. Hume. *Harmonic and Inter Harmonic Cross Modulation in HVdc Links*. PhD thesis, University of Canterbury, 2002.

[6] B.C. Smith, N.R. Watson, A.R. Wood, and J. Arrillaga. Steady state model of the ac/dc convertor in the harmonic domain. *IEE proceedings Pt C*, 142(2):109 to 118, March 1995.

[7] G.N. Bathurst, B.C. Smith, N.R. Watson, and J. Arrillaga. Harmonic domain modelling of high pulse converters. *IEE Proc.-Electr. Power Appl*, 146(3):335–340, May 1999.

[8] Q.N Dinh, J. Arrillaga, and B.C. Smith. Steady state model of a direct connected generator-HVDC converter units in the harmonic domain. *IEEE Proceedings on Generation, Transmission, and Distribution*, 145(5):559 to 565, sep 1998.

[9] G.W. Hill. On the part of the Lunar perigee which is a function of the mean motions of the Sun and the Moon. *Acta Mathematica*, 8:1–36, 1886.

[10] M.S. Branicky. *Studies in Hybrid Systems: Modeling, Analysis and Control*. Doctor of science in electrical engineering and computer science, Massachusetts Institute of Technology, 1996.

[11] IEEE. Special report on hybrid systems. *Proceedings of the IEEE*, 88, 2000.

[12] E V Larsen, D H Baker, and J C McIver. Low order harmonic interaction on ac/dc systems. *IEEE Transactions on Power Delivery*, 4(1):493–501, January 1989.

[13] D.J. Hume, A.R. Wood, B.C. Smith, and J. Arrillaga. Linearised direct harmonic solution method for a back-to-back HVdc link. *ICHQPs Conference, 14-16 sept. 1998, Athens, Greece.*, October 1998.

[14] C. Sainter, R. Hanitsch, C. Osauskas, and H. Laird. A harmonic transfer matrix model of a varible ac speed drive. *IEEE Postgraduate Power Conference*, 1999.

[15] C.M. Osauskas, D.J. Hume, and A.R. Wood. Small signal frequency domain model of an HVdc converter. *IEE Proceedings on Generation, Transmission and Distribution*, 148(6):573–578, November 2001.

[16] E. Mollerstedt and B. Bernhardsson. Out of control because of harmonics - an analysis of the harmonic response of an inverter locomotive. *IEEE sontrol systems magazine*, pages 70–81, August 2000.

[17] Ned Mohan, Tore M Underland, and William Robbins. *Power Electronics: Converters, Applications and Design*. Wiley, 2nd edition, 1995.

[18] Karnopp D. and Rosenberg R.C. *System Dynamics: a unified approach Power System Stability and Control*. John Wiley and Sons, N.Y., 1975.

[19] Chen W-K. *Linear Networks and Systems: Algorithms and Computer-Aided Implementations*, volume 2(Fourier Analysis and State Equations). John Wiley and Sons, N.Y., 2nd edition, 1990.

[20] A. Opal and J. Vlach. Consistent initial conditions of linear switched networks. *IEEE Transactions on Circuits and Systems*, 37(3):364–372, March 1990.

[21] Raymond A. DeCarlo and Pen-Min Lin. *Linear circuit analysis : time domain, phasor, and Laplace transform approaches*. Prentice Hall, 1995.

[22] D. Bedrosian and J. Vlach. Time-domain analysis of networks with internally controlled switches. *IEEE Transactions on Circuts and Systems - I:Fundamental Theory and Applications*, 39(3):199–212, March 1992.

[23] Vlach J., Wojciechowski J. M., and Opal A. Analysis of nonlinear networks with inconsistent initial conditions. *IEEE Transactions on Circuits and Systems - I:Fundamental Theory and Applications*, 42(4):195–200, April 1995.

[24] Massarini A., Reggiani U., and Kazimierczuk M. K. Analysis of networks with ideal switches by state equations. *IEEE Transactions on circutis and Systems - I:Fundamental Theory and Applications*, 44(8):692–697, August 1997.

[25] Kundur P. *Power System Stability and Control*. McGraw-Hall Inc, 1993.

[26] W.E. Boyce and R.C. DiPrima. *Elementary Differetial equations and Boundary Value Problems*. John Wiley and Son, Inc, New York, U.S.A, 6 edition, 1997.

[27] A. R. Wood. *An analysis of non-ideal HVdc convertor behaviour in the frequency domain, and a new control proposal*. PhD thesis, Department of Electrical and Electronic Engineering, University of Canterbury, Christchurch, New Zealand, November 1993.

[28] H. D. Laird, S. D. Round, and R.M. Duke. A frequency domain analytical model of an uncontrolled single-phase voltage-source rectifier. *IEEE Transactions on Industrial Electronics*, 47(3):525–531, June 2000.

[29] M. Schwartz, W. R. Bennett, and S. Stein. *Communication systems and techniques*. IEEE - Classic reissue, 1996.

[30] Haykin S. *Communication Systems*. John Wiley and Sons inc, 3rd edition, 1994.

[31] N.M. Wereley. *Analysis and control of linear periodically time varying systems*. PhD thesis, Department of Aeronautics and Astronautics, MIT, 1991.

[32] Bélanger P.R. *Control Engineering: A modern approach*. Saunders College Publishing, 1995.

[33] Aprille T. J. jr and Trick T. N. Steady-state analysis of nonlinear circuits with perodic inputs. *Proceedings of the IEEE*, 60(1):108–114, January 1972.

[34] El-Bidweihy E. A. and Al-Badwaihy K. Steady-state analysis of static power converters. *IEEE Transcations Industry Applications*, 1A-18:405–410, July 1982.

[35] Roberts S.M. and Shipman J.S. *Two-Point Boundary Value Problems: Shooting Methods*. American Elsevier Publishing Company, New York, U.S.A, 1972.

[36] Hall G. and Watt J.M. *Modern Numerical Methods for Ordinary Differential Equations*. Clarendon Press, Oxford, U.K., 1976.

[37] Aprille T. J. jr and Trick T. N. A computer algorthim to determine the steady-state response of non-linear oscillators. *IEEE Transactions on Circuit Theory*, 19(4):354–360, July 1972.

[38] Welsch G., Brachtendorf H.G., Sabelhaus C., and Laur R. Steady-state analysis of nonlinear circuits with perodic inputs. *IEEE Transactions on Circuits and Systems 1: Fundamental Theory and Applications*, 48(18):1252–1257, October 2001.

[39] Parkhurst J.R. and Ogborn L.L. Determing the steady-state output of nonlinear oscillatory circuits using multiple shooting. *IEEE Transactions on Computer-Aided Design of Integrated Circuits and Systems*, 14(7):882–889, July 1995.

[40] Armanazi A.N. Steady-state analysis of piecewise-linear systems with periodic inputs. *Proceedings of the IEEE (Letters)*, 61:789–790, June 1973.

[41] Armanazi A.N. *State-space analysis of piecewise-linear systems and networks*. D.E.Sc dissertation, Columbia University, 1971.

[42] Kato T. Efficient steady-state method with sensitivities of switch timings by the shooting method. *IEEE Conference record of the Power Conversion Conference (Yokohama)*, pages 550–556, 1993.

[43] Bedrosian D.C. and Vlach J. An accelerated steady-state method for networks with internally controlled switches. *IEEE Transactions on circutis and Systems - I:Fundamental Theory and Applications*, pages 520–530, 1993.

[44] J.C. Contreras-Sampayo, J. Usaola-Garcia, and A.R. Wood. Steady-state algorithm for switching power electronic devices. *IEE Proc.-Elect. Power Appl*, 148(2):245–250, March 2001.

[45] B.C. Smith. *A harmonic domain model for the interaction of the HVdc convertor with ac and dc systems*. PhD thesis, University of Canterbury, New Zealand, 1996.

[46] G.N. Bathurst. *A Newton solution for the harmonic analysis of power systems with multiple non-linear devices*. PhD thesis, Electrical Engineering department, University of Canterbury, New Zealand, April 1999.

[47] M Szechtman, T Weiss, and C V Thio. First benchmark model for HVDC control studies. *Electra*, 1(135):55 to 75, April 1991.

[48] D. Maksimovic and S. Cuk. A unified analysis of PWM converters in discontinuous modes. *IEEE Transactions on Power Electronics*, 6(3):476–490, 1991.

[49] P. Marino R. Carbone, A. Lo Schiavo and A. Tesla. A new method based on periodic convolution for sensitivity analysis of multi-stage conversion systems. *9th International Conference on Harmonics and quality of power*, 1:69–74, October 2000.

[50] B.C. Smith, N.R. Watson, A.R. Wood, and J. Arrillaga. A Newton solution for the steady state interaction of ac/dc systems. *IEE Proceedings on Generation, Transmission and Distribution*, 143(2):200 – 210, March 1996.

[51] E.V. Persson. Calculation of transfer functions in grid controlled convertor systems. *IEE Proceedings*, 117(5):989 to 997, May 1970.

[52] L. Hu and R. Yacamini. Harmonic transfer through convertors and HVdc links. *IEEE Transactions on Power Electronics*, 7(3):514 to 525, July 1992.

[53] A R Wood and J Arrillaga. Hvdc convertor waveform distortion - a frequency domain analysis. *IEE proceedings Pt C*, 142(1):88 to 96, January 1995.

[54] S. Chen, A.R. Wood, and J. Arrillaga. Hvdc converter core saturation instability; a frequency domain analysis. *IEE Proceedings Pt. C*, 143(1):75 to 81, January 1996.

[55] D. J. Hume. *Harmonic and interharmonic cross-modulation in HVdc links*. PhD thesis, Department of Electrical and Computer Engineering, University of Canterbury, Christchurch, New Zealand, July 2002.

[56] G. Floquet. Sur les èquations diffèrentielles linèaires a coefficients pèriodiques. *Annales de L'Ecole Normale Supèrieure*, 12:47–89, 1883.

[57] J.J. Rico, M. Madrigal, and E Acha. Dynamic harmonic evolution using the extended harmonic domain. *IEEE Transactions on Power Delivery*, 18(2):587–594, April 2003.

[58] T. Noda, A. Semlyen, and R.Iravani. Harmonic domain dynamic transfer function of a nonlinear time-periodic network. *IEEE Transactions on Power Delivery*, 18(4):1433–1441, October 2003.

[59] A. Ramirez, A. Semlyen, and R.Iravani. Harmonic domain characerization of the resonant interaction between generator and transmission line. *IEEE Transactions on Power Delivery*, 20(2):1753–1762, April 2003.

[60] Jonsson T. and Bjorklund P. Capacitor commutated converters for hvdc. *Stockholm Power Tech Conference*, pages 44 – 51, 1995.

[61] R. Mohan Mathu and Rajiv K. Varma. *Thyristor-Based FACTS Controllers for electrical transmission systems*. IEEE Press and John Wiley-Interscience, New York, 2002.

[62] G. Schmidt and A. Tondl. *Non-linear Vibrations*. Cambridge University Press, Cambridge, U.K, 1986.

[63] J.J. Stoker. *Nonlinear Vibrations*. Interscience Publishers, New York, U.S.A., 1950.

[64] D.R. Cunningham and J.A. Stuller. *Circuit Analysis*. John Wiley and Sons, New York, U.S.A., 1995.

[65] D.M. Mitchell. *Switching Regulator Analysis*. McGraw Hill, New York, U.S.A, 1991.

[66] J.G. Kassakian, M.F. Schkecht, and G.C. Verghese. *Principles of power electronics*. Addison-Wesley Publishing Company, Reading, Massachusetts, U.S.A, 1991.

[67] V.A. Caliskan, G.C. Verghese, and A.M. Stankovic. Multifrequency averaging of dc/dc converters. *IEEE Transactions on Power Electronics*, 14(1):124–133, 1999.

[68] A.R. Wood and J. Arrillaga. The frequency dependent impedance of an HVdc converter. *IEEE Transactions on Power Delivery*, 10(3):1635 to 1641, July 1995.

[69] J. Arrillaga. *High Voltage Direct Current Transmission*. Peter Peregrinus Ltd, London, U.K., 1983.

[70] Sadek K., Pereira M., Brandt D.P., Golè A.M., and Daneshpooy A. Capacitor commutated converter circuit configurations for dc transmission. *IEEE Transactions on Power Delivery*, 13(4):1257–1264, October 1998.

[71] Zeineldin H.H., El-Saadany E.F., and Kazerani M. Capacitor commutated contverter(sic) using an adaptive active capacitor for HVdc system. *Transactions of CCECE 2003 - CCGEI 2003*, pages 529 – 534, 2003.

[72] Toshihiko T, Masafumi N, and Shigeyuki F. A new approach to the capacitor-commutated converter for HVdc - a combined commutation-capacitor of active and passive capacitors. *Power Engineering Society Winter Meeting*, pages 968–973, 2001.

[73] Balzer G and Muller H. Capacitor commutated converters for high power HVdc transmission. *IEE Seventh International Conference on AC-DC Power Transmission, 2001.*, 3:60–65, 2001.

[74] Meisingset M. and Golè A.M. A comparison of convential and capacitor commutated converters based on steady-state and dynamic considerations. *IEE Seventh International Conference on AC-DC Power Transmission, 2001.*, pages 49 – 53, 2001.

[75] CIGRE and IEEE joint Task force. Guide for planning dc links terminating at ac locations having low short circuit capacities, part 1: Ac/dc interaction phenomena. Technical Report 68, CIGRE Publication, July 1992.

[76] Graham J., Jonsson B, and Moni R.S. The Gabari 2000 MW interconnection back-to-back HVdc to connect weak ac systems. *ABB Utlities, Ludvika, Sweden*, 2002.

[77] Muller H and Balzer G. Analysis of subsynchronous oscillations at capacitor commutated converters. *IEEE Bologna PowerTech Conference*, 3, 2003.

[78] Gomes S, Martins N, Jonsson T, Menzies D, and Ljungqvist R. Modeling capacitor commutated converter in power system stability studies. *IEEE Transactions on Power Systems*, 17(2):371–377, May 2002.

[79] B. Nobel and J.W. Daniel. *Applied Linear Algebra*. Prentice-Hall, Englewood Cliffs, New Jersey, 1988.

[80] D Clark. Intel makes its push for chips using dual microprocessors; 'multicore' technology breaks from past efforts to boost computing speed. *Wall Street Journal (Eastern Addition)*, page B3, March 2 2005.

[81] J D Ainsworth. Harmonic instability between controlled static convertors and ac networks. *IEE Proceedings*, 114(7):949 to 957, July 1967.

[82] M. Hernes and B. Gustavsen. Simulation of shaft vibrations due to interaction between turbine-generator train and power electonic converters at the Visund oil platform. *PCC-Osaka*, page 1381 to 1386, 2002.

[83] D.J. Hume, A.R. Wood, and C.M. Osauskas. Frequency-domain modelling of interharmonics in HVdc systems. *I-EE Proceedings Generation, Transmission and Distribution*, 150(1):41 – 48, Jan 2003.